

UNIVERSITY OF BIRMINGHAM

DEVELOPMENT OF LONG-ACTING NALTREXONE LOADED EVA SUBCUTANEOUS IMPLANTS FOR THE TREATMENT OF OPIOID DEPENDENCE

by

Gábor Drávavölgyi

A thesis submitted to the University of Birmingham for the degree of DOCTOR OF PHILOSOPHY

School of Pharmacy

College of Medical and Dental Sciences

University of Birmingham

November 2021

UNIVERSITY OF
BIRMINGHAM

University of Birmingham Research Archive

e-theses repository

This unpublished thesis/dissertation is copyright of the author and/or third parties. The intellectual property rights of the author or third parties in respect of this work are as defined by The Copyright Designs and Patents Act 1988 or as modified by any successor legislation.

Any use made of information contained in this thesis/dissertation must be in accordance with that legislation and must be properly acknowledged. Further distribution or reproduction in any format is prohibited without the permission of the copyright holder.

ABSTRACT

Opioid dependence has become an essential and severe public health crisis in the last two decades. An overwhelming increase in overdose deaths and public health department visits linked to the misuse of illicit and prescription opioids are highly publicised aspects of the opioid epidemic. Among several strategies, medication-assisted therapies have proven to be the most effective way to tackle the opioid epidemic. Naltrexone (NTX) is one of the most widely used drugs among the accepted pharmaceutical treatment options. Oral dosage forms of NTX have been commercially available since 1994 to treat opioid dependence. However, orally taken NTX formulations have several limitations, which may subsequently reduce the efficacy of the pharmacotherapy. First, the oral bioavailability of NTX is low, ranging from 5 to 40%, due to the extensive first-pass hepatic metabolism. Therefore, high orally taken daily doses are required to achieve an effective pharmacological response. This results in a repetitive fluctuation in drug plasma concentration that may cause mild or severe side effects. Second, the oral route of administration requires strict patient dosing compliance.

Several attempts have been made to develop innovative NTX formulations to address these limitations. These subdermal implantable or injectable extended-release NTX formulations bypass the gastrointestinal tract, enhance patients' adherence to the medication, ensure constant NTX blood levels and improve patient convenience by reducing dosing frequency. Unfortunately, most of them are under development or in a clinical phase. Moreover, they require complex manufacturing processes, increasing the cost of the final products and consequently decreasing the accessibility of such innovative and more effective NTX-based pharmacotherapies for poorer social classes.

In this research project, the main aim was to develop novel subcutaneously implantable long-acting poly(ethylene-co-vinyl) acetate (EVA)-based formulations of both the hydrochloride salt form of NTX (NTX HCl) and its neutral base form (NTX base) prepared using a cost-effective one-step hot-melt extrusion (HME) process. HME is a solvent-free, continuous technology that can be easily scaled for mass production. The prepared Implantable Drug Delivery Systems (IDDS) demonstrated sustained release for over 90 days, which can provide long-term delivery of NTX into the bloodstream from the subcutaneous tissue, eliminating mild or severe side effects due to the repetitive fluctuation in the NTX plasma concentration, which can otherwise be caused by conventional daily oral administration. Such long-acting simple matrix devices might be new, cost-effective alternatives on the market to support abstinence-based treatment for patients suffering from opioid addiction.

First, appropriate analytical protocols were developed and validated. Then, monolithic dispersion NTX HCl-EVA systems were developed. Different parameters influencing processability and critical quality attributes (CQA) of the formulations were investigated. *In vivo* investigations of the chosen final formulation showed long-term blood concentrations in male beagle dogs.

The manufacturing HME process of the final monolithic dispersion NTX HCl-EVA formulation was also further investigated. A process window was determined by analysing six HME process settings. The impact of process temperature and screw speed on CQAs was determined, and where appropriate, identification of any relationship was supported by statistical analysis. After selecting the most appropriate HME process setting, a larger batch size (approximately 100 implants) was manufactured, and their stability was assessed over six months under accelerated conditions (40 °C/ 75% RH). The stability study confirmed that no changes occurred in the final NTX HCl-EVA formulations under accelerated stability conditions, which could significantly affect their CQAs.

Our study also aimed to explore the influence of different cellulose-ether (CE) additives, namely hydroxypropylcellulose (HPC) and hydroxypropylmethylcellulose (HPMC), as swelling or pore-forming agents on NTX HCl release from EVA subcutaneous IDDSs. The results showed that the drug release could be tailored effectively by the incorporation of CE-additives, reducing the required initial NTX HCl concentration in the systems. This would result in significant cost savings as the NTX HCl is more expensive than CE-additives.

Finally, novel NTX base-loaded EVA IDDSs were manufactured, and their several CQAs were assessed and compared to NTX HCl-loaded EVA systems. This study explored that if the drug release mechanism was based on pure Fickian-diffusion through the polymeric EVA matrices, a significantly higher drug release rate could be achieved with the same drug level.

Acknowledgements

First and foremost, I would like to express my sincere appreciation to my supervisor Dr Christopher McConville for his constant assistance and guidance in my PhD study. I also extend my gratitude to my friends and lab mates in the School of Pharmacy for their kindness and support.

COVID-19 impact statement

As I have completed my PhD laboratory work by the deadline of 30th August 2020, there have been some impacts on my project as a result of the COVID-19 pandemic.

The main impact was related to the Raman spectroscopic measurements investigating the distribution of the components of the cellulose-ether-loaded NTX HCl-EVA28 implants (Chapter 4). Unfortunately, I did not get to test some remaining samples.

Table of Contents

1 Introduction 1
1.1 Opioid epidemic crisis and its management by the global healthcare system 1
1.1.1 The scope and origins of the opioid epidemic crisis 1
1.1.2 The acute and long-term effects of opiod drugs 2
1.1.3 Management of the opioid epidemic crisis 3
1.2 Medication-assisted therapies for treating opioid dependence 4
1.2.1 Full or partial opioid agonist treatments 4
1.2.2 Full opioid receptor antagonist treatment; Naltrexone (NTX) 7
1.2.3 Limitations of orally taken NTX formulations 8
1.3 General need for improved dose delivery in pharmaceutical therapies 9
1.4 Long-acting depot formulations, injectable and implantable systems 10
1.4.1 Rationale for the development of long-acting delivery systems 10
1.4.2 Limitations of long-acting oral administration 13
1.4.3 General considerations for long-acting drug deliveries 14
1.4.4 Marketing perspectives 16
1.4.5 Types of long-acting formulations 16
1.5 Polymer based long-acting implants 17
1.5.1 Classification 17
1.5.2 Mass control mechanism 20
1.5.3 Manufacturing technologies 27
1.5.4 Hot-melt extrusion (HME) 30
1.6 Long-acting formulations of NTX 37
1.7 Research hypothesis and objectives 41
2 Product development of NTX HCl loaded EVA implant 42
2.1 Introduction 42
2.2 Materials and methods 43
2.2.1 Materials 43
2.2.2 Hot-melt extrusion of EVA 44
2.2.3 Flexibility testing of blank implants 44
2.2.4 Reversed-phase HPLC methodologies 45
2.2.5 Homogeneity of the implants 49
2.2.6 Validation of HPLC methods 49
2.2.7 Stability of NTX HCl in various dissolution media 50
2.2.8 Solubility of NTX HCl in water 50
2.2.9 *In vitro* drug release 50

2.2.10 Rheological evaluation of the NTX HCl/EVA blends 50
2.2.11 Differential scanning calorimetry (DSC) 52
2.2.12 Scanning electron microscopy (SEM) 52
2.2.13 Preparation of NTX HCl-EVA implants from different grade EVA polymers 52
2.2.14 Preparation of NTX HCl-EVA28 implants with varying drug loadings 53
2.2.15 *In vivo* characterisation 53
2.2.16 Statistical data analysis 55
2.3 Results 55
2.3.1 Flexibility of the blank EVA implants 55
2.3.2 Development and validation of the different HPLC methods 57
2.3.3 Development of the NTX HCl dissolution method 62
2.3.4 The influence of EVA grade on the processability, stability and release of NTX HCl from the implants 64
2.3.5 The influence of drug loading on the processability, homogeneity, stability and release of NTX HCl 67
2.3.6 *In vivo* performance of the produced NTX HCl-EVA28 implants 79
2.4 Discussion 82
2.5 Conclusion 92
3 Process development for NTX HCl loaded EVA implants and 6 months stability study 93
3.1 Introduction 93
3.2 Materials and methods 95
3.2.1 Materials 95
3.2.2 Hot-melt extrusion 95
3.2.3 HPLC analysis, assay, homogeneity, impurity content, *in vitro* drug release and statistical analysis 95
3.2.4 DSC analysis 95
3.2.5 Comparison of drug release profiles 96
3.2.6 Flexibility testing 96
3.2.7 Stability study 97
3.3 Results 98
3.3.1 Average drug content and homogeneity of the implants 98
3.3.2 NTX HCl degradation 99
3.3.3 Tensile testing 101
3.3.4 Morphological investigations of the implants 102
3.3.5 *In vitro* NTX HCl release 105
3.3.6 6-month stability study 109
3.4 Discussion 112

3.5 Conclusions 114
4 The influence of cellulose-ether additives on drug release of NTX HCl loaded EVA implants. 115
4.1 Introduction 115
4.2 Materials and methods 116
4.2.1 Materials 116
4.2.2 Hot-melt extrusion 116
4.2.3 Drug content analysis and *in vitro* release testing 117
4.2.4 Morphological characterisation of the extrudates 118
4.3 Results 119
4.3.1 Processability and drug content of the implants 119
4.3.2 Morphological characterisation 119
4.3.3 *In vitro* NTX HCl release 123
4.4 Discussion 128
4.5 Conclusion 130
5 Development of NTX base loaded EVA systems 132
5.1 Introduction 132
5.2 Materials and methods 133
5.2.1 Materials 133
5.2.2 Diffusion experiments 134
5.2.3 Hot-melt extrusion 135
5.2.4 Purity profiling, drug content analysis and *in vitro* release testing of the implants 135
5.2.5 Morphological characterisation of the implants 135
5.3 Results 136
5.3.1 Diffusion study 136
5.3.2 Formulation study of NTX forms with different types of EVA 138
5.4 Discussion 146
5.5 Conclusion 149
6 General discussion and future works 150
6.1 General discussion 150
6.2 Future works 153
References 155

1 Introduction

1.1 Opioid epidemic crisis and its management by the global healthcare system

1.1.1 The scope and origins of the opioid epidemic crisis

Opioid dependence can be defined as a chronic recurrent disorder in personal regulation of opioid use arising from repeated or continuous use of opioids. Opioid use disorder can be associated with a wide range of mental and physical comorbid disorders and increased mortality[1]. Over the past two decades, the issue of opioid use disorder has grown into a global crisis. In particular, the escalating problem of addiction to heroin and opioid pain analgesics has evolved into the so-called opioid epidemic[2]. The severity of the opioid epidemic is indicated by the number of addiction patients around the world. In 2018, an estimated 35.6 million people suffered from substance use disorder globally[3]. Most patients used opioids. In the US alone, 10.1 million people misused opioids in 2019. Among them, 9.7 million people abused prescribed opioid drugs for pain management[4]. According to the WHO report from 2018, approximately 0.5 million deaths could be attributed to substance use disorder. 115 000 deaths were related to opioid overdose[5]. Alongside overdose deaths, other consequences of opioid use disorder include the rising spread of infectious diseases (e.g., hepatitis C and HIV[6]) and also, the increased risk of new-born infants having opioid dependence because their mother suffered from drug use disorder during the pregnancy[7]. Additionally, other societal burdens generated by this epidemic, such as criminal activities and the loss of worker productivity associated with opioid misuse and withdrawal symptoms, are also important to be mentioned.

The root cause of this epidemic is not only to be found in the resurgence of illicit synthetic opioids, such as heroin, or in the recent increased use of high-potency fentanyl and its derivatives. In the late 1990s, a widespread view recognised pain as a symptom that had not been addressed sufficiently so far in pharmaceutical therapies. The efforts stressed patients' rights in the assessment and management of pain. This subjective approach led to the liberalisation of prescribing opioids for chronic, non-cancer pain. Consequently, due to the increased availability of prescribed opioids, the misuse of this very addictive family of Active Pharmaceutical Ingredients (API) also increased[8]. It is also believed that the aggressive marketing from pharmaceutical companies and the intense prescription of opioid analgesics (e.g., OxyContin® by Purdue Pharma L.P.) in the mid to late 1990s also contributed to the uncontrollable misuse of prescribed pharmaceuticals, thus increasing the number of prescribed and illicit drug abusers[9].

1.1.2 The acute and long-term effects of opiod drugs

Opioid action and effects

Opioid receptors are a family of G protein-coupled receptors located both in the central and peripheral nervous systems. They can be divided into three subtypes (μ, δ and κ)[10]. In the absence of endogenous opioids (endorphins, enkephalins, dynorphins), inhibitory neurons (e.g., GABAergic interneurons) secrete neurotransmitters (e.g., GABA) that prevent nearby neurons from releasing dopamine. Conversely, the presence of endogenous opioids in the nervous system activates the group of opioid receptors located on the inhibitory neurons leading to the suppression of neurotransmitters that prevent dopamine release. As a consequence, dopamine-secreting neurons can freely release dopamine. In the pain-processing regions of the central nervous system (e.g., thalamus, brainstem and spinal cord), increased dopamine levels temper pain signals resulting in feeling less pain[11]. Additionally, dopamine release occurring in the mesolimbic pathway (usually referred to as the reward pathway) regions in the brain, such as the nucleus accumbens, prefrontal cortex and ventral tegmental area, results in a calming effect[12].

Acute doses of exogenous opioid drugs (e.g., heroin, fentanyl, morphine, codeine, hydrocodone, oxycodone) easily cross the blood-brain barrier and stimulate the μ-opioid receptor isoforms (μ_1, μ_2, μ_3) predominantly, inducing analgesia, sedation, euphoria, endocrine dysregulation, blood pressure, antitussive activity or respiratory depression[10,12]. Exogenous opioid drugs and their active metabolites bind to the opioid receptors more intensely and for a more extended period compared to endogenous opioids. As a result, exogenous opioid drugs can manage more severe pains. Additionally, they can cause increased feelings of pleasure and may be responsible for the sense of euphoria that characterizes the opioid high, which is the main reason for illicit use. However, exogenous opioids indirectly have high inhibitory activity at peripheral chemoreceptors (located in the vascular system) that play an essential role in the rhythmic respiration processes, responding to changes in blood oxygen and carbon dioxide level. Therefore, opioid drugs can be easily overdosed, causing hypoxia and even death, mainly by the depression of the respiratory system[13].

Opioid dependence

Long-term opioid exposure causes physical and psychological dependence[14]. The physical dependence on opioids is evolved by the down-regulation and adaptive changes of the opioid receptors, causing an overall decrease in the acute receptor response. This desensitization of the receptors results from the essential controlling mechanism to avoid receptor hyperstimulation[15].

These neuroadaptive changes result in the attenuation of the pharmacological response to opioid drugs. Therefore, increased doses are needed to achieve the original pharmacological effect[16]. This phenomenon is usually referred to as opioid tolerance. Opioid tolerance developed during the pharmacological treatment or illicit use can lead to incredibly debilitating withdrawal symptoms (e.g., anxiety, restlessness, insomnia, abdominal pain, fever, tremor, diarrhoea, vomiting). It is generally suggested that withdrawal symptoms are generated by the decreased dopamine concentration in the mesolimbic system[17,18]. In many cases, withdrawal symptoms can be violently intensive. As a result, long-term prescribed opioid users and illicit drug abusers administer these APIs not necessarily to manage pain or to experience euphoria but also to treat their severe withdrawal symptoms. After reduction or abrupt cessation of regular opioid doses, withdrawal symptoms can last 14 days or more[1].

On the other hand, the characteristic feature of psychological dependence on opioid drugs is a strong internal drive to use opioids, directed primarily by the need to accommodate the reward centre of the brain[19]. This manifests as patients' inability to effectively prioritize well-being over continuous opioid use. Patients often experience a subjective sensation of an urge or craving to use opioids, therefore acting out of character, leading to interpersonal, financial and legal problems[12].

1.1.3 Management of the opioid epidemic crisis

In order to alleviate the opioid epidemic, a number of initiatives and treatments have been implemented and developed over the years. Preventive measures mainly focus on restricting opioid prescription in chronic pain management and physician drug monitoring programs[20]. Preventive interventions for the younger population also show positive outcomes in decreasing the misuse of opioids[21]. Initiatives also urge preventing overdose deaths by increasing the accessibility of naloxone. Naloxone is short-acting, high affinity opioid receptor antagonist drug used for the acute treatment of overdoses[2,22]. Naloxone was approved in the 1970s, and for decades it was only available only in the emergency care units as injectable liquid formulations. In 2014, the US Food and Drug Administration (FDA) approved two generic formulations of naloxone, an auto-injector (Evzio®) and an intranasal kit (Narcan®), allowing first responders, including family members of individuals at risk, for immediate naloxone administration[23]. However, these pharmaceuticals can still be obtained only with a prescription, which is still a barrier to overcome. In addition, the development of abuse-deterrent formulation alternatives to existing opioid painkillers containing special additives to avoid misuse is well-supported by pharmaceutical authorities[24].

Besides the initiatives mentioned above, pharmacological treatments have been proven to be the most effective way of mitigating the opioid crisis. Although the number of medication-assisted therapies has advanced in the last 20 years, they show limited effectiveness.

1.2 Medication-assisted therapies for treating opioid dependence

In general, two main types of opioid dependence treatments can be differentiated: Agonist therapy, known as opioid substitution treatment; and antagonist therapy, also known as opioid blockade treatment. The three FDA approved medications which are commonly used as the standard of care for patients suffering from opioid use disorders are methadone (a full μ-opioid receptor agonist), buprenorphine (a partial μ-opioid receptor agonist) and naltrexone (a full μ-opioid receptor antagonist)[25].

1.2.1 Full or partial opioid agonist treatments

Methadone

Methadone, as a full μ-opioid receptor agonist, occupies and activates the same receptors in the central nervous system as opioid substances do. However, the rate of activation is much slower, and the extent of pharmacological response is smaller. Therefore, patients with an opioid history do not feel as much euphoria as in the case of other opioid drugs. Methadone has been successfully used in the treatment of opioid use disorder since 1974 and several studies have described its clinical benefits[26]. However, despite its clinical advantages, methadone also has limitations. The drug itself, because of its full agonist activity, can cause high euphoria among opioid naïve patients (individuals who have no or less history of opioid misuse), increasing the street value of the drug[27]. Additionally, methadone can cause overdose in situations where individuals do not use it in pre-determined doses or combine it with other substances that can further strain the central nervous system (e.g., alcohol, antidepressants, heroin)[28]. Discontinuation of methadone maintenance treatment is also challenging and requires clinical supervision as dependence to methadone can be developed during treatment due to its agonist activity[29]. Because of these reasons, daily doses of methadone can only be dispensed under strict regulatory supervision in licensed methadone treatment clinics and cannot be prescribed by physicians and practitioners, decreasing the risk of any misuse or illicit use concerns[30]. This restriction and the required constant clinical support make this type of medication-assisted therapy expensive and hard to access for many groups[31]. Moreover, daily visits to methadone treatment centres could be another obstacle for a successful treatment program among patients with poor compliance[32].

Buprenorphine

Buprenorphine is a partial μ-opioid receptor agonist, which means it has low activity but high affinity on these specific receptors. Because of that, it is less sedating than methadone, and the risk for overdosing is lower[33]. Additionally, buprenorphine has an antagonist effect on the κ-opioid receptors. Thus, it can reduce craving and depression during the treatment, which is considered to be a significant therapeutic benefit over methadone treatment[34]. Buprenorphine was first approved in France in 1998 and became FDA approved in 2002 as part of opioid dependence therapy[35]. To date, several studies showed the effectiveness of this medication in the treatment of opioid use disorders[36,37]. According to a comprehensive Cochrane database systematic review, buprenorphine and methadone were found to be almost equally effective in the treatment of opioid dependence, as long as buprenorphine is applied in an adequate dose (> 6 mg)[38]. Because of its proven efficacy, there are a number of formulation options of buprenorphine available on the market, such as oral tablets, sublingual tablets (Zubsolv®), sublingual films (Suboxone®), buccal films (Bunavail®), extended-release injections (Sublocade®) and non-biodegradable implants (Probuphine®). However, there may be problems and limitations associated with the use of this substance. Although its agonist activity is lower than methadone, buprenorphine can still be lethal, especially if combined with central nervous system depressants (e.g., alcohol, antidepressants, heroin)[39]. Moreover, this medication also precipitates withdrawal symptoms if the therapy is discontinued[36]**Error! Bookmark not defined.**. In addition, because of its opioid agonist nature, buprenorphine has the potential for abuse too. Therefore, in many formulations, it is used in combination with naloxone, a short-acting opioid receptor antagonist drug substance (e.g., Suboxone®, Zubsolv®, Bunavail®). The role of naloxone in such formulations is to deter from any attempt to misuse the buprenorphine products (e.g., preparation of injections from tablet formulations). Naloxone, if injected with buprenorphine, can reduce the agonist effect of buprenorphine and cause unpleasant withdrawal symptoms in opioid dependent patients[40]. Despite these limitations, unlike methadone, buprenorphine can be prescribed by physicians, but only under certain conditions. In the US and in the UK, health care workers need a specific license, which is a legal requirement for prescribing[41,42]. Therefore, access to buprenorphine-waivered prescribers can be a challenge in some areas, limiting its accessibility. Although in Canada and several European countries (e.g., France, Belgium, Croatia, Luxembourg, Norway), there are no such restrictions, prescribing this synthetic opioid derivative requires extreme cautions and patient monitoring from general health care workers. The less stringent dispensing and distributing regulations for buprenorphine make this substance suitable to be formulated as extended-release dosage forms,

in contrast to methadone. In addition to increasing patient compliance, diversion and abuse can be eliminated by using these formulation options[43,44]. However, they only can be used with extreme caution, taking into consideration patient compliance history and the willingness to remain within the therapy program.

According to the literature review, the main disadvantages of using methadone and buprenorphine in the treatment of opioid use disorder can be summarized as follows: 1) Both compounds carry the risk of abuse and overdose; 2) dependence on these substances can be developed during the treatment, making the discontinuation phase challenging at the end of the therapy, increasing the risk of relapse is significant; 3) the accessibility is highly limited for certain groups, as the prescription and dispensing of products containing these substances need to follow strict legal requirements; patient compliance and willingness has a pivotal role in the efficacy of the treatment.

As can be seen, most of the limitations above can be traced back to these substances' opioid receptor agonist activity. In contrast, naltrexone (NTX), a full opiate receptor antagonist drug, has the main advantage over methadone and buprenorphine in that its therapeutic effect is not related to the activation of opioid receptors. Thus, the distribution of NTX products and, consequently, patient access do not encounter strict regulatory barriers. However, according to market research, NTX is significantly underutilized compared to methadone and buprenorphine (***Error! Reference source not found.***), with naltrexone accounting for the smallest share of the market in 2018, which is most likely due to limitations of the currently available products on the market, and the low number of alternative formulation options.

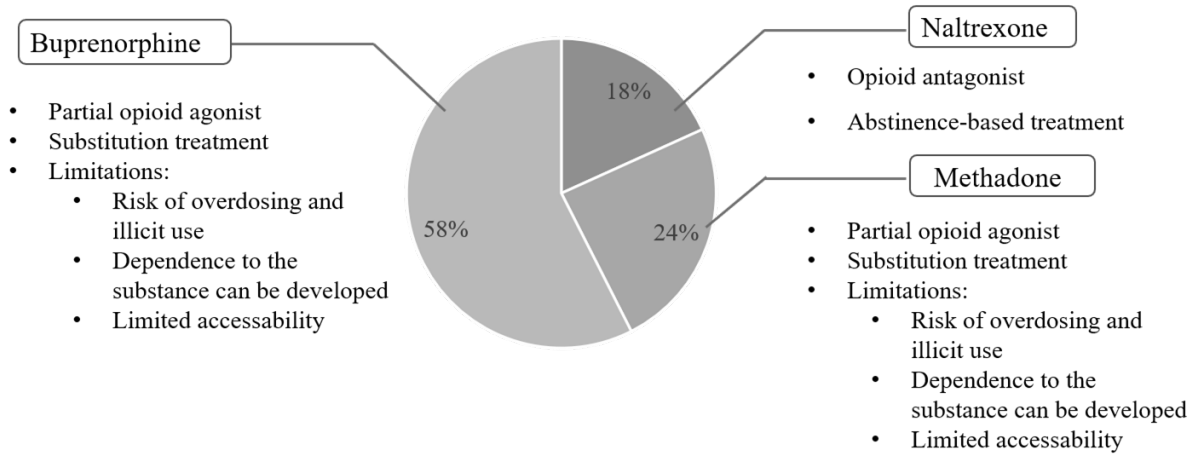


Figure 1 Global opioid use disorder market share, by drug in 2018

1.2.2 Full opioid receptor antagonist treatment; Naltrexone (NTX)

NTX is a noroxymorphone derivative most commonly used in clinical practice as an opioid receptor antagonist for treating opioid dependence and alcoholism. Although it was first synthesized in 1963 by Endo Laboratories[45] and the first clinical investigations of NTX in heroin abuse were published in 1973[46], the drug was FDA approved only in 1984 and promoted to treat addiction to different types of opiates, such as heroin, oxycodone and morphine, branded as Trexane® (oral tablet). Later, its therapeutic indication was extended, and in 1994 NTX became FDA approved as the first adjunct in the treatment of alcohol dependence and renamed as ReVia® (DuPont Merck Pharma, Inc.).

NTX, as a pure opiate antagonist, inhibits the dopamine release-enhancing effects of opioid analgesics by binding to the various opioid receptors (μ-, δ- and κ-receptors) in the central nervous system. This leads to an inhibition of the subjective effects of opioid analgesics[47]. Vereby et al. investigated the NTX plasma concentration and its blockade activity on opioid receptors in response to intravenously administered heroin. Their study showed that 2 ng/mL plasma level of NTX resulted in an 85.6% inhibition of 25 mg IV injected heroin[48]. The main advantages of NTX over the other commonly used drugs in the treatment of drug addiction (e.g., methadone and buprenorphine) is that this substance does not develop opioid effects (euphoria) in the induction period, or dependence to the substance during the treatment. Moreover, there are no withdrawal issues upon discontinuation of the therapy[49]. Similarly to buprenorphine, its antagonist effect on the κ-opioid receptors might reduce craving and depression with the treatment[50]. However, the use of NTX requires at least one week long period of opioid detoxification prior to the start of the abstinence-based treatment, significantly reducing the number of patients who are willing to start the therapy[51].

The basis of treating alcohol dependence with NTX relies on another mechanism. The reinforcing effects of ethanol are based on the activation of brain reward circuity through the mesolimbic dopamine pathway. Alcohol increases the release of β-endogenous opioid peptides, which inhibit the suppressing effect of GABA interneurons on dopamine release, resulting in higher dopamine concentration in the body, leading to euphoria. NTX is thought to block the bindings of β-endorphins to the μ-opioid receptors on the GABAergic neurons, thus preventing dopamine release, resulting in reduced craving for alcohol during the treatment[52]. Based on the similar mechanism, several studies are focused on promoting the indication of NTX to treat eating disorders, usually in combination with bupropion[53]. Although a number of further promising indications are reported in the literature (e.g., low-dose naltrexone for treating

multiple sclerosis[54], chronic pain disorders[55], inflammatory bowel disease[56], chronic fatigue syndrome[57], and even cancer[58]), their mechanism are not fully elucidated, and no definite conclusions can be drawn from the completed clinical trials.

The drug is extensively metabolized in the liver by the aldo-ketoreductase enzyme family (AKR1C1, AKR1C2 and AKR1C4), resulting in several metabolites, among which 6-β-naltrexol (6βNTX) is the major metabolite and shows some extent of biological activity (***Error! Reference source not found.***)[59]. 6βNTX has 1/12th to 1/185th the potency compared to NTX according to *in vivo* animal models but has a significantly longer half-life[60]. However, the pharmaceutical effect of NTX is attributed to both the parent and active primary metabolite[61].

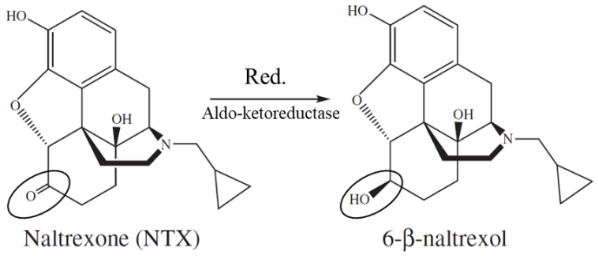


Figure 2 Chemical structure of NTX and its main metabolite 6-β-naltrexol

Due to extensive first-pass metabolism in the liver, orally administered NTX can be characterised by poor bioavailability, ranging from 5 to 40%[61]. According to the investigations by Meyer et al.[62], only 5% of the orally administered NTX hydrochloride (NTX HCl) reached the systematic circulation due to extensive hepatic first-pass metabolism. The mean elimination half-life of NTX and 6βNTX appeared to be approximately 4 and 12 hours, respectively. 48 hours after *oral* administration, not more than 1% of the administered NTX dose was excreted in the urine, while 25% was recovered as free 6βNTX. Both NTX and 6βNTX showed dose proportional drug concentrations in regard to AUC and C_{max} over the range from 50 to 200 mg.

1.2.3 Limitations of orally taken NTX formulations

Despite the fact that ReVia® and Depade®, orally administered tablets with a dose of 25-100 mg NTX HCl, have been on the market since 1994, the oral administration of NTX cannot be considered as the most successful strategy in the treatment of drug addiction and alcohol dependence. They have several limitations which may subsequently reduce the efficacy of the pharmacotherapy. Firstly, as mentioned above, only a small fraction of the administered dose becomes available for action in the systematic circulation after oral administration because of the high rate of first-pass metabolism in the liver. Secondly, the daily administration of fixed doses (25, 50 and 100 mg) of NTX shows a pharmacokinetic profile that can be characterised

by a rapid increase in plasma levels, which peaks within an hour, then is followed by a sudden decrease to below the minimum effective plasma concentration (2 ng/mL), within 8 hours after dosing[63]. This results in a repetitive fluctuation in drug plasma concentration that may cause mild or severe side effects, such as fatigue, nausea, headache, and vomiting[64]. Such side effects can significantly reduce patient adherence and treatment retention[65,66]. Moreover, the correct self-administration of the prescribed medication in the predefined time intervals is a particular problem in such treatments. In many cases, the individuals being treated are unwilling to give up the euphoric feeling associated with alcohol or drug use and thus discontinue the treatment[67,68].

Due to these limitations, there is a need for developing alternative delivery options of NTX, that by-pass the gastrointestinal tract and ensure constant plasma levels for extended time intervals, reducing the dosing frequency.

The following sections of this literature review focus on the general importance of improved dose delivery in pharmaceutical therapies. The existing long-acting formulations of NTX are presented after the general overview of extended-release formulation strategies, mainly focusing on polymeric implantable systems and their manufacturing technologies.

1.3 General need for improved dose delivery in pharmaceutical therapies

There has always been a need in the field of pharmaceutics to produce safer, more effective, economic, and less aggressive medications to support clinical therapies. As a result of biopharmaceutical research, in the 1950s, relevant changes took place in the pharmaceutical industry when the concept of bioavailability was adopted into practice. Along the way of defining bioavailability[69] and developing the framework of the Biopharmaceutical Classification System (BCS)[70], it became apparent that therapeutic benefits do not only rely on the higher potency and specificity of APIs. The selected route of delivery (parenteral or non-parenteral) and type of formulation (tablets, capsules, injectables, implants, patches, inhalations, creams etc.) have a major influence on the bioavailability and pharmacokinetic profiles of the administered active agents in the physiological environment[71]. Also, they can determine the possible side-effects and absolute toxicity of the drug product[72,73]. Furthermore, patient compliance, a usually overlooked factor, could also be a significant bottleneck to the successful clinical performance of the formulation being developed[74]. Even though there are several strategies and technologies in practice, each of the conventional drug delivery systems

currently available has its own therapeutic limitations and drawbacks that must be improved[75]. The biggest challenges that a successful drug delivery system need to overcome are[76]:

- to protect the API over untimely deactivation,
- to increase the retention time of the API in the host body,
- to overcome transport challenges associated with various physiological barriers,
- to decrease the accumulation of the API in non-targeted organs,
- to target the API release to the desired region of the body, or to direct the already absorbed API from the systematic circulation to the targeted cells and tissues,
- to overcome biocompatibility, integration, and sterility issues,
- to deliver APIs continuously for extended periods while maintaining them within their therapeutic window.

Looking at the wide range of innovative strategies and medications developed so far, a special class of drug products, namely controlled drug delivery systems, can offer several ways to decrease and overcome the challenges mentioned above.

Controlled drug delivery systems constitute an essential and expanding part of pharmaceutical interventions. Currently, controlled drug delivery represents 37.8 billion USD of the 1,250 billion USD annual global pharmaceutical market[77] and is projected to grow by 7.8% per year until 2027[78]. It includes both improved tuneable rate- and target-controlled administration of small molecules and biological macromolecules into the body[79]. These systems have been developed to achieve predetermined release rates and/or triggered release, utilizing passive physiological inductions (interstitial fluid diffusion, pH, temperature, enzymatic environment, glucose level etc.), and active, external physical, chemical or even remotely controlled stimulations[80,81].

1.4 Long-acting depot formulations, injectable and implantable systems

1.4.1 Rationale for the development of long-acting delivery systems

Each drug has a therapeutic plasma concentration, so-called therapeutic window, above which it is toxic (maximum safe concentration) and below which it is ineffective (minimum effective concentration). In the case of the administration of conventional dosage forms, the release of the API usually follows rapid first-order kinetics and demonstrates ‘peaks and troughs’ in which the plasma drug concentration increases rapidly, peaks and then declines eventually to almost zero according to the rate of elimination (*Figure 3*).

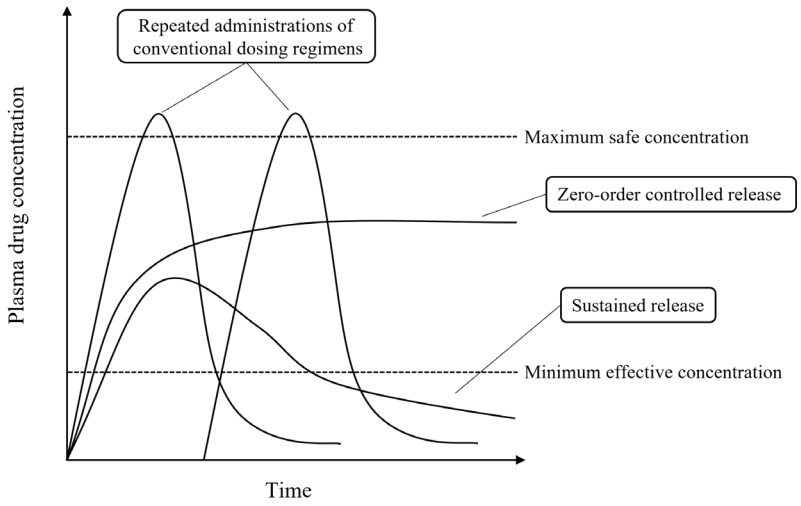


Figure 3 Schematic representation of plasma drug levels after the administration of different dosing regimens

Most pharmaceutical treatments require constant drug blood levels within the effective therapeutic window of the API. For this reason, frequently repeated, predominantly routine intravenous or immediate-release oral administrations of fixed doses are applied in predetermined time intervals to ensure sufficient drug concentration. However, this common practice may cause uncertain fluctuation in drug concentration at the desired site of action and in the whole body as well, resulting in under- or overexposure of the drug substance, or even toxic side effects, owing to the essential pharmacokinetic and pharmacodynamic inter- and intra-subject variability among patients. This problem is more pronounced in the administration of drugs with narrow therapeutic windows or relatively short biological half-lives (*Figure 3*).

Furthermore, intermittent scheduled medications require full patient adherence and/or healthcare professional supervision, inherently making the therapy expensive, hard to access for certain groups, and more importantly, reducing patient compliance. These drawbacks are more expressed in chronic disease treatments such as:

- cancer chemotherapy[82],
- HIV/AIDS prevention[83] and medication[84],
- diabetes management[85],
- tuberculosis[86],
- cardiovascular[87], antihypertensive[88] disorders,
- asthma[89],
- depression[90] and other mental illnesses[91],
- alcohol[92] and narcotic use disorder[2,93] treatments.

In a report from 2003, the World Health Organisation has highlighted an average adherence rate of 50% in developed countries among patients suffering from chronic diseases[94]. According to another study, 30 to 70% of the prescribed medication program fails or declines in efficacy due to patient non-adherence[95]. For instance, low adherence rates appeared to be in asthma (33%) and diabetes (51%) treatment[90], but unquestionably, the highest non-adherence rate can be seen among patients suffering from substance abuse and mental health disorders, such as alcoholism, drug addiction and schizophrenia (60%)[91].

Besides chronic diseases, frequently repeated administrations may decrease the efficacy of a well-designed hormone replacement or even vaccination program[96]. The need for extended or prolonged release medication also exists in long-term therapies that target hard-to-access body sites. For example, repeated intravitreal injections can be painful and traumatic for patients, and additionally, involve low, but significant risk for infections[97].

For these reasons, the need for formulations in which, in addition to concentration (mg/mL), the third dimension, time, can also be designed into the product, has become particularly important. Thereby, the desired duration of pharmacological action can be provided to patients (concentration/time). Long-acting dosage forms can maintain the plasma concentration in the desired therapeutic window with a single dose, significantly reducing dosing frequency, and ideally, minimizing drug exposure.

Several terminologies are used to express that the drug delivery systems in question effects over a longer period. Until now, there is no consensus in the terminology in this field. The United States Pharmacopeial Convention nomenclature refers to extended-release products as a type of modified-release systems designed to release the active agent at slower rates compared to immediate-release formulations[98]. However, this terminology can be further interpreted. Basically, two main types of long-acting drug release can be differentiated regarding their apparent pharmacokinetic profiles. Sustained-release (also called extended- or prolonged release) formulations release the drug at a continuously changing rate over a prolonged period of time, maintaining the drug level within its therapeutic concentration range. By contrast, controlled-release delivery systems operate at a drug release rate that aims to ensure an approximately constant plasma level throughout the product lifetime that would be similar to that attained by intravenous infusion. However, both terms are regularly used interchangeably.

1.4.2 Limitations of long-acting oral administration

Most of the conventional treatments rely on the use of orally administered medications. Drug products designed for oral drug delivery are convenient, easy-to-use for patients, and have a long shelf-life. Moreover, these non-invasive pharmaceuticals can be manufactured cost-effectively in bulk, without strict sterility issues. Because of these benefits, it is evident that a primary design goal to produce long-acting products aims for oral administration.

The concept of long-acting medication has long been implemented into the orally taken formulation designs. Typical examples are dissolution- and diffusion-controlled systems (e.g., tablets, capsules, pellets) based on the use of hydrophobic (e.g., ethylcellulose (EC), poly(propylene)) (PP) or hydrophilic (e.g., methylcellulose (MC), hydroxypropyl methylcellulose (HPMC), polyethylene oxide (PEO)) additives. The drug release can occur from either matrix or reservoir constructs. Such sustained-release systems have been on the market since the 1950s[99]. Osmotic pressure-activated controlled-release tablets (produced by trademarked OROS® technology) are in clinical practice from the 1980s, pioneered by Alza Corporation[100]. Despite their great history and popularity, the use of these formulations in long-term therapies is extremely limited.

Firstly, their duration of action is highly defined because of their relatively short residence time, typically 8-12 h, in the gastrointestinal tract. In general, the minimum intake frequency of extended-release oral dosage forms is one dose per day, depending on the half-lives of the active substance to be administered. Secondly, in many cases, especially in the new era of drug candidates, the active agent to be formulated does not possess preferable physicochemical and stability properties that make them suitable for the oral delivery route. The issues associated with poor aqueous solubility, low permeability, low pre-systemic stability (e.g., against hepatic first-pass metabolism) and short half-lives are getting more and more expressed in the optimisation of oral dosage forms of the new generation of small-molecule drug candidates[101,102,103,104]. Nonetheless, the increasing number of clinically approved biopharmaceutic macromolecules also demand further improvements in their formulation strategies to produce more effective delivery alternatives[105,106].

Furthermore, upon a certain ratio of the orally administered drug volume reaches the systematic circulation, it distributes according to its relative affinities to all tissues throughout the body. This leads to a high drug wastage, as only a small fraction of the delivered drug reaches the desired site of action. Nonetheless, most of the undesirable toxicity and side effects are

associated with the accumulation of drug substances in cells, tissues and organs that are not targeted in the therapy, radically decreasing the therapeutic index of the API.

In addition, given the high complexity of the gastrointestinal system, and the consequent inconsistent drug uptake makes it challenging to produce extended-release dosage forms whose pharmacological response is sufficiently predictable and independent of patient-to-patient variability. Therefore, only drugs with large therapeutic range are advantageous to be formulated as extended-release oral delivery systems to circumvent any possible under- and overexposure concerns.

1.4.3 General considerations for long-acting drug deliveries

Temporal injectable and implantable long-acting delivery formulations constitute a significant class within controlled drug delivery systems. The primary design goal of such systems aims to maintain therapeutic drug plasma concentrations within the therapeutic window for prolonged time interval (*Figure 3*). Retaining the plasma concentration of the API in this specific range requires that the rate of API uptake (liberation, absorption), distribution and clearance (metabolism and elimination) processes (*Figure 4*) should be well-balanced[107].

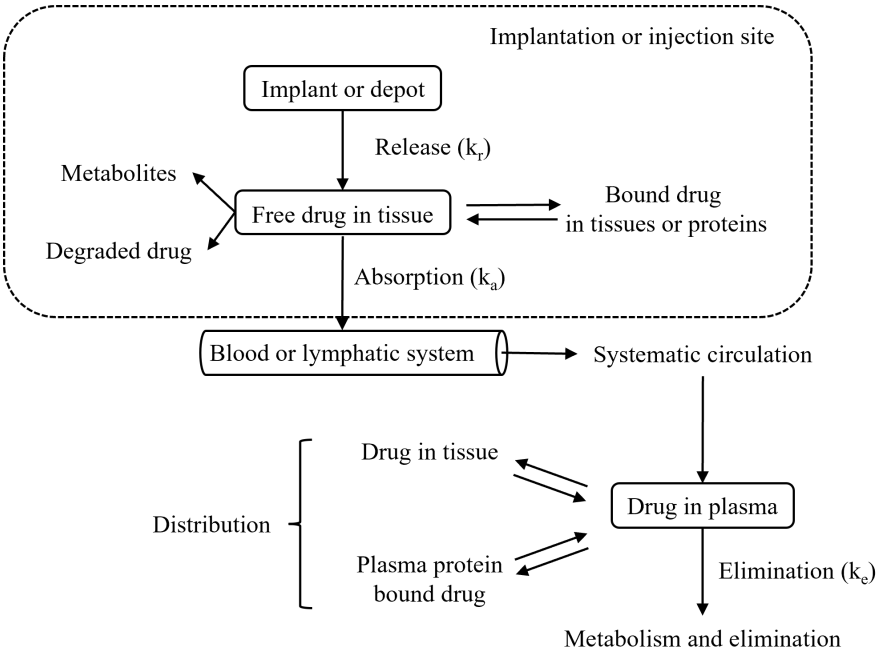


Figure 4 Schematic representation of pharmacokinetics for APIs delivered as long-acting injectable and implantable dosing regimens[107]

Generally, three main principles can be used to obtain long-term drug action:

- Modification of the biological system (k_a and k_e)

  e.g., inhibit renal clearance by probemicid

- Modification of the API (k_r, k_a and k_e)
    e.g., use of prodrugs, different crystal morphology and different polymorphs
- Modification of dosage forms (k_r)

Modification of dosage forms has been proven to be the most effective way to deliver APIs for longer periods, as this strategy can provide the most predictable pharmacological response among patients. In these systems the pharmacological action is controlled via drug release regulation ($k_a > k_r$). However, the knowledge of this complex physiological cascade from different formulations and implantation sites is essential in a particular development process, as other factors may also be responsible for the rate of absorption and excretion (k_a and k_e), which determine the apparent pharmacokinetic profile of the product[108,109,110]. During the application of these products, the drug release rate can be constant (controlled release system, following approximately zero-order release kinetics) or predetermined at a decreasing rate (sustained release system, following approximately first-order release kinetics).

The development of injectable and implantable extended-release drug formulations has long been an objective in the pharmaceutical industry[111]. These devices ensure continuous or programmed drug delivery into multiple body sites and organs, for local treatment or at a systematic level via various routes, including transdermal, parenteral, ophthalmic, and vaginal delivery ranging from days to months. Long-acting injectable and implantable drug delivery systems enable the achievement of the desired pharmacological response with enhanced bioavailability and lower cumulative exposure of the API, minimizing material wastage and toxic side effects (e.g., hepatic, and renal toxicity)[110]. Additionally, the extended pharmacological impact of the drug product reduces the frequency of required intake of medications. Therefore, it overcomes compliance issues, making the treatments of chronic diseases and preventive actions more convenient for patients[73,112].

Consequently, the role of this class of pharmaceuticals is becoming increasingly important in the global healthcare system as the range of patients suffering from chronic and life-threatening diseases expands. Although, healthcare professional assistance and supervision are mostly required for the administration or implantation process, and also for intermittent monitoring, these systems have become extremely popular in various pharmacotherapies. The importance of these products is indicated by their global market size, which is expected to reach an estimated USD 31.6 billion by 2025[113].

1.4.4 Marketing perspectives

Answering clinical needs and obtaining clinical benefits by such innovative formulation designs also add commercial value to already marketed drugs by promoting further use and extending patent protection, that is an essential part of product life-cycle management[114]. It is also worth to be borne in mind the potential of long-acting parenteral formulations already in drug discovery and early clinical development stage. For example, 'rescuing' failed compounds – generally designed for oral administration and rejected because of their poor water solubility – by these means can even generate profits for the developing company[115]. Clearly, this would require a significant paradigm shift in the conventional drug development process. Also, advanced manufacturing strategies can reduce development time and cost while improving the efficiency of getting the products faster to the market[116].

1.4.5 Types of long-acting formulations

Based on the market analysis of commercially available products, the types of long-acting pharmaceutical systems that have been approved can be classified into two main groups according to their drug release performance[117]. In passive delivery systems, drug release is controlled only via internal physiological inductions after administration, such as interstitial fluid diffusion, pH, temperature, enzymatic environment, among others. Drug products that can be categorised into this class involve drug eluting stents, injectable prodrugs, slow-dissolution crystal suspensions, emulsions, liposomes, in-situ gelling systems, micro- and nanoparticles, hydrogels, and pre-formed implantable devices based on non-biodegradable and biodegradable polymers. Active systems, on the other hand, are controlled by a positive post-implantation driving force that results from the product itself, allowing the regulation of dosing due to patients' needs for certain pharmacotherapies. This class of drug delivery systems mainly consists of programmable pump devices. The most common indication in which these systems are used is insulin delivery in diabetes management, generally with inbuilt glucose level monitoring[118]. Polymer based systems that can be categorized into this class involve implantable osmotic pumps[117].

Although, a wide variety of other promising long-acting formulation strategies are under development, to date, none of them have been used in regulatory approved pharmaceutical devices. Examples include, among others, nanoporous systems (e.g., titanium and carbon nanotubes[119,120], porous silica[121]) and microchip technologies [122,123]. Microneedle arrays (also called microarray patches) also have increasingly high potential in the field of extended-release formulations[124], thanks to its cost-effective, scalable, and customizable production technologies

(e.g., micromoulding[125], dip coating[126], spraying[127], 3D-printing[128]). Also, their easy-to-use formulation designs make them suitable for several clinical applications[129].

Of the large number of formulation strategies presented above, this literature review focuses only on pre-formed (shaped) polymeric implantable systems, as the development of such a product is the subject of the dissertation.

1.5 Polymer based long-acting implants

In these dosage forms, the extended release of the API is achieved by embedding the drug into a polymeric matrix, which then governs the release rate via different types of mechanisms.

1.5.1 Classification

Polymer-based systems fall into two main categories, namely passive and active systems. Passive systems consist of non-biodegradable and biodegradable implants, while osmotic pumps can be classified as active systems[117].

Non-biodegradable systems

Non-biodegradable systems are generally prepared using synthetic polymers, such as poly(siloxanes)[130,131], poly(urethanes)[132,133], and co-polymers, such as poly(ethylene-vinyl-acetate) (EVA)[134,135] and poly(vinylidene fluoride)[136]. These polymers are relatively inexpensive, possess beneficial mechanical properties, and the sustained drug release from them can be easily tailored by their composition and processing parameters[137,138]. In such systems, the drug release is mainly based on diffusion. In most dosage forms, they are applied as rate-controlling membranes, which enclose a solid inner core that contain the API. The thickness and permeability properties of the applied rate-controlling membrane polymer determine the rate of diffusion, and consequently drug release[139]. Due to their long-term biocompatibility and high degree of flexibility, they are mainly used for the preparation of contraceptives (e.g., Norplant®, Implanon®)[140], ophthalmic drug delivery systems (e.g., Ocusert®, Vitrasert®)[141] and various drug-eluting coatings/surfaces of stents for vascular disease treatments (e.g., Cypher®, Taxus®, Endeavor® and Xience V® stents)[142,143]. In addition to reservoir systems, they can be used in matrix constructs as well, where the active agent is homogeneously dispersed inside the polymeric carrier (e.g., Probuphine® implant)[144]. Drug-polymer interaction, drug concentration[145], and the porous structure of the system[146] can all have influence on their performances in the biological environment. Their main drawback is that at the end of the treatment they need to be removed from the patient, usually by minor surgical intervention.

Biodegradable systems

Biodegradable systems have attracted much more popularity over non-degradable systems. Their most significant benefit is that they degrade, absorb, and eventually excrete from the body after use[117]. Therefore, at the end of the delivery lifetime, there is no need for minor surgery to remove the product from patients, thus, increasing patient acceptance and compliance, and also reducing hospitalization costs. The biodegradation mechanism itself is a chemical decomposition of the applied material in-vivo, and usually proceeds via enzymatic degradations and/or hydrolysis[147]. A detailed understanding of the erosion and degradation kinetics of the applied polymers is of importance in terms of drug release kinetics. Erosion is generally the main driving force of drug release, besides diffusion, and can take place via the following different mechanism, namely, bulk erosion surface erosion and autocatalyzed bulk erosion[148]. The type of erosion and degradation mechanism determine the drug release kinetics of the device[149].

Commonly used materials to produce biodegradable drug products can be classified into two main groups depending on their source as either natural or synthetic biodegradable polymers. Natural polymers are derived from plants and animals[150]. Examples include proteins (e.g., collagen[151]), polysaccharides (e.g., chitosan[152]) and different types of cellulose derivatives[153]. They require cost-intensive purification steps before processing and show high lot-to-lot variability by nature. This feature makes their use in controlled systems significantly more difficult as the target drug release profile is more complicated to achieve consistently with varying physicochemical properties of raw materials[154]. On the other hand, synthetic biodegradable polymers are produced via controlled polymerization reactions with different types of monomers, usually derived from natural sources[150]. Although these chemical reactions make the production process more expensive, the constant quality of the final product ensures predictable and reproducible drug release profiles in controlled delivery systems. The most commonly applied synthetic polymers that have been used to produce such systems are synthetic aliphatic polyesters of poly-α-hydroxy acid family including poly(lactic acid), poly(glycolic acid), poly(lactic-co-glycolic acid), poly(aspartic acid) and poly(caprolactone) [155]. Poly(anhydrides)[156], poly(ortho esters)[157] and poly(urethanes)[158] are also frequently used in pharmaceutical products. The range of suitable polymers is still increasing. However, introducing a new synthetic bioerodible polymer in this field is challenging as the regulatory requirements are strict. In particular, the toxicological and immunogenetic evaluation of matrix

degradation by-products requires detailed investigation protocols, as these characteristics show high variability among each administration site[159,160].

The commercialised long-acting products based on these polymers are generally parenteral controlled drug delivery systems. Bioerodible pre-formed implants, usually in cylindrical- or wafer-shaped geometries can be used in the treatment of different cancer chemotherapies (e.g., Gliadel® wafer, Zoladex® implant)[161,162] and ocular diseases (e.g., Ozurdex® implant)[163].

Although long-acting injectables are not the subject of the present dissertation, to illustrate the benefits of biodegradable systems, it is worth mentioning in this section a few formulations that have been used in medicine for many years. These systems have also been proven the most successful formulation strategies in the long-acting platform of pharmaceutics. Microsphere formulations consist of multiple units that can range in size from 10 to 100 μm. The active agent is homogeneously dispersed in each matrix unit and may have an outer shell-like layer covering the drug reservoir core. The formulation is generally suspended in water-based vehicles, prior to dosing via a small gauge needle. A poly(lactic-co-glycolic acid)-based microparticulate formulations has become a substantial part in prophylactic treatment of prostate cancer over the past 30 years (e.g., Lupron® Depot portfolio)[164], and in the medications of mental illnesses (e.g., Risperidal® Consta®)[165] and narcotic use disorders (e.g., Vivitrol®)[166]. In-situ forming injectable depot systems are drug-containing viscous polymer solutions or suspensions generally prepared before use that form a semisolid depot when administered into the physiological environment. The solvent exchange at the injection site leads to the precipitation of hydrophobic polymers creating a finely porous spongelike microstructure through which the water uptake and drug release occur. The invention of Dunn and co-workers led to the licensed technology called Atrigel® System[167]. The N-methyl-2-pyrrolidone solution of poly(lactic-co-glycolic acid) associated with different types of drugs is injected intramuscularly, subcutaneously or into a periodontal pocket (e.g., Eligard® portfolio, Atridox®)[168].

Besides the inherent advantage of biodegradable systems, that there is no need of removal after the treatment, their biggest drawback is that there are several factors needed to be considered in their formulation and development, making the road to market slower and riskier. Furthermore, the use of these products usually does not have the potential to eliminate drug effect rapidly and effectively in the event of any undesirable or unexpected side effects, as their size and mechanical properties do not make surgical removal, if needed, easy due to their partial degradation in the biological environment.

Osmotic pumps

In addition to the dosage forms mentioned above, active osmotic pumps based on the osmotic principle should also be mentioned in this classification, as they can also be used as implants (e.g., Chronogesic™, Viadur®)[169]. These systems consist of two main parts: the osmotic material enclosed by a semipermeable membrane and the drug reservoir. The two parts are separated by a membrane which does not allow the diffusion of water. During the operation of the system, water is taken up from the biological environment (e.g., from subcutaneous tissues) by diffusion through the semipermeable membrane, the osmotic material dissolves, or swells and because of the resulting osmotic pressure the drug pumps out through the hole from the reservoir. Two main types, based on the design and place of the drug releasing orifice have been trademarked and marketed: Alzet® implantable osmotic pumps[170], and Duros® implantable osmotic systems[171].

1.5.2 Mass control mechanism

The mass transport strategies commonly used to achieve prolonged drug action in such systems are diverse, and usually, several factors and mechanisms operate simultaneously or in sequence, therefore their classification is complex. However, in most cases, one of the transport mechanisms can be considered as the rate-limiting step in the entire release process[172]. Thus, four general control mechanisms by which the liberation of the drug from the applied matrix can be distinguished[73,173]:

- diffusion control (e.g., non-biodegradable or biodegradable systems)
- chemical and enzymatic reaction control (e.g., biodegradable systems)
- osmotic pressure control (e.g., osmotic pumps),
- swelling control (e.g., hydrogels).

Diffusion mechanism

Diffusion is a process in which the mass transfer is regulated by a concentration gradient. In diffusion-controlled system the construct of the product and their microstructure plays a pivotal role in the drug releasing process. Long-acting implants are available as matrix (non-divided) and reservoir (divided) constructs (*Figure 5*).

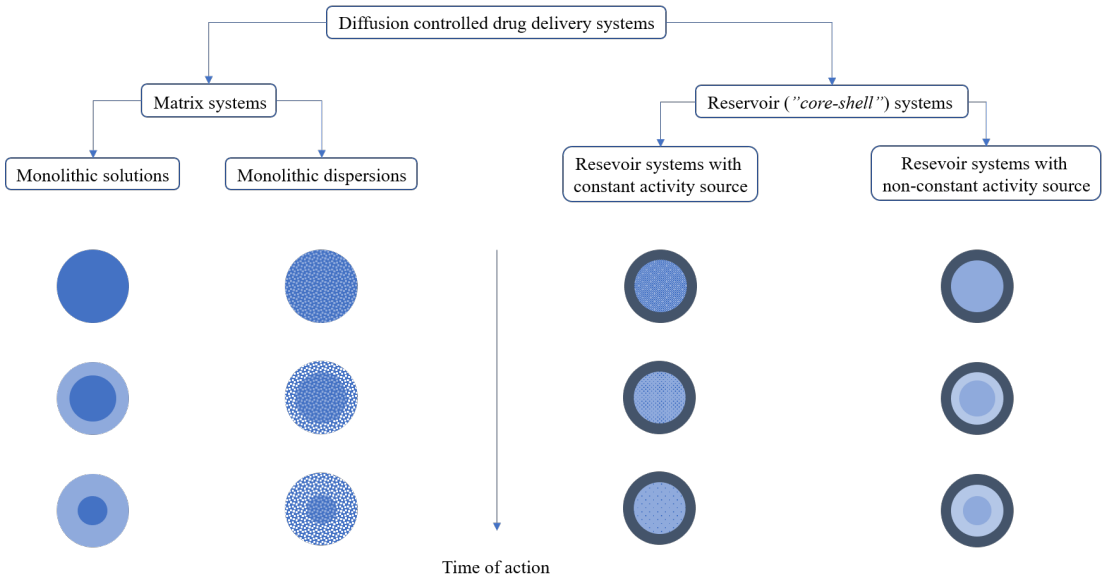


Figure 5 Matrix and reservoir systems

In the matrix form, drugs are dispersed homogeneously in their crystalline or amorphous forms, or dissolved (molecularly dispersed) inside a polymeric matrix unit[174]. The morphology of the product depends on the drug-polymer miscibility and drug content[134]. Monolithic solutions contain the drug compound in a concentration level (c_{ini}) that does not exceed the API's saturation concentration in the polymeric matrix (c_s), thereby resulting in a solid solution system ($c_{ini} < c_s$). On the other hand, monolithic dispersion systems enclose a drug amount that is much greater than its saturation concentration in the polymer ($c_{ini} > c_s$).

The APIs are released as the drugs dissolve in water or in body fluids and diffuse through the fluid filled porous network (monolithic dispersion systems), or only diffuse through the polymer matrix (monolithic solution systems) to obtain the sustained release of the drug. These systems may exhibit relatively high initial burst release associated with drug content on or near the surfaces exposed to the release medium. Ideally, only drug diffusion across the matrix is rate-limiting and remains constant, as long as the shape, structure, permeability and drug morphology (e.g., crystalline, amorphous, molecularly dispersed) does not change during release. In this case, a drug is released from the outer regions of the matrix first, these regions become depleted, and the drug content remaining inside the core diffuses through the depleted zones. This is known as a moving boundary and the net result is that the release rate is decreasing as a function of time[175]. Although zero-order kinetic is considered to be advantageous, in most cases, it can be approximated with prolonged timely changing kinetics as well.

One promising strategy for tailoring drug release from non-biodegradable monolithic dispersion systems is the incorporation of pore-forming agents. Several studies showed the drug-release promoting effect of different types of hydrophilic additives (e.g., D-mannitol, polyethylene-glycol, polysorbate, polyethylene-oxide and even bovine serum albumin) embedded in the systems, developed mainly for oral administrations[176,177,178], surface coatings[179,180] and even intravaginal delivery[181]. In these works the pore channels are formed during the application of the devices in the physiological environment. In contrast, the concept of drug-loaded porous foam extrusion in a therapeutic field was outlined in the work by Koutsamanis et al.[146]. In this study, chemical pore former additives were used to produce non-biodegradable porous thermoplastic polyurethane foams with sufficient flexibility to be used for removable implantable drug delivery system (IDDS). Different types of hydrogen carbonates were added to the mixtures to be formulated, and the pores were continuously formed during the hot-melt extrusion (HME) manufacturing process by the thermal decomposition of the additives. However, the main drawback of this concept is the application of a relatively high processing temperature required for thermal decomposition of the hydrogen carbonates (above 150 °C) and their residues remaining in the extrudates. HME assisted by supercritical gases, such as CO_2 or N_2 could be more preferable for this purpose[182]. However, no comprehensive study can be found in the literature to date that focuses on the production of non-biodegradable IDDSs using such technologies.

The aforementioned researches aimed to enhance the API release from the non-biodegradable monolithic dispersions. In contrast, only one study was found in the literature that aimed to tailor the API release by decreasing the release rate from non-biodegradable matrix IDDSs. Constantini et al. developed a nalmefene hydrochloride loaded EVA-based subcutaneous implants[183]. Their results showed that 100% of the initial drug content (35% w/w) was dissolved from the extrudates within 20 days *in vitro*, following a first-order release mechanism. The release rate could be decreased and eventually fine-tuned to obtain a perfectly zero-order release by coating the rods with an additional porous EVA layer. However, the main drawback of this approach is the cost-intensive coating process itself.

In the reservoir form, an inner core is coated with an inert (e.g., silicon rubber, ethylene-co-vinyl acetate and thermoplastic polyurethane) rate-controlling membrane whose thickness and permeability properties can control the diffusion of the drug into the body (*Figure 5*). Depending on the drug concentration/saturation in the inner core ($c_{ini} < c_s$ or $c_{ini} > c_s$), drug release can be programmed into the design following both zero- or first-order drug release

kinetics. However, in most cases, reservoir constructs are used to provide systems with truly zero-order release kinetics[175]. Like monolithic systems, these products can also show some degree of burst effect, which can be related to the amount of material diffused into the rate-controlling outer layer during storage.

In each system, several factors significantly contribute to the apparent diffusion, thus to the drug release. The release kinetics of the reservoir systems with constant activity source mainly controlled by Fickian diffusion, which is affected by surface area/volume ratio, diffusion distance and polymer-drug permeability. The permeability of the APIs through the polymer network is highly dependent on their solubility in the matrix, which is greatly influenced by the composition, glass transition temperature, and crystallinity of the polymer. In other systems with non-constant activity sources, additional factors must be considered. In these systems, the release kinetics depend to a large extent on the volume fraction of the drug and its effect on the porous microstructure continiously forming during the release process. Thus, in general, the release is directly proportional to the amount of drug embedded in the matrix[117].

Several mathematical models have been developed and introduced into practice to describe diffusion mechanism and predict the drug release from certain products. Each of them derived from Fick's laws of diffusion (*Eq. 1.4.1* and *Eq. 1.4.2*).

Fick's first law of diffusion:

$$J = -D\frac{\partial c}{\partial x} \qquad \text{(Eq. 1.4.1)}$$

and Fick's second law of diffusion:

$$\frac{\partial c}{\partial t} = D^2\frac{\partial^2 c}{\partial x^2} \qquad \text{(Eq. 1.4.2)}$$

J: flux, the rate of transfer per unit area of section
D: diffusivity, diffusion coefficient
C: drug concentration
x: length in direction of diffusion
t: time

The developed describing/predicting models can be derived from theoretical analyses, namely solving Fick's basic differential equations for specific geometries to a given set of appropriate initial and boundary conditions[175]. For example, from monolithic solution systems with cylindrical geometry the drug release under perfect sink conditions can be described by the following function[175].

$$\frac{M_t}{M_\infty} = 1 - \frac{32}{\pi^2}\sum_{n=1}^{\infty}\frac{1}{q_n^2}exp\left(-\frac{q_n^2}{R^2}Dt\right) * \sum_{p=0}^{\infty}\frac{1}{(2p+1)^2} * exp\left(\frac{(2p+1)^2\pi^2}{H^2}Dt\right) \quad \text{(Eq. 1.4.3)}$$

M_t: cumulative drug release at time t
M_∞: cumulative drug release at infinite time
D: diffusion coefficient
q_n: Bessel function (cylindrical coordinates)
n and p: summation indices
R: radius of the cylinder
H: length of the cylinder
t: time

In a similar way, the following equation can be derived for cylindrical reservoir systems with constant activity source[175]:

$$M_t = \frac{2\pi HDKc_s}{ln\left(\frac{R_0}{R_i}\right)} * t \quad \text{(Eq. 1.4.4)}$$

M_t: cumulative drug release at time t
D: diffusion coefficient
R_i: radius of the inner core
R_0: radius of the cylinder
c_s: solubility of the drug in the inner core
K: partition coefficient of the drug between the membrane and core
H: length of the cylinder
t: time

Other semi-empirical approaches were also developed, that have been proved more reliable on the occurring processes and based on some basic theories and assumptions[174]. In 1961, Takeru Higuchi proposed a simple equation to quantify the drug release over time from monolithic dispersion systems ($c_{ini} > c_s$) with slab geometries (ointment films)[184]. His theory was based on a simple representation of the drug concentration-time profile within the matrix. The connection between the theory and Fick's laws led to his famous equation (*Eq. 1.4.5*). He further interpreted his equation in 1963, in which the porous structure of the product already appears (*Eq. 1.4.6*)[185]. *Eq. 1.4.5* and *Eq. 1.4.6* can be written in a more general form (*Eq. 1.4.7*), which is known as the *"square root of time"* release kinetic.

$$M_t = A\sqrt{Dc_s(2c_{ini} - c_s) * t} \quad \text{(Eq. 1.4.5)}$$

$$M_t = A\sqrt{Dc_s\frac{\varepsilon}{\tau}(2c_{ini} - \varepsilon c_s) * t} \quad \text{(Eq. 1.4.6)}$$

$$M_t = K\sqrt{t} \quad \text{(Eq. 1.4.7)}$$

M_t: cumulative drug release at time t
A: surface area exposed to the release medium
D: diffusion coefficient
c_s: solubility of the drug in the matrix
c_{ini}: drug concentration in the matrix
ε: porosity of the matrix
τ: capillary tortuosity
t: time
K: Higuchi constant

The Higuchi equation relies on several assumptions, the most important of these is that the matrix geometry should not change during the application, and the diffusivity must remain constant over time[184]. However, in practice, these prerequisites are normally not met. Peppas and his co-workers developed a more comprehensive model that yielded important information on drug delivery mechanisms[186,187]. The *"power law model"* (Korsmeyer-Peppas model) is useful to investigate drug release from polymeric drug delivery systems when the release mechanism is unknown or when more than one type of controlling mechanism is involved. This semi empirical model establishes the exponential drug release–time relationship. According to the model the entire drug delivery process is divided into two sub-processes: diffusion-controlled and relaxation-controlled drug release mechanism (e.g., swelling of the matrix) (*Eq. 1.4.8*). The two constants (k_1 and k_2), representing the contribution of the two processes to the overall release mechanism can be generalized into one *k* constant. In *Eq 1.4.9* the *k* constant (velocity constant) describes the characteristic of the polymeric matrix, and the *n* exponent is related to the controlling drug release mechanism (*Table 1*).

$$\frac{M_t}{M_\infty} = k_1\sqrt{t} + k_2 t \qquad \text{(Eq. 1.4.8)}$$

$$\frac{M_t}{M_\infty} = kt^n \qquad \text{(Eq. 1.4.9)}$$

Table 1 Interpretation of n exponent and drug release mechnaism of active agent from controlled deivery systems with different geometries

Planar (thin films)	Spheres	Cylinders	Release mechanism model
n exponent			
0.5	0.43	0.45	Fickian diffusion (Case I)
0.5 < n < 1.0	0.43 < n < 0.85	0.45 < n < 0.89	Anomalous transport
1.0	0.85	0.89	Relaxation transport (Case II)

Drug release mechanism from biodegradable system

In the case of biodegradable system, the drug release mechanism is more complex compared to the release mechanism from non-biodegradable devices, making the formulation development more complicated. Degradation and diffusion mechanisms operate simultaneously. Generally, the release mechanism from such systems has three main stages of release. First, in the so-called burst release phase the drug releases from the surface of the device and from the pores which are connected to the surface. In the latent second stage (lag-phase), drug release mainly corresponds to diffusion through the matrix and the low rate of degradation of the polymer. In the last third step, the complete disintegration of the device facilitates the immediate release of the remaining entrapped drug[188].

Erosion and biodegradation processes occur mainly via hydrolytic breakdown and/or enzyme-catalyzed cleavage at the administration site[189,190]. The role of molecular weight, molecular weight distribution[191,192], polymer crystallinity and glass transition temperature, copolymer composition[193], shape, size and other physicochemical factors[194] (e.g., ionic strength, pH) on degradation mechanisms are well investigated. The effect of such factors is based on modifying water uptake of the polymeric systems, which is an essential step for the hydrolytic cleavage between the monomer units leading to matrix erosion. The issue of water uptake can be further complicated by the addition of any additives, including the active agent, that might alter the osmotic pressure and thus the water uptake into the system during relase, which might alter the degradation performance of the polymer. It can be considered as a limitation of drug loading, especially when the goal is formulating hydrophilic active substances[195]. On the other hand, incorporated hydrophobic drugs can change the erosion mechanism to surface from bulk erosion, as the water uptake of the system is reduced because of the poor dissolution of the drug[196].

Certain drug-polymer incompatibility issues can also be traced back to uncontrolled degradation processes in the system. Encapsulation of a large amount of basic substance can change the pH in the microenvironment of the administered product. Under these extreme pH conditions, the matrix tends to degrade at a higher rate[197].

The apparent microstructure of the device, determined by both the manufacturing processes and the physiological environment at the implantation site, can also affect the erosion process. For example, in porous systems the interconnected channels are not only responsible for shepherding the dissolved drug out to the physiological environment, but also to let the implant get rid of self-degradation products. The accumulated hydrolytic by-products in the bulk of the

device can autocatalyze other degradation processes resulting in the higher rate of non-consistent bulk erosion[198].

1.5.3 Manufacturing technologies

A number of manufacturing strategies are available to produce long-acting implants. However, several aspects need to be considered before developing or selecting the right manufacturing strategy. Firstly, the development and operating costs of the applied technology should be in line with the therapeutic benefits underlying the product's marketing strategy, thereby generating a profit for the maufacturer[116]. In general, the primary consideration is mass production, thus the process must be robust and scalable, continuously ensuring the consistent quality of the product and the predefined target profile of the product. Also, these large-scale technologies should have a low environmental footprint. In addition to these aspects, it is also advisable to keep in mind the latest "trends". Of these, personalized medicine and the advancement of continuous technologies in the pharmaceutical industry has played a prominent role in the recent period.

Based on the literature review the following manufacturing strategies are used both in academia and in industry.

Solvent casting

In solvent casting methods, the polymer is dissolved in a suitable solvent, and the active agent is added to the resulting polymer solution. The mixture is then cast into a mould, where the slow evaporation of the solvent occurs. In this way mainly films and laminar implants can be produced[199,200]. Langer and Folkman embedded a biologically active macromolecule (soybean trypsin inhibitor) in different polymers in this way. The sustained release of the macromolecule was achieved by the slow diffusion through the tortuous network of interconnected pores[201]. Their work can be considered a significant milestone, as it was previously largely thought that the extended release of large macromolecules could not be achieved by entrapping them in a polymer matrix.

The main disadvantage of this method is the use of vast amounts of organic solvents, which can present in trace amounts in the product, causing toxic side effects in the body. Also, upon gradual solvent removal, the dispersed active agent can form precipitated drug aggregates, significantly decreasing the homogeneity of the drug product[202].

Solvent extrusion

The solvent extrusion method is similar to the solvent casting method, except that in this case the polymer is not fully dissolved in the solvent. The matrix former is only plasticized by the solvent to an extent that the rheological properties make the drug-polymer mixture suitable to force it through a syringe, resulting in rod-like shaped implants. The slow evaporation of the solvent may result in a solid fine porous structure[203]. This technique can also be implemented at elevated temperatures, thereby accelerating solvent removal. In this case, the system tends to have higher porosity accelerating the rate of drug release[204]. This process, similarly to solvent casting, is cost-intensive and time consuming due to the need for solvent removal.

Compression

The most significant advantage of compression is that its use does not require heat and solvents, making the formulation of heat-sensitive or solvent-sensitive materials, such as proteins and peptides, possible[205]. These systems tend to have a higher rate of drug release compared to products produced by other production techniques, most likely because of the high porosity of the products[206]. Because of that, they may require additional formulation steps, such as coating or sintering, to ensure prolonged release[206]. Kau et al. treated compressed poly(lactic-co-glycolic acid)-based tablets at elevated temperature, above the glass transition temperature of the polymer, that was low enough to avoid destroying the embedded antibiotics. After this sintering step, the resulting product could achieve constant release of doxycycline for up to 28 days *in-vitro*[207].

In some cases, compression only provides shaping, and the fusion between the polymer and the active agent takes place in a preliminary technology step. Carmustine-loaded Gliadel® wafers are produced by spray drying of a drug- poly(lactic-co-glycolic acid) solutions, forming 5-10 μm particles that are subsequently compressed into wafers, with a high moisture-sensitive porous structure[208]. Maturavongsadit et al. demonstrated that using direct compression combined with a preliminary solvent-based phase inversion step, high drug-loaded (up to 85% w/w) biodegradable subcutaneous tablets can be produced, which can ensure up to 6 months constant dolutegravir release *in-vitro*[209].

Injection moulding

Conventional injection moulding technology consists of the injection of low viscosity thermoplastic polymer melts at high speed through a narrow orifice into a mold cavity, where it cools under high pressure, then it is ejected after cooling to take the final shape[210]. The technology has the advantages of being solvent-free, can be easily scaled-up and automated,

enabling economic and continuous production of a variety of products in large series.[210] A range of different polymers are good candidates and widely used to produce various types of long-acting implantable drug delivery systems (e.g., drug eluting subdermal implants, vaginal rings and intrauterine devices). Among others, poly(ethylene-co-vinyl-acetate), thermoplastic poly(urethanes)[211], poly(ε-caprolactone)[212], poly(lactic-acid)[213] and poly(lactic-co-glycolic acid)[214] are extensively studied and applied as carriers for this versatile technology.

However, in addition to its significant advantages, injection moulding usually requires a prior technological step, as a single screw extruder operating inside the equipment cannot provide efficient mixing between the matrix polymer, additives, and the API to be formulated. Usually, it is combined with hot-melt extrusion to increase the homogeneity in the final product. This may increase the time and cost of the industrial manufacturing line. Moreover, in some cases, the heat and shear effects underlying the technology can cause degradation of the formulated drug and have a significant contribution to the morphology of the matrix-forming polymer, significantly affecting the pharmacokinetic behaviour of the product[212].

Reactive injection moulding forms a separate group in injection moulding technologies. This technique is widely used for the processing of thermosetting materials, such as silicone elastomers, and is mainly related to the production of intravaginal rings in the field of long-acting medical products[215]. Commercial examples include Estring®, Femring®, Progering® and Annovera® among others. These materials are processed by chemical crosslinking of functionalized, linear, poly(dimethylsiloxane) molecules to produce implants with the desired pharmacokinetic profile[216].

3D-printing

In the field of drug formulation, 3D printing is a very promising and versatile formulation strategy. 3D printing, also defined as additive manufacturing, is a process of gradually construct three-dimensional objects, usually in a layer upon layer manner, according to a pre-designed digital model constructed by computer software. As a specific part of pharmaceutical therapies is undergoing a paradigm shift from bulk to patient-customized medications, 3D-printed drug delivery systems may offer a promising step forward for the provision of personalized care. This is because the performance of the product can be fine-tuned to meet the needs of a given patient or group of patients to achieve the most effective therapeutic effect possible[217]. Additionally, 3D-printing has the potential to manufacture different prototypes at the very beginning of the development process for initial investigations (e.g., geometry, drug content), according to which decisions can be made about the design of the scaled-up production line for

bulk manufacturing. Although the literature in this field is massive and several recently published reviews summarize the benefits, the pharmaceutical industry seems still sceptic and laggard about adopting this economical and extremely adaptable technique into clinical practice. Most likely due to the uncertain regulatory issues. However, the first FDA approved 3D-printed medication (Spritam®) indicated a great step forward in this field[218].

1.5.4 Hot-melt extrusion (HME)

In the last few decades, the formulation of APIs by HME is getting more and more important as the extruded formulations of different types of pharmaceutics are suited for several clinical applications. Nonetheless, besides the clinical benefits that can be achieved by this solvent-free processing method, it possesses all the benefits of continuous technologies as well. Owing to its increasing and unquestionable importance in the pharmaceutical field a number of well-established reviews summarised its impact in the last two decades[219,220,221,222].

Basics of HME

HME has a great history in the polymer industry, and besides injection moulding, it is the most commonly used method for processing thermoplastic polymers. By construction, extruders can be divided into three main categories: the common screw extruders (single- or twin-screw), the older ram (piston) and radial screen extruders. Among these, the latter two designs have little practical significance in the pharmaceutical field. The performance of screw extruders is most simply characterised by the diameter of the screw: larger diameter can mean exponential productivity[223]. The predecessor of single-screw extruders was patented as early as the 19th century but became widespread in the plastic industry only in the 1930s. Twin-screw versions broke into the industry only a decade later due to the more complicated mechanical construction and became preferable for pharmaceutical applications.

Pharmaceutical HME is the process of using heat and pressure to generate a new form of the applied raw materials that possess advantageous physical and/or physicochemical properties for further medical applications. The main criterion of HME regarding the applied materials is that at least one component must be melted in the extrusion process. The process itself consists of several steps. First, the drug-polymer mixture is fed through a hopper into a temperature-controlled barrel at an adjustable rate utilizing a dosing unit (volumetric or gravimetric). Inside the barrel, the mixture is conveyed through several heated zones by means of continuously rotating single screw or twin screws. The divided zones allow setting of a temperature program for optimal processability. The first zone (feeding zone) of the extruder is usually water-cooled

to avoid any static build-up at the feeding hole caused by untimely heat transition of the fed materials. In the following compression zones, the mixture is simultaneously heated above the glass transition and melting temperature of the polymer and compressed into a homogeneous melt. The drug-polymer melt is eventually conveyed through a pumping zone providing homogeneous pressure, flow, and temperature to eventually force the system through a die, which determines the shape (e.g., films, fibres, tubes) and size of the extrudate. With an appropriate die design, two extruders can be coupled to produce coaxial fibers or multi-layered extrudates. In these processes, the molten polymers conveyed by two different – mainly single screw – extruders are transferred into two different spinning pumps that are combined into a spinning block. The pumps ensure accurate flow of the molten polymers to the spinneret where coaxial fibers form.

Co-rotating or counter-rotating twin-screws provide uniform residence time, shorter exposure to high temperature, and higher mixing capability. Both screw constructs usually have flighted (conveying), kneading, mixing, and for some specific applications, backward-pumping elements assembled on the extruder shafts and can be characterised by their geometry (pitch, width, and offset angle). Depending on the geometry and the upbuilt configuration of the screw elements on the shaft, the balance between dispersive (elongational) and distributive (recombination) mixing can be controlled. In conclusion, the applied screw design determines the mixing, pressure, and flow profile of the process, which has a pivotal role on the produced extrudates in terms of homogeneity and morphology[224].

During HME, three main controllable processing parameters can be defined. These are the feeding rate, screw speed and process temperature or barrel temperature profile in the case of extruders equipped with several heated zones. Detailed understanding of the effects of these critical process parameters (CPP) on the critical quality attributes (CQA) of the final product is essential in the development step of a new drug product.

One of the most significant CQA of an extruded product is the morphology of the API in the system, which has a huge impact on the pharmacokinetic performance of the product. By the end of the HME process the API may be in three main physical forms in the extruded system. First, when the fed crystalline drug does not go through any morphological changes, the API remains in crystalline form thoroughly dispersed in the matrix. Owing to the number of influences (e.g., heat, pressure, shear) during the process, the API may achieve higher energy levels and/or a certain amount of it can be dissolved in the molten polymeric carrier. If the cooled system can stabilize such states, the final product may contain dispersed amorphous

regions or a truly molecularly dispersed form (solid solution) of the drug. The combination of such forms is also possible.

Pharmaceutical applications of HME

The first publication about the use of HME for producing drug delivery systems can be attributed to Follonier et al. in 1994[225]. In their work, sustained release of freely water-soluble salt forms of several model drugs was achieved by HME using different matrix forming polymers and plasticizers. Aitken-Nichol et al. developed a film formulation by HME for transdermal delivery in 1996[226]. In the late 1990s, further studies were published about the development of sustained release formulations for orally administered dosage forms[227,228].

HME has been successfully implemented in the manufacturing process of several dosage forms (e.g., tablets, pellets, granules, films, foams and implants). One of the most frequently exploited applications of HME is the bioavailability enhancement of poorly water-soluble APIs by producing solid dispersion systems[229]. In these systems, water soluble thermoplastic polymers, such as poly(ethylene glycol), poly(vinyl pyrrolidone) and different types of methacrylate co-polymers (Eudragits) are chosen as a matrix former to solubilise the drugs during the HME process, and in some cases, to solubilise them in the release media as well during release. The extrudates can be further processed (e.g., pelletizing, milling) and compressed into tablets or filled into capsules. The greatest milestones of this specific application can be attributed to the commercialisation of the reformulated dosage forms of Rezulin® (troglitazone) and Kaletra® (liponavir/ritonavir) oral tablets[230]. In addition, several other active substances with poor solubility have been further formulated by HME and successfully marketed. Examples include Onmel™ (itraconalzole), Noxafil® (pozakonazol), Belsomra® (suvorexant), Zithromax® (azithromycin) and Eucreas® (metformin/vidagliptin), among others[231].

While the majority of research articles and industrial applications of HME are focusing on oral delivery, commercially available melt-extruded medical implants have proven their potential in several long-term pharmaceutical therapies. In that regard, the use of HME can be traced back to the commercialisation of Lacrisert® in 1981, a hydroxypropyl cellulose (HPC) ocular insert for treating dry-eye syndrome[232]. Although, this rod-shaped implant produced by HME cannot be classified as classic drug delivery systems. The slow dissolution of the HPC matrix in the conjunctival sac stabilises the tear film and provides continuous lubrication to the eye. Zoladex® bioerodible implants based on PLGA has been a significant part of prostate cancer treatment since its approval in 1996[162]. Ozurdex®, a dexamethasone loaded PLGA ophthalmic implant has been on the market since 2009 for treating macular edema[163].

The use of EVA to produce melt-extruded medical implants have been discussed in several research publications and numerous approved products can be found on the market[233]. This polymer family possesses great mechanical and rheological properties making it suitable for HME. EVA polymers also have advantageous physicochemical features (e.g., permeability) and high biocompatibility providing great potential in long-term therapies. The first commercialized product based on EVA was a pilocarpine loaded reservoir device (Ocusert®), that was FDA approved in 1974. This ocular insert for treating glaucoma was produced by Alza Corporation. However, the main application of EVA is contraception. NuvaRing® (Organon Inc.), a contraceptive vaginal ring containing two active components (ethinyl estradiol and etonogestrel) was approved by FDA in 2001. This reservoir (core-shell) type implant is produced by coextrusion, where the inner core contains the solubilized and oversaturated (or supersaturated) form of the two drug substances and the outer layer (membrane) controls the drug release. The driving force of drug release is the constant concentration gradient between the inner core and the biological environment, ensured by the oversaturated state of the active compounds in the core. The product ensures constant treatment for 21 days. Van Laarhoven and his co-workers found that the two applied hormones form an eutectic mixture in EVA[234]. The physical interaction between the two steroid hormones resulted in a great decrease in etonogestrel (0.69% w/w) release (approx. 13%) by increasing the ethynyl estradiol concentration from 0 to 1% w/w. Their further study investigated the effect of drug loading and their physical state in the core, process temperature and storage conditions on drug release[134]. Organon introduced another implantable medical device (Implanon®) in 2006. This etonogestrel loaded single-rod contraceptive implant, inserted subcutaneously in the upper arm, can prevent ovulation for a 3-year period. Implanon® has recently been reformulated with barium sulphate, an X-ray-active additive and renamed to Nexplanon®. The other melt extruded application of EVA as matrix drug delivery system can be attributed to the ProNeura® extended-release platform developed by Titan Pharmaceuticals in the US. During manufacturing, the drug and EVA are dry-blended and extruded (T_{proc}≈ 110 °C) to form rod-shaped like implants. A special feature of the implants within this platform is that in the monolithic dispersions produced by HME, the active ingredient and the EVA carrier form two separate phases[235]. In this case, drug delivery is not based on the classical Fickian diffusion of the drug through the matrix polymer. The sustained release is achieved by the dissolution of the active substance particles, that leave pores behind for further access of biological fluid. The slow diffusion of the dissolved API through the continuously evolving tortuous network of interconnected pores is responsible for the sustained release for extended periods of six months or longer. Numerous

patents by Patel and his co-workers describe different HME formulation strategies based on EVA for several other drug substances (e.g., triiodothyronine, buprenorphine, nalmefene, apomorphine, loratadine)[236,237,238,239]. However, the company's portfolio based on the ProNeura® technology consisted of three products for the treatment of Parkinson's disease, hypothyroidism, and opioid dependence. Among these, only the Probuphine® (buprenorphine loaded subcutaneous implant) reached the market in 2016. The two patents of Patel and Bucalo provide an insight into the development process of Probuphine® implant. They reported that drug loading could be achieved in the range of 15 to 85% w/w[236]. Additionally, the initial burst release due to the drug content on or near to the implant surface was decreased by using a washing step in ethanol[239]. The ratio of the peak to the steady-state plasma level could be decreased from approximately 4.5 to 2 ng/mL. However, based on the recently pressed new marketing strategy of Titan Pharmaceuticals, the development and distribution of each implant is discontinued, and the company has started focusing on two new products which are in preclinical phase.

Beside PLGA and EVA, several other types of polymers are commonly used in HME formulation to produce long-acting implantable devices. In a study conducted by Chen et al sustained release of 5-fluorouracil was achieved by a PCL based needle-shaped implant for stereotactic injection directly into tumours minimizing the systematic exposure of the drug[240]. In this solid dispersion system, the major portion of the active substance remained in its crystalline state, and the drug release mainly based on the pore formation inside the implant during application. Clark et al. developed a TPU-based hot-melt extruded intravaginal ring that could achieve a sustained release of an antiretroviral microbicide agent (UC781) for treating HIV[241]. Their work proved that even a relatively high drug loading (10% w/w) could be solubilized in the matrix polymer, forming a monolithic solution system. However, the dissolved drug content tended to recrystallize on the implant surface during storage under room temperature. The authors found that a simple PVP/glycerol (10/3% w/w) surface coating sufficiently prevented the recrystallization phenomena even under elevated storage conditions (50 °C) for 16 months.

Advantages of HME

According to the literature review, the significant advantages of HME can be summarized as follows:

- HME is a continuous manufacturing process and for this reason the batch sizes are flexible to market needs and can cover R&D as well as production needs. Therefore, in some cases, no scaling-up is needed. Additionally, the process parameters can be easily controlled to ensure consistent product quality based on real-time data (e.g., drug content and morphology, geometry) acquired by several process analytical tools (e.g., NIR and Raman probes)[242,243], minimizing waste and raw material consumption. Also, it can operate at low cost without taking up much space[244].
- HME is an organic solvent free technology, involving the fact that no solvent wasting, and regeneration are needed. More importantly, the manufactured products do not require time- and energy-consuming drying technological steps prior to further applications[219].
- A single unit hot-melt extruder combines several processing steps shortening the manufacturing time and cost[220].
- HME can be easily scalable, if needed[220].

Limitations of HME and possible solution strategies

Despite the large number of advantages, there are also obstacles to the application of HME. During the extrusion process the formulated active substances and the matrix polymer are exposed to different influences such as:

- pressure, caused by the extruding melt,
- shear stress, caused by the rotating screws,
- heat stress,
- and chemical stress, due to any possible interaction between the drug and the matrix polymer or other additives.

Owing to these influences, chemical degradations of the API and the polymeric carrier may occur during processing, which can significantly limit the formulation opportunities and conditions, as the concentration of different contaminants (degradation products) must meet strict regulatory requirements[245]. Based on examples available in the literature, the mechanism of API degradation during extrusion can be diverse, typically hydrolysis (e.g., due to the water content of the formulated raw materials), solvolysis, and oxidation[246,247]. Furthermore, the decomposition of the matrix polymer can influence not only the pharmacokinetic performance of the extruded product, but the polymer side-products can induce or accelerate the degradation

of the API as well[248,249]. Therefore, in a HME product development, it is essential to apply an appropriate strategy to control the amount of different types of by-products.

In regard to homogeneity, extruding above the melting point of the active ingredient is extremely advantageous since it can then be dispersed or dissolved in the matrix with high efficiency with a short residence time. If the probability of decomposition is sufficiently small in the molten state, the degree of degradation may remain below the permissible level[250]. However, several APIs show significant degradation after HME formulation above their melting temperature[251,252]. In these cases, the process temperature should be 20-30 °C above the glass transition temperature of the matrix polymer and must remain below the melting temperature of the API. Even full amorphization or drug dissolution in a matrix carrier can be achieved by HME under the melting point of the API[253]. However, several publications also report the degradation of crystalline drugs during HME formulation under their melting points[254,255]. According to these results, it can be assumed that the rate of drug degradation is likely in connection with the in-situ forming amorphous or molecularly dispersed drug content. Namely, the molecularly dispersed or amorphous phases tend to have lower stability than the more energetically stable crystalline form. Consequently, when the goal of the formulation is to achieve a fully amorphous or molecularly dispersed (dissolved) form of the API in a polymeric matrix, it is hard to avoid degradation. As the degradation rate constant increases with temperature according to the Arrhenius equation, the easiest way to reduce degradation is to adjust the lowest process temperature and residence time. In this way, not only the thermal decompositions but also the possible reactions with the drug and polymeric component can be moderated. However, controlling of these parameters is very complex[256].

Lowering of the process temperature is limited by the increase in polymer viscosity. The rates of this effect vary on case-by-case basis depending on the rate of interaction between the API, the matrix polymer, and other additives (e.g., plasticisers). Plasticisation of the system is essential to reduce the glass transition temperature of the polymer, hence, to decrease the process temperature, the pressure and shear stresses. Plasticisation using small molecular additives or low-molecular-weight polymers is a way to decrease viscosity and the minimum processing temperature. Unfortunately, plasticiser content may also change the functional performance and long-term chemical, or physical stability (e.g., recrystallization of molecularly dispersed form) of the API in the products[257]. In some special cases, even the dissolved drug compound can show a certain extent of plasticization on the system[258].

Another way to moderate heat stresses is to reduce the residence time of the melted system in the extruder. It can be achieved by two main methods. Firstly, the API can be fed into the extruder as close as it is possible to the end of the barrel, near the die. Secondly, the screw speed can be increased to a level where dispersion is still achievable[246,247].

The literature also mentions several other possibilities for suppressing degradation processes of certain APIs caused by heat stresses. In these publications, the formulations are accomplished with the stabilized form of the API. Preparing molecular inclusion complexes with cyclodextrins may protect the drug from heat stress and oxidative influences[259]. In some cases, drug-polymer interaction may reduce the degradation in the system[260]. Antioxidants can also be used to avoid oxidative decompositions[261]. The degradation of both the API and polymeric matrix can be significantly reduced by the application of Vitamin-E, as an antioxidant agent[262,263]. In-situ salt formation between basic and acid functional groups of the active substance and a salt-forming additive is recently reported as an effective way to decrease the rate of drug decomposition processes[264].

1.6 Long-acting formulations of NTX

In general, long-acting formulations of NTX consist of intramuscularly administered suspensions and subcutaneously implanted pellets or tablets. These parenteral delivery routes have the advantage for systematic delivery, while avoiding first pass metabolism. However, other approaches using long-acting prodrug formulations of NTX for oral and transdermal delivery can also be found in the literature[265,266]. There have been several attempts reported to produce long-acting parenteral formulations of NTX dating back to the late 1970s. Sullivan and Kalkwarf produced a solid dispersion of NTX in natural glyceride. The subcutaneously implanted formulation proved its long-acting effect in mice[267]. Misra and Pontani developed a subcutaneously implantable pellet formulation of NTX containing cholesterol and glyceryltristearate with 3 months constant drug delivery reported in rats[268]. The use of insoluble pamoate acid salt and metal complexes (e.g., zinc and aluminium) of NTX were also attempted and tested in mice by Gray and Robinson[269].

Along with the propagation of biodegradable polymers, the first attempts for a bioerodible formulation of NTX appeared as early as the 1970s[270,271]. The first human study can be attributed to Chiang and co-workers who embedded NTX base (dose of 63 mg) into poly(lactic-co-glycolic acid) (PLGA) beads (1.5 mm in diameter) and implanted them into three healthy individuals. Their results showed that the plasma concentrations of NTX were maintained at a

constant level (range 0.3 to 0.4 ng/mL) for a month, however, this was below the 1-2 ng/mL required for clinical efficacy. Moreover, 2 of the 3 patients showed severe inflammation at the implantation site[272]. Later, several other biodegradable formulations were developed and successfully commercialised. For example, Depotrex®, manufactured by Biotek Inc., is a PLGA microsphere formulation of NTX base intended to be injected subcutaneously. In a study, Comer and colleagues[273] assessed the efficacy of the formulation on 12 heroin dependent individuals. Two arms were designed, with 6 participants receiving 192 mg, and the other 6 participants receiving 384 mg of NTX. The administered NTX doses sufficiently blocked the effect of IV administered heroin HCl (0-25 mg) depending on the applied dose for 3 to 5 weeks. The long-acting formulation effectively maintained the NTX drug plasma of levels above 1 ng/mL for approximately 3 to 4 weeks after the administration of 192 and 384 mg doses. No local tissue reaction was observed at the implantation sites and no other severe side effects were reported.

Vivitrol®, previously known as Vivitrex®, by Alkermes Inc., is also an injectable microsphere formulation, but with the difference that it is not administered subcutaneously but intramuscularly. NTX is incorporated in 75:25 PLGA at a concentration of 337 mg of NTX base per one gram of microspheres. The formulation provides continuous NTX administration for 4 weeks in the treatment of opioid and alcohol dependence[274]. Dunbar et. al investigated the pharmacokinetics and tolerability of single and multiple doses of Vivitrol® with different study groups[275]. Their results found that the ratio of the primary active metabolite and the parent substance appeared to be lower with the long-acting subcutaneous systems (6βNTX/NTX AUC_{∞} = 2.44 and 2.28, with the dose of 190 mg and 380 mg respectively) than that seen with the oral administration (6βNTX/NTX AUC_{∞}= 28.1, with the dose of 50 mg). The administration of a single dose long-acting NTX microsphere formulation with a dose of either 190 or 380 mg NTX base ensured effective plasma levels (>1 ng/mL) for 24 and 35 days, respectively. The maximum plasma level concentrations (C_{max}) showed relatively similar values with both administration modalities (10.2 and 12.9 ng/mL for microsphere formulation vs. 10.6 ng/mL for the oral tablet). No adverse effects were reported during the study, with the formulations well-tolerated.

Injectable in-situ forming implant formulations of NTX have not been commercialized yet. However, Kamali et al. presented a PLGA/N-methyl-2-pyrrolidone/ethyl-heptanoate based formulation design, and compared its *in-vivo* performance with Vivitrol® on rabbits[276]. Their

study showed that the in-situ forming depot formulation and Vivitrol® had similar pharmacokinetic profiles in rabbits.

NTX implants are usually inserted into the subcutaneous tissue area of the lower abdominal wall under local anaesthesia. Based on the literature review, only 4 NTX-loaded sustained release implants are available, with most of them not approved in certain countries for regular use.

The first NTX implant was reported by Gooberman et al. in their patent from 1997[277]. This implant is known as Wedgewood® implant, produced by Wedgewood Pharmacy in the US. In this formulation, 1000 mg of NTX HCl was compressed with a pharmaceutically acceptable carrier (magnesium stearate) to form a subcutaneously implantable tablet, which had a thickness of 8 mm and a diameter of approximately 13 mm. These implants completely dissolve in approximately 5 to 7 weeks and disappear from the implantation site. According to a pharmacokinetic investigation conducted by Olsen et al. the Wedgewood® implant ensured effective drug plasma concentrations (> 1 ng/mL) for more than 40 days with a median C_{max} of 12.3 ng/mL[278]. However, two patients out of ten reported severe local tissue reaction.

The Prodetoxone® implant, is also an implantable tablet, produced in a similar way as the Wedgewood® implant. Although, this formulation contains 10 mg of triamcinolone, a corticosteroid to reduce severe tissue reaction, most likely due the magnesium stearate content. This implant is manufactured by Fidelity Capital in Russia, and approved for regular clinical use in Russia only. One study investigated the pharmacokinetic performance of this formulation[279]. They reported the prolonged presence of NTX in the blood samples collected from 60 patients for up to 60 days. The study showed relatively high drug plasma levels (20-40 ng/mL), which were maintained by the end of the study.

Navin and Kunal described a new composition for implantable NTX tablets to avoid the use of magnesium stearate and triamcinolone, which can be responsible for particular side effects at the implantation site (e.g., rash, itch, swelling)[280]. According to their patent, NTX HCl is dispersed in a polymeric solution, containing PLGA and Eudragit NE (methacrylate copolymer). The suspension is then discharged and dried. The milled powder mixture then compressed into tablets, which can provide controlled release for 3 to 6 months, depending on the composition.

The O'Neil implant®, also called OLANI (**O**'Neil **L**ong **A**cting **N**altrexone **I**mplant) implant produced by Go Medical Industries in Australia, consists of NTX base-loaded biodegradable

poly(lactic acid) (PLA) microspheres, that are compressed into tablets (8 mm diameter, 5 mm thickness), then coated with another PLA layer[281]. These tablets are implanted subcutaneously in the abdominal site, where the drug release is controlled by passive diffusion and the slow surface and bulk erosion of the matrix[282]. According to a pharmacokinetic study the drug level was between 1 and 2 ng/mL, for 3 months with 10 implanted tablets, and for 5 months with 20 implanted tablets. The product was further tested on a bigger population and compared its efficacy with methadone. An open-label clinical study investigated the heroin usage of individuals after prison release[283]. 23 individuals received the O'Neil implant® and 21 were allocated to methadone. The study found that the therapeutic effect of O'Neil implant® is equivalent to that of methadone treatment.

Although their is potential for the injectable microsphere and subcutaneous tablet formulations, in emergency situations when opioid therapy is required as part of anaesthesia or analgesia, extreme caution should be exercised, as NTX inhibits the effect of opioid analgesics. As there is no practical way to remove such long-acting formulations from the body, due to their size or decreased mechanical properties, usually another non-opioid medication must be chosen, or a higher dose of narcotic analgesics is recommended to reverse the NTX blockade. However, in these cases, opioid-induced respiratory problems may occur, requiring extreme caution[274].

An interesting extended delivery strategy of NTX was investigated in a proof-of-concept clinical study by Wermeling et al. in 2008[284]. The microneedle-assisted percutaneous delivery of NTX for systematic administration was conducted according to the following steps. First, the skin was pre-treated with a microneedle array patch, making opened micropores on the surface. Then, a covering patch containing a NTX HCl-based gel was applied on the treated surface. The slow diffusion of the hydrophilic salt form of the drug through the perforated skin surface resulted in effective drug plasma levels (> 1 ng/mL) for more than 70 hours in six healthy subjects, while the maximum concentration did not exceed the value of 4.5 ng/mL. The microneedle-assisted delivery was well tolerated by the patients with mild side effects on the application site. Brogden et al. reported further development of the concept based on their finding that diclofenac, an anti-inflammatory agent, can prolong the closure time of the formed micropores. The application of NTX HCl/diclofenac-containing gel patches on the treated skin resulted in approximately 120 hours of effective drug plasma levels, above the 1 ng/mL[285]. However, the clinical efficacy of microneedle-assisted drug delivery may be questionable in a long-term therapy related to patient adherence and compliance issues. The fact that this type of

NTX administration does not require unpleasant injections or a surgical intervention makes it a promising strategy for patients with high compliance.

Summary

Based on the literature review, each long-acting NTX formulation commercially available show effective performance for treating opioid use disorder. Of these products, the market dominance of Vivitrol® is unquestionable. However, several clinical studies cite monthly administration of Vivitrol® as the main limitation to its effective use in the treatment of opioid dependence. Patients with poor compliance are not willing to complete the standard 24 week long treatment and discontinue the therapy after the first or second dose. Additionally, emergency discontinuation of Vivitrol® therapy is very limited as there is no practical way for removing the injected microsphere formulation from the muscular tissue area. And finally, the solvent extraction process for the manufacture of injectable microsphere formulations of NTX involves several technological steps and requires an extensive amount of organic solvents[286]. This cost-intensive manufacturing protocol increases the market price of the product, consequently decreasing its accessibility for certain groups. The price of long-acting NTX injection treatments usually varies from USD 700 to USD 1100 per month (cost of one injection). The cost of the oral form for one month is significantly less expensive, generally ranging from USD 25 to USD 60 per month.

1.7 Research hypothesis and objectives

The objective of this thesis was to develop a less expensive long-acting NTX formulation alternative that could address the limitations associated with other commonly used NTX products. This study aimed to investigate the feasibility of a non-biodegradable, NTX-loaded EVA implant produced by HME, adopting a pre-exisiting Probuphine® (buprenorphine) subdermal implant. The extruded rod shaped implants would be implanted into the subcutaneous tissue area of the upper arm via a minor surgical procedure and were developed to provide 2 ng/mL drug plasma levels for up to 3 months. Such a sustained-release product can be easily removed from the patient at the end of the treatment period, or in the case of any unexpected adverse effect or emergency situation. In addition, the HME technology is a continuous, solvent-free, easily scalable, and controllable manufacturing process, which makes it suitable for cost-effective mass production. Therefore, this non-biodegradable long-acting NTX product may have significant unexploited potential in the antagonist treatment of opioid dependence.

2 Product development of NTX HCl loaded EVA implant

2.1 Introduction

The primary objective of this project was the development of a subcutaneously administered sustained-release formulation of the hydrochloride salt form of NTX. NTX HCl is commonly administered in oral form and must be taken daily to reduce the symptoms associated with opiate withdrawals and recovery. However, the effectiveness of the oral formulation is compromised due to poor patient compliance with the dosing regimen, repetitive fluctuation in API plasma concentration, causing mild or severe side effects and the extensive first-pass metabolism in the gastrointestinal tract, significantly reducing the fraction of the administered dose reaching the systematic circulation. These problems can be overcome by the development of a NTX HCl implant that can be implanted subcutaneously, providing an extended release of NTX into the bloodstream.

Previous clinical studies proved that a concentration of 2 ng/mL of blood per day of NTX is required for effective treatment. The required blood level can be ensured and tailored by inserting different numbers of implants with dimensions of 40 mm in length and 2 to 4 mm in diameter. This is similar in dimensions to other subcutaneous implants currently available on the market. These implants are intended to be capable of providing an effective blood concentration of 2 ng/mL for up to 3 months.

This chapter describes the preformulation studies of a subcutaneous NTX-loaded EVA matrix implant, manufactured via HME.

The main objectives of this chapter were as follows:

- For patient compliance and adherence reasons, the implant needs to be flexible. Therefore, the first step was to determine the range of EVA polymers with varying vinyl acetate content (VA-content), melt-flow index (MFI) and the dimension of implants that have sufficient flexibility for further investigation.
- After selecting the appropriate matrix polymers, the second step involved the development and validation of reversed-phase high-performance liquid chromatography (HPLC) methods and protocols for content assay, *in vitro* dissolution testing and related substance studies.

- By means of the developed and validated analytical protocols, the influence of EVA grade on the average drug content, degradation profile and release of NTX HCl from the implants was determined.
- Generally, in matrix type drug delivery systems, the drug release is directly proportional to the amount of drug embedded in the matrix. However, in monolithic dispersion systems, the drug content has a great influence on drug release rate as well, which must be tailored to ensure a sufficient level of sustained release of the formulated drug compound. For that reason, the influence of drug loading on processability, homogeneity, stability and release of NTX HCl from the implants was also determined.
- Finally, the *in vivo* performance of the formulations considered suitable for clinical applications was investigated in male beagle dogs. The study was designed to provide a preliminary assessment of local tolerance and pharmacokinetics in the dogs following implantation of sterilised placebo EVA and drug-loaded implants with differing concentrations of NTX HCl.

2.2 Materials and methods

2.2.1 Materials

EVA copolymers with different VA-content and MFI values were provided by Celanese Corp. (Texas, United States) and Polysciences Inc. (Warrington, United States) as a hydrophobic carrier (*Table 2*).

Table 2 Applied EVA matrix polymers

VA-content (%)	Melt Flow Index	Manufacturer	Form
8.9	1.07	Celanese Corp.	pellet
9.1	8.14	Celanese Corp.	pellet
18.2	159.73	Celanese Corp.	pellet
27.7	2.89	Celanese Corp.	pellet
28.0	25.00	Polysciences Inc.	flake
28.1	42.46	Celanese Corp.	pellet
39.1	60.40	Celanese Corp.	pellet

NTX HCl was provided by Sanofi Chimie (Aramon, France). The chemical reference standards (CRS) of NTX HCl and Naltrexone Impurity C were purchased from EDQM. Acetonitrile (HPLC grade), toluene (reagent grade), dichloromethane (reagent grade) were obtained from Fisher Scientific (Leicestershire, UK). Octanesulphonic acid sodium salt (purity ≥99%), 1M

hydrochloride acid and orthophosphoric acid (≥85 w/w%) were purchased from VWR (Leicestershire, UK).

2.2.2 Hot-melt extrusion of EVA

The appropriate amounts of NTX HCl and EVA were weighed into a sealed plastic container and roll mixed for approximately 10 min. The NTX HCl-EVA blends (approx. 15-20 g) were fed into a Rondol laboratory scale 10 mm twin screw extruder (Rondol Indsitries, Nancy, France) using a Lambda Doser powder feeder (Lamda Instruments, Brno, Czech Republic) and extruded through 2, 3 or 4 mm dies. The feed rate, screw speed and temperature of the extruder were dependent on the grade of EVA and NTX HCl loading used. The extrudates were allowed to cool and subsequently cut into 40 mm lengths to produce either blank, 20, 30, 35, 40 or 50% w/w NTX HCl-loaded EVA implants with either a 2, 3 or 4 mm diameter and 40 mm length.

2.2.3 Flexibility testing of blank implants

Blank implants with 40 mm length and varying diameters (2, 3 and 4 mm) were manufactured from different grades of EVA polymers with varying (8.9, 9.1, 18.2, 27.7, 28.0, 28.1 and 39.1%) VA-contents and MFI values by HME. Different processing temperatures were required for the different EVA grades to obtain extrudates with sufficient quality. The applied processing temperature profiles are shown below in *Table 3*. The filaments were allowed to cool down to room temperature and subsequently cut into 40 mm long rods.

Table 3 Processing temperature profiles used for extrusion of blank implants from different types of EVA

VA-content (%)	Melt Flow Index	Temperature (°C)		
		Zone 1	Zone 2	Zone 3
8.9	1.07	100	150	150
9.1	8.14	100	150	150
18.2	159.73	80	90	80
27.7	2.89	90	120	120
28.0	25.00	90	120	110
28.1	42.46	90	110	100
39.1	60.04	70	80	80

The flexibility of the blank implants with varying diameters (2, 3 and 4 mm) was analysed using an Instron Model 5848 MicroTester (Instron, Norwood, MA, United States) set up for a 3-point flexibility test and their flexibility compared to that of a reference (blank Nexplanon). First, the blank implants were placed in the flexibility tester in a position where the two standard points

were positioned to the 1 cm and 3 cm length of the 4 cm long implants. Then the height of the load cell was adjusted to zero at a level where it reached the surface of the implants (*Figure 6* left side). This state induced the start of the flexibility test. Then the load cell height decreased at 0.1 mm per minute until the distance reached at least the diameter of the measured implant (100% elongation) (*Figure 6* right side). The reaction force (N) of the implant was determined by the force transducer with the decreasing height of the probe cell. The flexibility (N/mm) for each implant was defined as a slope, calculated by linear fitting on the measured points in the linear region on the force-extension curve (*Figure 7*).



Figure 6 Images demonstrating the 3-point flexibility test on an example of the reference implant (Nexplanon)

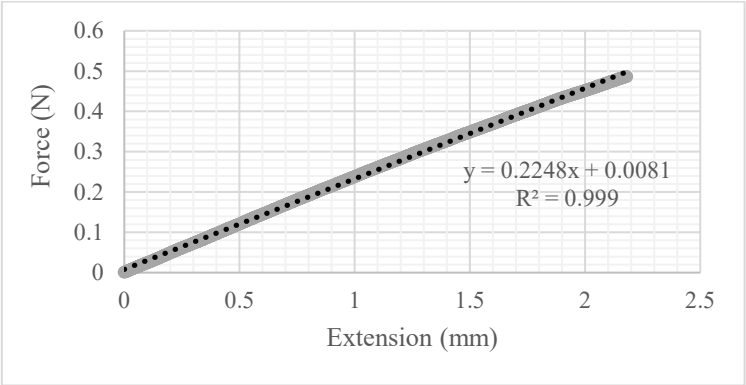


Figure 7 Determination of flexibility on an example of the reference Nexplanon blank implant

2.2.4 Reversed-phase HPLC methodologies

The HPLC methods are based on the related substance method in the Ph.Eur. 9.0 monograph No. 1790 for NTX HCl. The HPLC method for assay only differs in the mobile phase compositions to shorten the analysis time. The basic analytical conditions are summarised in *Table 4*.

Table 4 Analytical conditions for HPLC measurements

Equipment:	Dionex Ultimate 3000 HPLC with Multi-wavelenght UV-Vis detector or Agilent 1260 HPLC with Diode array UV-Vis
Wavelength:	230 nm
Column:	ZORBAX Eclipse Plus 5 µm C18, 4.6 x 150 mm
Column temperature:	25 °C
Flow rate:	1.2 mL/min
Injection volume:	10 µL
Mobile phase A:	1.1 g/L solution of sodium octane sulfonate adjusted to pH=2.3 with phosphoric acid
Mobile phase B:	Acetonitrile

HPLC related substance method

The related substance method used to detect impurities due to the degradation of NTX HCl was in accordance with the Ph.Eur. 9.0 monograph No. 1790 for NTX HCl. The gradient program is summarised in *Table 5*.

Table 5 Mobile phase composition of the related substance HPLC method

Time (min)	Mobile Phase A (% v/v)	Mobile Phase B (% v/v)
0 - 45	90 to 55	10 to 45
45 - 47	55 to 90	45 to 10
47 - 55	90	10

The proposed concentration of NTX HCl in the injected *test solution* and *reference solution* was 2.00 and 0.002 mg/mL, respectively. The applicability of chromatographic conditions was checked before and after every measurement sequence by the injections of a *system suitability solution*, where the resolution had to be at least 2.0 between the peaks due to NTX and Impurity C. The retention time of NTX was approximately 16 min, with a run time of 55 min. The solutions required for sample analysis were prepared as follows.

Preparation of NTX HCl test solution (2.00 mg/mL NTX HCl):

The test solution was prepared by dissolving 20.0 mg of NTX HCl in 0.1 M HCl and diluting to 10.0 mL with the same solvent.

Preparation of NTX HCl system suitability solution (0.002 mg/mL NTX HCl and 0.002 mg/ml NTX impurity C):

0.2 ml of the NTX HCl test solution was diluted to 20.0 mL with 0.1 M HCl to produce the NTX HCl system suitability stock solution. The system suitability solution was prepeared by dissolving 5.0 mg of NTX Impurity C CRS (EDQM, Batch No. 1) in 0.1 M HCl and diluting to 10.0 mL with the same solvent. A further dilution of 1.0 mL to 25.0 mL was performed. 1.0

mL of this solution was combined with 1.0 mL of the NTX HCl system suitability stock solution and diluted to 10.0 mL with 0.1 M HCl.

Preparation of NTX HCl reference solution (0.002 mg/ml NTX HCl):
1.0 mL of NTX HCl test solution was diluted to 10.0 mL with 0.1 M HCl. 0.2 mL of this solution was diluted to 20.0 mL with 0.1 M HCl to produce the NTX HCl reference solution.

Sample preparation for HPLC related substance method was performed as follows. 6 implants were cut into small pieces and homogenised by shaking. Equivalent to 20 mg of NTX HCl was measured into 40 mL glass tubes then 2.5 mL of dichloromethane (DCM) was added. The samples were shaken at 37 °C/ 60 rpm in a Unitron HT Infors shaking incubator until the whole amount of polymer was dissolved. After the complete dissolution of the polymer, 10 mL of 0.1 M HCl was added to the systems and shaken manually for 2 minutes. After the two phases were separated (approx. 0.5 hour), 1.5 mL of the upper phase was measured into 1.5 mL Eppendorf tubes and centrifuged for 5 minutes at 13000 rpm. 10 µL of the centrifuged samples were injected and analysed by NTX HCl related substance HPLC method (*Test solution 100% approx. 2.00 mg/mL of NTX HCl*). 1 mL of the centrifuged samples was diluted to 1 in 1000 with 0.1 M HCl then injected and analysed by NTX HCl related substance method (*Reference solution 0.1% approx. 0.002 mg/mL of NTX HCl*).

Calculation of impurity content respectively:

$$Impurity\ Content\ (\%) = \frac{A_{test\ solution} * 0.1}{A_{reference\ solution}}$$

where

- $A_{test\ solution}$ – area of the peak due to the impurity in the *Test solution*
- $A_{reference\ solution}$ – area of the peak due to NTX HCl in the *Reference solution*
- *0.1* – dilution factor (*Test solution 100%, Reference solution 0.1%*)

The disregard limit was 0.25 times the area of the peak due to naltrexone in the chromatogram obtained with reference solution.
The contents of each impurity were established from the average results of 3 replicates. Known impurities were identified according to their relative retention time to naltrexone, as written in the Ph.Eur. monograph.

HPLC assay method

The NTX HCl assay method was isocratic with the following mobile phase composition:

Time (min)	Mobile Phase A (% v/v)	Mobile Phase B (% v/v)
0 - 10	75	25

With this method the retention time of NTX HCl was approximately 4.4 min, with a run time of 10 min. The required standard solution was prepared as follows.

Preparation of NTX HCl standard solution (0.20 mg/mL NTX HCl):

20.0 mg of the NTX HCl CRS (EDQM, Batch No. 2) was dissolved in 0.1 M HCl and diluted to 10.0 mL with the same solvent. 1.0 mL of this solution was further diluted to 10.0 mL with 0.1 M HCl to produce the NTX HCl standard solution.

Calculation of NTX HCl assay:

$$Assay\ (\%) = \frac{m_{std} * A_{sample} * D_{sample}}{m_{sample} * A_{std} * D_{std}} * 100$$

where

- m_{std} and m_{sample} – weighed mass of NTX HCl standard and extrudates
- A_{std} and A_{sample} – area of the peak due to NTX HCl on the standard and sample chromatogram respectively
- D_{std} and D_{sample} – dilution factor of NTX HCl standard and extrudates (the dilutions with 0.1 M HCl)

The drug contents were established from the average results of 4 replicates.

Sample preparation for HPLC assay methods was based on the work of Constantini et al.[183] and performed as follows. 6 implants were cut into small pieces and homogenised. Approximately 60-70 mg was measured into 40 mL glass tubes then 5.0 mL of toluene was added. The samples were shaken at 37 °C/ 60 rpm in an orbital shaking incubator (Unitron HT Infors) until the whole amount of polymer was dissolved. After the complete dissolution of the polymer, 10 mL of 0.1 M HCl was added to the systems and shaken manually for 2 minutes. After the two phases were separated (approx. 0.5 hour), 1.5 mL of the lower phase was measured into 1.5 mL Eppendorf tubes and centrifuged for 5 minutes at 6500 rpm. 1 mL of the centrifuged samples was diluted to 1 in 10 with 0.1 M HCl then injected and analysed by NTX HCl assay method.

The sample preparation procedure in the case of release samples consisted of a single preparation step. 1 mL of the dissolution media was measured into a 1.5 mL Eppendorf tubes

and centrifuged for 5 minutes at 13000 rpm. 10 µL of the centrifuged samples were then injected and analysed by NTX HCl assay HPLC method.

Calculation of NTX HCl content in dissolution samples:

$$Concentration\ (mg/mL) = \frac{m_{std} * A_{sample}}{A_{std} * D_{std}}$$

where

- m_{std} – weighed mass of NTX HCl standard
- A_{std} and A_{sample} – area of the peak due to NTX HCl on the standard and sample chromatogram respectively
- D_{std} – dilution factor of NTX HCl standard

2.2.5 Homogeneity of the implants

The homogeneity of drug content along the 4 cm long implants was determined by analysing the drug content in 1 cm sections of the rods and comparing. The implants were cut up to four 1 cm long pieces, and each section was analysed for drug content by the HPLC assay method written above in *Section 2.2.4*. Each batch was investigated by analysing 4 implants (16 measurements).

2.2.6 Validation of HPLC methods

The NTX HCl related substance method was an already validated and authorised Ph.Eur. HPLC method, therefore, this report only contains the system suitability results by the presentation of 5 injections of the System Suitability Solution containing 0.002 mg/mL NTX HCl CRS and 0.002 mg/mL NTX.HCl Impurity C CRS. Although other parameters were also validated in our lab. To verify that all degradation products appear in the test solutions to be injected after the sample preparation (liquid/liquid extraction with DCM), the thermally stressed drug substance (190 °C/ 240 min) was tested without the matrix polymer, as well as in the presence of the matrix polymer. The sample preparation protocol was validated for precision over 12 determinations, using 6 replicates on 2 consecutive days.

The NTX HCl assay HPLC method was partly validated according to International Conference on Harmonization (ICH) guideline[287]. The linearity was determined across the entire concentration range of the assay using 10 different concentrations ranging from 0.001 to 0.300 mg/mL. The accuracy was validated over 12 determinations, using 6 concentrations and 2 replicates of each concentration. The range of the assay was determined from the linearity and

accuracy data. The repeatability was validated using 6 determinations at 100%, while the intermediate precision was determined over two days using another 6 determinations at 100% prepared on a different day. The limit of detection (LOD) was calculated using the formula LOD = 3.3*(SD/S), while the limit of quantification (LOQ) was calculated using the formula LOQ = 10*(SD/S). SD = the standard deviation between the y-intercepts from the two linearity curves and S = the mean slope of the line for the same linearity curves.

2.2.7 Stability of NTX HCl in various dissolution media

20 mg of NTX HCl was dissolved in 10 mL of each of the potential dissolution media (Water, 0.1 M HCl, 0.05 M Phosphate Buffer at pH 6.8, 7.4 and 8.2). The solutions were placed in an orbital shaking incubator (Unitron HT Infors) at 37°C and 60 rpm, while a solution of NTX HCl in water was also stored in a fridge at 5-8°C. The stability of NTX HCl was determined after 16 hours, 1, 2, 3, 4, 5, 6 and 7 days using the NTX HCl related substance HPLC method. Each dissolution media was evaluated in triplicate.

2.2.8 Solubility of NTX HCl in water

An excess amount (100 mg) of NTX HCL was added to 1 mL of water and placed in an orbital shaking incubator (Unitron HT infors) for 72 h at 37°C and 60 rpm. After 72 h, the solutions were removed from the incubator and left to equilibrate to room temperature. The solutions were subsequently filtered through a 0.45 µm membrane filter and aliquots suitably diluted for analysis using the NTX HCl assay HPLC method. The solubility was evaluated in triplicate.

2.2.9 *In vitro* drug release

NTX HCl release from each implant was determined by placing the rods into a sealed 150 mL glass bottle containing 50 mL of purified water and placed into an orbital shaking incubator (Unitron HT Infors) at 37 °C and 60 rpm. Teflon rings were placed on the middle of the implants to act as sinkers to stop them from floating. 1 mL of the dissolution media was taken on each sampling day, and the sample volume was replaced with fresh deionised water. The collected samples were centrifuged and analysed for drug content using the NTX HCl assay HPLC method (*Section 2.2.4*).

2.2.10 Rheological evaluation of the NTX HCl/EVA blends

Rheological experiments were carried out using a Discovery HR-1 Rheometer (TA Instruments, New Castle, DE, United States). The rheological properties of the melted samples were investigated by a dynamic oscillatory measurements with parallel plate geometry (*Figure 8*).

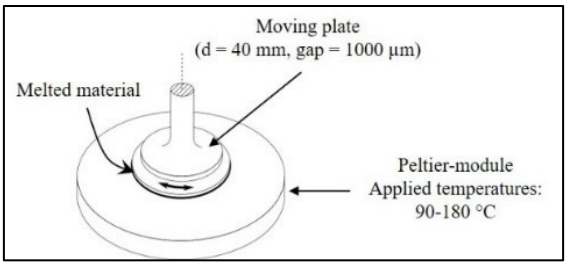


Figure 8 Illustration of the dynamic oscillatory measurement geometry

Several NTX HCl/EVA blends were melted and homogenized on the Peltier-module before each measurement. After the blends were melted and thoroughly mixed, the upper parallel plate was lowered to produce a gap between the plates of 1000 µm. The excess blends were removed before the oscillation experiment was begun. Prior to analysis, each sample was conditioned at the initial measuring temperature for 60 s.

The first step was to determine the Linear Viscoelastic Region (LVR) of the samples at 3 different temperatures by running an *oscillatory amplitude sweep* test. This type of measurement involved the oscillatory stress / strain / torque to be increased, in a logarithmic ramp (1-100000 µNm), at a fixed frequency (1 Hz) and temperatures (90, 135 and 180 °C) covering the interested temperature region. Then, the *oscillatory temperature ramp* tests were performed within the LVR, at fixed frequency (1 Hz) and under constant stress condition (1000 µNm) using a chosen torque value from the *oscillatory amplitude sweep* test result, in order to maintain the response of the samples in the LVR. The cooling temperature ramp (5 °C/ min) was used from 180 to 90 °C. By this cooling procedure the geometry always stayed in contact and the sample did not drain or expand out of the gap during the measurements (*Figure 9*).

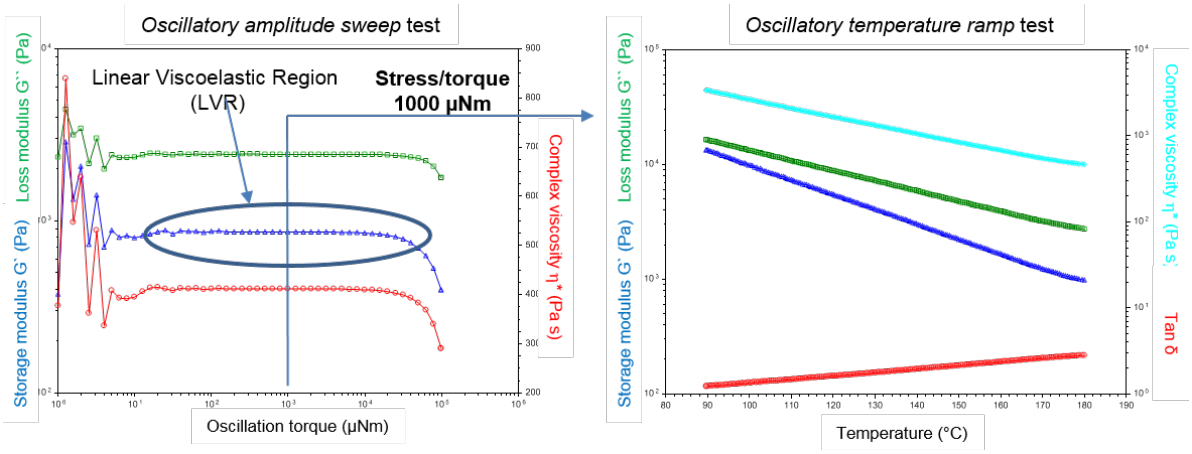


Figure 9 Illustration of the dynamic oscillatory measurement process

2.2.11 Differential scanning calorimetry (DSC)

Thermal analysis of NTX HCl, EVA polymers, physical mixture of NTX HCl and EVA polymer, and NTX HCl-loaded extrudates was carried out using a DSC250 TA Instruments DSC. The sample was weighed (~10 mg each) and sealed in a Tzero® aluminium pan. The pan was then equilibrated at the initial temperature for 1 min, which was followed by heating to 255 °C at the ramp rate of 10 °C/min under nitrogen atmosphere.

The degree of crystallinity of NTX HCl in the implants was evaluated from the heat of fusion using the following equation:

$$X_c(\%) = \frac{\Delta H_m}{\Delta H_m^0} * 100$$

where

- ΔH_m – heat of fusion measured from the DSC thermogram
- ΔH_m^0 – heat of fusion of crystalline NTX HCl

(44.757 J/g, measured by DSC using the NTX HCl chemical reference standard)

The enthalpy values were normalised based on the NTX HCl conent of the implants, measured by HPLC assay method.

2.2.12 Scanning electron microscopy (SEM)

Microscopic sample morphology was investigated using a Hitachi TM-3030 (Hitachi, Tokyo, Japan) scanning electron microscope (SEM). The cross-section of each sample was fixed with a conductive double-sided carbon adhesive tape and covered with a gold layer to increase the conductivity of the sample surface and improve the signal. Samples were then observed under SEM at 15kV. Finally, the elemental analysis was carried out by means of the energy dispersive X-ray (EDX) spectroscopic function of the equipment where it was required.

2.2.13 Preparation of NTX HCl-EVA implants from different grade EVA polymers

20% w/w drug-loaded implants with 2 mm diameter and 40 mm length were manufactured from different EVA polymers with varying VA-content and MFI values by HME. Different processing parameters were applied to produce extrudates with sufficient quality. The applied process parameters are shown in *Table 6*. The filaments were let cool to room temperature and manually cut, usinga scalple into rods of 4 cm length. Average drug content of each batch and degradation of NTX HCl in the produced implants was assessed by a validated HPLC assay and related substance method (*Section 2.2.4*). Drug release tests were performed as described in *Section 2.2.9*.

Table 6 Processing parameters used for the extrusion of drug loaded implants with varying EVA grade

EVA grade	Feeding rate (g/min)	Screw speed (rpm)	Temperature (°C)		
			Zone 1	Zone 2	Zone 3
EVA 28.1 MFI:42.46	90	100	100	110	100
EVA 27.7 MFI:2.89	90	100	100	165	160
EVA 39.1 MFI:60.64	90	100	75	90	90

2.2.14 Preparation of NTX HCl-EVA28 implants with varying drug loadings

Drug loaded implants with varying NTX HCl content (20, 30, 40 and 50% w/w) were prepared by HME from EVA28 (MFI: 42.46). The dimensions of the rod-shaped products were 4 cm in length and 3 mm in diameter. Different processing temperatures were required for different drug loadings to obtain extrudates with adequate quality. Other parameters remained constant. The applied processing parameters are shown below in *Table 7*. The filaments were allowed to cool to room temperature then manually cut, using a scalple into rods of 4 cm length.

Table 7 Processing parameters used for extrusion of drug loaded implants with varying drug content

Polymer/ Manufacturer	Drug loading (%w/w)	Feeding rate (g/min)	Screw speed (rpm)	Temperature (°C)		
				Zone 1	Zone 2	Zone 3
EVA28.1 (MFI:42.46) Celanese	20	90	90	100	120	100
	30	90	90	100	120	100
	35	90	90	100	130	100
	40	90	90	100	135	110
	50	90	90	100	145	110
EVA28.0 (MFI:25.00) Polysciences	35	90	90	100	130	100

Drug content and homogeneity of each batch was assessed by a validated HPLC assay method and a sample preparation protocol. The homogeneity of drug content along the 4 cm long implants was estimated by analysing the drug content of the 1 cm regions of 3 implants. The degradation of NTX HCl was determined by a related substance HPLC method. Drug release tests were performed as described in *Section 2.2.9*.

2.2.15 *In vivo* characterisation

The preliminary assessment of local tolerance and *in vivo* release of NTX from the implants and their dose-ranging influence were investigated in young adult male beagle dogs (Marshall

BioResources). Due to the preliminary investigative nature of this 29 day study, no specific regulations or guidelines were applicable. The work performed followed Good Laboratory Practice principles. The in-life experimental procedures were undertaken during the course of this study were subject to the provisions of the United Kingdom Animals (Scientific Procedures) Act 1986 Amendment Regulations 2012.

The sterilised palcebo and NTX HCl-EVA rods were implanted subcuteneoulsly into the flank of the dogs. To ensure that the sterilisation agent (ethylene-oxide) did not induce degradation of the NTX HCl, implants with 35% w/w drug-loadings were analysed by the related substance HPLC method before and after the sterilisation procedure (*Section 2.2.4*). After the acceptable purity profile of NTX HCl in the sterilised implants was confirmed, the implants were implanted on the left and right lateral flank regions (one implant per site) of the animals under general anesthesia, according to *Table 8*.

Table 8 In vivo study design

Group	Number of animals	Implant 1 Left flank (NTX HCl% w/w)	Implant 2 Right flank (NTX HCl% w/w)	Estimated total NTX HCl exposure (mg/animal)*
PK1	2	0	30	111
PK2	2	35	35	259
PK3	2	0	40	148
PK4	2	40	40	296

* Based on an approximate total weight of 370 mg/implant; 2 implants

At various time points, blood samples were collected into tubes containing ethylene-diamine-tetra-acetic acid (EDTA) and stored at -70 ± 10 °C prior to the quantitative analysis of NTX by a validated LC/MS/MS method. Pharmacokinetic evaluation appropriate to the data was performed. The pharmacokinetic analysis included the determination of the maximum plasma concentrations (C_{max}), their times of occurrence (T_{max}) and the areas under the plasma concentration-time curves to the last measurable plasma concentration (AUC_{0-t}) using the computer program WinNonlin® (Pharsight Corporation, USA). A non-compartmental analysis using the log-linear trapezoid rule with a log-linear extrapolation was applied. No formal statistical analysis was performed.

Throughout the study period (29 days), all dogs were monitored for complications, including irritation, inflammation or other site-specific adverse effects.

The animals were euthanised at the end of the study (day 29) with implantation site excised from all animals and the implanted rods removed. The resected implantation sites, surrounding

tissues and any migration tracts were histopatologically examined, while the implants were analysed for their remaining NTX HCl content.

2.2.16 Statistical data analysis

Statistical analysis was performed to evaluate significant differences between different extruded implant characteristics using Student's t-test. Post-hoc comparisons of the means were performed using Tukey's range test. The level of $p<0.05$ was accepted as significant. All statistical analysis was performed using Minitab® 19 software.

2.3 Results

2.3.1 Flexibility of the blank EVA implants

For patient compliance and adherence reasons, the implant needs to have some level of flexibility. In order to select a suitable dimension of the product, flexibility tests were performed to assess the applicability of the implants for clinical use. All of the blank implants showed a reversible deformation during the measurements. However, the force required for certain elongations varied as a function of implant diameter, VA-content and MFI value of the EVAs. *Figure 10* and *Figure 11* demonstrate that the flexibility of the implants decreased with an increase in the diameter and a decrease in the VA-content of the EVA.

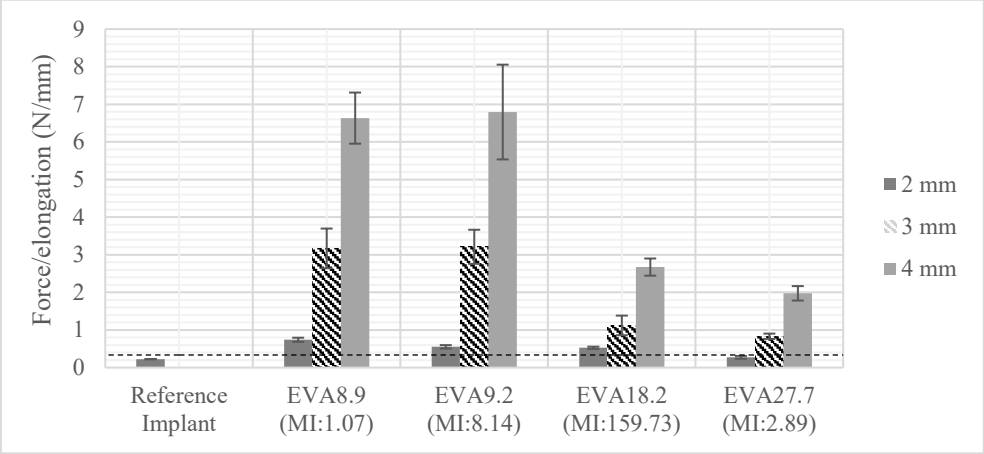


Figure 10 The flexibility data for the blank implants with varying VA-contents (8.9, 9.2, 18.2 and 27.7) and diameter (2,3, and 4 mm). The dashed line represents a 50% upper limit, where anything above this is 50% less flexible than the reference. Error bars represent ±1 standard deviations of n=3 replicates.

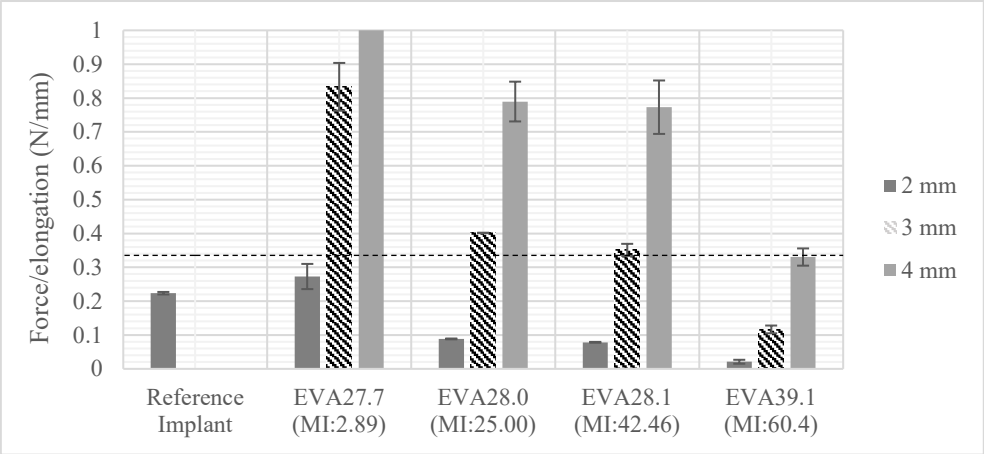


Figure 11 The flexibility data for the blank implants with varying VA-contents (27.7, 28.0, 28.1 and 39.1) and diameter (2,3, and 4 mm). The dashed line represents a 50% upper limit, where anything above this is 50% less flexible than the reference. Error bars represent ±1 standard deviations of n=3 replicates.

As can also be seen in *Figure 11*, blank implants manufactured from EVAs with similar VA-contents (27.7, 28.0 and 28.1) but with different MFI values (2.89, 25.00 and 42.46) exhibited different levels of flexibility. Blank implants produced from EVA with an MFI value of 2.87 required significantly larger force for the same elongation ($p<0.05$). At the same time, implants produced from EVA with MFI values of 25.00 and 42.46 showed almost a similar level of flexibility.

The Nexplanon placebo implant was used as a reference. The flexibility limit for the implants was set at not less than 50% of the Nexplanon implant. Based on the results, only 2 mm implants with a VA-content of 27.7, 28.0 and 28.1 and 3 mm implants with a VA-content of 39.1 were acceptable. However, 4 independent people were asked to visually inspect and compare the flexibility of the produced implants to that of the Nexplanon reference. Based on the visual inspection, 3 mm implants from EVA with VA-content of 27.1, 28.0 and 28.1 were also acceptable. 4 mm implants extruded from EVA with VA%-content of 28.0, 28.1 and 39.1 also showed acceptance among the individuals. The data are summarised in *Table 9*.

Table 9 Summary of the diameters and EVA grades that were acceptable for an implant based on flexility data and visual inspections. + represents acceptance based on flexibility data, while ± represents the points where visual inspection scored the implant acceptable, but 3-point flexibility test didn't.

Implant diameter	VA%-content						
	8.9 (MI: 1.07)	9.2 (MI: 8.14)	18.2 (MI: 159.73)	27.7 (MI: 2.89)	28.0 (MI: 25.00)	28.1 (MI: 42.46)	39.1 (MI: 60.40)
2 mm	-	-	-	+	+	+	+
3 mm	-	-	-	±	±	±	+
4 mm	-	-	-	-	±	±	±

Based on the flexibility data, EVAs with 27.7, 28.0, 28.1 and 39.1% VA-content were selected for further investigation.

2.3.2 Development and validation of the different HPLC methods

HPLC related substance method

The applicability of the already authorised method described in the Ph.Eur. monograph was checked by injecting the system suitability test solution 5 times. An example system suitability chromatogram is presented in *Figure 12*. The measured parameters are summarised in *Table 10*. The RSD% values calculated for different performance parameters are less than 2% in each case. Based on these results it can be confirmed that the related substance method described in the corresponding Ph.Eur. monograph was succesfully established and could be used for this reserch project to assess the degradation profile of NTX HCl. An example chromatogram of the test solution is presented in *Figure 13*. All of the known impurities could be indentified on the chromatograms according to their relative retention time to NTX.

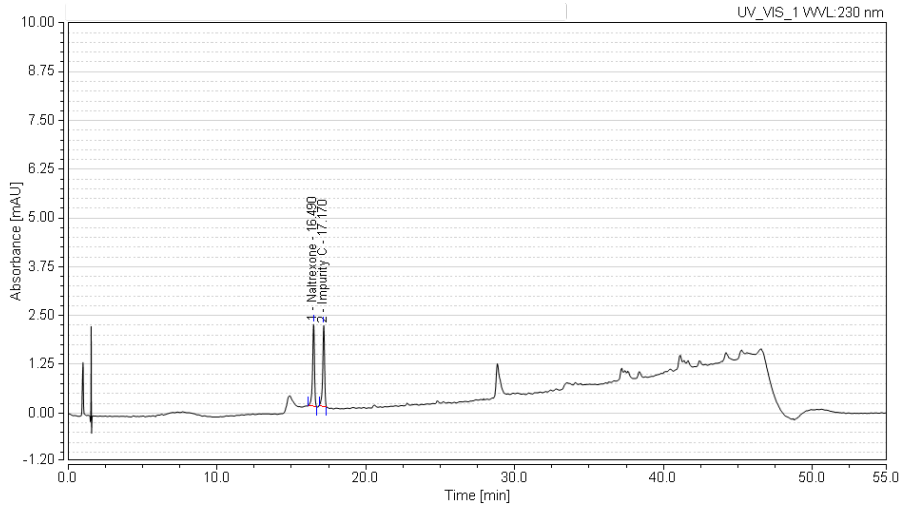


Figure 12 System suitability chromatogram for NTX HCl related substance method

Table 10 System suitability parameters from 5 injections for NTX HCl related substance HPLC method

Inj.	Naltrexone				Impurity C				Resolution between NTX and Imp C
	Ret. time (min)	No. Plates	Assy-metry factor	Area (mAU*min)	Ret. time (min)	No. Plates	Assy-metry factor	Area (mAU*min)	
1	16.45	96052	0.81	0.297	17.13	101053	0.80	0.308	3.19
2	16.46	96295	0.81	0.293	17.14	100512	0.80	0.312	3.2
3	16.51	97613	0.81	0.287	17.19	101732	0.81	0.306	3.19
4	16.56	99115	0.84	0.291	17.24	104831	0.79	0.307	3.22
5	16.57	99245	0.83	0.286	17.25	104422	0.81	0.303	3.25
Mean:	16.51	97664	0.82	0.29	17.19	102510	0.80	0.31	3.21
STDEV:	0.06	1506.67	0.01	0.00	0.06	1985.13	0.01	0.00	0.03
RSD%:	0.33	1.54	1.72	1.55	0.32	1.94	1.04	1.06	0.79

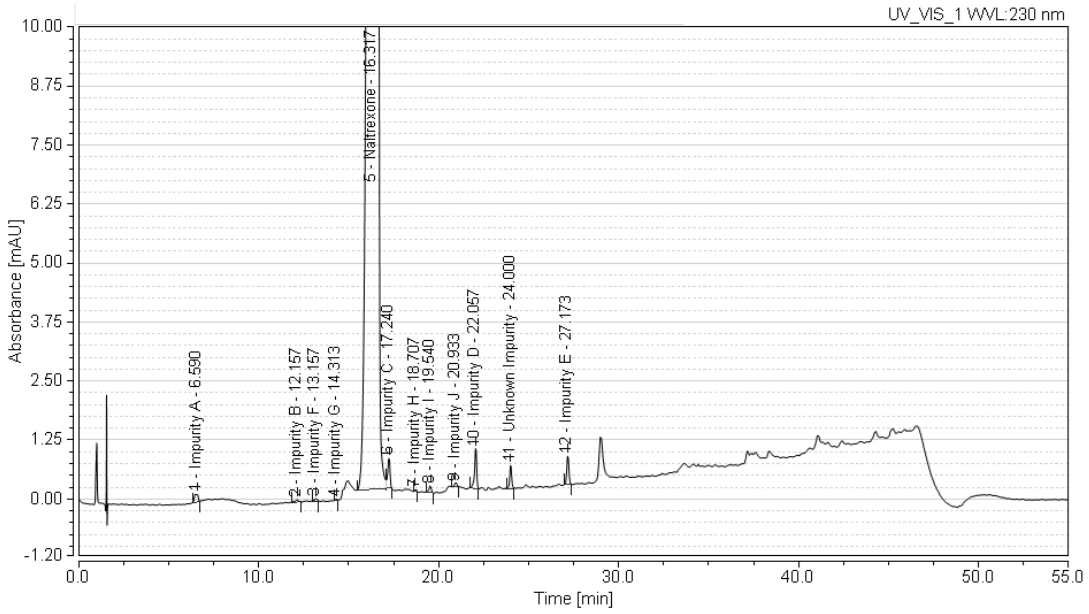


Figure 13 Example chromatogram of the NTX HCl test solution using the NTX HCl related substance method

The influence of the applied sample preparation protocol on the detected impurities was investigated. As can be seen in *Figure 14*, all of the detected impurities on the chromatogram related to the test solution of heat-stressed NTX HCl appeared at the same retention times and with concurrent intensity values on the test solution chromatograms prepared by the liquid/liquid (L/L) extraction method. No additional peaks can be found on the test solution chromatogram prepared from the heat-stressed API by dissolving it only in 0.1 M HCl. These results indicate that the L/L extraction and the presence of the EVA matrix did not influence the diffusion of degradation products from the DCM phase into the 0.1 M HCl phase. According to this investigation, it could be stated that the developed sample preparation protocol was suitable to determine the purity profile of the active ingredient in the extruded products.

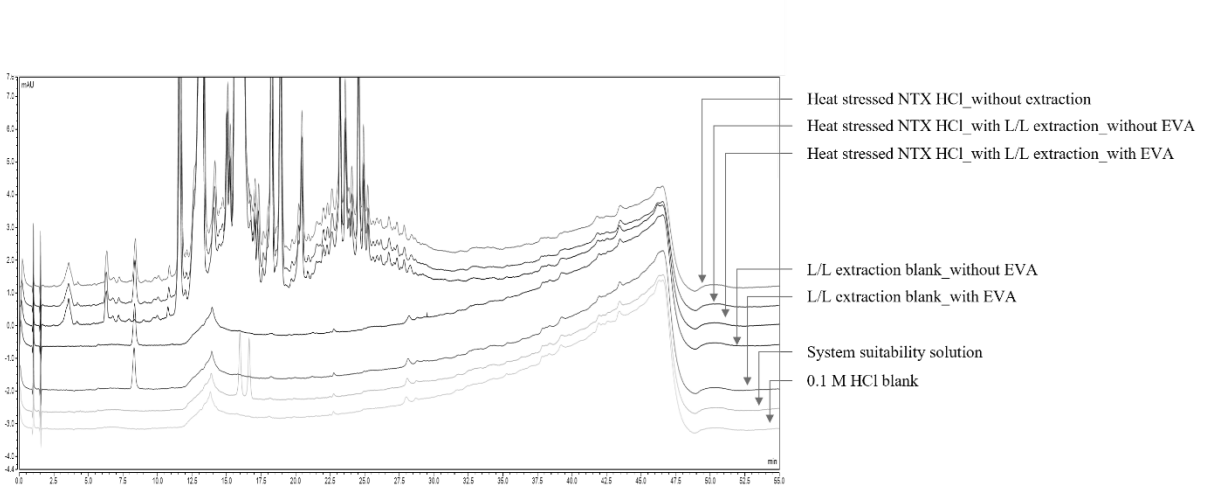


Figure 14 Verification of the sample preparation (liquid/liquid extraction) protocol in regard to detected impurities

In order to justify the applicability of the developed sample preparation protocol (L/L extraction with DCM), the repeatability was validated using 6 determinations on the sample loaded with 20% w/w NTX HCl prepared from EVA28.1 (MFI:42.46) by HME at the processing temperature of 120 °C, while the intermediate precision was determined over two days using another 6 determinations on a sequent day on the same sample. The measured impurity profiles are presented in *Table 11* and *Table 12*. As can be seen, the developed method show acceptable repeatability and precision.

Table 11 Repeatability data for NTX HCl related substance method from 6 determinations on Day 1

Impurity	Impurity content (%) Day 1 Preparation					
	1	2	3	4	5	6
Imp. A	< D.L.	< D.L.	< D.L.	< D.L.	< D.L.	< D.L.
Imp. B	< D.L.	< D.L.	< D.L.	< D.L.	< D.L.	< D.L.
Imp. C	0.03	0.03	0.03	0.03	0.03	0.03
Imp. D	< D.L.	< D.L.	< D.L.	< D.L.	< D.L.	< D.L.
Imp. E	0.04	0.04	0.03	0.04	0.04	0.04
Imp. F	< D.L.	< D.L.	< D.L.	< D.L.	< D.L.	< D.L.
Imp. G	no detect.	no detect.	no detect.	no detect.	no detect.	no detect.
Imp. H	< D.L.	< D.L.	< D.L.	< D.L.	< D.L.	< D.L.
Imp. I	< D.L.	< D.L.	< D.L.	< D.L.	< D.L.	< D.L.
Imp. J	< D.L.	< D.L.	< D.L.	< D.L.	< D.L.	< D.L.
Unknown Imp.	< D.L.	< D.L.	< D.L.	< D.L.	< D.L.	< D.L.
Total Impurity	0.07	0.07	0.06	0.07	0.07	0.07

"D.L." = under disregard limit (0.025%)

Table 12 Intermediate precision data for NTX HCl related substance method from 6 determinations on Day 2

Impurity	Impurity content (%) Day 2 Preparation					
	1	2	3	4	5	6
Imp. A	< D.L.	< D.L.	< D.L.	< D.L.	< D.L.	< D.L.
Imp. B	< D.L.	< D.L.	< D.L.	< D.L.	< D.L.	< D.L.
Imp. C	0.03	< D.L.	0.03	0.03	0.03	0.03
Imp. D	< D.L.	< D.L.	< D.L.	< D.L.	< D.L.	< D.L.
Imp. E	0.04	0.04	0.04	0.04	0.04	0.04
Imp. F	< D.L.	< D.L.	< D.L.	< D.L.	< D.L.	< D.L.
Imp. G	no detect.	no detect.	no detect.	no detect.	no detect.	no detect.
Imp. H	< D.L.	< D.L.	< D.L.	< D.L.	< D.L.	< D.L.
Imp. I	< D.L.	< D.L.	< D.L.	< D.L.	< D.L.	< D.L.
Imp. J	< D.L.	< D.L.	< D.L.	< D.L.	< D.L.	< D.L.
Unknown Imp.	< D.L.	< D.L.	< D.L.	< D.L.	< D.L.	< D.L.
Total Impurity	0.07	0.04	0.07	0.07	0.07	0.07

"D.L." = under disregard limit (0.025%)

HPLC assay method

For sufficient analysis of drug content from the extrudates and release samples, an HPLC method with a short runnning time (10 min) was developed and validated for its linearity, range, accuracy, precision (repeatability and intermediate precision), limit of detection (LOD) and limit of quantification (LOQ). A sample chromatogram is presented in *Figure 15*. The method was found to be linear across the concantration range of 0.001 to 0.300 mg/mL with an r^2 of 0.999 (*Figure 16*) and to have an accuracy of 99.0 to 102.0% (*Table 13*). The method was shown to be precise with a mean for the repeatability of 99.9% and a RSD% of 0.55%, while the intermediate precision had a mean of 100.1% and a RSD% of 0.53%. The mean across the 12 determinations prepared over 2 days was 100.0% with a RSD% of 0.52%. The range of the assay was found to be 0.001 to 0.300 mg/mL, while the LOD and LOQ were 0.0002 mg/mL and 0.0008 mg/mL respectively.

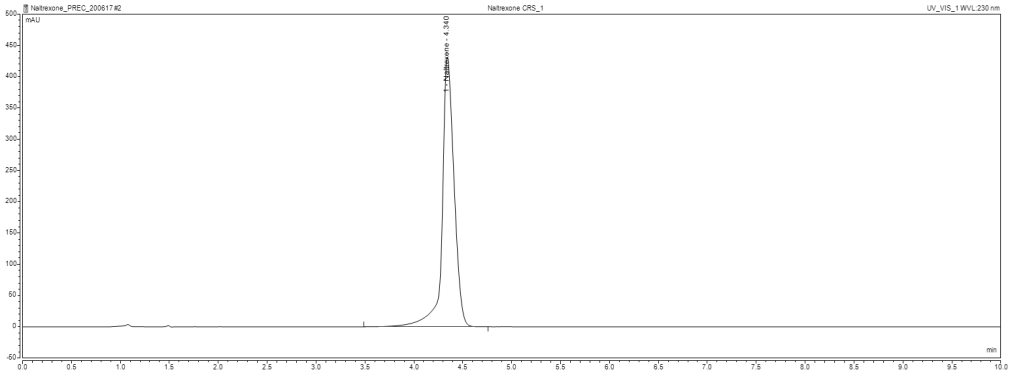


Figure 15 Example chromatogram for the NTX HCl assay method

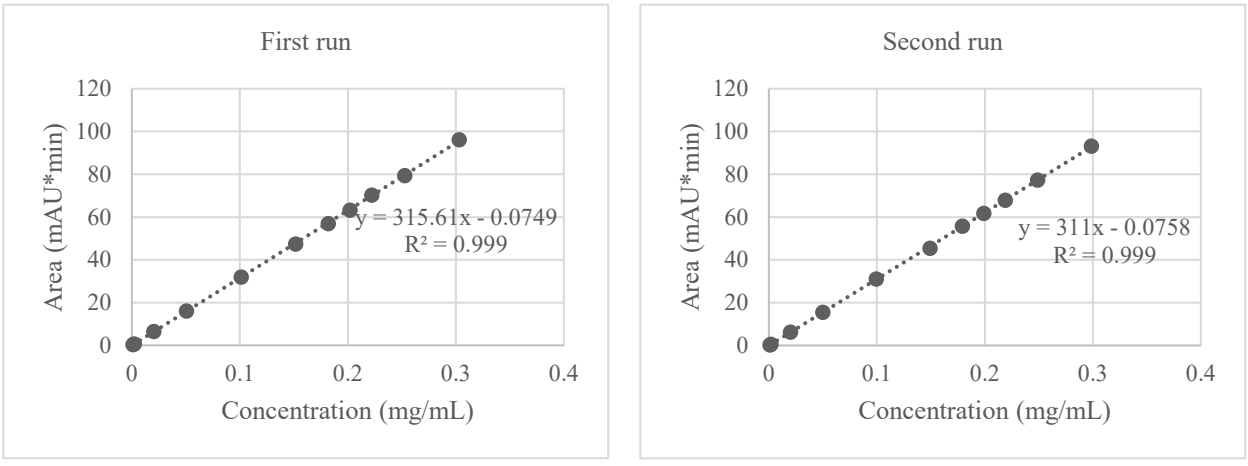


Figure 16 Linearity of the NTX HCl HPLC assay
The concentration of NTX HCl standard solutions range from 0.001 to 0.300 mg/mL

Table 13 Accuracy data for the NTX HCl HPLC assay from 6 determinations and 2 replicates of each concentration

Solution 1			Solution 2		
Concentration (mg/mL)	Area (mAU*min)	Recovery (%)	Concentration (mg/mL)	Area (mAU*min)	Recovery (%)
0.001	0.313	99.0	0.001	0.313	101.0
0.051	15.720	101.4	0.054	16.632	100.4
0.103	31.855	100.8	0.101	31.435	101.4
0.151	46.643	100.7	0.150	45.754	99.4
0.295	64.190	102.0	0.200	62.195	101.3
0.300	93.410	101.5	0.298	91.187	99.7

Table 14 Repeatability and precision data for NTX HCL HPLC assay from 6 determinations at 0.200 mg/mL concentration level

Prepa-ration	Day 1			Day 2		
	Concentration (mg/mL)	Area (mAU*min)	Assay value (%)	Concentration (mg/mL)	Area (mAU*min)	Assay value (%)
1	0.202	63.258	100.9	0.199	62.019	100.4
2	0.201	62.088	99.5	0.204	63.475	100.3
3	0.202	62.591	99.9	0.201	61.826	99.1
4	0.203	62.79	99.7	0.202	62.82	100.2
5	0.199	61.358	99.4	0.196	61.157	100.6
6	0.203	63.045	100.1	0.202	62.804	100.2
		Mean:	99.92		Mean:	100.13
		STDEV:	0.55		STDEV:	0.53
		RSD%:	0.55		RSD%:	0.53

In order to justify the applicability of the developed sample preparation protocol (L/L extraction with toluene), the accuracy was validated over 12 determinations. Known amounts of NTX HCl were added to the sample matrix at 6 concentration levels, and 2 replicates of each concentration level were measured by the HPLC assay method with a sample preparation protocol based on L/L extraction with toluene. Measured data are summarised in *Table 15*. The measurement of NTX HCl content in the extrudate through the developed HPLC method and sample preparation protocol was found to be accurate within a range of 99.0 and 102.0%, which is identical with the accuracy values measured just for the HPLC method alone, without sample preparation.

Table 15 Accuracy data for the sample preparation protocol related to NTX HCl HPLC assay from 6 determinations and 2 replicates of each concentration

Run 1		Run 2	
Theoretical concentration (mg/mL)	Recovery (%)	Theoretical concentration (mg/mL)	Recovery (%)
0.089	101.87	0.083	99.93
0.178	99.88	0.192	99.06
0.274	99.03	0.265	98.98
0.348	99.00	0.350	101.24
0.433	98.90	0.417	100.99
0.525	99.54	0.516	100.98
Mean:	99.70	Mean:	100.20
STDEV:	1.055	STDEV:	1.017
RSD%:	1.058	RSD%:	1.015

The repeatability of the developed sample preparation protocol was also validated using 6 determinations on the sample loaded with 35% w/w NTX HCl prepared from EVA28.0 (MFI:25.00) by HME at the processing temperature of 130 °C, while the intermediate precision was determined over two days using another 6 determinations on a different day on the same sample. As can be seen in *Table 16*, the mean across 12 determinations prepared over 2 consecutive days was 34.62% w/w with a RSD% of 1.116, which considered acceptable for assay methods in the industrial environment, where the limit is generally 2% for RSD%.

Table 16 Repeatability and intermediate precision data for the sample preparation protocol related to NTX HCl HPLC assay from 12 determinations over two consecutive days

Precision	Measured drug content (w/w%)	
Preparation number	Day 1	Day 2
1	35.26	34.46
2	35.01	34.04
3	34.93	34.48
4	34.71	34.1
5	35.08	34.51
6	34.77	34.33
Mean:	34.64	
STDEV:	0.387	
RSD%:	1.116	

2.3.3 Development of the NTX HCl dissolution method

NTX HCl stability in different dissoultion media

Figure 17 demonstrates that the NTX HCl was stable for up to 7 days in purified water and 0.1M HCl stored at 37 °C as well as purified water stored at between 5 and 8 °C. However, significant degradation occurred after 1 day in phosphate buffered media, with the rate of

degradation being proportional to the increase in pH from 6.8 to 8.2. The NTX HCl in water solution stored at 37 °C showed an increase in some of the known and unknown impurity peaks, but their level was below the disregard limit and no new impurity peaks were identified. There was also no increase in the known impurity peaks and no new impurity peaks for the NTX HCl in 0.1M HCl stored at 37°C. The chromatograms for the NTX HCl in phosphate buffers of varying pH showed a significant increase in the known impurity peaks to well above the disregard limit, with the addition of new unidentified impurity peaks after 24 hours. Moving forward in the development, purified water was selected as release media for further investigations.

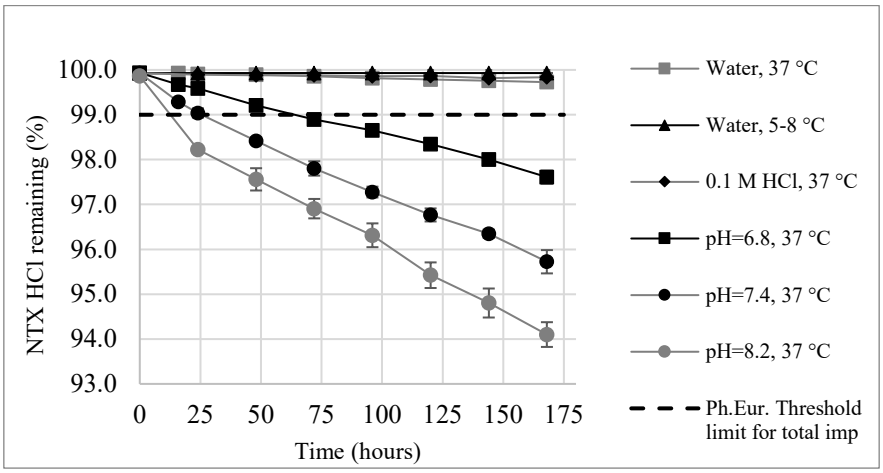


Figure 17 Stability of NTX HCl in different dissolution media. The dashed line represents the Ph.Eur. threshold limit for purity. Error bars represent ±1 standard deviations of n=3 replicates

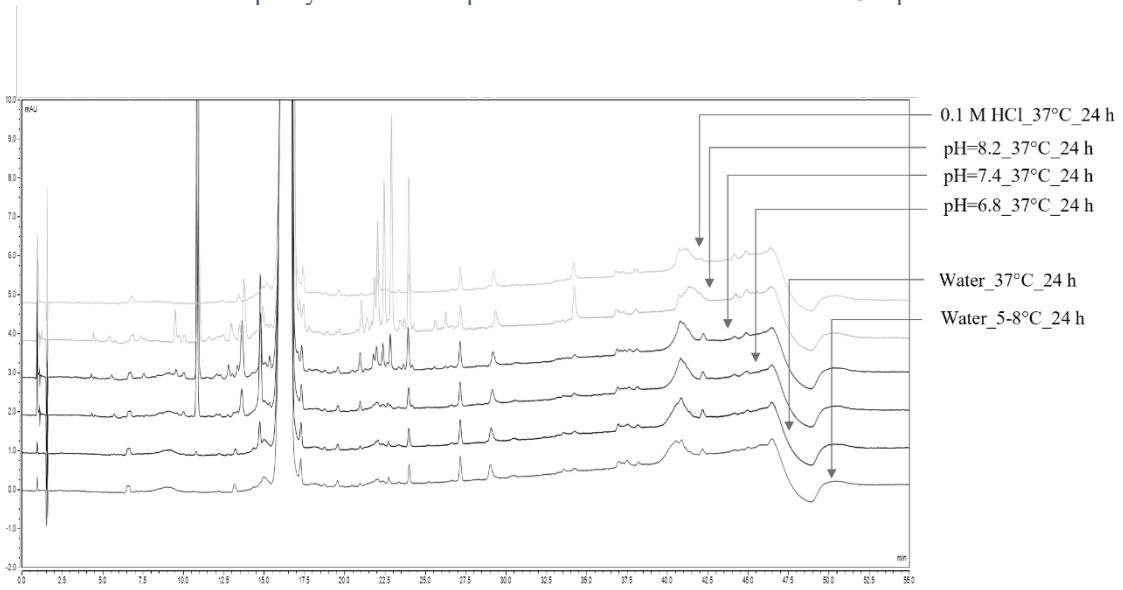


Figure 18 Example chromatograms of varying NTX HCl solutions after 24 h exposure at 37 °C/ 60 rpm

Determination of solubility of NTX HCl in water

The solubility of NTX HCl in water at 37 °C was shown to be 115.8±2.2 mg/mL (n=3).

2.3.4 The influence of EVA grade on the processability, stability and release of NTX HCl from the implants

Different extrusion temperature profiles along the barrel were required to produce implants with adequate quality depending on the grade of EVA applied. As indicated in *Table 6*, EVA28.1 (MFI:42.46) implants could be formulated at 110 °C, whereas EVA27.7 (MFI:2.89) based drug-polymer mixture had to be extruded at as high as 165 °C. In contrast, implants containing the EVA with the highest VA-content were easily manufactured at a processing temperature of 90 °C. After each extrusion batch, the barrel was opened and cleaned for the next experiment. During the cleaning processes, significant amounts of drug were visible adhering to the surface of the conveying elements, generally after the mixing zone in the case of batches produced from EVA27.7 and EVA39.1. This material wastage was noticeable in the measured average NTX HCl concentrations of the produced implants. The drug levels in the extruded implants measured by the validated HPLC assay method are presented in *Figure 19*. The results demonstrated that EVA implants with 28.1% VA-content contained the required amount of NTX HCl, while implants produced from EVAs with 39.1% and 27.7% VA-content had lower and more variable NTX HCl contents (n=4), indicating a significant level of inhomogeneity along and/or between the analysed rods.

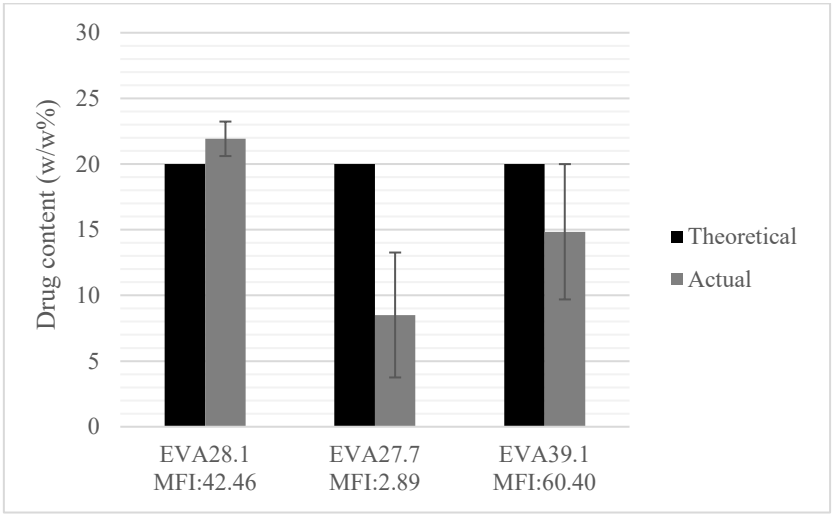


Figure 19 Actual and theoretical contents of NTX HCl in each of different EVA implants. Error bars represent ±1 standard deviations of n=4 replicates

The investigation of NTX HCl degradation in the extruded implants by the related substance HPLC method revealed that the content of different types of impurities (know and unknown) did not exceed the acceptable limits stated in the Ph.Eur. monograph related to NTX HCl in all cases (*Table 17*). However, in the case of EVA27.7 implants, which required the highest processing temperature (165 °C), a significant increase in total impurity content was detected,

mainly due to the increase of Impurity B (oxidative degradation product) and an unknown impurity (with unidentified chemical structure) on the measured chromatograms (data not shown).

Table 17 Summary of purity profiles of 20% w/w NTX HCl-EVA implants

Impurity	Average content (%) (n=3)			Ph.Eur. limit (%)
	EVA28.1 MFI:42.46	EVA27.7 MFI:2.89	EVA39.1 MFI:60.40	
Imp. A	< D.L.	< D.L.	< D.L.	0.1
Imp. B	< D.L.	0.07	< D.L.	0.1
Imp. C	0.02	0.03	< D.L.	0.2
Imp. D	< D.L.	< D.L.	< D.L.	0.2
Imp. E	0.04	0.04	0.04	0.2
Imp. F	< D.L.	< D.L.	< D.L.	0.2
Imp. G	no detection	no detection	no detection	0.2
Imp. H	< D.L.	< D.L.	< D.L.	0.1
Imp. I	< D.L.	< D.L.	< D.L.	0.1
Imp. J	< D.L.	< D.L.	< D.L.	0.1
Unknown Imp.	< D.L.	0.05	< D.L.	0.1
Total Impurity	0.06	0.19	0.04	1.0

"< D.L." = under disregard limit

In-vitro drug release of the implants was performed in purified water for 14 days at 37 °C. *Figure 20* shows the results of dissolution testing of the implants manufactured for this study. Implants produced from EVA28.1 (MFI:42.46) had more than 40% cumulative drug release in 14 days following a nearly perfect zero-order release pattern. At the same time, the other two investigated implants showed a significantly lower release rate, where only approximately 15% cumulative drug release was achieved. The EVA27.7 (MFI:2.89) implants also performed a nearly zero-order release over the period of the study, similarly to the EVA28.1 implants. The decreased release rate compared to EVA28.1 implants is most likely due to the significantly lower drug content that was measured. However, the EVA39.9 (MFI:60.64) implants released the embedded NTX HCl in a different manner. The related dissolution curve shows a linear increase up to day 5, from which time point the growth became slower but still constant. This release pattern can suggest some kind of structural changes in the matrix polymer during the release study, slowing the release kinetic of the formulated API.

Thermal investigation of EVAs using DSC resulted in distinct thermograms, as can be seen in *Figure 21*. In all cases, the thermograms showed a broad glass transition in the temperature range from approximately -48 °C to 0 °C. No significant shift could be seen in glass transitions. However, well-defined differences could be seen in the melting transitions of the 3 different

EVA polymers. EVA27.7 and EVA28.1 showed 2 well separated melting peaks, correlating with the lamellar thickness distribution of the crystalline domains, where the first endothermic peaks appeared at the same temperature (48 °C), while the second peaks differed with 5 °C to each other (70 °C and 75 °C). On the other hand, in addition to the melting peak at 48 ° C, the thermogram associated with EVA39.1 also has a melting peak at a lower temperature, at approximately 21 °C, overlapped with the polymer's broad glass transition. However, the offset of this transition appeared to be at 37.5 °C.

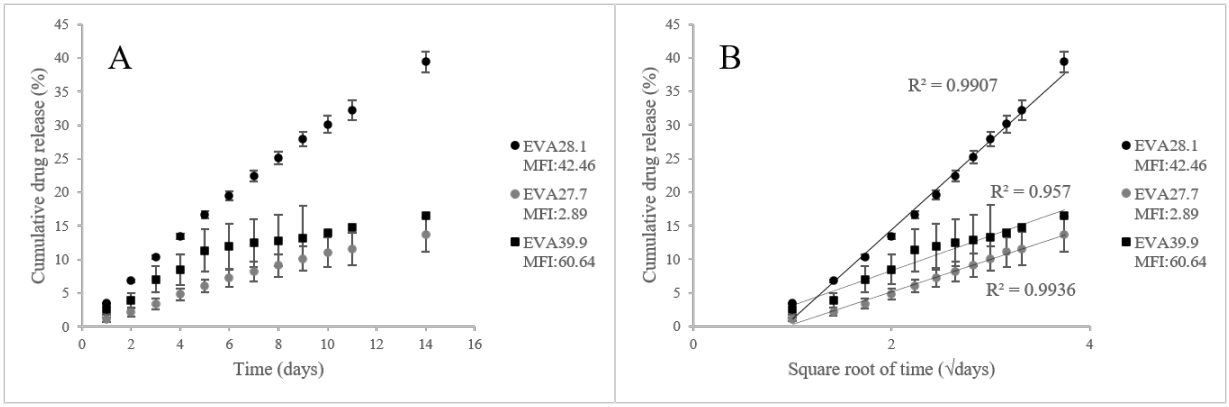


Figure 20 In vitro cumulative release (%) of NTX HCl vs. time (A) and *in vitro* cumulative release (%) of NTX HCl vs. square root of time (B) from 20% w/w drug-loaded implants manufactured using different grades of EVA. Error bars represent ±1 standard deviations of n=6 replicates

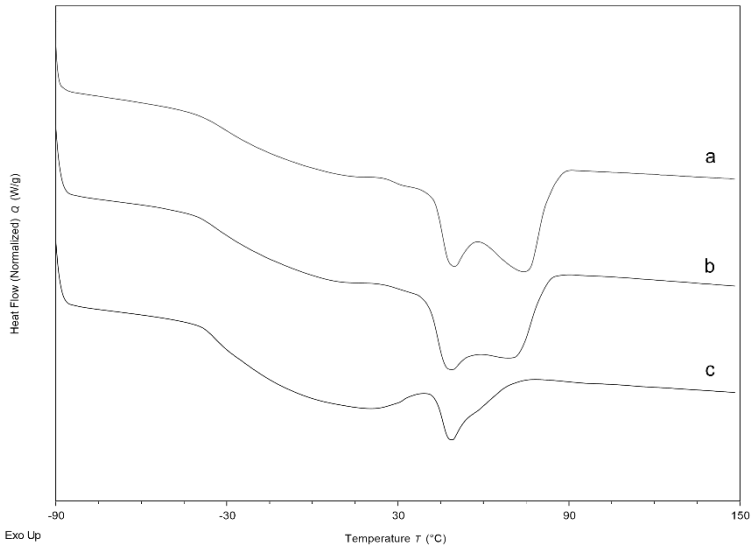


Figure 21 DSC thermogram of pure EVA27.7 (MFI:2.89) (a), EVA28.1 (MFI:42.46) (b) and EVA39.1 (MFI:60.64) (c)

2.3.5 The influence of drug loading on the processability, homogeneity, stability and release of NTX HCl

Rheological investigations of NTX HCl-EVA28 blends

HME processability of drug-polymer mixtures highly depends on their rheological properties. Therefore, several drug/polymer mixtures with varying drug levels were tested by dynamic oscillatory measurements to evaluate their processability and required processing temperature range. The tests were performed in a cooling mode, starting at 180 °C, almost 40 °C below the melting point of NTX HCl (227 °C). Two EVA polymers, EVA28.1 (MFI:42.46) and EVA28.0 (MFI:25.00), were chosen for this investigation. These polymers were presumed to be applicable for further development based on the results from the previous experiments.

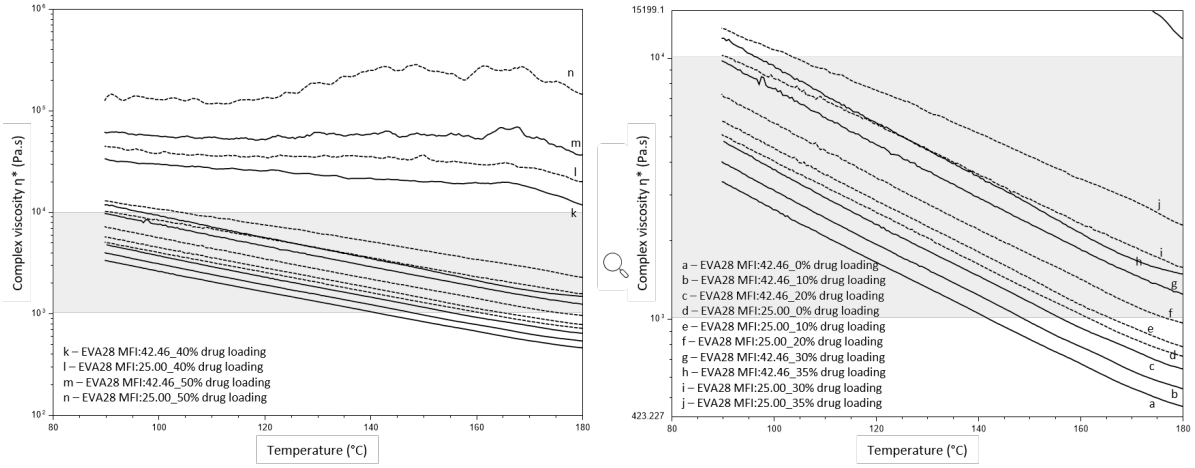


Figure 22 Effects of NTX HCl concentrations on complex viscosities of the both EVA28.1 (MFI:42.46) (solid lines) and EVA28.00 (MFI:25.00) (dashed lines) polymers in a function of temperature. The shaded area indicates the generally accepted viscosity range (10^3-10^4 Pa.s) for small scale extrusion[288].

Complex viscosities of the neat polymers and the drug-loaded mixtures as the function of temperature are shown in *Figure 22*. For EVA polymers and 10, 20, 35% w/w drug-loaded mixtures, the complex viscosities increased in almost a parallel manner with decreasing temperature. Furthermore, increasing NTX HCl concentration resulted in increased complex viscosity values due to an increase in the solid drug particle. The rheological difference between the two applied polymers is also well presented on the recorded data points. The EVA with a lower MFI value (25.00) showed higher complex viscosity compared to the EVA with a higher MFI value (42.46), even up to 50% w/w drug-loading.

Mixtures with 40 and 50% w/w NTX HCl concentration showed different rheological behaviours. In these cases, the detected rheograms were almost horizontal, which would suggest that these mixtures lost their elastic nature due to the large amount of solid NTX HCl they contain. These results were not surprising, as at such higher drug concentrations (40 and 50%

w/w), the determination of LVR by *oscillatory amplitude sweep* test was not possible at lower temperatures (90 and 135 °C) even under higher applied stress/torque conditions. However, at 180 °C, each system showed sufficient elasticity to measure their complex viscosity values by the used experiment setup. Complex viscosity of mixtures up to 35% w/w NTX HCl loadings was in the recommended range for optimal extrusion (10^3-10^4 Pa.s)[288] in a temperature range from approximately 100 to 150 °C. However, the viscosity of 40 and 50% w/w drug-loaded systems was greater than the generally accepted "rule-of-thumb" viscosity range.

Extrusion of NTX HCl-EVA28.1 (MFI:42.46) implants with varying drug loadings

Extrusion experiments aiming to explore the effects of drug loading was only performed with EVA28.1 (MFI:42.46) as the available amount of EVA28.0 (MFI:25.00) was limited. For this study a die with diameter of 3 mm was applied. Depending on the drug loading of the produced NTX HCl-EVA28 (MFI:42.46) implants, differing processing temperatures were required for the extruder (*Table 7*) to obtain sufficient quality. The manufacturing temperatures were highly influenced by drug loadings, with the lower NTX HCl concentration requiring lower processing temperatures. The surface structure of the extrudates was also influenced by drug loading. While implants with NTX HCl concentrations up to 35% w/w could be processed into smooth-surfaced extrudates over a processing temperature range from 100 to 130 °C, it was not possible to obtain extrudates with similar quality when higher API concentrations (40 and 50% w/w) were used, even at higher processing temperatures. In these cases, extrudates showed a "shark-skin" surface structure (pictures are not shown). However, higher drug-loaded implants could be produced at increased processing temperature (up to 145 °C). It must be noted that applying extrusion temperatures above 150 °C resulted in a significant discolouration, and cracks were seen on the extrudates. Therefore, these samples were not part of further examinations.

Among the extruded products, implants with NTX HCl up to 40% w/w showed acceptable average content and homogeneity (*Figure 23* and *Figure 24*). The values did not exceed the predefined ±10% acceptance limit to the expected theoretical concentration. However, the 50% w/w drug-loaded implants could only be produced with lower and more variable NTX HCl levels, even after several attempts. Although increased processing temperatures were required to produce samples with higher drug loadings, the measured degradation profiles of the formulated API did not show a significant increase in degradation products in any cases. As shown in *Figure 25*, the total amounts of impurities were far below the acceptable 1.00 % total impurity limit, given in the Ph.Eur. monograph related to NTX HCl. In addition, none of the

detectable known and unknown impurities exceeded their specified content limit (data are not shown).

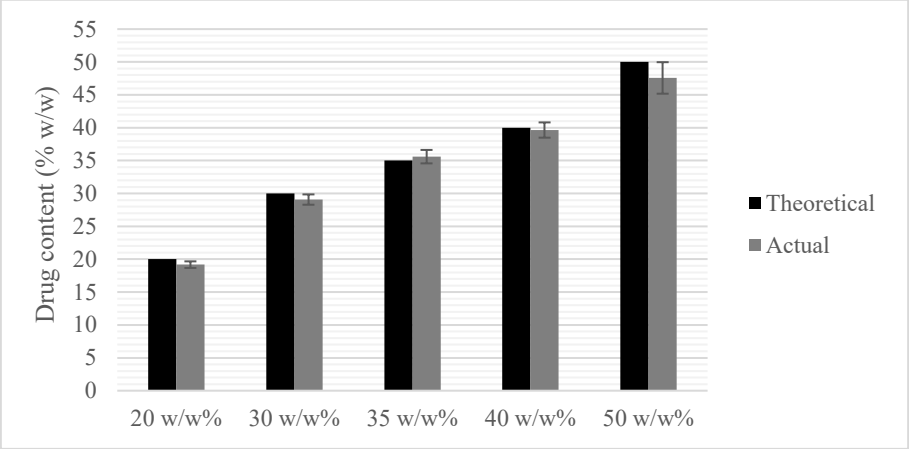


Figure 23 Actual and theoretical contents of NTX HCl in each of the different drug loaded EVA implant batch. Error bars represent ±1 standard deviations of n=4 replicates.

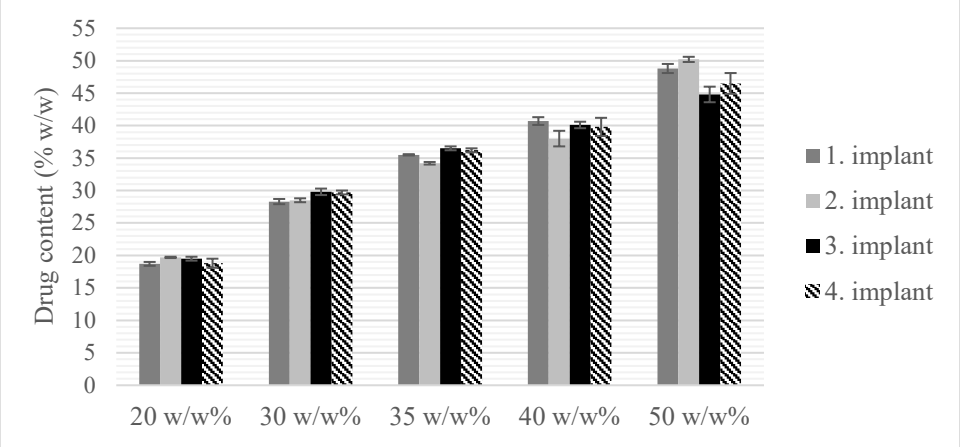


Figure 24 Homogeneity of NTX HCl between the 4 different sections of each implants with different theoretical drug loadings. Error bars represent ±1 standard deviations of n=4 replicates.

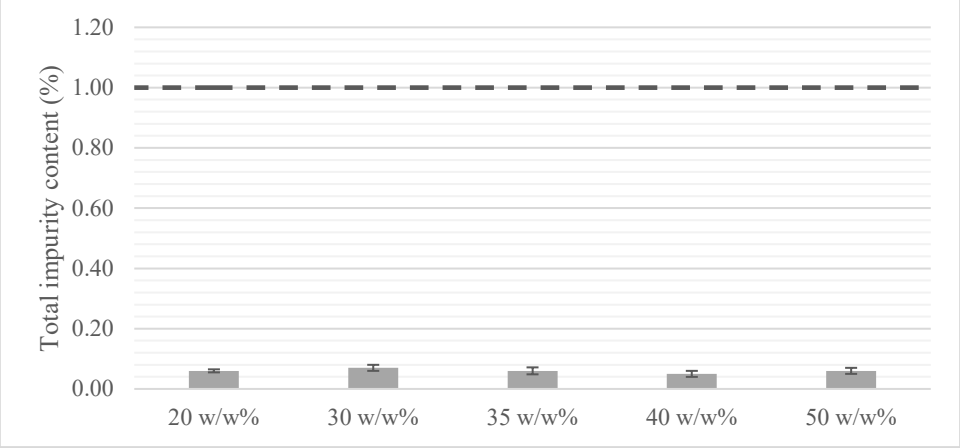


Figure 25 Total impurity content of EVA28-NTX HCl implants with varying drug loadings. The dashed line represents the 1.00% Ph. Eur. threshold limit for total impurity content. Error bars represent ±1 standard deviations of n=3 replicates.

Morphological characterisation of extrudates produced from EVA28.1 (MFI:42.46) with varying drug loadings

DSC measurements were performed in order to investigate the physical state and the morphology of NTX HCl and the matrix polymer. The DSC scans of pure NTX HCl, EVA28.1, and the extruded samples with a drug loading of 20, 30, 40 and 50% w/w are shown in *Figure 26*. Thermograms of the extruded products showed a well-defined melting peak at around 227 °C related to the crystalline ratio of NTX HCl. The measured normalised enthalpy values related to the melting of crystalline NTX HCl is summarised in *Table 18*. Based on the calculated crystallinity values, it could be assumed that a significant portion of the formulated NTX HCl converted to its amorphous state or molecularly dispersed (dissolved) into the molten matrix during the extrusion, which remained stable in the extruded products until the investigations. It can also be concluded that as the drug loading increased, the amorphous or dissolved fraction of the NTX HCl content in the extruded products decreased. At 50% w/w drug loading, the extent of amorphization or dissolution was only 3%, while at 20% w/w drug loading, almost 25% of the formulated NTX HCl went through physical state changes. The DSC curves also show that in all cases, where the tested sample contained the matrix polymer, the glass transitions associated with the amorphous ratio of EVA28.1 appeared in the same temperature range, with the inflexion point of approximately -31 °C. No significant shifts could be seen related to this type of phase transitions. The measured thermograms also revealed a slight change in the crystalline structure of the matrix polymer after the extrusion process. While 3 well-defined melting peaks related to 3 different crystalline types of EVA28.1 appear on the thermogram of the pure EVA28.1 at 31, 46 and 69 °C, the heating curves of the extruded samples showed only 2 well-separable peaks in the same temperature range (20-100 °C) at around 46 and 69 °C.

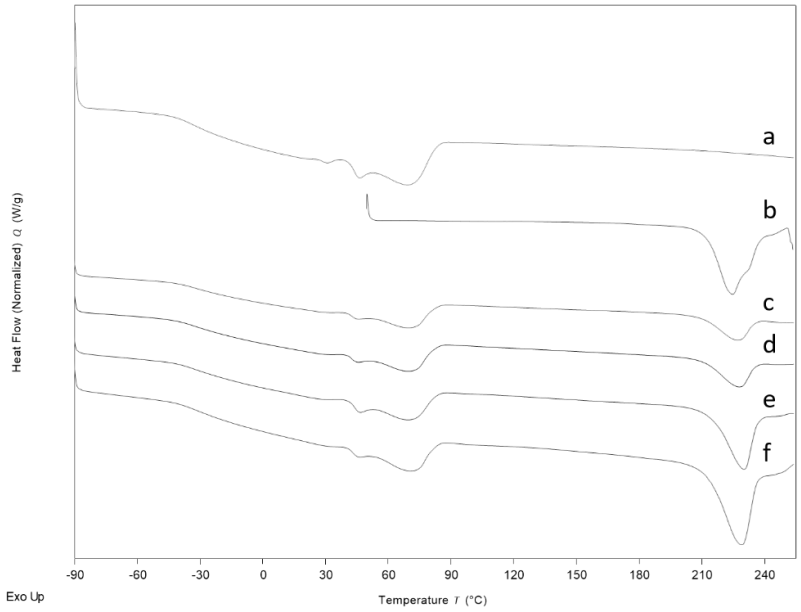


Figure 26 DSC thermograms of pure EVA28.1 (a), NTX HCl (b) and extrudates of NTX HCl-EVA28.1 systems with 20 (c), 30 (d), 40 (e) and 50% w/w drug loadings

Table 18 Normalised melt enthalpy and calculated crystallinity of NTX HCl

Sample	Melt enthalpy, ΔH (J/g)	Calculated crystallinity of NTX HCl (%)
Pure NTX HCl	51.76	100.00
20% w/w extrudate	38.56	74.50
30% w/w extrudate	40.00	77.28
40% w/w extrudate	47.74	92.23
50% w/w extrudate	50.29	97.17

SEM images of the cross-section of the implants showed that NTX HCl and EVA28.1 form well-separable phases in the products, demonstrating that the HME process produced monolithic dispersion systems in all cases (*Figure 27*). The EDX spectra, recorded from several points in the SEM images, showed the signals of Cl atoms presented in the dispersed NTX HCl particles, which appeared with no or only reduced intensity in the areas recorded from the matrix polymer (*Figure 28*). The SEM images also revealed the differences in the drug particle sizes and shapes. Some areas on the SEM images showed larger drug crystals with well-defined edges, while other parts of the cross-section showed smaller particles with a flocculent structure. It can also be stated that although the distribution of the NTX HCl particles could be considered homogeneous in the cross-section of the extrudates, in some areas, especially at

higher drug concentrations, several drug particles were present together, forming enriched clusters in the system.

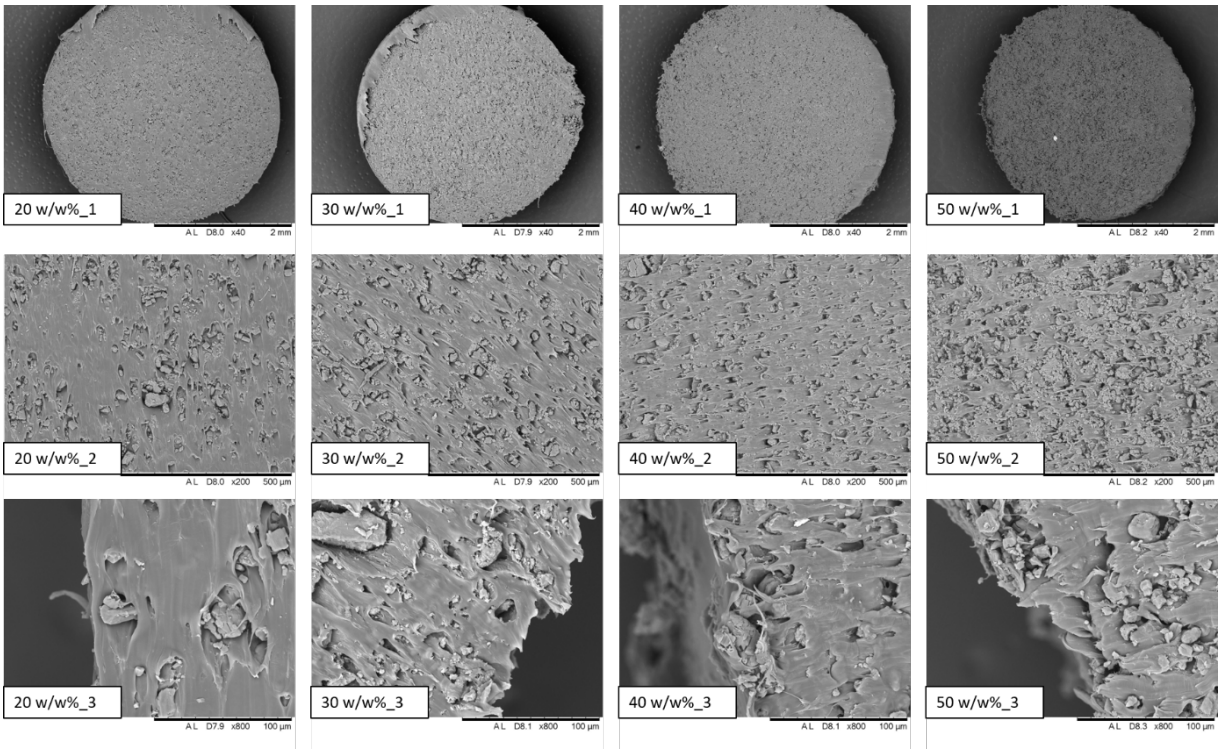


Figure 27 SEM images of cross-sections of NTX HCl-EVA28.1 implants with varying drug loadings. The images in the first row were taken at 40x magnification from the cross-section of the implants. The images in the second row represent 200x magnification from the centre (bulk) of the cross-sections, while the third row shows images taken from the edges of the implants at 200x magnification.

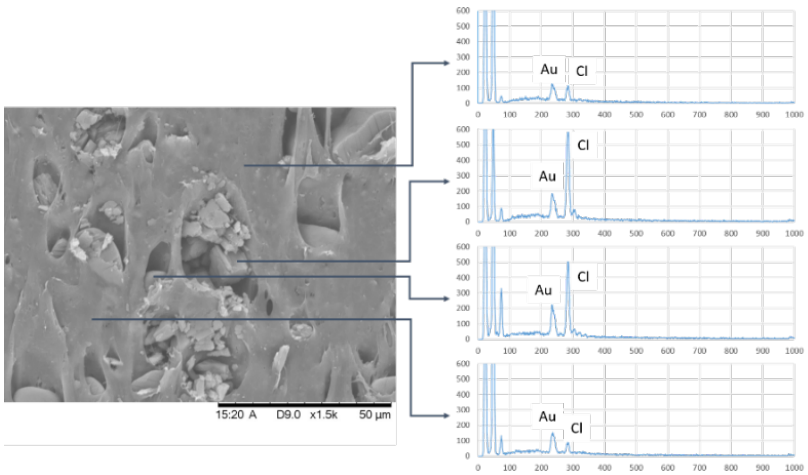


Figure 28 Energy-dispersive X-ray spectra recorded from several points in the cross-section of 30% w/w NTX HCl EVA28 (MFI:42.46) implant

In vitro characterisation of extrudates produced from EVA28.1 (MFI:42.46) with varying drug loadings

Drug release from the produced extrudates with increasing drug loadings was performed in demineralised water at 37 °C. The percentage cumulative drug release profiles are presented in *Figure 29*, *A_1 and A_2*.

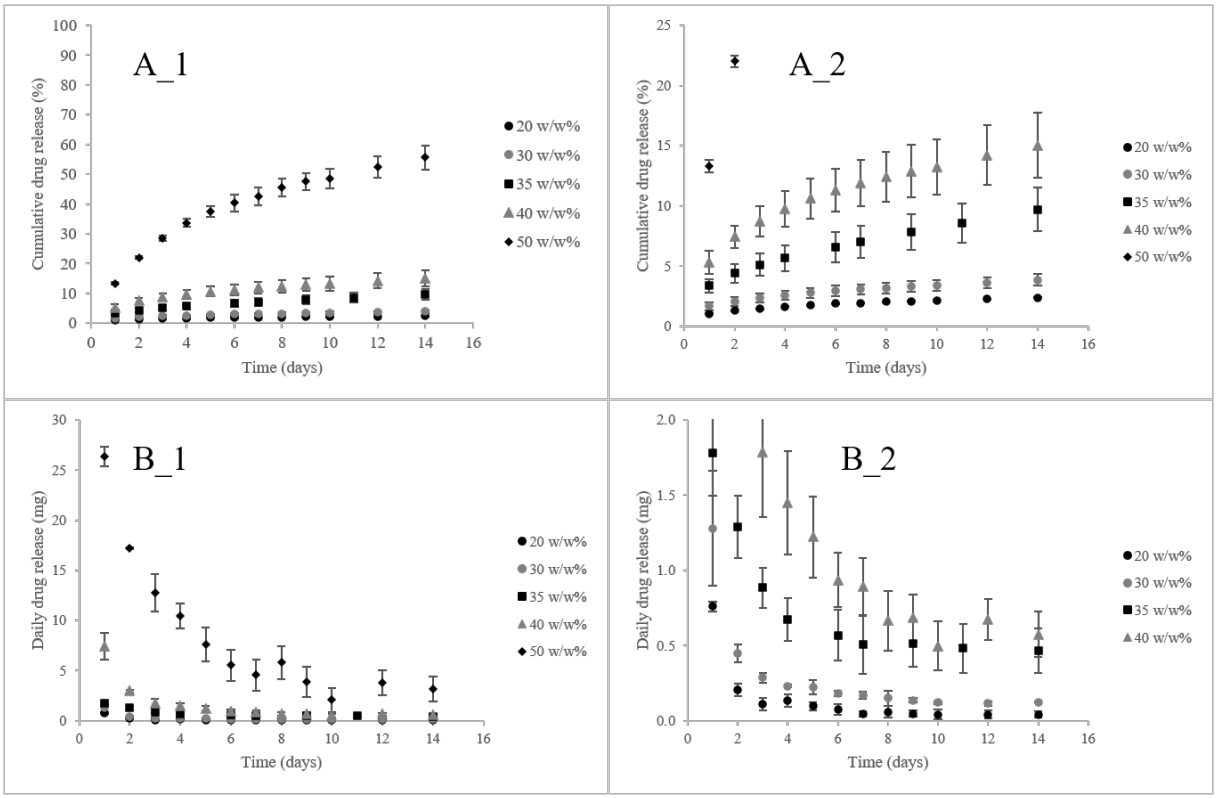


Figure 29 In vitro release of NTX HCl from NTX HCl-EVA28 (MFI:42.46) implants containing different drug loadings. (A_1 and A_2) Total NTX HCl released over time (% total ± 1 SD; n=4/group). (B_1 and B_2) NTX HCl release rate over time (mg released/day, ± 1 S.D.; n=4/group). Figures with sign 2 represent the magnification of figures wih sign 1.

Each system had a relatively large NTX HCl 'burst' release after the first day, followed by a gradual decrease in release on subsequent days, as expected from matrix-type drug delivery systems. The release profiles also demonstrate that as the NTX HCl loading was increased, the release increased substantially in all cases. In particular, for the implants with 50% w/w drug loading, the cumulative release was approximately 22% in the first 2 days with more than 50% of the embedded drug content released within 14 days, whereas the release from implants with lower drug loadings showed significantly lower drug release rates. Even the 40% w/w implants showed only ~15% cumulative drug release after 14 days, while at the lowest (20% w/w) drug loadings, the released drug amount did not exceed 3% after two weeks. The release rates of NTX HCl from the implants over 14 days, expressed as mg/day, are illustrated in *Figure 29, B_1* and *B_2*. The profiles clearly show, that the initial drug concentrations influenced the

magnitude of the initial "burst" release. 50% w/w loading in the implants resulted in 26.40±0.98 mg (13.3±0.49%) released NTX HCl after the first day of the experiment, while 20, 30, 35 and 40% w/w implants released approximately 0.8±0.03 mg (1.03±0.04%), 1.28±0.38 mg (1.66±0.35%), 1.78±0.40 mg (3.38±0.55%), and 7.45±1.30 mg (5.32±0.93%) of NTX HCl, respectively, over the same period. As can also be seen on the daily release profiles, after the significant decline in the first 5 to 8 days, the release rates stabilised by day 8 for implants with drug-loading of 20, 30, 35 and 40% w/w resulting in approximately 0.05, 0.10, 0.50 and 0.60 mg/day release rate, respectively. In contrast, 50% w/w drug-loaded implants showed almost continuously declining daily release over the time of the study.

Following the completion of the in vitro study, the implants were dried for 2 days at room temperature. SEM images of the cross-sections of the dried implants clearly showed the pores formed near the surface of the implants, which remained after the drug particles dissolved over the time of the experiment (*Figure 30*). It can also be seen in the images that the porous structure formed by dissolving the NTX HCl particles remained stable and did not collapse over the release study. Furthermore, both the pores' size and the porous structure's radial depth left behind increased with increasing initial drug concentration.

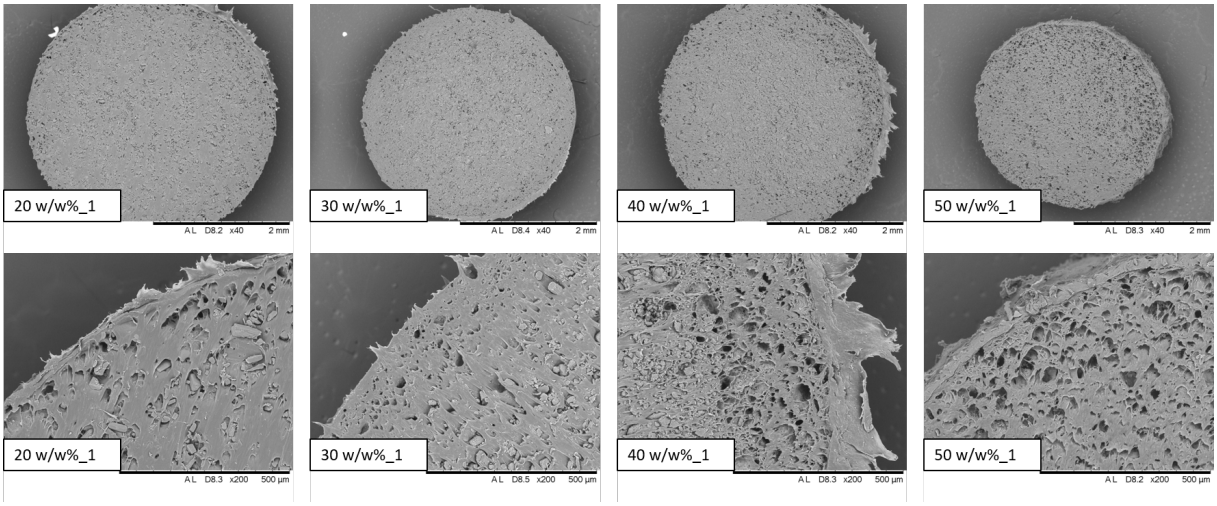


Figure 30 SEM images of cross-sections of NTX HCl-EVA28.1 implants with varying drug loadings after 14 days *in vitro* release study. The images in the first row were taken at 40x magnification from the cross-section of the implants. The images in the second row represent 200x magnification from the centre (bulk) of the cross-sections, while the third row shows images taken from the edges of the implants at 200x magnification.

In order to investigate the drug release mechanism from the implants, the release data obtained from the *in vitro* release experiment were separately fitted to two mathematical models, i.e., the Higuchi model and the Korsmeyer-Peppas model. As each implant released less than 60% of their initial drug content and significant dissolution or swelling of the hydrophobic matrix polymer did not occur under the applied experiment conditions, the models mentioned above

were considered applicable to describe the drug release mechanism. The calculated parameters for both models are summarized in *Table 19*. The evaluation of the r^2 values indicates that the dissolution kinetics obeyed the semi-empirical "*square-root-of-time law*" of Higuchi and the "*power law*" of Korsmeyer and Peppas, demonstrating that the NTX HCl released from the cylindrical implants by diffusion at each concentration level.

Table 19 Results of mathematical models fitting for the release rate of NTX HCl loaded implants at different drug loadings

Drug loading (% w/w)	Higuchi model $M_t/A=k_H*t^{1/2}$		Korsmeyer-Peppas model $M_t/M_\infty=k*t^n$	
	slope	r^2	n	r^2
20	0.090	0.983	0.304	0.998
30	0.214	0.995	0.317	0.999
35	0.716	0.998	0.398	0.997
40	1.222	0.992	0.365	0.998
50	7.644	0.979	0.461	0.992

The dissolution kinetics of the implants was predicted up to 90 days by extrapolating the models fitted to the 14 days long averaged *in vitro* data to give a rough estimation about the amount of NTX HCl released for extended periods. The predicted release profiles are presented in *Figure 31*. As can be seen, generally, the Higuchi model estimated higher release values than the Korsmeyer-Peppas model. According to the calculations, the Higuchi model predicted 35, 22, 8 and 5% cumulative drug release by day 90 for 40, 35, 30 and 20% w/w implants, respectively. At the same time, the Korsmeyer-Peppas model estimated 30, 21, 7 and 4% release for 40, 35, 30 and 20% w/w implants, respectively, over the same period. The used two models can be applied only up to 60% cumulative drug release. Therefore the prediction of the release kinetic of the 50% w/w drug-loaded sample is presented on the figure only up to 15 days. However, the Higuchi model predicted 100% release at 43 days, whereas the Korsmeyer-Peppas model estimated complete dissolution at 47 days for the samples with the highest initial drug concentration. The predicted daily drug release profiles of the 35 and 40% w/w samples clearly show a declining release rate over time, which roughly estimated 0.2 and 0.4 mg/day drug release at day 40 and 0.15 and 0.25 mg/day by day 90 calculated by the Higuchi model for the 35 and 40% w/w drug loadings, respectively.

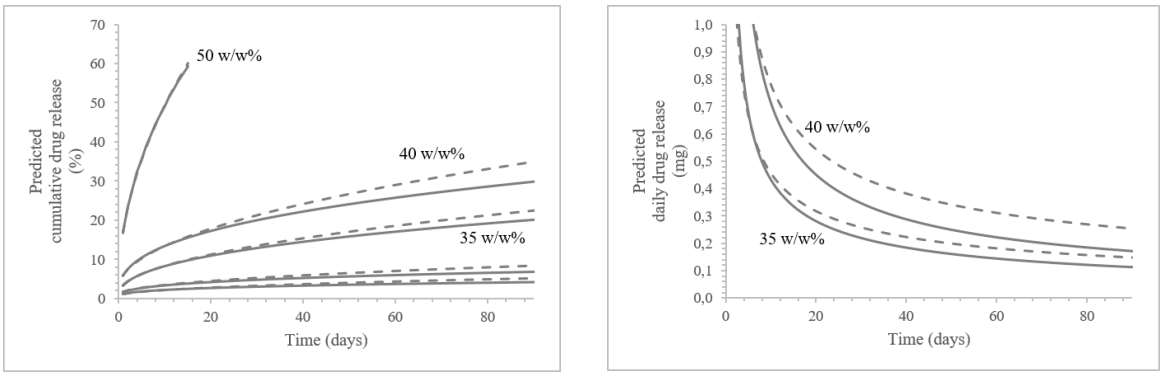


Figure 31 Predicted per cent cumulative release (left side) and predicted daily release (mg) (right side) of NTX HCl from implants according to Higuchi (dashed line) and Korsmeyer-Peppas (solid line) model fitted to the experimental data from the 14 days long *in vitro* release study

Based on these results, further investigations focused on 35 and 40% w/w implants because preferable sustained NTX HCl release could only be obtained at these drug loadings.

Comparison of Ø=3 mm implants produced from EVA 28.0 (MFI:25.00) and EVA28.1 (MFI:42.46) with 35% w/w NTX HCl loading

The previous *in vitro* dissolution study demonstrated that only the implants with 35 and 40% w/w drug concentrations showed presumably sufficient release profiles for further investigations. The EVA28.1 (MFI:42.46) matrix polymer from Celanese Corp. was used to prepare these samples. However, in further clinical studies, using a matrix polymer manufactured under GMP conditions was highly recommended. Unfortunately, only a limited amount of EVA28.0 (MFI:25.00) was available from Polysciences Corp. for this purpose. In order to investigate whether the implants made from the EVA polymer with the same VA-content but with significantly lower MFI value show the same performance, the preparation of samples by the use of GMP compliant EVA28.0 (MFI:25.00) matrix polymer was attempted at 35 and 40% w/w NTX HCl concentration levels.

While the 35% w/w batch was extrudable at a processing temperature of 130 °C, the 40% w/w sample could not be produced even at higher temperatures (up to 150 °C) with the extruder used. The prepared 35% w/w samples showed acceptable average drug content and similar homogeneity with the EVA28.1 (MFI: 42.46) implants with the same NTX HCl concentration (*Figure 32* and *Figure 33*).

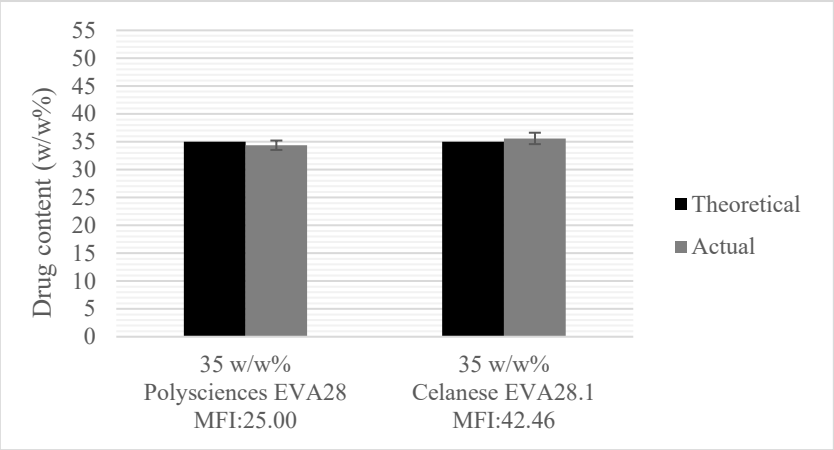


Figure 32 Actual and theoretical contents of NTX HCl in the 35% w/w NTX HCl loaded implants produced from EVA28.0 (MFI:25.00) and EVA28.1 (MFI:42.46). Error bars represent ±1 standard deviations of n=3 replicates.

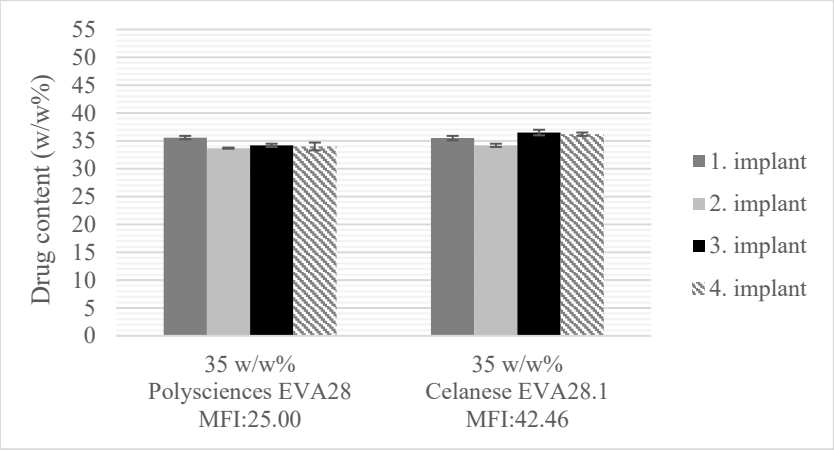


Figure 33 Homogeneity of NTX HCl between the 4 different sections of each implants produced from EVA28.0 (MFI:25.00) and EVA28.1 (MFI:42.46). Error bars represent ±1 standard deviations of n=4 replicates.

Although the total NTX HCl impurity content measured in the prepared implants were also well below the acceptable 1 % limit, the content of Impurity B (4,5α-epoxy-3,14-dihydroxymorphinan-6-one; noroxymorphone), an oxidative degradation by-product showed a significant increase compared to the implants made of EVA28 with the same NTX HCl concentration (data are not shown) (*Figure 34*). In addition, DSC measurements for the implants produced from the Polysciences EVA with a lower MFI value (25.00) showed no endothermic peak at the melting temperature of the formulated NTX HCl (227 °C), indicating that the drug went through complete amorphisation during the process (*Figure 35*). The measured thermogram also showed a slight difference in the crystalline structure of the extruded Polysciences EVA. The melting peaks of EVA appeared on the thermogram related to the Polyscience implant with a slight shift compared to the extrudate made of Celanese EVA polymer.

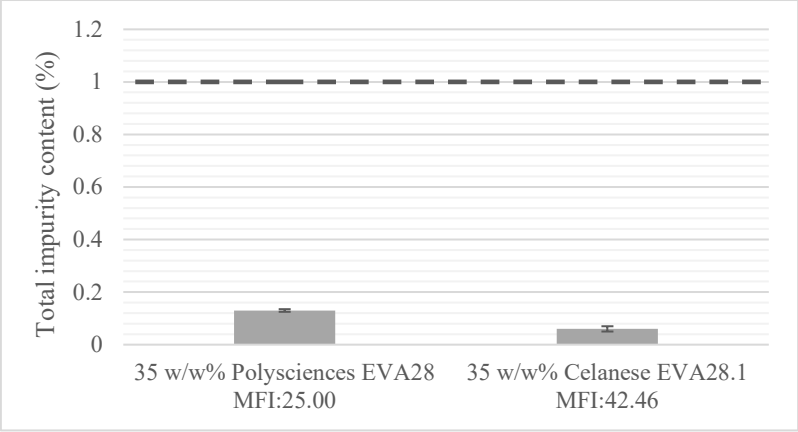


Figure 34 Total impurity content of 35% w/w implants produced from EVAs with MFI:25.00 and MFI:42. The dashed line represents the 1.00% Ph. Eur. threshold limit for total impurity content. Error bars represent ±1 standard deviations of n=3 replicates.

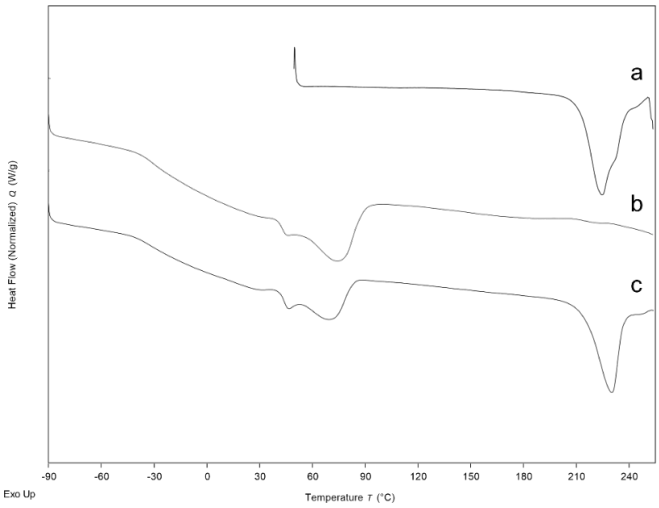


Figure 35 DSC thermograms of pure NTX HCl (a) and 35% w/w extrudates produced from EVAs with MFI:25.00 (b) and MFI:42.46 (c)

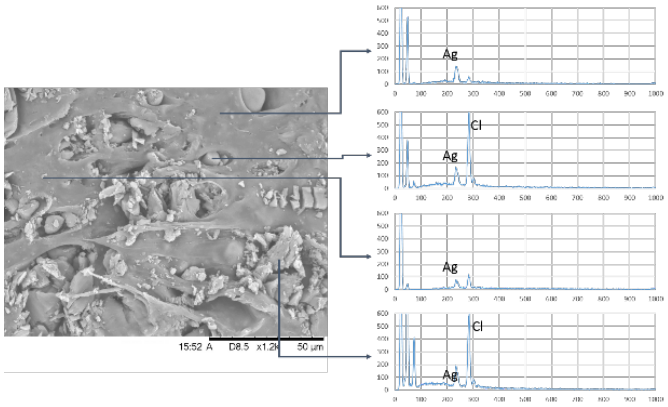


Figure 36 SEM image and energy-dispersive X-ray spectra recorded from several points in the cross-section of 35% w/w NTX HCl EVA28 (MFI:25.00) implant

Furthermore, the two types of implants with a drug loading of 35% w/w produced from Polysciences EVA28 and Celanese EVA28 had a similar release pattern as shown in figure, no significant ($p<0.05$) differences could be seen on the two release profiles (*Figure 37*).

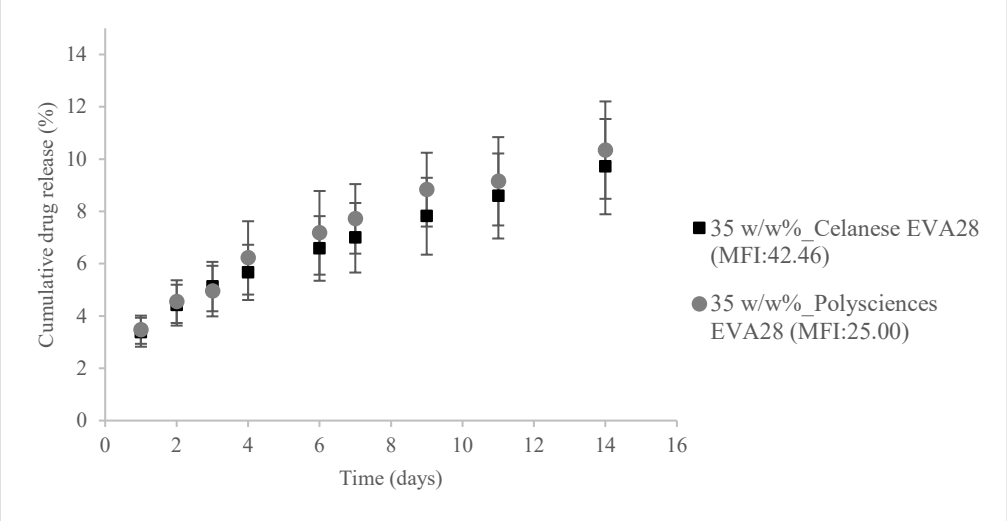


Figure 37 In vitro cumulative release (%) of NTX HCl vs. time from 35% w/w drug-loaded implants manufactured using EVA28.0 (MFI:25.00) and EVA28.1 (MFI:42.46). Error bars represent ±1 standard deviations of n=6 replicates

It should also be noted that the flexibility of the both 35% w/w implants produced from the two different types of EVA matrix polymer was found to be similar and suitable for clinical use by the four individuals who were included in the first flexibility study involving the blank implants (*Section 2.3.1*).

2.3.6 *In vivo* performance of the produced NTX HCl-EVA28 implants

The implants were assessed for their local tolerance, *in vivo* drug release and dose-ranging influence in a dog model according to the study design described in *Table 8*. All dogs tolerated the implant procedure well throughout the 29-day study period. However, significant swellings were observed around the implantation sites on all animals as early as the fourth day after the surgical procedure. The macro- and histopathological examination of the surrounding tissue areas performed after 4 weeks of treatment revealed capsule formation around the implants and dose-related subcutaneous inflammation and granulomas in the surrounding tissues. At implant site 1 (left flank), histomorphological changes were observed with increased incidence and severity in groups PK2 and PK4 (animals exposed to 35 and 40% w/w drug-loaded implants, respectively), compared to the other groups (PK1 and PK3) that received a placebo treatment only. In contrast, inflammation at implant site 2 (right flank) was detected with similar incidence in all four study groups. However, the severity and/or extent of the inflammation at

implant site 2 was increased in dogs from groups PK3 and PK4 that received 40% w/w drug-loaded implants. Subcutaneous granulomas were also observed at the right flank implant site in dogs in groups PK3 and PK4.

Plasma NTX levels following subcutaneous implantation of placebo and drug loaded EVA rods in the 8 dogs involved in this study are depicted in *Figure 38*. With the exception of group PK1 animals, NTX concentrations were quantifiable out to the last measured time point at approximately 692 hours post implantation. For group PK1 the NTX blood concentrations were under the limit of quantitation (0.2 ng/mL) at the 360 hour time point. Generally, plasma levels achieved C_{max} within 6 hours after implantation in almost all dogs, ranging from approximately 1 ng/mL in group PK1, to approximately 4 ng/mL in group PK2 and around 11-12 ng/mL in group PK4. Considering the data related to subject PK3_1 as an outlier, the extent of exposure as estimated by the mean AUC was the highest in group PK4, at approximately 2000 ng.h/mL. Mean AUC_{0-t} for group PK2 and PK1 were around 380 and 58 ng.h/mL, respectively.

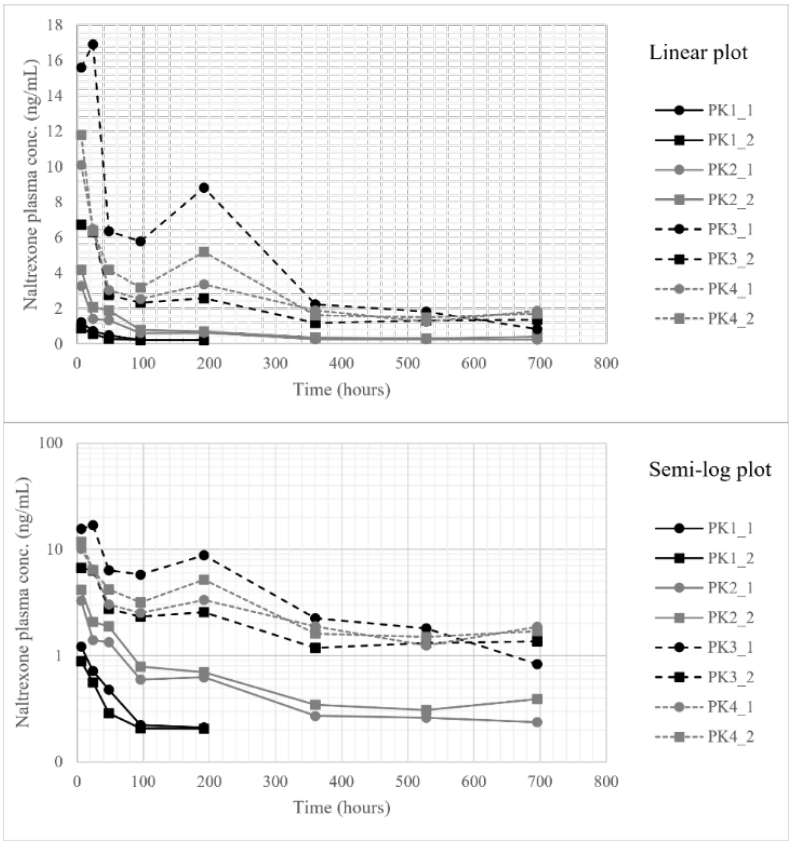


Figure 38 Plasma NTX concentrations in dogs after subcutanoeus implantation

The pharmacokinetic data are summarised in *Table 20*. According to the measured blood concentration results, it can be stated that the mean AUC_{0-t} across the groups did not appear to be proportional with the expected overall NTX exposure based on the initial drug concentration

in the implants. However, the total NTX HCl exposure calculated by the determination of the remaining NTX HCl content in the retrieved implants from the animals after the study (*Table 21*) showed correlation with the AUC_{0-t} results. As can be seen in *Figure 39*, higher amount of NTX HCl released *in vivo* from the implants developed higher AUC_{0-t} values. Interestingly, the point related to the animal marked as PK3_1 was highly out of trend. Additionally, the total NTX HCl released amount calculated from the residual drug concentrations of the explanted implants clearly show that higher initial drug concentrations delivered higher proportions of NTX HCl *in vivo*.

Table 20 Pharmacokinetic parameters of NTX following subcutaneous administraton over 29 days

Group/ # of dog	C_{max} (ng/mL)	T_{max} (hours)	AUC_{0-t} (ng.h/mL)
PK1_1	1.22	6	73.0
PK1_2	0.886	6	42.6
		Mean:	57.8
PK2_1	3.27	6	308.0
PK2_2	4.17	6	453.0
		Mean:	380.5
PK3_1	16.9	24	3100.0
PK3_2	6.72	6	1350.0
		Mean:	2225.0
PK4_1	10.10	6	1670.0
PK4_2	11.80	6	2010.0
		Mean:	1840.0

Table 21 Residual drug contents for NTX HCl-EVA28 rods after in vivo release and calculated total NTX HCl exposure

	Implant 1 (left flank) Drug content (%w/w)		Implant 2 (right flank) Drug content (%w/w)		
Group/ # of dog	Theoretical loading of NTX HCl before implantation*	Actual loading of NTX HCl after explantation**	Theoretical loading of NTX HCl before implantation*	Actual loading of NTX HCl after explantation**	NTX HCl released*** (mg)
PK1_1	Placebo	-	30.00	23.13	25.419
PK1_2		-		21.63	30.969
PK2_1	35.00	25.19	35.00	25.73	70.596
PK2_2		25.35		25.98	69.079
PK3_1	Placebo	-	40.00	8.43	116.809
PK3_2		-		18.30	80.29
PK4_1	40.00	22.85	40.00	24.90	119.325
PK4_2		18.88		24.64	134.976

* Based on the batch characterisation

** Drug concentration of the rods analysed by the in-house developed HPLC assay method

*** Based on an approximate total weight of 370 mg/implant

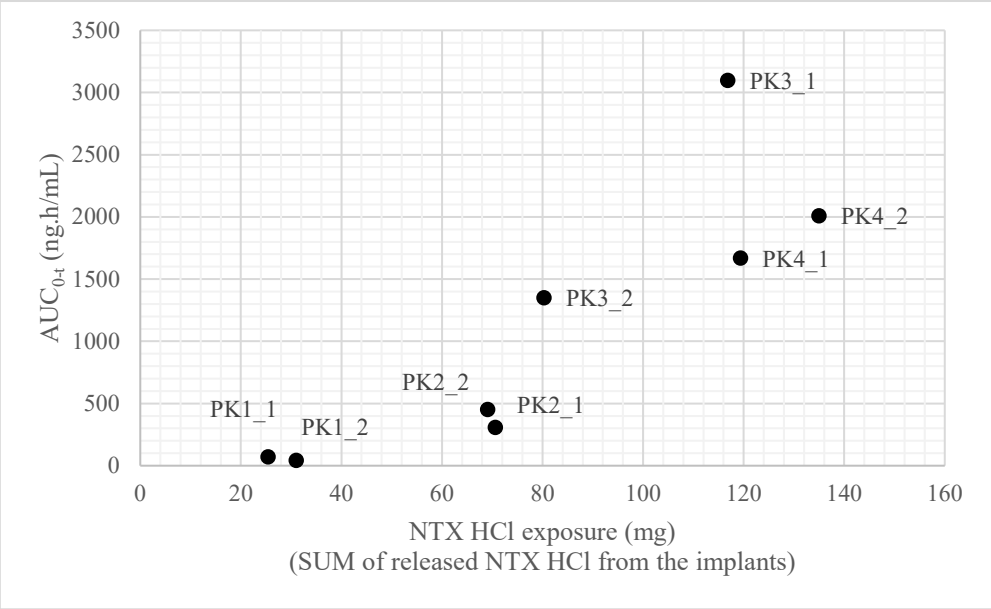


Figure 39 Total NTX HCl exposre vs. AUC_{0-t}

2.4 Discussion

Flexibility of blank implants

The differences in the flexibility of the blank implants could be well detected by the applied 3-point bending test. The results clearly showed that the diameter of the rods and VA-content of the applied EVA polymers had a great influence on the level of flexibility (*Figure 10* and *Figure 11*). EVA has a semi-crystalline structure, consists of crystalline and amorphous regions. The VA-groups inhibit crystallization of the polyethylene chain segments through steric hindrance by acetate side chains, enabling variation of softness and crystallinity of EVA without the addition of low molecular weight plasticizers. As the VA-content increases, the volume of the amorphous regions with higher molecular mobility increases that results in an increase in flexibility[289]. Another attribute that generally has a great influence on the physical properties of polymers is their molecular weight or molecular weight distribution. MFI value is practical measure for the ease of flow of melted plastics at fixed, standardized pressure and temperature. Usually, this value is considered as an indirect measure of molecular weight and viscosity of the polymer. The higher MFI value corresponds to low molecular weight and low viscosity[290]. As shown by the flexibility data for EVA27.7 (MFI: 2.89), EVA28.0 (MFI: 25.00) and EVA28.1 (MFI: 42.46), the effect of the MFI value on the flexibility became significant only at the level of 2.89, at constant (approximately 28%) VA-content. This data is consistent with those reported in the technical data brochure for DuPont™ Elvax® EVA polymers with VA-content of 28%, where polymers with MFI value of 3 has an elastic modulus of 28 MPa, whereas

polymers with MFI values of 25 and 40 have an elastic modulus of 18 and 19 MPa, respectively[291].

The Nexplanon placebo implant was used as a reference, which has demonstrated user acceptability in relation to comfort and insertion. Nexplanon is a commercially available subdermal contraceptive implant with a dimension of 4 cm in length with a diameter of 2 mm. The flexibility limit was set to have 50% of the Nexplanon placebo implant. Only 4 types of rods met this criterion. However, the visual inspection conducted by 4 independent people demonstrated sufficient flexibility for 6 further blank implants (*Table 9*). This study demonstrated that the predetermined limit for implant flexibility was quite stringent. Thus, in the following, the results from the measurements aimed at the flexibility/elasticity of the implants were used only for batch-to-batch comparison and no conclusions regarding clinical application were drawn from the data.

Development of reversed phase HPLC methods and sample preparation protocols

The primary objective of developing and maintaining adequate product quality is to maximize the therapeutic efficacy and safety of the formulated drug compound. Ensuring consistent quality can only be achieved by analyzing the critical quality attributes of the drug products (e.g., drug content, purity content and drug release) with reliable and accurate analytical protocols. Today, as it has become an essential requirement for the manufacturers to follow the Good Manufacturing Practice (GMP) guidelines consistently, laboratories need to demonstrate that the chosen analytical methods and protocols are fit for their purpose[292]. Namely, they must be validated. For these reasons, the analytical protocols used in this project were validated according to the ICHQ2 guideline[287].

Our measurements described in *Section 2.3.2* demonstrated that both the analytical protocols developed for the determination of the NTX HCl content and its impurity profile in the implants had adequate performance characteristics that made them suitable to support the development of the NTX HCl implants.

Development of an *in vitro* dissolution method

One of the most important requirements for a dissolution method is that the concentration values measured correspond to the actual concentration values in the dissolution medium. This can only be ensured if the active substance does not go through any significant degradation during the test, reducing the accuracy of the determination[293]. Our study demonstrated that the NTX HCl showed significant degradation at higher pH ranges, with the degradation rate being

proportional to the increase in pH from 6.8 to 8.2 (*Figure 17*). In addition to identified by-products (e.g., Impurity B, D and G), the measured chromatograms also showed a very high proportion of other decomposition substances with unidentified chemical structures ("unknown impurities") (*Figure 18*). The demonstrated degradation of NTX HCl in solutions at higher pH levels are in accordance with the study earlier published by Abdelkader and his coworkers[294]. In this work, the authors attributed the reason for decreased stability of NTX HCl to be oxidation, in which the electron loss from the molecule is more likely to occur in the neutral form of NTX. In the case of NTX HCl, with a pKa value of 8.13 at 37 °C, the drug is completely ionised, positively charged at acidic pH levels when it is more difficult to achieve an electron loss[295]. Our results also supported this hypothesis, as the degradation profiles were partially dominated by Impurity B (4,5α-epoxy-3,14-dihydroxymorphinan-6-one; noroxymorphone) and Impurity D (17,17'-bis(cyclopropylmethyl)-4,5a:4',5'a-diepoxy3,3',14,14'-tetrahydroxy-2,2'-bimorphinanyl-6,6'-dione; pseudonaltrexone), which substances can be identified as oxidative by-products of the morphine backbone[296,297]. The HCl-content of the media can explain the significantly higher chemical stability of NTX observed in water (with neutral pH) after the dissolution of the HCl salt, which decreased the pH to acidic levels. In another study, conducted by Andhariya et al., an accelerated *in vitro* release testing method for NTX loaded PLGA microspheres was developed[298]. Their work demonstrated that the addition of an antioxidant agent (0.0625 w/v% sodium ascorbate) in the release media (pH=7.4) could protect NTX against oxidative degradation up to 10 days at 37 °C. However, based on practical consideration, we decided to use water as the dissolution media, with all samples stored in the fridge until analysed, which was conducted within 5 days of the sample being taken. The solubility of NTX HCl in water at 37 °C was shown to be 115.8±2.2 mg/mL. Therefore, to ensure perfect sink conditions for all of the implants, the volume of media used during the dissolution testing was decided to be 50 mL of water, with complete media replacement.

The release experiments presented in this and the following chapters of the thesis have demonstrated the discriminatory capability of the developed *in vitro* dissolution methods to detect the effect of process-parameter and formulation changes on drug release, which is the quintessence of drug release testing[299].

The influence of EVA grade on the processability, drug content, stability and drug release

The two most important properties of EVA copolymers are the VA-content and the MFI value, which determine their processability and drug release. EVAs with higher VA-contents have lower crystallinity and lower melting temperature, whereas the MFI values are considered to be

an indirect measure of molecular weight and viscosity of the polymers, as mentioned earlier. In order to investigate the effect of monomer composition and molecular weight (or molecular weight distribution) on the processability, stability and release of NTX HCl, several implants were produced by HME from varying grades of EVA. All extruded rods were loaded with 20% w/w NTX HCl and had the same geometry (2mm in diameter and 4 cm in length). Depending on the VA-content and MFI values of the matrix polymers applied, the extrusion behaviour differed. For example, EVA27.7 with the lowest MFI value of 2.89 required the highest processing temperature, while EVA39.1 with an MFI value of 60.64 could easily be extruded at 90 °C (*Table 6*). Generally, the melting properties of the polymers have a great infleunce on their extrusion behaviours. As all of the used polymers showed complete melting at 90 °C on their measured DSC curves (*Figure 21*), and the applied processing temperatures were at or above this temperature in all cases, the differences in processability can be explained only by the differences in the rheological properties of the polymer melts. The MFI values of the polymers are intended to express the rheological properties, namely, the melt viscosity of the polymers. Thus, a correlation can be observed, with the required processing temperatures being inversely proportional to the MFI values.

Although all of the formulated NTX HCl-EVA blends could be processed relatively well, the critical quality attributes of the produced samples greatly differed. First, the average NTX HCl content and its homogeneity in the implant showed significant ($p<0.05$) differences. This was most likely due to the observed adherence of NTX HCl on the surface of the screw elements. This phenomenon can be attributed to the non-perfect mixing during the extrusion processes. It can be assumed that in the case of EVA39.1, the viscosity of the polymer melt was too low during the extrusion process. Therefore the shear stress responsible for mixing was not high enough to ensure perfect mixing. In contrast, the EVA27.7-based blend was probably too viscous to “wet” the drug particles, thus the formation of a continuously advancing phase along the extrusion barrel was not achieved. Additionally, a significant increase in impurity content was measured in the EVA27.7 implants because of the higher processing temperature and shear stress required for the extrusion.

Drug release patterns measured from the extruded implants revealed other interesting differences between the polymers involved in this study. Although the cumulative release curves related to EVA28.1 and EVA27.7 differed significantly, most likely due to the differences in the incorporated amount of NTX HCl, both of them showed a nearly zero order release. Release performance of these two systems obeyed perfectly the ”square root-of-time”

law of Higuchi (r^2= 0.9907 and 0.9936), which describes the diffusion-controlled release from non-biodegradable matrix systems (*Figure 20*). On the other hand, drug release from EVA39.9 implants followed diverse kinetic compared to the 2 other systems. According to several publications in the literature, EVAs with higher VA-content, therefore lower degree of crystallinity are expected to perform higher drug release[300,301]. Although EVA39.9 implants could be manufactured only with about 5% lower NTX HCl content than proposed, these systems showed lower-than-expected NTX HCl release even with reduced drug concentrations. This slower drug release performance indicated that other parameters besides VA-content had an influence on drug release. The work published by Almeida et. al have been already reported the unexpected release performance of this type of polymer in higher temperature release media (e.g., 37 °C) compared to other systems produced from different grades of EVA[302]. In this study the authors attributed the slower drug release from EVA systems with approximately 40% VA-content to the rearrangement of the porous structure remaining after the dissolution of drug particles from the implants. According to this hypothesis, the drug release from EVA39.1 implants can be explained as follows. Drug particles situated on or near the implant surfaces dissolved into the surrounding release media, ensuring constant release up to the fifth day of the study. However, the evolved porous structure collapsed from this time point due to the molecular rearrangement for achieving an energetically more stable structure at 37 °C. This rearrangement resulted in the partial closure of the interconnected network, decreasing the rate of NTX HCl release. The measured DSC thermogram of EVA39.1 could confirm this assumption, as this grade of EVA showed partial melting at the temperature the dissolution study was undertaken.

Based on the results described above, EVA polymers with 28% VA-content and higher MFI values (>2.89) were selected for further investigations.

The influence of drug loading on the processability, drug content, stability and drug release

In non-biodegradable matrix drug delivery systems, drug release is directly proportional to the drug content incorporated into the polymer matrices. Therefore, to investigate the influence of drug loading on the release performance, processability, drug content and stability, several implants with varying NTX HCl loadings were manufactured by HME from EVA polymers with a VA-content of 28%.

Based on the preliminary rheological investigations of different NTX HCl-EVA28 blends, several conclusions could be drawn regarding the processability of the systems to be

formulated. First, the results mainly showed the negative effect of increasing NTX HCl concentration on the rheological properties of different drug-polymer melts (*Figure 22*). Higher NTX HCl concentrations resulted in higher complex viscosity values, which was detectable even at 10% w/w NTX HCl. The reduced flow properties could be attributed to the solid-state nature of the drug particles, which therefore acted as a filler, increasing the complex viscosity of the polymer melts, even at higher temperature range (up to 180 °C). These results were consistent with the processing temperatures required to extrude NTX HCl-EVA28 blends with varying concentrations of NTX HCl (*Table 7*). While EVA28 implants with 20% w/w drug loading could be produced at 120 °C, those with 50% w/w drug loading could only be extruded at 145 °C. Although the NTX HCl-EVA28 blends with 40 and 50% w/w drug loadings showed major decrease in their rheological properties, they could be processed by HME, even though the measured viscosity values for these blends appeared to be much higher than the recommended range for optimal extrusion (10^3-10^4 Pa.s)[288]. It must be noted that this complex viscosity range is informative, and the processability of different systems would rather depend on the performance and special features of the used extruder. Secondly, a significant difference was observed in the rheological properties of the two EVA28 polymers and the drug-polymer blends produced from them. Mixtures made from the EVA polymer with the lower MFI value showed significantly higher complex viscosity at the corresponding NTX HCl concentration levels. This observation was not surprising, since the main purpose of the MFI value is to practically denote the flow properties of polymer melts, as mentioned earlier. The extruder could only handle the rheological differences between the two polymers up to the NTX HCl concentration level of 35% w/w. EVA28 (MFI:25.00) implants with a NTX HCl level of 40% w/w could not be processed.

Differences in the flow properties of the investigated systems were also noticeable in the average drug content of the implant batches and the drug homogeneity in the length of the implants (*Figure 23* and *Figure 24*). 40 with the 50% w/w implants showing greater variability assay results compared to lower drug-loaded implants. This was due to the highly increased viscosity of these systems, which was confirmed by the rheological study performed. The viscoelastic nature of EVA did not dominate during the extrusion of 40 and 50% w/w systems. Therefore the mixing efficiency was not sufficiently high enough to ensure a homogeneous product leaving the die at the end of the barrel.

From thermal investigations of the manufactured extrudates, it could be deduced that the formulated NTX HCl exhibited a phase transition during the HME process (*Figure 26* and

Figure 35). The decrease in the crystallinity of NTX HCl can be explained by two types of phase-transition processes. First, the drug may have been molecularly dispersed (dissolved) into the polymer melt and remained in this state, kinetically stabilised by the matrix former. On the other hand, a certain amount of drug particles may have been melted during the HME process and did not recrystallise upon cooling, forming amorphous regions in the implants. As the melting point of NTX HCl appeared to be at 227 °C on the related DSC curve, almost 100 °C above the applied process temperatures, this assumed melting could have occurred due to the frictional heat generated during processing. The extent of the first hypothesized process, namely the dissolution of NTX HCl into EVA melts, if it occurred, was still likely to be very small because of the highly hydrophilic nature of the NTX HCl and the highly hydrophobic nature of the EVA polymer. Therefore, the miscibility of these two components with different physicochemical properties is very unlikely, even at elevated temperatures[303]. This was confirmed by the morphological characterisation of the 35% w/w EVA28 (MFI:25.00) implants. The DSC curve related to this sample did not show an endothermic peak that corresponds to the melting of NTX HCl (*Figure 35*), but at the same time, two well-separated phases – with different elemental compositions (EDS spectra) – could be seen in the SEM images from the same sample (*Figure 36*). Based on this observation, the phase transition of NTX HCl that was detected by DSC measurements was more likely due to the amorphisation, despite the fact that processing temperatures were far below the melting temperature of NTX HCl. However, none of the measured thermograms from the extrudates showed a distinct glass transition related to the amorphous NTX HCl content, possibly due to the matrix effect of EVA, because of which this transition was not detectable on the DSC curves. There are several publications in the literature where amorphisation has taken place similarly, well below the melting point of the formulated API[253].

It is well known that APIs in their amorphous state tend to have lower heat stability, which can be an obstacle for formulation by HME[254]. However, the samples investigated in this study showed no or acceptable increase in purity content related to NTX HCl (*Figure 25* and *Figure 34*) even though a significant portion of the drug was present in the amorphous state. Although a significant increase of oxidative degradation by-products (e.g., Impurity B) was observed in the case of 35% w/w EVA28 (MFI:25.00) implants, the measured purity content of NTX HCl was well below the threshold limits stated in the corresponding Ph.Eur. monograph. The significantly decreased stability of NTX HCl in this sample can be explained by the increased

shear stresses required for extrusion due to the lower MFI value of matrix polymer used and the consequent complete amorphisation of NTX HCl during the process.

In vitro dissolution experiments of the implants showed that each formulation had a release characteristic of matrix-type drug delivery systems (*Figure 24*). The magnitude of the initial ”burst” depended on the implants’ NTX HCl loading. At lower NTX HCl loadings, the probability that the drug particle was situated on or near the surface of the implants was reduced. Hence, the released amount of NTX HCl on the first day of the study appeared to be lower than it was observed with higher drug-loaded implants. Moreover, the release profiles also presented that as the NTX HCl loading was increased, the release rose substantially in all cases. This can be explained by the suggested drug release mechanism. It can be assumed that the release mainly occurred through a porous network filled with the release media. Pores were formed by the drug itself, which upon dissolution, left behind a void space, and thus providing further access to the release medium to form additional pores in the matrix. Thus, the dissolved NTX HCl diffused through the continuously evolving tortuous network of the interconnected pores resulting in the sustained drug release. In this respect, it can be concluded that the initial drug loading highly contributed to the extent of pore formation, therefore, to the release rate. This theory was confirmed by the SEM images about the implants taken before and after the release study (*Figure 27* and *Figure 30*). The extent of the observed empty porous structures was larger at higher drug loadings, which was in accordance with the measured release profiles of the implants. Diffusion-based drug delivery was also confirmed by the results of two widely used mathematical models (Higuchi and Korsmeyer-Peppas equation) describing drug release mechanisms from drug products (*Table 19*). However, the calculated values of the *n* exponents in the Korsmeyer-Peppas model related to the controlling mechanism appeared to be considerably less than 0.45. This was most likely due to the polydisperse nature of the drug distribution in the implants, according to which drug particles and particle clusters are present with varying sizes affecting the drug release (*Figure 27*)[304].

The release performances of 35% w/w implants produced from EVAs with differing MFI values (25.00 and 42.46) were identical, no significant difference could be seen in their release characteristics (*Figure 37*). This would suggest that the morphology of NTX HCl in the extruded implants had no significant influence on drug release. This was not surprising since APIs tend to have higher solubility in their amorphous state[229]. As the water solubility of crystalline NTX HCl is already exceptionally high (115.8±2.2 mg/mL), amorphisation could not contribute significantly to solubility enhancement, therefore, could not increase the release.

Based on the Higuchi and Korsmeyer-Peppas equations, the predicted release of NTX HCl delivered from the rods clearly showed that only the 35 and 40% w/w implants could ensure sufficient sustained release for longer periods (*Figure 31*). In contrast, 50% w/w implants presumably release all of the incorporated drug amounts within 40 days, whereas the release from 20 and 30% w/w implants is not high enough to be relevant for further clinical applications. It should be noted here that these predictions assumed the contribution of all of the drug content in the release mechanism. However, in such binary systems, a specific drug loading threshold can be defined, where all of the embedded drug particles form a continuous network. Thus, all of the formulated drug can contribute to drug release. This threshold commonly referred to as "the percolation threshold", which is generally defined at a critical porosity value of ~0.20, which corresponds to the drug level of 23-25% w/w in the NTX HCl-EVA28.1 cylindrical implants, with 4 cm in length and 3 mm in diameter[305]. Therefore, the predictions for the samples with drug loading above 25% w/w were considered to be valid.

Although 35 and 40% w/w implants showed promising release characteristics, the delivered drug amounts from one rod were still lower than required for clinical efficacy in humans. Generally, the orally taken daily dose of NTX HCl is 50 mg which ensuring 2 ng/mL effective drug plasma levels in adults. A previous clinical study conducted by Meyer et al. showed that only 5% of the orally administered naltrexone hydrochloride reached the systematic circulation due to extensive hepatic first-pass metabolism[62]. Thus a dose of 2.5 mg/day from the subcutaneous implants is presumably sufficient to achieve therapeutic efficacy. However, the estimated daily release from the developed implants appeared to be 0.2 and 0.4 mg/day at day 40 and 0.15 and 0.25 mg/day by day 90 calculated by the Higuchi model for the 35 and 40% w/w drug loadings, respectively. In this respect, a sufficient drug level would be achieved and tailored by using several implants.

In vivo performance of the produced samples

The *in vivo* pharmacokinetic investigation in male beagle dogs demonstrated that NTX HCl was delivered from the NTX HCl-EVA28 implants providing detectable NTX blood levels in almost all study groups throughout the 29-day study. As the clearance rate of NTX is extremely high in both dogs and humans, it can be stated that the measured blood levels were due to the sustained release of NTX from the implants[306]. Interestingly, the residual drug content analysis confirmed that 35 and 40% w/w implants (except for subject PK3_1) released approximately the same amount of NTX HCl in the 29-day long *in vivo* study as it was predicted from the 14-day long *in vitro* experimental data by the Higuchi and Korsmeyer-Peppas model to day 29

(*Table 21* and *Figure 31*). For example, 35% w/w implants (subjects PK2_1 and PK2_2) released almost 9-10% of the initial drug loading over 29 days *in vivo*. The predicted *in vitro* cumulative release for this sample appeared to be around 14% at day 29. In the same respect, the 40% w/w implants (subjects PK3_2, PK4_1 and PK4_2) showed a total release of about 15-20% in vivo, while the predicted cumulative release curve of 40% w/w implants showed a release of about 20% at day 29. However, such a correlation in the case of 30% w/w implants could not be observed. Although the *in vitro* model prediction by the Higuchi and Peppas models should be handled with caution, it could be concluded that a promising correlation exists between the release performed *in vitro* and *in vivo*. Even though the subcutaneous tissue area is constricted and has lower fluid volumes compared to the constant shaking and relatively large volume of release medium used in the *in vitro* study.

If subject PK3_1 is considered as an outlier and therefore not involved in the analysis, a correlation can be observed between the total amount of NTX HCl delivered from the implants and the measured NTX plasma concentrations (*Figure 39*). However, the measured drug levels were relatively lower than the total NTX HCl exposure calculated from the residual drug content analysis. This was probably due to the observed dose-related inflammation in the vicinity of the implants, which resulted in the formation of a biofilm layer surrounding the implants. NTX HCl was likely accumulated in this layer, modulating the subsequent systematic NTX absorption. It is well known that inflammatory tissue response to intramuscularly or subcutaneously administered dosage forms has a negative influence on drug absorption[307].

Based on the results related to the subject PK3_1, it can also be assumed that if the concentration of NTX in the surrounding biofilm layer reaches a certain limit, the drug may burst out of this depot and then be absorbed in the appropriate tissues reaching the systematic circulation. This hypothesis can explain the significantly higher blood levels observed in the subject PK3_1, where the highest total NTX HCl exposure was calculated. In that regard, multiple implants inserted close together can reduce the relative surface area of the capsule forming around the implants. Hence, the sufficient NTX HCl concentration can build up easier to burst out of the biofilm layer.

In the case of NTX HCl-based subcutaneous tablets, a similar inflammatory side reaction has been reported in the literature, probably due partly to the HCl content of the NTX HCl salt form[278]. To solve this problem, an anti-inflammatory agent (e.g., NSAIDs or triamcinolone) can be used simultaneously, orally administered or can be incorporated into the matrix with the NTX HCl.

Results from the *in vivo* experiment showed that 35 and 40% w/w implants could produce sufficient level of sustained release of NTX HCl. Although the 40% w/w implants produced higher release than the 35% w/w implants, it was decided that the final formulation would use the EVA28.0 (MFI:25.00) matrix polymer from Polysciences Inc.. The main reason for this decision was that we wanted to conduct the following process development studies using a GMP grade EVA that would be suitable for clinical evaluation and commercialization of the final product. Reasonably proced GMP grade EVAwas only availabe from Poysciences Inc. and thus a decicison was made by the sponsor to move forward with theis EVA.

2.5 Conclusion

In this chapter, appropriate analytical protocols were developed and validated to support the development process of the final formulation. Then, during the pre-screening process, several variables were investigated. The influence of EVA grade (VA-content and MFI value) and drug loading on the processability, stability and *in vitro* drug release were studied. In summary, higher VA-content resulted in slower drug release, whereas lower MFI value affected the processability and, consequently, the drug stability. Drug loading also had a great influence on the processability, homogeneity and *in vitro* release. Implants with higher drug loadings could only be formulated with lower homogeneity and performed a higher drug release rate, which above 40% w/w NTX HCl concentration appeared to be insufficient to achieve long-term release. At the same time, implants with lower NTX HCl loadings, below 35% w/w, showed significantly slower release than was expected. Our experiments also revealed the mechanism of drug release from the implants, mainly controlled by the diffusion of NTX HCl through a porous network filled with the release media. We also demonstrated that the amorphisation of NTX HCl during extrusion has an acceptable effect on the evolution of degradation by-products. *In vivo* investigations showed that 35 and 40% w/w implants provide long-term blood concentrations in male beagle dogs. Although the exhibited plasma levels were lower than was expected, our investigations proved that relevant NTX HCl was delivered from the implants, which amount presumably accumulated in the surrounding capsule formed by inflammatory tissue response. This problem can be presumably solved by the administration of anti-inflammatory drugs simultaneously or by positioning several implants close together. However, further animal studies would have been required to prove these assumptions.

Based on our decision, the final formulation had 35% w/w NTX HCl drug loading produced from EVA28 (MFI:25.00) and had a diameter and length of 3 mm and 4 cm, respectively.

3 Process development for NTX HCl loaded EVA implants and 6 months stability study

3.1 Introduction

In HME, several processing parameters can be varied, including processing temperature, screw speed, screw configuration and feeding rate[220]. Each parameter has specific functions and, at the same time, correlates with the others, thereby controlling the process. For example, the process temperature, or temperature profile ensures that at least one component in the feed mixture melts influencing the rheological or flow properties along the length of the barrel[220]. Furthermore, screw configuration and screw speed shape the mixing, shear stress and pressure distributions to which the API-polymer blend is exposed, and more importantly, control its residence time in the extruder[308]. Finally, the feeding rate mainly determines the fill rate of the screw channels, which controls the pressure profile built up in the barrel and directly influencing the effective length of the applied screw design involved in mixing[309]. As can be concluded, each of the process parameters mentioned above has a great influence (directly or indirectly) on the most critical characteristic of the extrusion process, namely on the mixing efficiency, which has a pivotal role on the homogeneity and morphology of the extrudate. In addition, owing to the mechanical and thermal stresses that occur during HME, both the formulated API and the matrix polymer can undergo significant degradation, thereby affecting the pharmacokinetic behaviour and clinical applicability of the resulting product.

Because of the high complexity of the HME process described above, determining the interaction between each critical process parameter (CPP) and understanding their influence on the critical quality attributes (CQA) of the final product is a crucial step in HME production. With the role of the Quality by Design (QbD) concept emerging in both the research and industrial arenas, this step is usually performed by mathematical modelling tools[310]. Several works have been published on the influence of HME process parameters on the CQAs of the formulated extrudates[311,312,313,314]. In most studies, the Design of Experiment (DoE) approach has been successfully applied for process optimisation purposes. The objective of process optimisation by DoE is to determine the critical factors and their optimum level using statistical tools to achieve an optimal response, or in other words, to achieve an optimal product property[315]. The statistical techniques usually applied in DoE for optimisation include the frequently used response surface designs, such as the factorial designs, the central composite, D-optimal and mixture designs, among others[316]. However, the main disadvantage of these DoE

approaches is that they require a relatively large number of experiment runs. Furthermore, investigation of additional points (e.g., central points) and replicates in the chosen design are also highly recommended, not only to increase the prediction efficiency of the calculated model but also to detect the level of significance of certain factors on the selected response more reliably. However, in many cases, the number of experiments required to calculate a reliable model cannot be performed due to limited raw materials. It should also be noted here that in addition to process optimisation based on statistical methods, computational simulations of HME processes may also have the potential to discover optimal process parameters settings[315,317].

The primary aim of this chapter was to assess a process window that allows the technology to be transferred to a larger scale extruder for the mass production of the previously developed 35% w/w NTX HCl-EVA28 implants (see *Chapter 2*) with sufficient quality. Additionally, a 6-month accelerated stability study of the final formulation was performed to provide evidence on how the implants vary over time under the influence of increased temperature and humidity, which is essential for commercialisation[318].

The main objectives of this chapter were as follows:

- 6 different process settings were investigated to assess the impact of manufacturing process parameters (process temperature and screw speed) on several quality attributes and, where appropriate, identify any relationships that were supported by statistical analyses.
- After the appropriate HME process settings was selected to achieve the sufficient implant quality which was in good agreement with the product profile indetified in the previous chapter, a larger batch size (approximately 100 implants) was manufactured, and its stability was analysed for 6 months under accelerated conditions (40 °C/ 75 % RH).

3.2 Materials and methods

3.2.1 Materials

For this study an EVA28.0 (MFI:25.00) was purchased from Polysciences Inc. (Warrington, United States). All other materials used for further analytical procedures were the same as those used in *Chapter 2*.

3.2.2 Hot-melt extrusion

The extrusion method is described in detail in the previous chapter, *Section 2.2.2*. In this study, a 3-mm diameter die was used. The applied processing parameters varied according to *Table 22*.

Table 22 Investigated process settings

Sample	Feeding rate (g/min)	Processing temperature (°C)	Screw speed (rpm)
Proc1	60	125	90
Proc2	60	135	90
Proc3	40	135	60
Proc4	80	135	120
Proc5	60	145	90
Proc6	80	145	120

3.2.3 HPLC analysis, assay, homogeneity, impurity content, *in vitro* drug release and statistical analysis

The methods were the same as described in the previous chapter, *Section 2.2*.

3.2.4 DSC analysis

The method was the same as described in the previous chapter, *Section 2.2*. The degree of crystallinity of NTX HCl and the matrix polymer were evaluated from the heat of fusion using the following equation:

$$X_c(\%) = \frac{\Delta H_m}{\Delta H_m^0} * 100$$

where

- ΔH_m – heat of fusion measured from the DSC thermogram
- ΔH_m^0 – heat of fusion of crystalline NTX HCl (44.757 J/g, measured by DSC using the NTX HCl chemical reference standard) and 100% crystalline polyethylene (277.1 J/g)[319]

The enthalpy values were normalised based on the average NTX HCl conent of the implants, measured by the HPLC assay method.

3.2.5 Comparison of drug release profiles

The similarity between the average drug release profiles related to different sampling time points was established from the calculation of the f_2 similarity factor. The method is based on the logarithmic transformation of the sum-squared error of differences between the test T_j and reference product R_j over all time points[320].

$$f_2 = 50 * log\left\{\left[1 + (1/n)\sum_{j=1}^{n}\left|R_j - T_j\right|^2\right]^{-0.5} * 100\right\}$$

where

- n – number of dissolution time points
- R_j – released average drug percent at each time point j
- T_j – released average drug percent at each time point j

3.2.6 Flexibility testing

The tensile properties of the produced implants were analysed using an INSTRON 5848 Microtester set up for a tensile test. The 1 cm sections of the rods were fixed at both ends, and an increasing tension (N) was applied (*Figure 40*). The extension (mm) of the implants was determined with increasing tension (500 mm/min). The modulus for each implant was calculated by linear fitting on the measured points in the linear region (Hookean region) on the stress-strain curve (*Figure 41*). The elastic modulus was defined as a slope of the fitted linear curve:

$$Modulus\ of\ elasticity = \frac{Stress}{Strain}$$

$$E = \frac{F/A}{\Delta L/L_0 * 100}$$

where

- F – tension (N)
- A – surface area (mm^2)= (3 mm /2)^2*π = 7.065 mm^2
- L_0 – initial length = 20 mm (because of the sample preparation)
- ΔL – extension (mm)

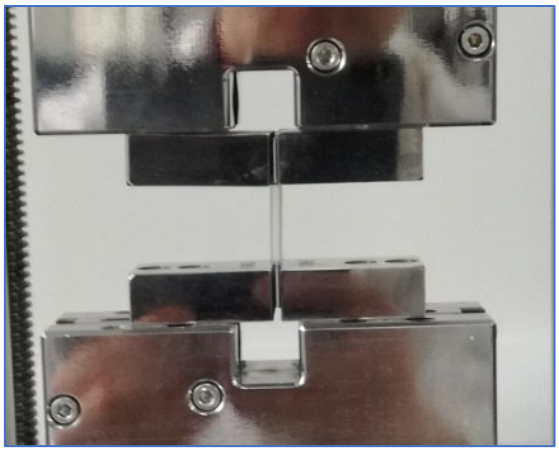


Figure 40 Tensile testing setup

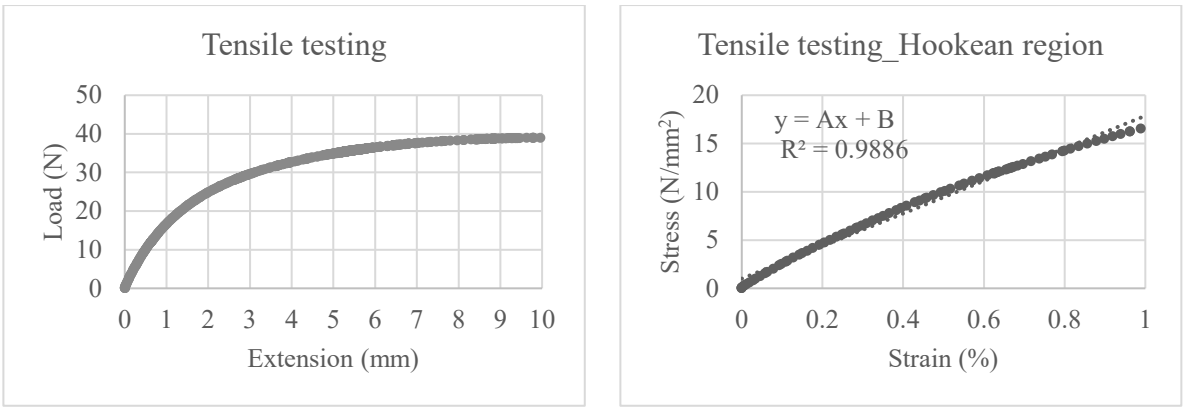


Figure 41 Determination of flexiblity on an example of an extruded Ø= 3 mm EVA rod

3.2.7 Stability study

Using the process parameters (135 °C/ 90 rpm, implants were manufactured at a larger batch size (approximately 100 implants). The implants were packed into an Alu/PE/PP sachet pouches and heat-sealed. The sachets were transferred into the Binder KMF 115 stability chamber and stored at 40 °C and 75% RH, for 6 months. CQAs of the implants were examined at several time points (0, 1, 2, 3 and 6 month) throughout the 6-months study period.

3.3 Results

3.3.1 Average drug content and homogeneity of the implants

The average NTX HCl content for the majority of the implants were within the target range of 35% w/w± 10% (*Figure 42*). However, drug content analysis revealed higher average NTX HCl contents for samples manufactured using Proc4 (38.81±1.00% w/w), Proc5 (39.22±1.37% w/w) and Proc6 (38.38±0.35% w/w). An increase in the variation of the measured values (%RSD>5) was observed for the Proc1 (%RSD=9.98) implants. The homogeneity of drug content along the length of the implants was also investigated. The results showed that the homogeneity was acceptable (%RSD<5) in all cases (*Figure 43*) except for a single implant (Proc4_2. implant) were the measured %RSD calculated from the drug content of the 4 different sections of the implant exceeded the target 5 %RSD value. However, the average drug contents differed significantly within the sample groups in batch Proc1, Proc4 and Proc5. These results were approximately in good agreement with the average drug content measurements, where the inhomogeneity within the correspondent batches appeared with a greater value of %RSD.

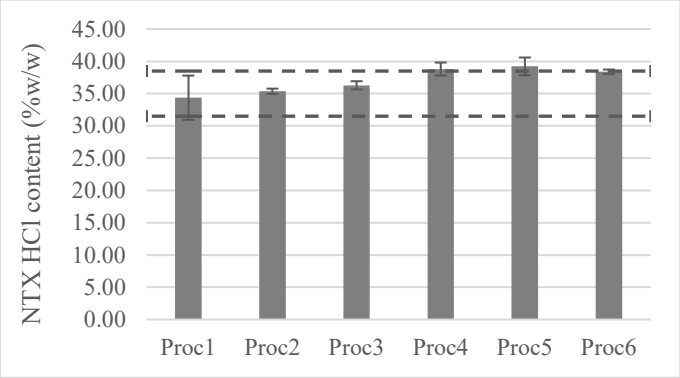


Figure 42 Average NTX HCl content of implants produced using different processing parameters. Dashed lines represent the 35% w/w ±10% limit. Error bars represent ±1 standard deviations of n=3 replicates.

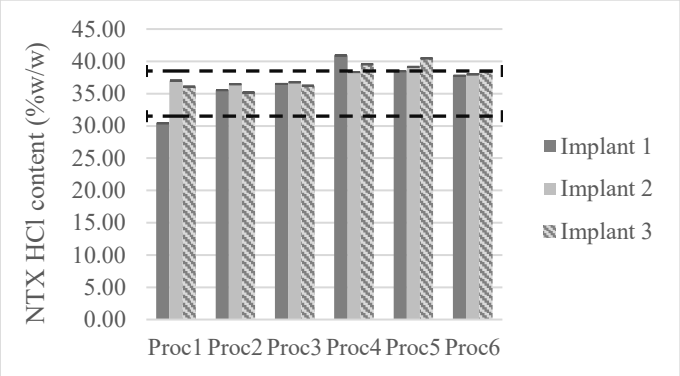


Figure 43 Homogeneity of NTX HCl between the 4 different sections along the implants. Dashed lines represent the 35% w/w ±10% limit. Error bars represent ±1 standard deviations of n=4 replicates.

To investigate the inflence of the process parameters on the actual drug content and homogeneity of the implants, a multifactor ANOVA analysis (using Minitab 19 software) was calculated for the measured data points (*Figure 44*). The model fitted to the drug content revealed that the process temperature and the screw speed had significant influence on the average NTX HCl content of the implants ($p<0.05$). The two-way interaction and polynomial terms for processing temperature and screw speed were also statistically significant ($p<0.05$). The value of the regression coefficient was 0.8304, indicating that the fitted model explains 83.04% of the variation in the average drug content of the batches. The homogeneity of the average drug contents related to each batch was statistically investigated by using the level of %RSD. The general model calculations revealed no significant effects of processing temperature ($p=0.282$) and screw speed ($p=0.764$) on the %RSD values. The same calculation were conducted for the intra-implant NTX HCl homogeneity. Similarly, the calculated *p* values were greater than 0.05, indicating the lack of statistically significant effect of the investigated process parameters.

Analysis of Variance

Source	DF	Adj SS	Adj MS	F-Value	P-Value
Proc. temp. (°C)	1	7.857	7.8570	11.36	0.006
Screw speed (rpm)	1	11.499	11.4991	16.63	0.002
Proc. temp. (°C)*Proc. temp. (°C)	1	10.762	10.7618	15.56	0.002
Screw speed (rpm)*Screw speed (rpm)	1	9.563	9.5625	13.83	0.003
Proc. temp. (°C)*Screw speed (rpm)	1	13.814	13.8136	19.97	0.001
Total	17	44.850			

Model Summary

S	R-sq	R-sq(adj)	R-sq(pred)
0.831653	83.04%	75.33%	60.24%

Coefficients

Term	Coef	SE Coef	T-Value	P-Value
Constant	297.9	98.2	3.03	0.011
Proc. temp. (°C)	5.09	1.51	3.37	0.006
Screw speed (rpm)	1.536	0.377	4.08	0.002
Proc. temp. (°C)*Proc. temp. (°C)	0.02414	0.00612	3.94	0.002
Screw speed (rpm)*Screw speed (rpm)	0.002430	0.000653	3.72	0.003

Figure 44 Results of the multifactor ANOVA analysis for drug content of the implants produced using different HME process settings

3.3.2 NTX HCl degradation

In order to investigate the influence of different process settings on the degradation of the formulated NTX HCl, RP-HPLC measurements were conducted. Although significant discolouration was observed in implants produced at higher processing temperatures, Proc5 and

Proc6 (*Figure 45*), for all formulations, the concentration of each detectable impurities was far below the threshold limits stated in the Ph.Eur. monograph for NTX HCl (*Figure 46*).



Figure 45 Appearance of the produced extrudates

A multiway ANOVA analysis calculated for the total impurity contents revealed the statistically significant effect of screw speed (p=0.002) and its interaction term with processing temperature (p=0.003) (*Figure 47*). The regression coefficient of the generated model was 0.7016, indicating a good fit between the response and the investigated continuous variables. According to the calculated coefficient values, the processing temperature had a positive effect, while the screw speed had a negative effect on the evaluation of the NTX HCl degradation.

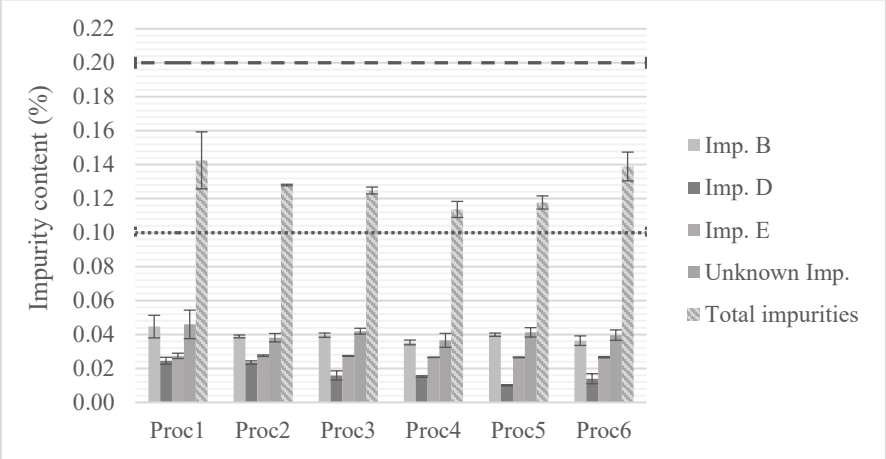


Figure 46 Detectable impurities of NTX HCl in the produced implants prepared using different HME process settings. The dotted line represents the 0.1% threshold limit for Impurity B and Unknown impurity, while the dashed line represents the 0.2% threshold limit for Impurity D and Impurity E according to the Ph.Eur. monograph for NTX HCl. The 1.0% threshold limit for total impurity content is not indicated in this figure. Error bars represent the ±1 standard deviations of n=3 replicates.

Analysis of Variance

Source	DF	Adj SS	Adj MS	F-Value	P-Value
Proc. temp. (°C)	1	0.000105	0.000105	1.52	0.242
Screw speed (rpm)	1	0.001015	0.001015	14.64	0.002
Proc. temp. (°C)*Proc. temp. (°C)	1	0.000009	0.000009	0.13	0.724
Screw speed (rpm)*Screw speed (rpm)	1	0.000155	0.000155	2.24	0.161
Proc. temp. (°C)*Screw speed (rpm)	1	0.000949	0.000949	13.68	0.003
Total	17	0.002788			

Model Summary

S	R-sq	R-sq(adj)	R-sq(pred)
0.0083267	70.16%	57.72%	32.85%

Coefficients

Term	Coef	SE Coef	T-Value	P-Value
Constant	2.062	0.925	2.23	0.046
Proc. temp. (°C)	0.0177	0.0143	1.23	0.242
Screw speed (rpm)	-0.01443	0.00377	-3.83	0.002
Proc. temp. (°C)*Proc. temp. (°C)	0.000021	0.000059	0.36	0.724
Screw speed (rpm)*Screw speed (rpm)	-0.000010	0.000007	-1.50	0.161
Proc. temp. (°C)*Screw speed (rpm)	0.000119	0.000032	3.70	0.003

Figure 47 Results of the multifactor ANOVA analysis for total impurity content of the implants produced using different HME process settings

3.3.3 Tensile testing

The mechanical properties of the implants were tested using the INSTRON 5848 Microtester set up for a tensile test. The calculated elastic modulus for Ø=3 mm blank and drug-loaded implants are presented in *Figure 48*. The elastic modulus of drug-loaded implants were approximately 3.6 fold higher compared to placebo extrudates. No statistical significance of the processing parameters was revealed by the ANOVA calculations (*Figure 49*). Therefore, influence of screw speed and processing temperature on the implants' tensile properties could be ignored.

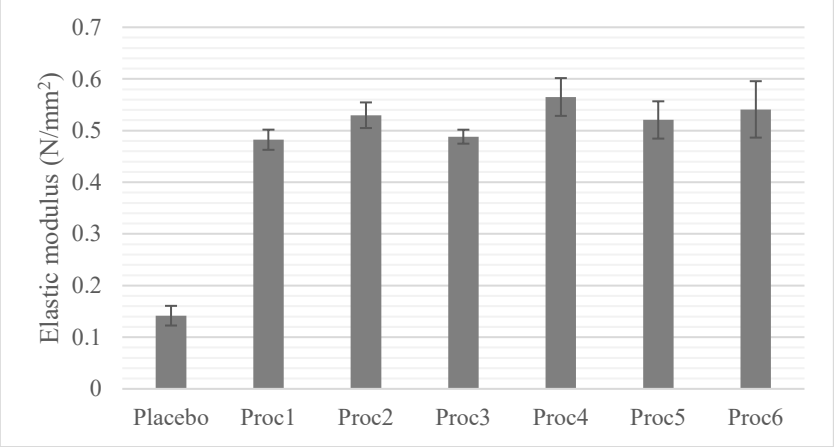


Figure 48 Calculated elastic modulus of the implants produced using different HME process settings. Error bars represent ±1 standard deviations of n=3 replicates.

Analysis of Variance

Source	DF	Adj SS	Adj MS	F-Value	P-Value
Proc. temp. (°C)	1	0.002309	0.002309	2.04	0.179
Screw speed (rpm)	1	0.000361	0.000361	0.32	0.583
Proc. temp. (°C)*Proc. temp. (°C)	1	0.001601	0.001601	1.41	0.258
Screw speed (rpm)*Screw speed (rpm)	1	0.000019	0.000019	0.02	0.899
Proc. temp. (°C)*Screw speed (rpm)	1	0.000167	0.000167	0.15	0.708
Total	17	0.028590			

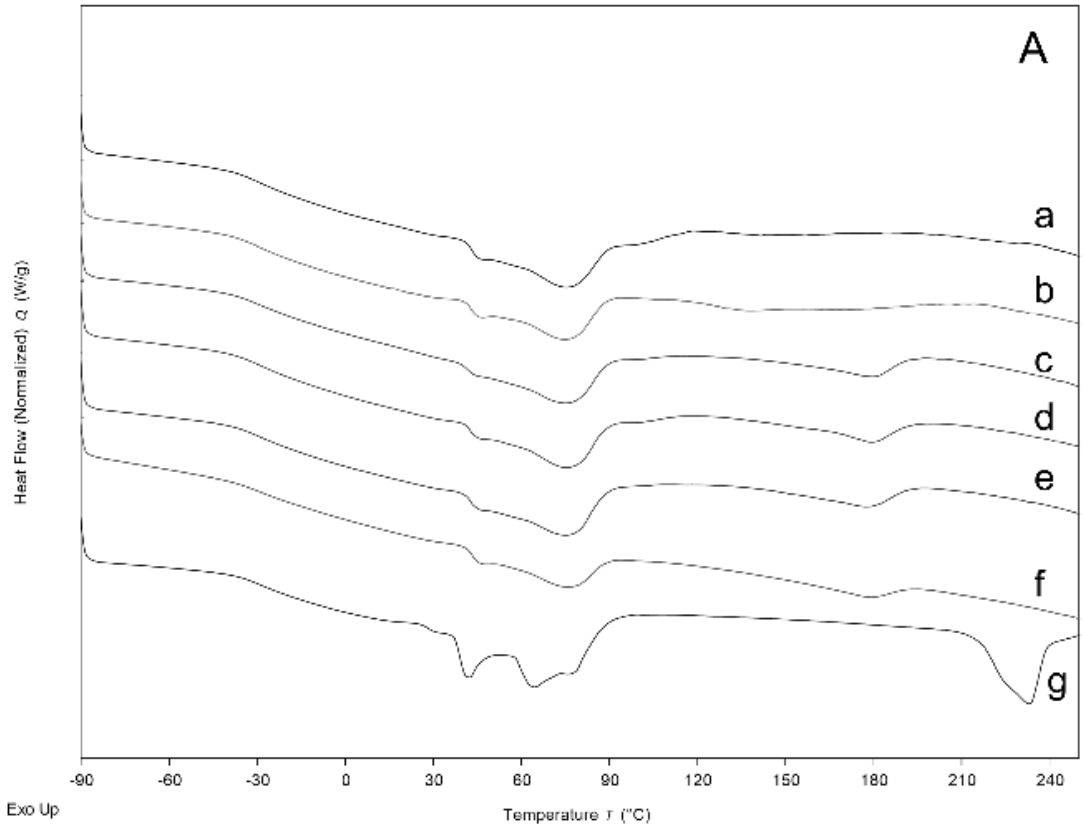
Figure 49 Results of the multifactor ANOVA analysis for tensile properties of the implants produced using different process settings

3.3.4 Morphological investigations of the implants

The DSC scans of the physical mixture of NTX HCl-EVA28 (35:65 %w/w) and the implants manufactured using different HME process settings are shown in *Figure 50*-A. The thermograms exhibited a wide glass transition range for EVA28 with the inflection point of approximatley -31 °C. Neither the extrusion process itself nor the varying process parameters affected this type of thermal transition. In contrast, significant structural change in the rate and structure of crystallinity of the matrix polymer could be observed due to the HME process. Multiple endothermic melting peaks for EVA28 are shown on the DSC curves of the physical mixture, while these melting transitions could be observed at different temperatures and with wider temperature range in thermograms of the implants. The calculated crystallinity of EVA28 based on the normalised melting enthalpies are summarised in *Table 23.* The calculated results clearly showed the approximately 2 fold decrease in the rate of crystallinity of EVA28 after the HME process. Although no replicates were measured, it could be suggested that the differences between the calculated crystallinity values related to the implants was not influenced by varying the process parameters.

The DSC results also indicated that the NTX HCl in the implants was completely amorphous as no endothermic peaks could be detected at the melting temperature of NTX HCl (227 °C). However, an interesting melting transition could be observed in the DSC scans of samples from Proc1 to Proc4 at approximately 180 °C. This transition could be attributed to the glass transition of the amorphous fraction of NTX HCl. This hypothesis was confirmed via the thermal investigation of the *in situ* formed glassy NTX HCl using the following experimentation. The pure drug was first heated in the DSC pan to 220 °C and held at this temperature for 1 minute. The reason for using this methodology, instead of heating the system above the offset of the drug's melting melting peak, was to avoid any degreadation of NTX HCl, as our preliminary investigations showed that the drug degraded immediately after the melting, above 230 °C. We suggested, that at this temperature the melting of NTX HCl started

and completed in the isothermal step, without no significant degradation. After the conditioning step at 220 °C for 1 minute the system was quenched at a cooling rate of 100 °C/min to -90 °C to avoid any recrystallistion of the possible glassy NTX HCl. The heating curve from -90 to 255 °C at a rate of 10 °C/min clearly showed the glass transition of the amorphous NTX HCl at around 180 °C, confirming that the heat transition observed in the DSC scans of Proc1 to Proc4 could be attributed to the glass transition of NTX HCl overlapped with the matrix signal (*Figure 50*-A and B). The lack of such transition in the DSC curves of samples Proc5 and Proc6 was probably due to the different distribution of drug particles in the implants. The amorphous drug particles did not form larger clusters, therefore there small glass transition signal was not added together to produce a sufficient signal that could be detected by DSC.



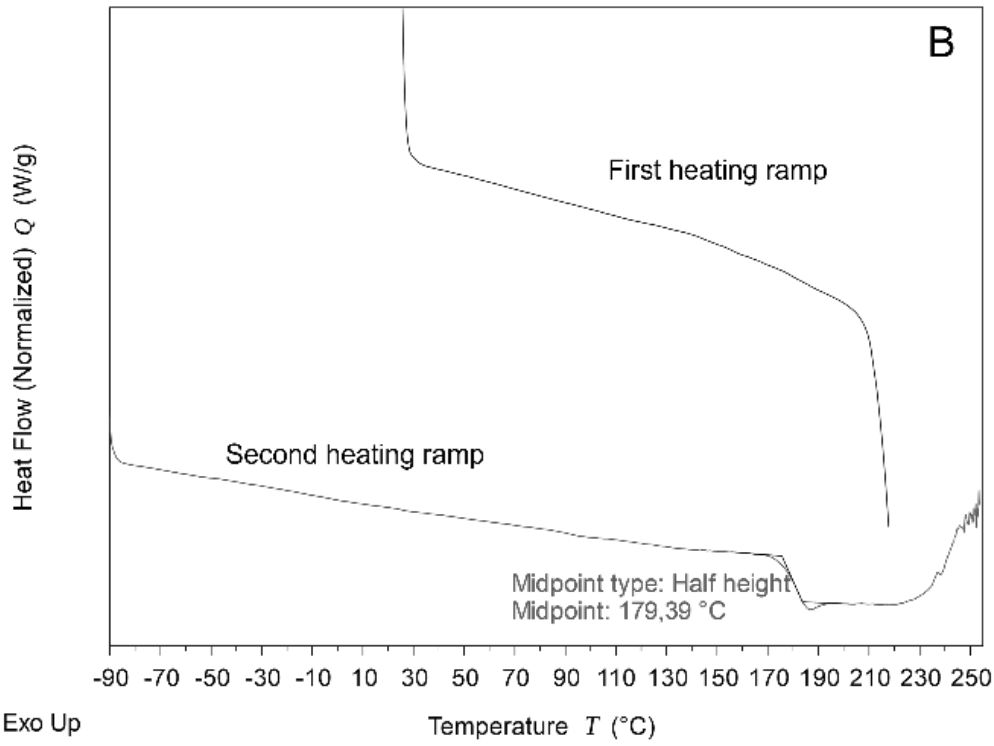


Figure 50 (A) DSC scans of the NTX HCl-EVA28 physical mixture (g) and the produced implants (Proc1-f; Proc2-e; Proc3-d; Proc4-c; Proc5-b; Proc6-a). (B) In situ formation of glassy NTX HCl. In the first heating ramp the sample heated up to 220 °C, then quenched. On the second heating ramp Tg of glassy NTX HCl was detected.

Table 23 Calculated crystallinity of EVA28 and NTX HCl in the physical mixture and implants

Sample	Crystallinity (%)	
	EVA28	NTX HCl
Physical mixture	20.3	100.0
Proc1	10.9	0.0
Proc2	10.9	0.0
Proc3	10.8	0.0
Proc4	10.9	0.0
Proc5	11.2	0.0
Proc6	11.1	0.0

The NTX HCl distribution and morphology on the cross sectional surfaces of the implants was characterised visually by SEM. The SEM images showed a homogeneous distribution of NTX HCl in the cross sectional areas of the implants (*Figure 51*). However, a higher amount of NTX HCl enriched clusters could be seen wherein smaller particles with flocculent structure forming higher pores. No noteworthy trend could be observed in relation to the homogeneity of NTX

HCl between the cross sectional surfaces of implants produced using varying HME process settings.

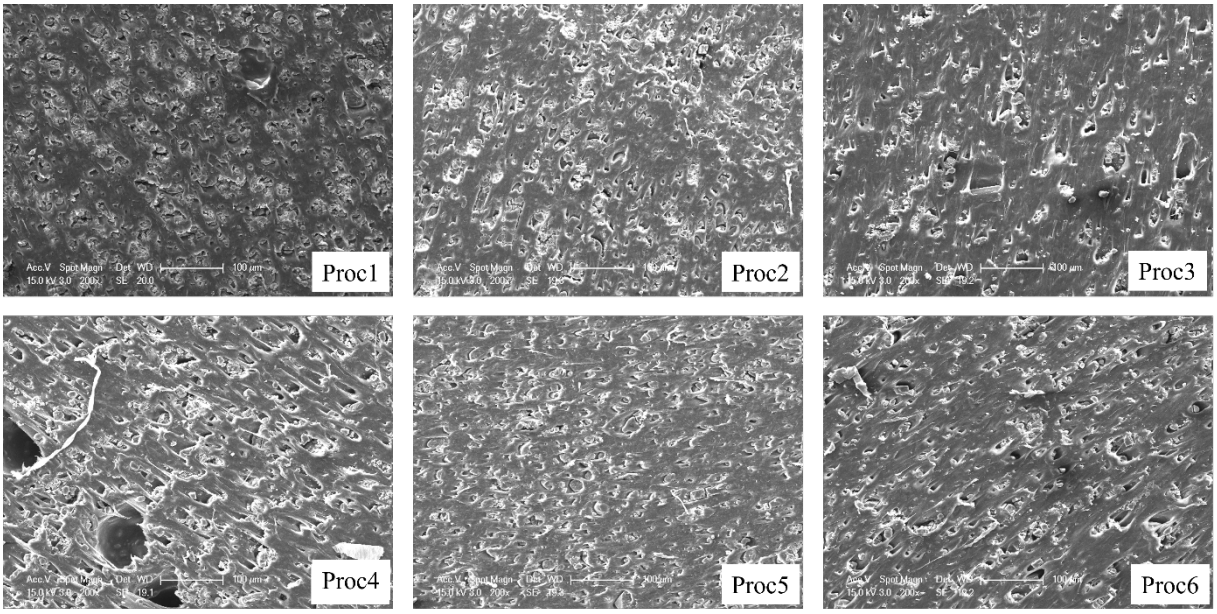
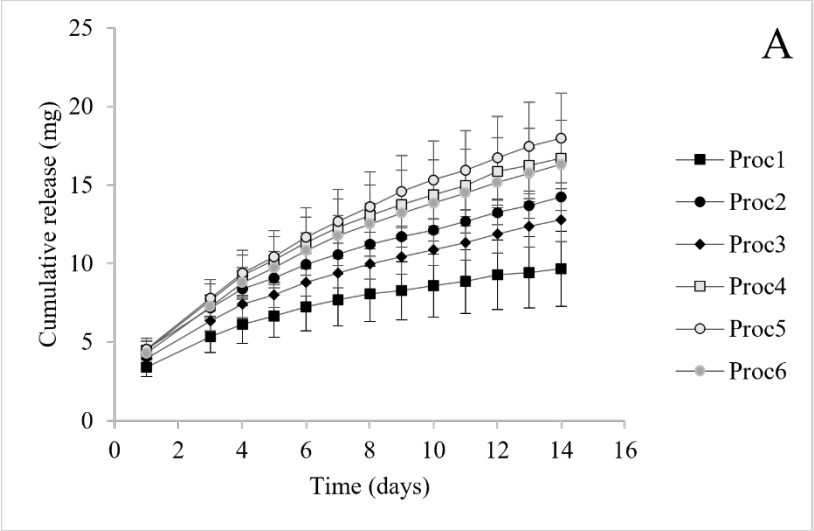


Figure 51 SEM images of cross-sections of NTX HCl-EVA28 implants produced using different process settings.

3.3.5 *In vitro* NTX HCl release

The influence of different process settings on the NTX HCl release kinetics from the implants was investigated in purified water at 37 °C. As shown in *Figure 52*, the implants exhibited a typical matrix release pattern. However, the total amount of NTX HCl released over the 14 days varied over a relatively wide range from 5 to 20 mg. After a significant decline in release over the first 5 to 9 days, the release rates stabilised by Day 8 or 9, resulting in approximately 0.5 to 1.0 mg/day for samples from Proc2 to Proc6. Proc1 implants demonstrated a significantly lower daily release rate (0.1 to 0.4mg) over the same period.



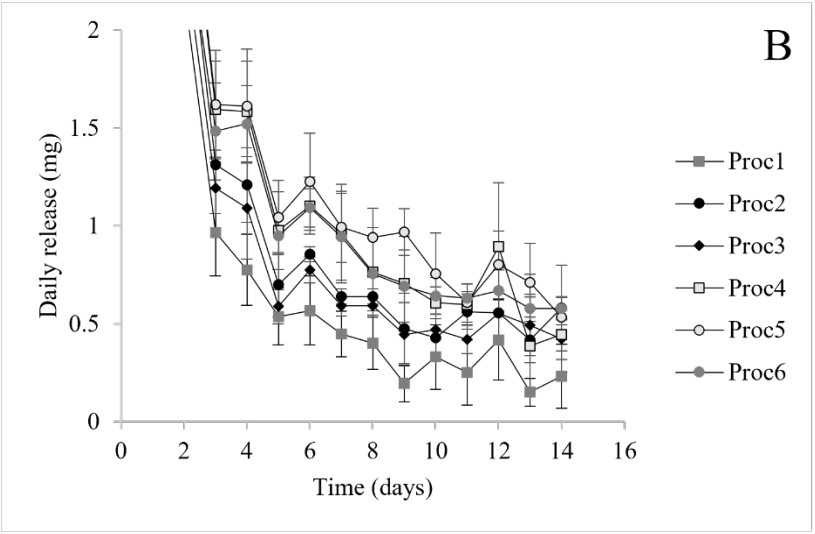


Figure 52 In vitro release kinetics of the the produced implants. (A) Cumulative and (B) daily NTX HCl release over time (mg released/day, ±1 SD; n=4/group).

The one-way ANOVA and post-hoc Tukey's test revealed a statistically significant difference in relase from Day 3 between Proc1 and Proc4 to Proc 6. The statistical test classified three groups from Day 8, which did not change by the end of the study (*Figure 53*). According to the pairwise comparison test, the cumulative NTX HCl release of Proc1 statistically differed from the Proc4 to Proc6 samples, while Proc2 showed no statistical difference from each group over the 14 days.

Grouping on Day 8

Factor	N	Mean	Grouping		
Proc5_D8	4	13.61	A		
Proc4_D8	4	13.066	A	B	
Proc6_D8	4	12.524	A	B	
Proc2_D8	4	11.231	A	B	C
Proc3_D8	4	9.986		B	C
Proc1_D8	4	8.087			C

Grouping on Day 14

Factor	N	Mean	Grouping		
Proc5_D14	4	17.99	A		
Proc4_D14	4	16.70	A	B	
Proc6_D14	4	16.318	A	B	
Proc2_D14	4	13.907	A	B	C
Proc3_D14	4	12.445		B	C
Proc1_D14	4	9.67			C

Figure 53 Results of post-hoc Tukey's pairwise comparison test for the measured release of NTX HCl (mg) on Day 8 and Day 14 from the implants produced using different HME process settings.

Multiway ANOVA-based model was also fitted for the total amount of NTX HCl released at the end of the study (Day 14). The general model showed that only the screw speed had a statistically significant effect (p=0.035) on the total amount of NTX HCl released from the implants over 14 days (*Figure 54*).

Analysis of Variance

Source	DF	Adj SS	Adj MS	F-Value	P-Value
Proc. temp. (°C)	1	3.551	3.5514	0.86	0.367
Screw speed (rpm)	1	21.489	21.4890	5.17	0.035
Proc. temp. (°C)*Proc. temp. (°C)	1	0.493	0.4928	0.12	0.734
Screw speed (rpm)*Screw speed (rpm)	1	0.645	0.6451	0.16	0.698
Proc. temp. (°C)*Screw speed (rpm)	1	16.933	16.9325	4.08	0.059
Total	23	260.901			

Model Summary

S	R-sq	R-sq(adj)	R-sq(pred)
2.03787	71.35%	63.39%	49.06%

Coefficients

Term	Coef	SE Coef	T-Value	P-Value
Constant	-288	196	-1.47	0.159
Proc. temp. (°C)	2.81	3.04	0.92	0.367
Screw speed (rpm)	1.818	0.799	2.27	0.035
Proc. temp. (°C)*Proc. temp. (°C)	-0.0043	0.0125	-0.34	0.734
Screw speed (rpm)*Screw speed (rpm)	0.00055	0.00139	0.39	0.698
Proc. temp. (°C)*Screw speed (rpm)	-0.01372	0.00679	-2.02	0.059

Figure 54 Results of multifactor ANOVA analysis for released NTX HCl (mg) over 14 days from the implants produced using different HME process settings

Based on the results so far, the process settings related to batch Proc2 were chosen to manufacture implants with a larger batch size for further investigations (T_{proc}=135 °C/ Screw speed= 90 rpm). This decision was due to the CQA of the Proc2 implants showing the highest correlation with the 35% w/w NTX HCl-EVA28 (MFI:25.00) implants developed in the previous chapter. Furthermore, although the predictive efficacy (*R-sq(pred)*) of the generated fitted models based on ANOVA analysis appeared to be relatively low in some cases, the response optimiser tool of Minitab on the calculated models was used to give an estimation of the process settings which could be used to achieve the optimal target quality of the implants (*Figure 55* and *Figure 56*). For this calculation 3 CQAs were involved. Drug content was optimised for the target 35% w/w±10% level, the total impurity content was minimised, and the total amount release NTX HCl at Day 14 was maximised. The calculated optimised process parameters showed a very high correlation with the chosen process settings (T_{proc}=136.51 °C/ Screw speed= 90.91 rpm).

Parameters

Response	Goal	Lower	Target	Upper	Weight	Importance
Drug release at D14 (mg)	Maximum	8.6372	21.3381		1	1
Total imp. cont. (%)	Minimum		0.1090	0.1618	1	1
Drug cont. (%w/w)	Target	31.5000	35.0000	38.5000	1	1

Variable Ranges

Variable	Values
Proc. temp. (°C)	(125, 145)
Screw speed (rpm)	(60, 120)

Solution

Solution	Proc. temp. (°C)	Screw speed (rpm)	Drug release at D14 (mg) Fit	Total imp. cont. (%) Fit	Drug cont. (%w/w) Fit	Composite Desirability
1	136.515	90.9091	14.7339	0.126170	35.7787	0.631434

Multiple Response Prediction

Variable	Setting
Proc. temp. (°C)	136.515
Screw speed (rpm)	90.9091

Response	Fit	SE Fit	95% CI	95% PI
Drug release at D14 (mg)	14.734	0.992	(12.573, 16.895)	(10.368, 19.100)
Total imp. cont. (%)	0.12617	0.00474	(0.11584, 0.13650)	(0.10529, 0.14705)
Drug cont. (%w/w)	35.779	0.911	(33.794, 37.764)	(31.768, 39.790)

Figure 55 Response optimisation results calculated using Minitab software. 3 CQAs (drug release at Day 14_maximised; total impurity content_minimised; drug content_35% w/w±10%) were involved in the calculation. The two independent variables were the process temperature and screw speed ranging from 125 to 145 °C, and from 60 to 120 rpm, respectively.

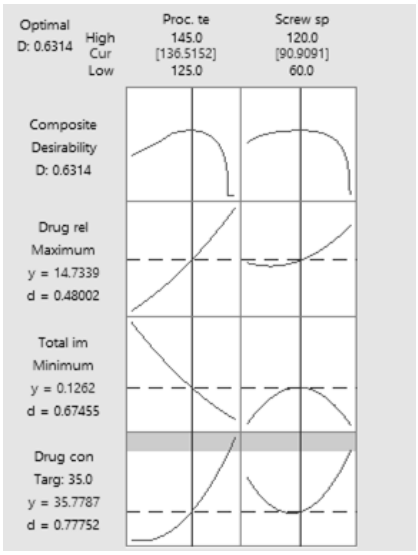


Figure 56 Response optimisation plot calculated using process temperature and screw speed with 3 CQAs (drug release at Day 14_maximised; total impurity content_minimised; drug content_35% w/w±10%) as responses

3.3.6 6-month stability study

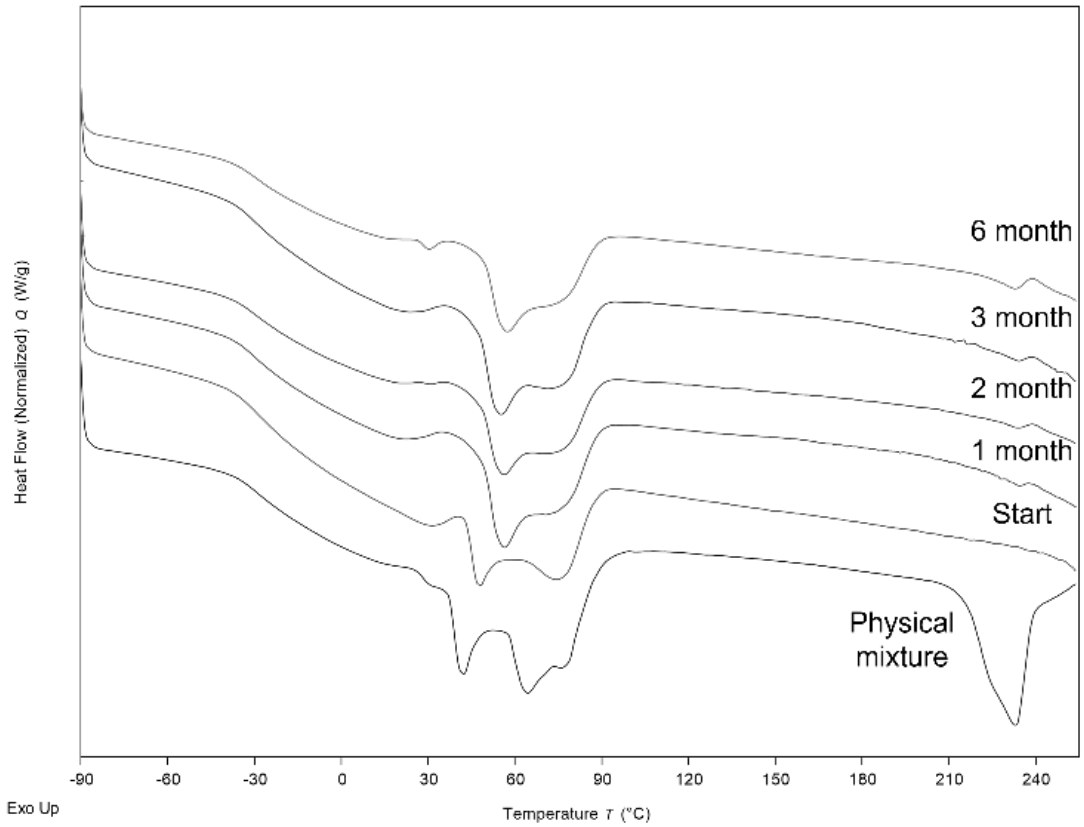
A large batch (100) of implants was manufactured using the selected (Proc2) process parameters (T_{proc}=135 °C/ Screw speed= 90 rpm) and stored for 6 months under accelerated conditions (40 °C/ 75%RH) in heat-sealed Alu/PE/PP sachet pouches (*Figure 57*).



Figure 57 Appearance of the produced implants (left side) and the heat-sealed sachet pouches prepared for the accelerated stability study (right side).

The stability samples were analysed for their several CQAs, including drug content, chemical stability, mechanical and morphological properties and *in vitro* release performance. The measured results are summarised in *Table 24*. No significant time-dependent change could be seen in terms of assay and purity profile of the NTX HCl. However, an increase in crystallinity of NTX HCl and the EVA matrix was observed, which had no impact on the tensile and release properties of the implants. Interestingly, the glass transition of the amorphous NTX HCl observed in the process screening step (*Figure 50_A*), did not appear in the DSC thermograms after storage which could be observed in the process screening step (*Figure 58*).

The release profiles of the implants at various sampling time points were compared using different comparison techniques, including model-independent (*f_2 similarity factor*) and model-based (*Higuchi constant*) methods. Both methods did not reveal any significant change in the dissolution profiles over the period of the stability study. The calculated f_2 values compared to the starting point was not less than 95, confirming a very good similarity between the release patterns, as in the industrial practice a similarity factor less than 50 indicates non-similarity between the average release curves of two products. Moreover, the calculated Higuchi constants for each release curve showed no statistically significant (p<0.05) differences between the group means related to different sampling time points based on one-way ANOVA and the post-hoc Tukey's pairwise comparison test.



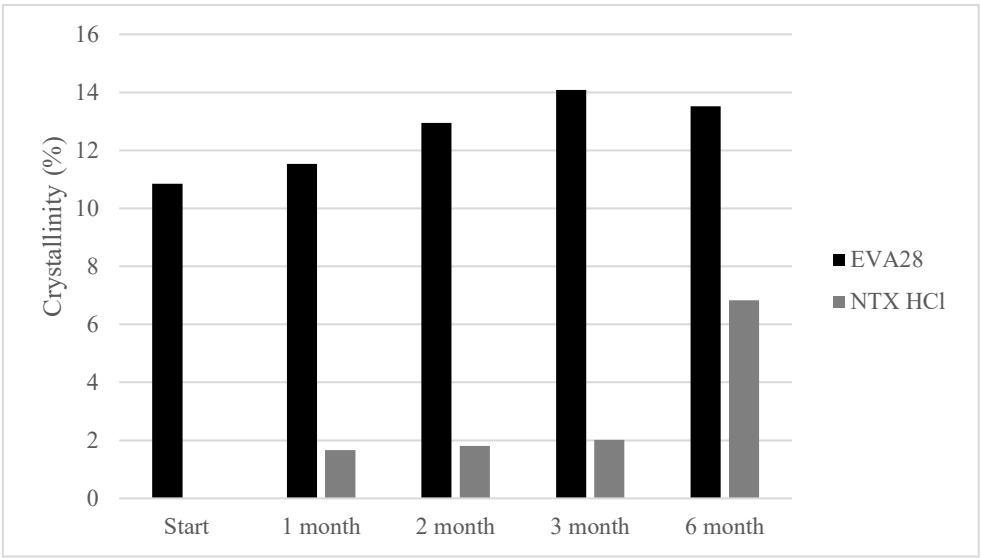


Figure 58 DSC curves of the stability samples (upper side) and the calculated crystallinity values (lower side) measured at different sampling time points

Table 24 Summary of stability study

Test attributes	**Requirements**	**40 °C / 75 % RH**									
		Start		**1 month**		**2 months**		**3 months**		**6 months**	
Appearance	*n.a*	Off-white rods		Off-white rods		Off-white rods		Off-white rods		Off-white rods	
Assay/CU (n=6) (Mean±SD)	35% w/w ± 10% (31.5–38.5% w/w)	34.3 ± 1.0% w/w %RSD: 2.8		36.0 ± 1.6% w/w %RSD: 4.4		33.0 ± 0.8% w/w %RSD: 2.4		35.1 ± 1.0% w/w %RSD: 2.8		34.3 ± 1.0% w/w %RSD: 2.8	
Related substances (n=3) *Complies with PhEur 9.0*	Imp. A 0.10%	< D.L.		< D.L.		< D.L.		< D.L.		< D.L.	
	Imp. B 0.10%	0.03 ± 0.0021%		0.03 ± 0.0004%		0.03 ± 0.0012%		0.03 ± 0.0016%		0.03 ± 0.0007%	
	Imp. C 0.20%	0.07 ± 0.0041%		0.07 ± 0.0005%		0.06 ± 0.0037%		0.06 ± 0.0008%		0.06 ± 0.0036%	
	Imp. D 0.20%	0.04 ± 0.0017%		0.04 ± 0.0015%		0.04 ± 0.0015%		0.03 ± 0.0020%		0.03 ± 0.0010%	
	Imp. E 0.20%	0.03 ± 0.0013%		0.03 ± 0.0011%		0.04 ± 0.0018%		0.03 ± 0.0009%		0.03 ± 0.0007%	
	Imp. F 0.20%	No detection		No detection		No detection		No detection		No detection	
	Imp. G 0.20%	< D.L.		< D.L.		< D.L.		< D.L.		< D.L.	
	Imp. H 0.10%	0.04 ± 0.0007%		0.04 ± 0.0041%		0.04 ± 0.0023%		0.02 ± 0.0016%		0.03 ± 0.0009%	
	Imp. I 0.10%	No detection		No detection		No detection		No detection		No detection	
	Imp. J 0.10%	No detection		No detection		No detection		No detection		No detection	
	Unknown Imp. 0.10%	< D.L.		< D.L.		< D.L.		< D.L.		< D.L.	
	Total 1.00%	0.20 ± 0.0035%		0.21 ± 0.0032%		0.21 ± 0.0056%		0.17 ± 0.0049%		0.19 ± 0.0061%	
Drug release (n=6) f_2 similarity factor (compared to the start point)	*Two dissolution profiles are declared similar, if* ***$50< f_2<100$***	100		98.99		95.82		98.89		99.33	
Drug release (n=6) Higuchi const.	*n.a*	2.34 ± 0.48		2.38 ± 0.53		2.06 ± 0.69		2.36 ± 0.67		2.40 ± 0.56	
Drug release (n=6) Total rel. at day 14	*n.a*	13.28 ± 0.79 mg		12.53 ± 1.24 mg		12.90 ± 1.51 mg		12.69 ± 0.71 mg		12.44 ± 1.36 mg	
Tensile (n=3) (Modulus±SD)	*n.a*	0.49 ± 0.06		-		-		0.54 ± 0.02		0.43 ± 0.05	
Degree of crystallinity	*n.a*	*NTX.HCl*	*EVA28*	*NTX.HCl*	*EVA28*	*NTX.HCl*	*EVA28*	*NTX.HCl*	*EVA28*	*NTX.HCl*	*EVA28*
		0.00%	10.85%	1.67%	11.53%	1.81%	12.95%	2.02%	14.08%	6.83%	13.52%

3.4 Discussion

Six different batches of implants were manufactured by using different HME process parameters. In this study, the two independent parameters were processing temperature and screw speed, which were varied at 3 different levels and their effect on the CQAs investigated. Although the study performed in this chapter cannot be considered as a standard DoE experiment, the evaluation method of the Minitab software based on the multifactor ANOVA analysis (*Fit General Model* tool) was able to show the significant effects of the studied process parameters in several cases.

Of particular interest in this study, the evaluation of NTX HCl content in the implants revealed the most intricate connection between this CQA and the processing parameters. Generally, the application of higher processing temperature and screw speed resulted in a significantly higher drug content in the implants, even though an appropriate proportion of drug-polymer mixture (35/65% w/w) was fed into the extruder each time. This phenomenon was most likely due to the phase transition of NTX HCl during the process, which was confirmed by the DSC measurements. It can be assumed that the amorphised and/or molten drug generally adhered better to the screw elements, and the extent of which was strongly temperature dependent, resulting in an accumulation of NTX HCl at a certain point along the barrel at higher process temperatures[321]. After a sufficient concentration and pressure profile developed, the screw elements conveyed the mixture with higher NTX HCl concentration. However, this hypothesis could not be confirmed, as the extruder used in this study could not monitor the torque during the process.

Statistical analysis revealed the significant negative effect of screw speed on the total impurity content of the implants (*Figure 47*). This result was not surprising as lower residence time resulted in shorter heat stress on the extruded amorphous systems. Furthermore, although the ANOVA calculation did not show a significant effect of the processing temperature on the degradation of NTX HCl, its interaction term with screw speed expressed a statistically significant positive effect on the degradation of NTX HCl. This means that the simultaneous increase of these two factors resulted in a higher degradation of NTX HCl, but with a much lower effect compared to the factor of screw speed alone. This could suggest that the amorphous and/or molten drug was slightly more sensitive against the shear stresses at higher temperatures.

Morphological characterisation of the implants confirmed that the total amount of NTX HCl went through amorphisation in all cases (*Figure 50*). Interestingly, although the glass transition

of the glassy drug was also seen on the DSC thermograms in some cases, this endothermic peak did not appear both in the samples produced in the product development step and the following stability samples. The hypothesis is that this transition was seen because of some level of inhomogeneity (i.e., drug enriched clusters) in the radial direction of the implant was not confirmed by the SEM analysis, where the NTX HCl distribution seemed homogeneous. It is conceivable that the radial inhomogeneity in question could be demonstrated by analysing a larger number of samples, as both the DSC and SEM can analyse only the small amount of the implants. Another solution could be to use an analytical method that can analyse larger volumes simultaneously, for example, the X-ray computed tomography (XRCT) technique, which differentiates the components and pores according to their densities[302].

The flexibility measurements showed a significant, almost 3-fold increase in the elastic moduli of the drug-loaded implants (*Figure 48*). This great decrease in flexibility can be explained as a result of cohesive energy on the high specific surface area of the fine amorphous drug particles dispersed in the polymeric matrix. The fine particles of NTX HCl acted as a filler with a high specific surface area. Additionally, the amorphous form tends to have higher surface energy than the thermodynamically more stable crystalline form, causing higher attractive forces[321]. Increased level of crystallinity in matrix polymer could also cause a decrease in flexibility. However, the degree of crystallinity in EVA28 decreased after the extrusion process, confirmed by DSC measurements (*Figure 50*), indicating that the detected change in flexibility resulted from the amorphous drug loading. Interestingly, the ANOVA analysis showed no significant effect of process settings, and therefore indirectly of drug content, on the mechanical properties of the implants, most likely due to the limitation of the applied measuring technique (*Figure 49*).

According to the average cumulative drug release curves of the implants, 3 distinct groups could be classified, which is in good agreement with the average drug content of the implant batches (*Figure 53*). However, statistical analysis revealed less significant differences between the sample groups because of the relatively high variability within the samples. This high variability in the measured NTX HCl release could question the reliability of the generated ANOVA-based model fitted on the total amount of NTX HCl released by Day 14, which revealed the significant impact of only screw speed (*Figure 54*). It is more likely that the average drug content and homogeneity of the samples determined the amount of the drug released, on which the process parameters have a very complex effect, as already mentioned above.

The 6-month stability study of a larger batch produced using the process settings (Proc2) that showed the highest correlation with the 35% w/w implants developed in the previous chapter was conducted. The implants were identical in all investigated CQAs to batch Proc2 manufactured using the same process settings throughout the 6 months study period. Only the purity profile differed, as NTX HCl with a different lot number was used to manufacture this stability batch. However, a significant change in this characteristic was not observed during the study, indicating that the drug was chemically stable under accelerated storage conditions. Furthermore, the crystallinity of NTX HCl increased significantly from the third to the sixth month, but this change in drug morphology did not affect the dissolution profile of the implants. The neglectable effect of drug morphology on the release performance was already observed and discussed in the previous chapter. Moreover, drug release characteristics measured at different sampling time points were compared using model-independent and model-dependent methods. Although the calculation of the f_2-value is very general in industrial practice because of its simplicity, it has many limitations, especially in formulation development decisions[322],[323]. Therefore, a statistical analysis on the calculated Higuchi constants related to each dissolution curve was conducted. No statistically significant difference was observed, confirming that the most critical attribute of the implants, namely the drug release performance appeared to be stable throughout the study period.

3.5 Conclusions

In this chapter, the influence of two HME process parameters on the performance of NTX HCl-EVA28 implants was studied. Several CQAs were chosen as response variables. Our results revealed the complex influence of processing temperature and screw speed on the drug content of the products, which is due to the morphological change of NTX HCl during the HME process. However, other performance characteristics are not influenced by these two process parameters or can be traced back to the complex evolution of the drug content. The larger stability batch produced with the selected process parameters showed a good agreement with the target product profile. Furthermore, this batch showed adequate stability under long-term (6 months) and accelerated (40 °C/ 60 %RH) storage conditions.

4 The influence of cellulose-ether additives on drug release of NTX HCl loaded EVA implants

4.1 Introduction

In binary EVA-based monolithic dispersion implantable drug delivery systems (IDDS) drug release mainly occurs through a porous network filled with the release media. The pores are formed by the hydrophilic drug itself, which leaves behind a void space upon dissolution, thus providing further access to the release medium to form additional pores in the hydrophobic matrix, through which the dissolved drug can diffuse out from the system. Accordingly, in these systems, a specific drug concentration can be defined (i.e., percolation threshold), below which a system-wide interconnected network of pores does not form. Thus, the complete release of the embedded drug particles cannot be achieved. On the other hand, increasing the initial drug loading above the percolation threshold results in increasing drug release rates as the tortuous pathways have a lower number of "dead ends", allowing the dissolved drug molecules to reach the surface of the medical device with less time delay[305]. However, if the initial drug concentration exceeds the percolation threshold to a great extent, the high release rate may make the device unsuitable for sustained drug delivery. Although the desired release profile can be achieved by appropriate selection of matrix polymer and drug loading (see *Chapter 2*), the application of specific release-controlling additives can be more advantageous from a therapeutic and even economic point of view. For example, the desired pharmacokinetic profile of IDDS can be achieved even at lower drug loadings by using a suitable pore-forming additive, while an appropriate release-controlling agent can tailor the release profile to be preferable for long term therapy or expand the time of treatment by lowering the release rate at higher initial drug concentrations.

Swelling or gelling agents have a great history in the pharmaceutical field and are widely used for oral administration (e.g., matrix tablets, osmotic pumps)[324] and injectable or implantable controlled release devices[80,325]. Furthermore, several applications for long term intravaginal drug delivery have been reported where such agents, mainly cellulose derivatives, are compressed with the API and enclosed in a hard polymer casing (e.g., polyurethane or silicone tubes)[326,327]. The controlled release occurred through orifices drilled onto the tubes. These designs require complex manufacturing processes that will likely prove challenging and cost-intensive to scale.

This study aimed to investigate the influence of two cellulose-ether (CE) additives, namely hydroxypropylcellulose (HPC) and hydroxypropylmethylcellulose (HPMC), as pore forming, swelling or gelling agents on NTX HCl release from EVA subcutaneous implants produced via a one-step HME process.

The main objective of this chapter were as follows:

- Firstly, the biodegradable hydrophilic CEs were added at two concentration levels, 5 and 10% w/w, to the systems containing two initial drug loadings, under and above the percolation threshold, 20 and 50% w/w, respectively. The influence of CE addtivies on processability was investigated. Additionally, the produced implants were characterised for their drug loadings, while the morphology of the samples was investigated by Raman spectroscopy and SEM.
- Secondly, NTX HCl-EVA implants were also manufactured with varying NTX HCl loadings (20, 30, 40 and 50% w/w) and their release performance compared to the composite systems.

4.2 Materials and methods

4.2.1 Materials

EVA copolymer with VA-content of 28% and an MFI of 150 was provided by Celanese Corp. (Texas, US) in a cryomilled powder form. CEs used were HPC (Alfa Aesar, Haverhill, US) and HPMC (Sigma-Aldrich, St. Louis, US). The properties of the additives are shown in *Table 25*.

Table 25 Properties of cellulose derivatives used for this study

Cellulose ether	Molecular weight (M_w)	Substitution (%)		Viscosity (5% water; 20°C)
HPC	≈ 100 000	Hydroxypropoxyl group	50-80%	75-150cps
HPMC	≈ 400 000	Methoxyl group	28-30%	3000-5600cps
		Hydroxypropoxyl group	7-12%	

All other materials used for manufacturing and further analytical procedures were the same as those used in *Chapter 2, Section 2.2.1*.

4.2.2 Hot-melt extrusion

The appropriate amounts of NTX HCl, EVA28, HPC and HPMC were weighed into a sealed plastic container and roll mixed for approximately 10 min. The formulations used in the current study are shown in *Table 26*.

Table 26 Composition of formulation investigated in this study

Formulation	Component (% w/w)				
	NTX HCl	HPC	HPMC	EVA	Total
20NTXHCl	20	-	-	80	100
30NTXHCl	30	-	-	70	100
40NTXHCl	40	-	-	60	100
50NTXHCl	50	-	-	50	100
20NTXHCl_5HPC	20	5	-	75	100
20NTXHCl_10HPC	20	10	-	70	100
50NTXHCl_5HPC	50	5	-	45	100
50NTXHCl_10HPC	50	10	-	40	100
20NTXHCl_5HPMC	20	-	5	75	100
20NTXHCl_10HPMC	20	-	10	70	100
50NTXHCl_5HPMC	50	-	5	45	100
50NTXHCl_10HPMC	50	-	10	40	100

The pre-blends (approx. 10 g) were fed into a Kapex laboratory scale 7.5 mm (15 L/D) twin-screw extruder (Kapex Manufacturing LLC, Saginaw, US) using a Lambda Doser powder feeder (Lamda Instruments, Brno, Czech Republic) and extruded through a 3 mm die at a screw speed of 30 rpm, a processing temperature of 140°C and with a feeding rate of 5 g/min. The resulting extrudates, 3.0±10% in diameter, were allowed to cool and cut into 20 mm long rods.

4.2.3 Drug content analysis and *in vitro* release testing

Drug content of 3 rods was assessed prior to *in vitro* release testing. The first and last 5 mm long segments were cut from the 20 mm long implants and their drug content measured by the method described in *Section 2.2.4.* Drug content and homogeneity of the different batches was assessed using the average of the 3*2=6 measurements. The remaining 10 mm long rods were then analysed for their *in vitro* release performance by placing the rods into a sealed 35 mL glass vials containg 20 mL of purified water and placed into an orbital shaking incubator (Unitron HT Infors) at 37°C and 60 rpm. Closed syringe needles were used to prevent the extrudates from floating and to ensure perfect sink conditions (*Figure 59*). 1 mL of the dissolution media was taken on each sampling day, and the sample volume was replaced with fresh deionised water. The collected samples were centrifuged and analysed for drug content using the NTX HCl assay HPLC method (*Section 2.2.4*). The statistical analysis of the results was identical as described in *Section 2.2.16*.

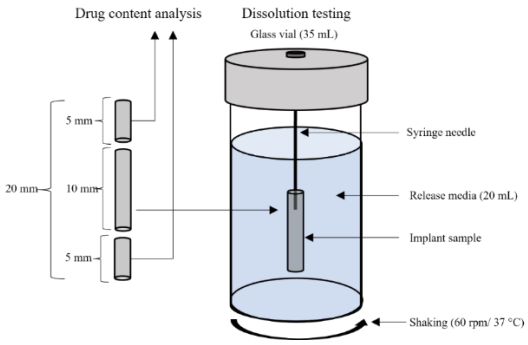


Figure 59 Depiction of the protocol used for drug content and *in vitro* release analysis

4.2.4 Morphological characterisation of the extrudates

The SEM measurements were the same as described in *Section 2.2*. The distribution of the components was analysed by Raman spectroscopy. The measurements were performed using a Thermo Scientific DXR Raman microscope (Thermo Fisher Scientific, Waltham, US). The spectra were collected from a selected cross-sectional area (*Figure 60*) by exciting the sample surface with laser light of a 780-nm wavelength at a laser power of 24mW. For each measurement, a X10 objective was used, and the aperture was selected to 25 mm. Each mapping was executed with a spatial resolution of 30 µm vertically and horizontally. The collected spectra were pre-processed by automatic baseline correction and normalisation prior to generating the chemical maps by the OMNIC for Dispersive Raman 9.9 software package (Thermo Fisher Scientific). The images from the cross-sectional distribution of each component were generated according to the correlation between the measured spectra at each point and the pure components' spectra.

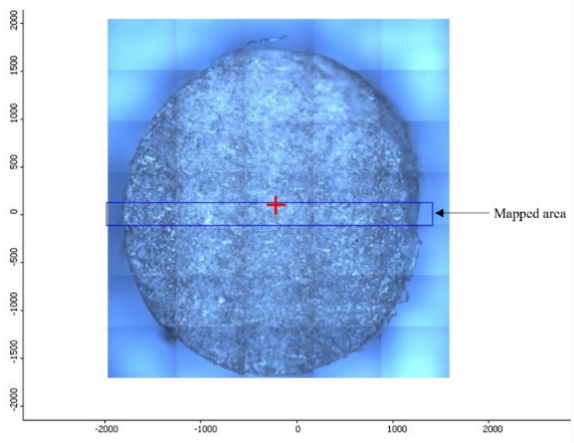


Figure 60 Optical microscope image with X10 objective about the cross section of an example extrudate (20NTX HCl_5HPC) and the area mapped for each Raman measurement executed for this study

4.3 Results

4.3.1 Processability and drug content of the implants

Each formulation could be manufactured with the selected processing parameters using the Kapex extruder. However, higher torques were required to extrude the systems with higher drug loadings and CE additives with a slight discolouration observed in these samples. 3 independent people were asked to visually inspect and compare the flexibility of the produced implants to that of the Nexplanon reference, as described in *Section 2.3.1*. Only the 50% w/w NTX HCl implants with 10% w/w CE additives showed unaccepted flexibility among the individuals.

Drug content of the implant batches was assessed by analysing 2 segments of 3 extrudates per formulation. The results clearly show that NTX HCl contents were approximately in the target ± 10w/w% range (*Figure 61*). However, the average NTX HCl content of the binary systems was slightly higher than expected. In the case of 20 and 30% w/w NTX HCl-EVA implants, the drug content exceeded the ±10% acceptance limit (22.5±0.55 and 33.33±0.42%). The variation of the measured values was acceptable in each batch (%RSD<5), indicating good homogeneity within the formulations.

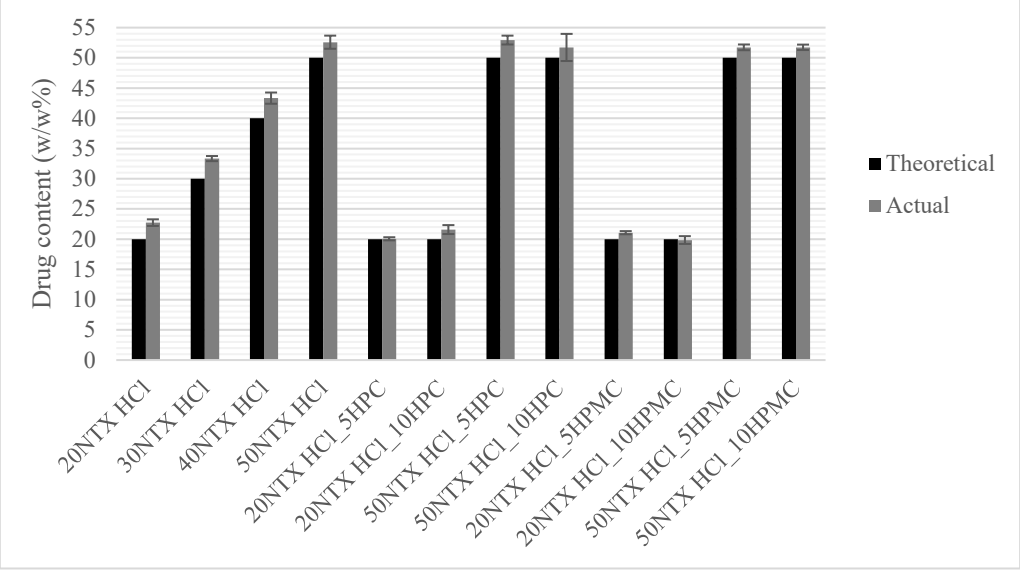


Figure 61 Actual and theoretical NTX HCl contents in each of the different formulation investigated in this study. Error bars represents ±1 standard deviation of n=6 replicates.

4.3.2 Morphological characterisation

SEM analysis was conducted on the produced CEs-loaded implants to investigate the morphology of the extrudates. As demonstrated in *Figure 62*, the cross-sectional areas of implants with lower drug loadings were less porous with well-defined particles and clusters within them, which distribution could be considered homogeneous in the dense EVA matrix.

On the other hand, the samples containing 50% w/w NTX HCl showed a relatively more porous and complex structure. Unfortunately, chemical mapping of the sample surfaces to differentiate NTX HCl particles from the other (non-EDS active) components by the EDS function of the SEM equipment was not conducted, as the equipment had limited access at the time of this study (see *Covid statement*). However, to investigate the distribution of each component in the implants, Raman microscopic analysis was performed. This analytical technique allowed each component in the system to be analysed simultaneously, as each material had sufficient Raman activity and showed different spectra with well-distinguishable characteristic peaks (*Figure 63*). Three chemical images were generated per formulation for EVA28, NTX HCl and the CEs. The results are shown in *Figure 64*. The images represent that each component was relatively well distributed in the radial direction of the extrudates. It can also be assumed that none of the formulated components formed one phase with another, as lower spectral concentrations for a certain component were measured in points, where other components showed higher intensity. According to these results, it is very likely that each component was presented in the system as separated particles, and no fusion among the components occurred during HME. Several NTX HCl-EVA28-HPMC implants (20NTXHCl_10HPMC, 50NTXHCl_5HPMC and 50NTXHCl_10HPMC) were not tested by Raman (see *Covid statement*). However, it can be assumed with high certainty due to their similar surface morphology, measured by SEM that their distribution profile is similar to that of the samples were measured.

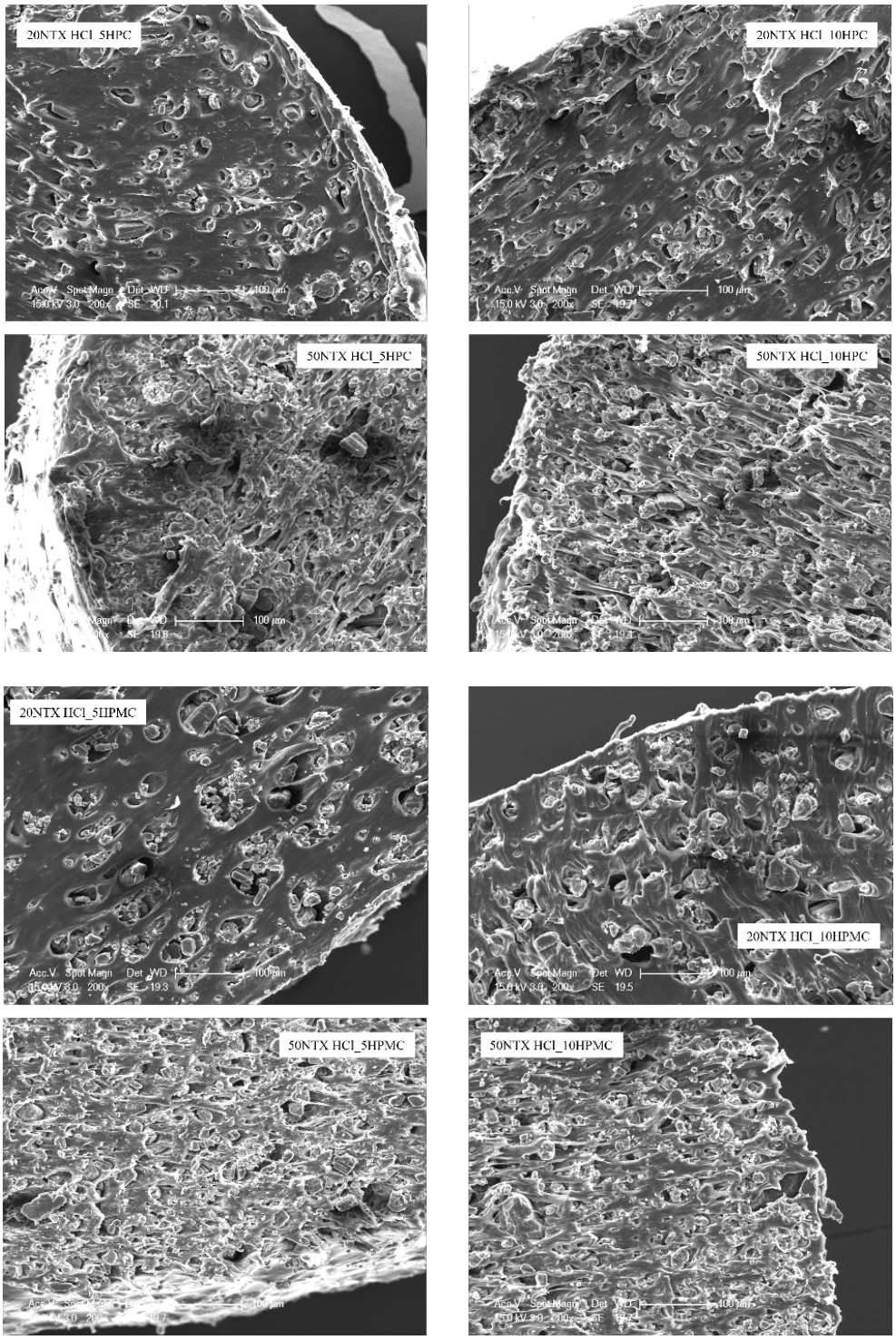


Figure 62 SEM images of cross-sections of NTX HCl-EVA28 implants with varying drug and CE additive loadings. The images represent 200x magnification from the edges of the implants.

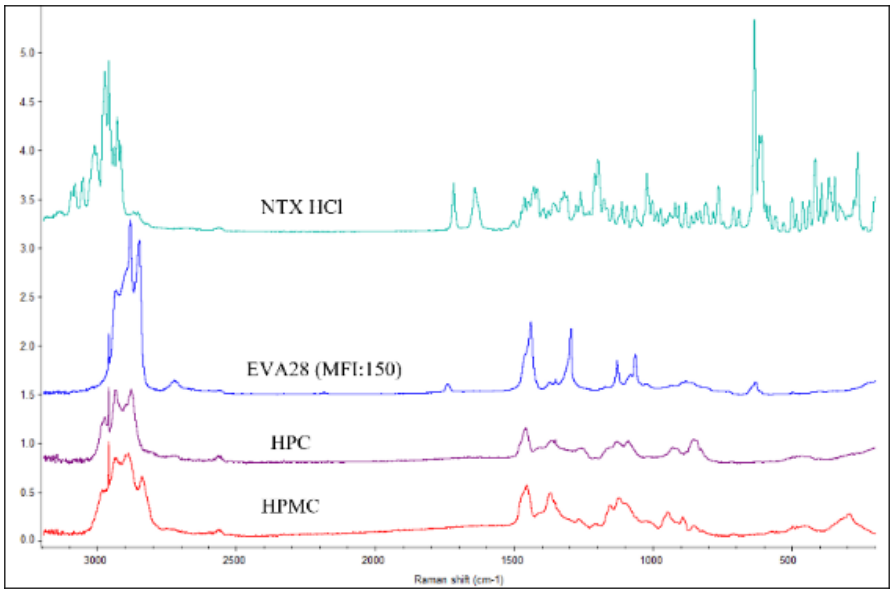
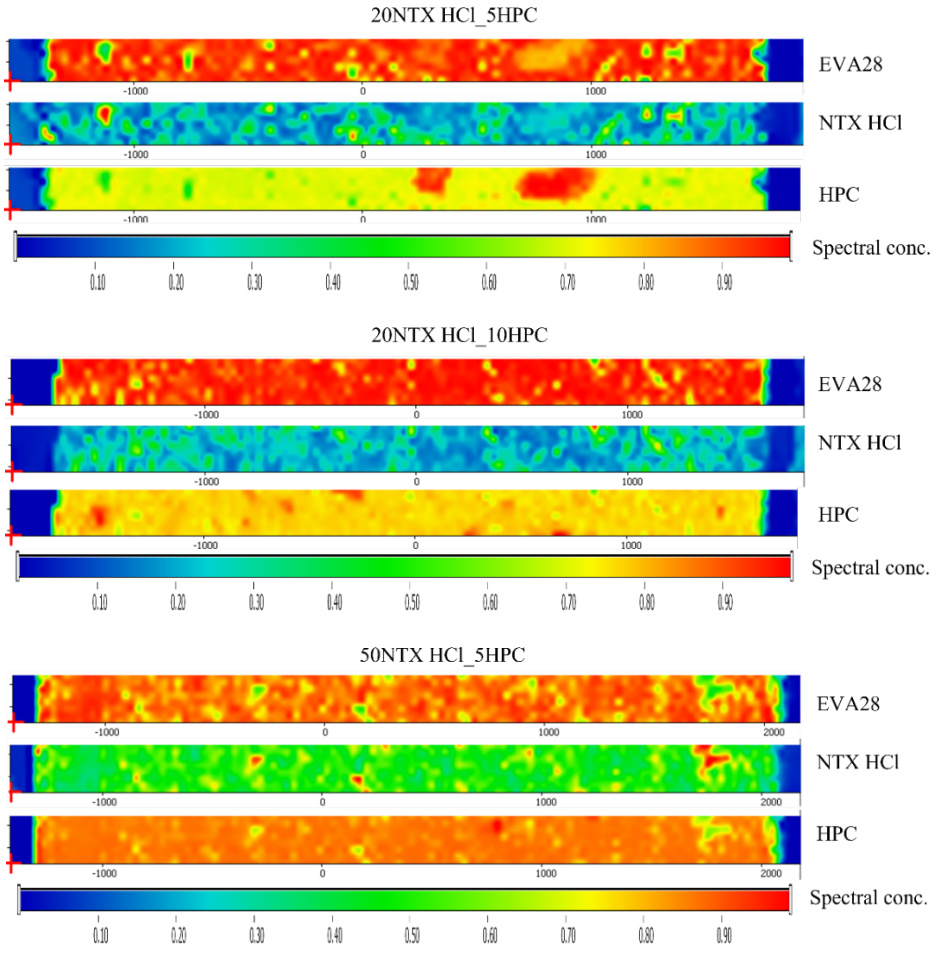


Figure 63 Representative average spectra of each material used for sthis study. 4 measurements were taken from each pure component. The spectra were then averaged, baseline-corrected and normalised by the Omnic software.



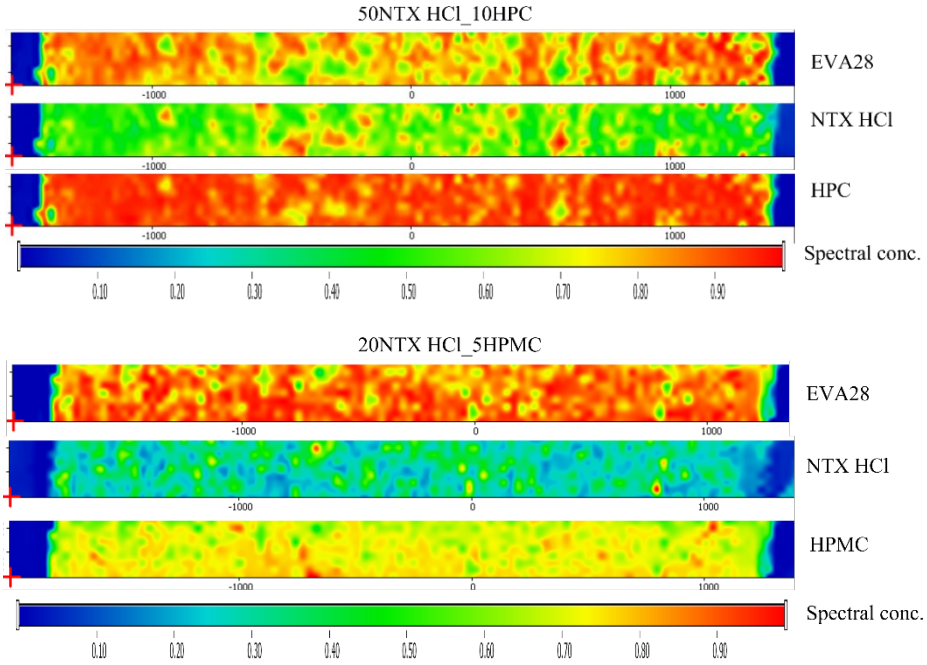


Figure 64 Chemical maps created based on the correlation between the spectra of the pure components and the meusured spectra on the analysed surface area with a spatial resolution of 30 µm. Low to high spectral concentrations (extent of correlation) in the images are described by colors blue to red.

4.3.3 *In vitro* NTX HCl release

Dissolution studies were conducted to investigate NTX HCl release from both the binary NTX HCl-EVA28 and ternary implants containing CE additives. The 50% w/w NTX HCl implants with higher CEs loadings (50NTXHCl_10HPC and 50NTXHCl_10HPMC) swelled and expanded to such an extent that they cracked on Day 4 and their investigation terminated. It is also important to mention, that by the end of the 27 day study, the remaining implants had acceptable mechanical properties, and their diameter did not exceed the 3±10% mm limit.

The release profiles are summarised in *Figure 65*. The amount and rate of NTX HCl release depended greatly on both the drug loading and the choice of CE additive. As the initial drug concentration was increased, the NTX HCl release increased substantially. In particular, for the 50NTX HCl samples, rapid and nearly complete release occurred by Day 9. However, the other binary systems, up to 40% w/w NTX HCl loading, showed a significantly (p<0.05) lower drug release rate following nearly zero-order kinetics over 27 days. 20NTXHCl samples with the lowest drug concentration (below the percolation threshold; approximately 23-25% w/w) released only 14.56±1.10% (3.57±0.24 mg), while 30NTXHCl and 40NTXHCl implants released 25.02±1.29% (7.18±0.06 mg) and 42.68±2.07% (18.98±0.04 mg) by the end of the study, respectively (*Figure 65 A_1*). As can also be seen form the daily release profiles, after the significant decline in release from day 3, the release rates stabilised by day 11 for the 20,

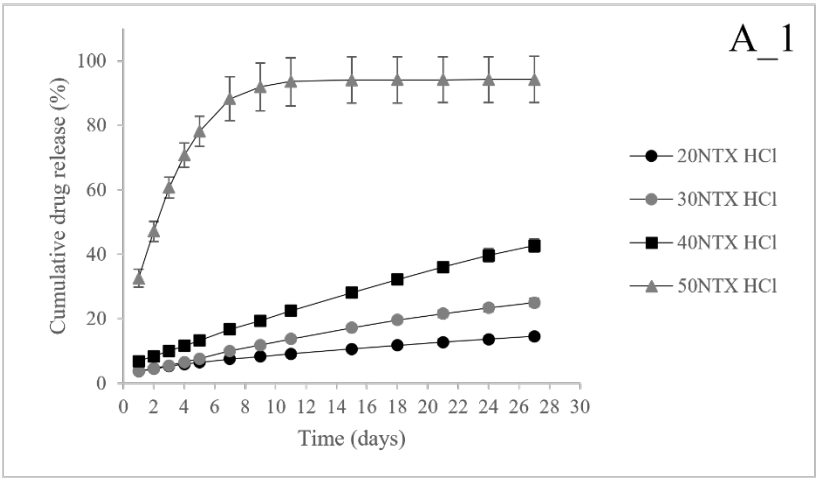
30 and 40NTX HCl implants with an approximate release rate of 0.12, 0.25 and 0.64 mg/day, respectively (*Figure 65 A_2*).

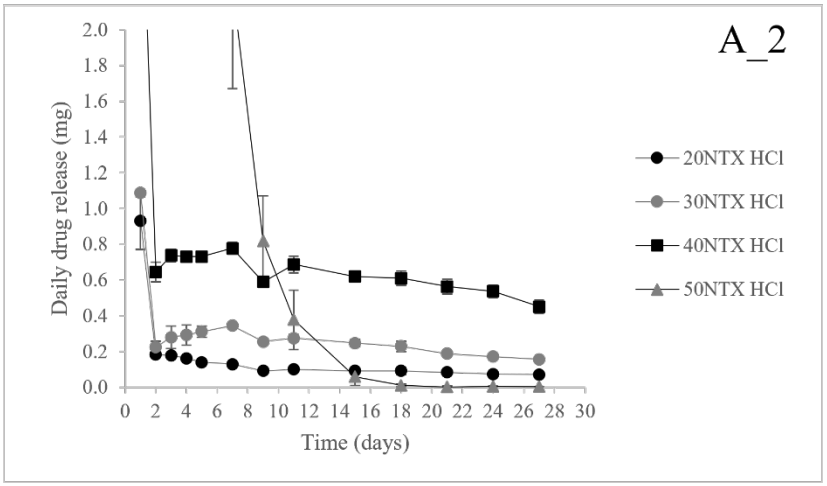
Figure 65 B_1 and *B_2* represents the effect of different CE additives on drug release of 20% w/w NTX HCl-loaded implants. The release rate was found to be significantly higher ($p<0.05$) in implants with 5 and 10% w/w HPC and 10% w/w HPMC additives compared to that of the binary system with the same NTX HCl loading. Cumulative drug release levels of 30.21±0.72% (6.43±0.06 mg), 92.52±0.97% (19.24±0.03 mg) and 70.33±3.50% (13.00±0.06 mg) could be reached with 20NTXHCl_5HPC, 20NTXHCl_10HPC and 20NTXHCl_10HPMC, respectively, by the end of the study period. That represents a 1.88, 5.39 and 3.64 fold increase in the release of NTX HCl compared to the 20NTX HCl binary system. It is also important to highlight that 20NTXHCl_5HPC and 20NTXHCl_10HPMC systems followed a nearly zero-order release kinetics from Day 2 with a daily drug release of 0.22 and 0.47 mg/day, respectively, which is close to 2 and 4 fold increase in the release of NTX HCl per day compared to 20NTXHCl implants (0.12 mg/day). However, 5% w/w HPMC additive had no signifcant ($p>0.05$) effect on the release kinetic.

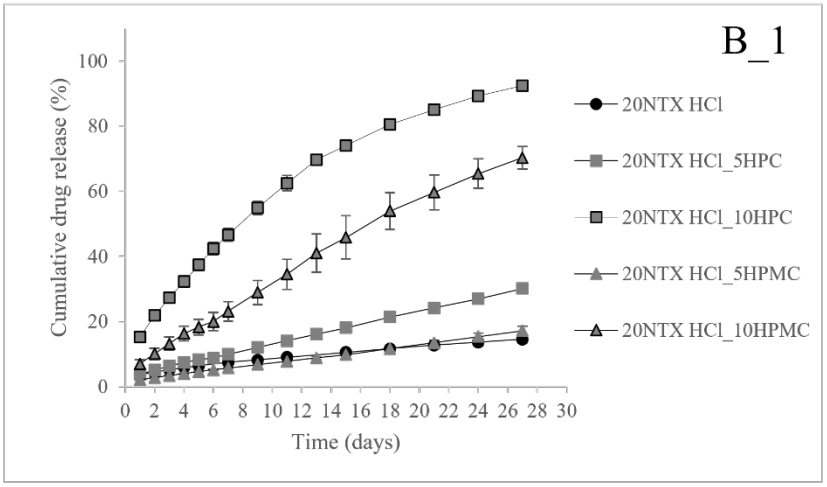
The influence of CEs on drug release in systems with 50% w/w NTX HCl loading compared to the binary system with the same drug concentration is demonstrated in *Figure 65 C_1* and *C_2*. Significant ($p<0.05$) decrease in release rate was observed in the case of 50NTXHCl_5HPC and 50NTXHCl_5HPMC. However, 5w/w % HPC additive resulted in a nearly first-order release kinetic that reached a plateau on Day 18 at approximately 80% release. On the other hand, HPMC at a level of 5% w/w affected the drug release preferably. As can be seen, its release followed a nearly zero-order kinetic with a daily release rate of approximately 1.2 mg/day.

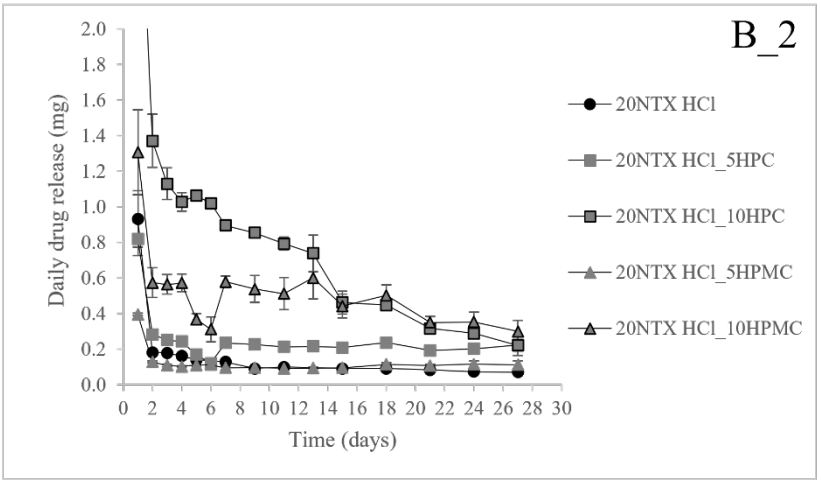
In order to understand the release mechanism, the release data were fitted to several mathematical models (*Table 27*). The Higuchi model showed a good fit ($r^2>0.95$) with the binary systems, indicating that the release occurred mainly through diffusion. This result was also confirmed by the Korsmeyer-Peppas and Peppas-Shalin model, as the calculated Korsmeyer-Peppas n exponents were less than 0.45, while in the Peppas-Shalin model, k_1 values, indicating the contribution of drug diffusion, were much higher than the k_2 values ($k_1>>k_2$), representing the contribution of polymer erosion. On the other hand, investigation of the release data of the ternary systems revealed anomalous transport mechanism according to the Korsmeyer-Peppas model, as the n exponents were in the range of $0.45<n<0.89$. The contribution of drug diffusion (k_1) and polymer erosion (k_2) in the release mechanism calculated

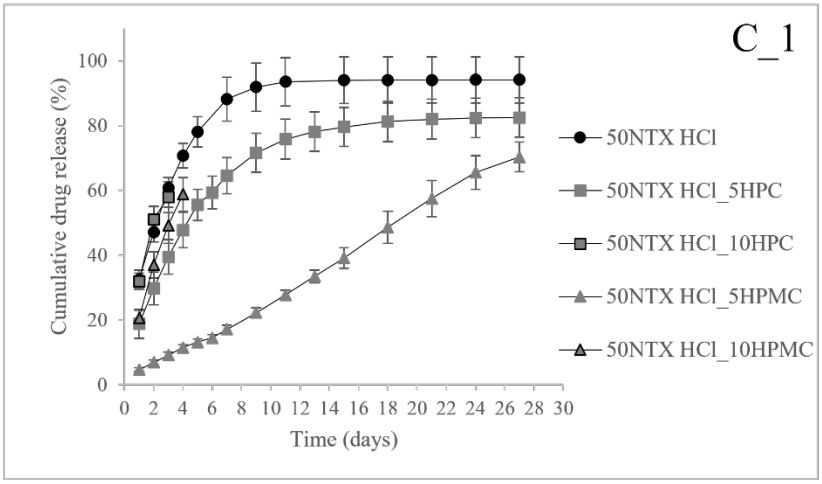
by the Peppas-Shalin model revealed that drug release in the ternary systems was mainly governed by drug diffusion ($k_1 > k_2$). However, polymer erosion also played a significant role in the release mechanism.











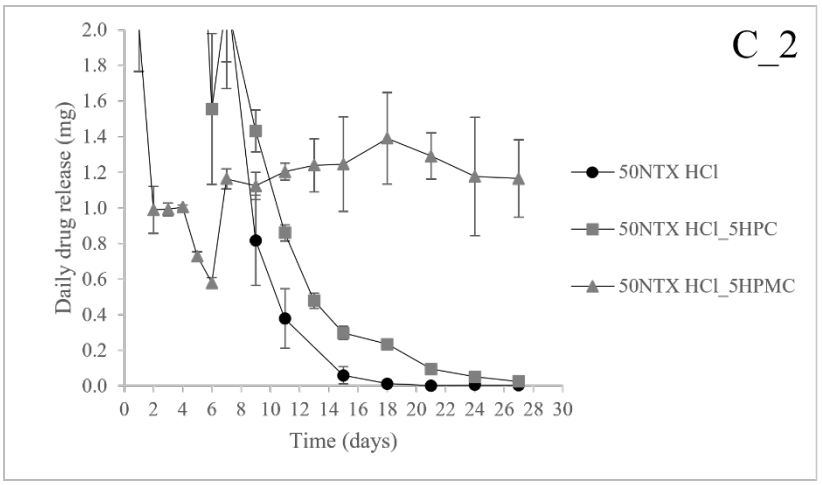


Figure 65 In vitro release of the produced implants. (A_1, B_1 and C_1) Total NTX HCl released over time (% total ± 1 SD; n=3/group). (A_2, B_2 and C_2) Daily NTX HCl release over time (mg released/day, ± 1 SD; n=3/group).

Table 27 Drug release kinetic results for the implants

Formulation	Higuchi model	Korsmeyer-Peppas model		Peppas-Sahlin model		
	$M_t/A=k_H*t^{1/2}$	$M_t/M_\infty=k*t^n$		$M_t/M_\infty=k_1*t^{1/2}+k_2*t$		
	r^2	n	r^2	k_1	k_2	r^2
20NTX HCl	0.9967	0.3577	0.9973	2.8105	0.0000	0.9983
30NTX HCl	0.9888	0.3778	0.9986	2.6309	0.0441	0.9986
40NTX HCl	0.9840	0.4400	0.9980	4.5088	0.0718	0.9990
50NTX HCl	n.a.****	n.a.***	n.a.***	n.a.***	n.a.***	n.a.***
20NTX HCl_5HPC	n.a.****	0.7609	0.9966	2.1326	0.6869	0.9982
20NTX HCl_10HPC**	n.a.****	0.6193	0.9992	12.8323	1.8095	0.9997
50NTX HCl_5HPC**	n.a.****	0.6161	0.9974	17.7493	2.7450	0.9963
50NTX HCl_10HPC*	-	-	-	-		-
20NTX HCl_5HPMC	n.a.****	0.7773	0.9956	1.1145	0.4043	0.9974
20NTX HCl_10HPMC**	n.a.****	0.7922	0.9984	4.3870	1.8416	0.9983
50NTX HCl_5HPMC**	n.a.****	0.8502	0.9975	2.8605	1.9584	0.9979
50NTX HCl_10HPMC*	-	-	-	-		-

* Implants expanded and cracked at the beginning of the *in-vitro* study at day 3 or day 4.

** Release data were processed up to 60% cumulative drug release.

*** The cumulative release (%) exceeded 60% at the beginning of the *in-vitro* study, therefore the models were not applicable.

**** The Higuchi model was not applicable.

The release profiles of the binary systems with 30 and 40% w/w NTX HCl loadings, and the 20NTXHCl_5HPC, 20NTXHCl_10HPMC and 50NTXHCl_5HPMC were predicted up to 90 days by extrapolating the Higuchi models fitted to the 27 days long averaged *in vitro* data to give a rough estimation about the amount of NTX HCl released for extended periods. The Korsmeyer-Peppas model was used for the prediction of the binary systems' release profiles, while the Peppas-Sahlin model was applied for the ternary formulations, as this model gave a best fit for the *in vitro* data. The predicted release profiles are shown in *Figure 66*.

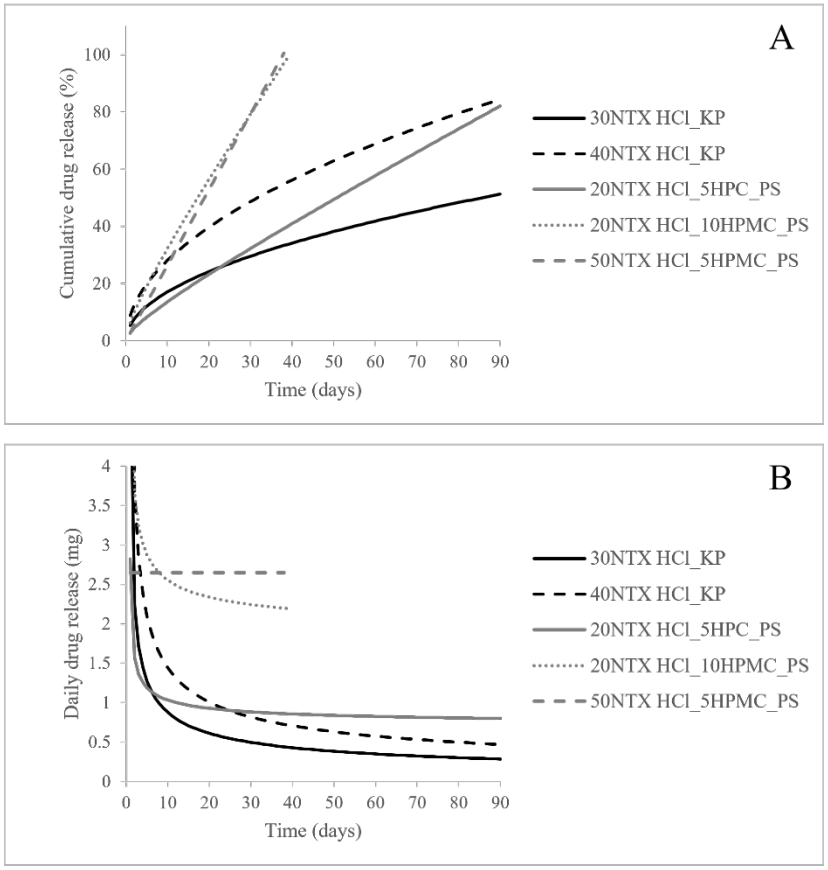


Figure 66 (A) Predicted cumulative release (%) and (B) daily release (mg) of NTX HCl from the implants according to the Korsmeyer-Peppas (KP) and Peppas-Sahlin (PS) models fitted to the experimental data from the 27 days long *in vitro* release study

According to the predictions, the daily release of 20NTXHCl_5HPC was estimated at approximately 1 mg/day from Day 20, while the binary systems, 30NTXHCl and 40NTXHCl, had only approximately 0.50 and 0.55 mg/day release rates, respectively. At the same time, the 20NTXHCl_10HPMC and 50NTXHCl_5HPMC implants were estimated to release 100% of the drug content within 40 days, with a release rate of 2.5-2.2 and 2.6 mg/day, respectively.

4.4 Discussion

NTX HCl-EVA28 implants with up to 50 w/w% drug loading with and without CE additives (up to 10w/w%) were successfully manufactured with the selected process parameters (T_{proc} = 140°C; Screw speed = 30rpm) on the Kapex extruder. The results from the drug content assay (*Figure 61*), SEM (*Figure 62*) and Raman microscopic measurements (*Figure 64*) showed that the extrudates had acceptable homogeneity both for NTX HCl and CEs, where each component was presented in different phases, forming separated particles within the implants. According to our measurements in this study and the results from the previous two experimental chapters, NTX HCl is not miscible with the EVA matrix carrier. Furthermore, as the selected grade of hydrophilic HPMC has a T_g of 186°C[328], nearly 40°C above the T_{proc}, it was very unlikely to

occur any fusion with EVA28 or NTX HCl. On the other hand, the T_g of HPC is approximately 80-85°C, calculated in a study conducted by Luebber et al.[329]. Accordingly, the fusion with the other hydrophilic component (NTX HXl) is feasible. However, the results from Raman microscopic measurements did not confirm this hypothesis, as higher spectral concentrations of HPC were measured in the areas where NTX HCl showed lower intensities.

NTX HCl release from the implants was highly influenced by the initial drug loading, as was previously demonstrated in *Chapter 2*. Higher drug loadings resulted in higher drug release due to the increasing number of pores, continuously forming during the release process (*Figure 65_A*). The results show that incorporation of the CE additives significantly influenced the release kinetics. The hydrophilic CE polymers absorbed water and swelled, forming a temporary hydrogel network stabilised by physical chain entanglements and H-bonds. Upon further water uptake, the hydrogel was continuously dissolved due to polymer chain disentanglement, for which the rate was depended upon the extent of different types of interaction forces. Thus, drug release could occur via the diffusion of the dissolved drug molecules through the hydrogel network and/or the water-filled pores left behind after the dissolution of different types of particles. Moreover, the swelled CE particles could expand the narrow throats between the pores, increasing the volume for diffusion[330]. Water uptake, swelling, hydrogel density and dissolution rate of the CEs depends highly on their molecular weight and chemical structure[331,332]. Generally, CEs with higher molecular weight form a denser hydrogel phase because of the many possibilities for physical chain entanglements, while CEs with lower substitution with hydrophobic groups tend to have higher solubility due to a higher probability for interactions between water and unsubstituted hydroxyl and/or other side chain hydrophilic groups.

Among the two competing phenomena of dissolution and swelling of the CEs, dissolution predominated in drug release experiments of the implants with 20% w/w NTX HCl loadings (*Figure 65_B*). The additives acted as a pore-former, increasing the porosity and pore sizes resulted in a higher drug release. Increasing CE content increased the NTX HCl release. However, the influence of HPC and HPMC on drug release significantly differed from each other. It can be explained by the higher water solubility and lower gel-forming behaviour of HPC. The selected HPC had a lower molecular weight (100 kDa) and also was substituted with hydrophilic hydroxypropoxyl groups making more possibilities to interact with water. In comparison, HPMC had a 4 fold higher molecular weight (400 kDa) and 28-30% of the -OH groups on the cellulose backbone was substituted with hydrophobic methoxyl groups (*Table*

25). It is also noteworthy that 20NTX HCl_10HPMC samples showed a nearly zero-order drug release, most likely due to the contribution of the better hydrogel-forming behaviour of HPMC.

In the case of 50% w/w NTX HCl-loaded implants, the water uptake of the swelling agents used at the concentration level of 10% w/w expanded the implants to a great extent and destroyed the samples at the beginning of the *in vitro* study. However, 5% w/w CE-loading was applicable (*Figure 65_C*). The better gelling behaviour of HPMC influenced the drug release more advantageously compared to the HPC loaded system. The HPMC additive could decrease the release rate of NTX HCl by forming a hydrogel network, resulting in a nearly zero-order release kinetic. Although 5% w/w HPC could also decrease the drug release, it was not sufficient enough for further considerations.

The release kinetic was further analysed by different mathematical models (*Table 27*). According to the Korsmeyer-Peppas model, drug release occurred via anomalous transport mechanism, which means both drug diffusion and polymer relaxation significantly contributed to drug release. However, the calculated k_1 and k_2 constant of the Peppas-Sahlin model revealed that the drug release was mainly governed by diffusion ($k_1 > k_2$) through the continuously formed hydrogel and porous network, rather than polymer erosion in the CE-loaded systems.

4.5 Conclusion

A one-step HME process was used in this study to prepare NTX HCl-EVA28 subcutaneous implants to investigate the pore-forming and swelling/gelling effect of different CEs on drug release. Morphological measurements revealed that the implants with acceptable mechanical properties and sufficient homogeneity could be produced with the selected HME process parameters that may be suitable for use as a removable subcutaneous IDDSs. We also demonstrated that an approximately 2 and 4 fold increase in drug release could be obtained by incorporating only 5 and 10% w/w swelling- or pore-forming CE-additives into the 20% w/w NTX HCl-loaded implants, and the release mainly followed zero-order kinetics. Applying different semi-empirical models on the 27 days long *in vitro* release data, the predictions up to 90 days showed that adding 5% w/w HPC into 20% w/w NTX HCl-loaded implants resulted in 2 fold higher daily release (≈1.0 mg/day) compared to 30 and 40% w/w NTX HCl-loaded systems (≈0.5 mg/day). Additionally, we also developed a ternary system that could advantageously decrease the release rate of 50% w/w NTX HCl-loaded system. By embedding 5% w/w HPMC into the 50% w/w drug-loaded implants, a system could be produced that

performed a zero-order release kinetic with an approximately 2.6 mg/day release rate for 40 days.

This innovative and cost-effective approach for tailoring drug release from NTX HCl-loaded EVA implants could greatly impact further developments of the subject of the first two experimental chapters of this thesis.

5 Development of NTX base loaded EVA systems

5.1 Introduction

EVA is one of the most commonly used non-biodegradable polymers to produce IDDSs for controlled drug delivery. These products can be divided into two main categories according to their drug release mechanism. In systems where the drug's permeability is neglectable due to its low miscibility or solubility in the hydrophobic polymer, the release mainly occurs through the tortuous network of interconnected pores that form during the release process. These systems are generally matrix constructs (e.g., ProNeura® platform by Titan Pharmaceuticals Inc.). The other class includes systems in which the physicochemical properties of the drug and matrix polymer allow mixing at the molecular level between the two components. Thereby passive Fickian diffusion of the drug through the polymer is thermodynamically possible. The majority of the commercially available EVA-based IDDSs control drug release by the latter mechanism. Most of them are reservoir type products, where the inner core contains the solubilised and oversaturated form of one or more APIs and the outer layer (membrane) controls the drug release (e.g., NuvaRing®, Implanon®, Ocusert®). The driving force of drug release is the constant concentration gradient between the implant and the biological environment, ensured by the oversaturated state of the API in the core. The drug release can be fine-tuned by the appropriate selection of polymers for the inner core and the rate-controlling membrane according to the API's apparent diffusion coefficient in them and also by the geometry of the implants[301].

The previous experimental chapters aimed to develop subcutaneous EVA implants with a monolithic dispersion design using the highly polar salt form of NTX. In these systems, the drug release was based on tortuosity and hydrogel controlled diffusion. This chapter focuses on developing monolithic solution and/or dispersion systems in which the drug release is governed by pure Fickian diffusion through different grades of EVA using the neutral base form of NTX with lower polarity and hydrophilicity compared to its HCl-salt form.

The main objectives of this chapter were as follows:

- First, the solubility and permeability of different forms of NTX in three grades of EVA were investigated.
- Then, implants with 10% w/w NTX HCl-salt and base loading were produced by HME, and their homogeneity, purity profile, morphology and release performance were compared to each other.

5.2 Materials and methods

5.2.1 Materials

EVA copolymers with a VA-content of 18% (MFI:159.73), 28% (MFI:150.00) and 39% (MFI:60.04) was provided by Celanese Corp. (Texas, US). EVA18 and EVA39 pellets were cryomilled prior to processing as follows. An appropriate amount of pellets were placed into a 50 mL screw-top grinding jar with a zirconium oxide ball, frozen in liquid nitrogen for 30 minutes, then ground with a Retsch MM200 mixer mill for 1 minute at 25 Hz. The jars were subjected to 4 freezing and milling cycles. Cryomilled powder of EVA28 was used as provided.

Anhydrous NTX base was produced from NTX HCl as follows. First, 20 mL of 20 mg/mL NTX HCl water solution was measured into a 250 mL separatory funnel, then the pH was adjusted to 7-8 by adding NaOH solution to the system. The precipitated NTX base was then extracted with 4 portions of DCM (5, 10, 10, 10 mL). The collected DCM solution of NTX base was dehydrated by anhydrous K_2SO_4 and filtered on sintered glass before evaporation of the solvent in a rotary evaporator. The NTX base was then collected and recrystallised from ACN[333]. The products were dried for two days under vacuum at 40 °C and stored in a desiccator above P_2O_5. The morphology and purity of the produced NTX base was verified by DSC and HPLC related substance method as described in *Section 2.2*. The purity of the produced NTX base met the requirements of the related Ph.Eur. monograph and the measured thermogram was in a good agreement with the results reported by Brittain et al.(T_m=175.90 °C; ΔH_m=69.01 J/g)[333].

All other materials used for manufacturing and further analytical procedures were the same as those used in *Chapter 2, Section 2.2.1*.

5.2.2 Diffusion experiments

In order to determine the equilibrium solubility of different NTX forms in several grades of EVA polymer, the ”immersion-method” described by van Laarhoven et al.[134] was used. Polymeric films (100 µm) were cut into 10x10 mm pieces and immersed in oversaturated water solution of NTX base and NTX HCl at 37 °C (*Figure 67*). After 6 weeks of conditioning in a shaking incubator (60 rpm), the films were removed, rinsed with water and analysed for drug content using the HPLC assay method described in *Section 2.2.4*. The films were produced as follows. Approximately 0.5 g of polymers were placed in an evacuable pellet press dies whose inner surface was covered by teflon sheets. The die was then heated to 130 °C, and the air bubbles from the molten polymer were removed by a vacuum pump. The die was cooled and the resulting polymeric cylinders were removed from the die. Appropriate slices were then cut from the cylinders and placed on the Peltier-plate module of the Discovery HR-1 Rheometer covered by teflon sheets. The polymer slabs were then heated up to 110 °C, and the height of the teflon covered parallel plate was slowly adjusted to 100 µm. The systems were then left to cool, and substantially the thin polymer films were easily removed from the teflon sheets.

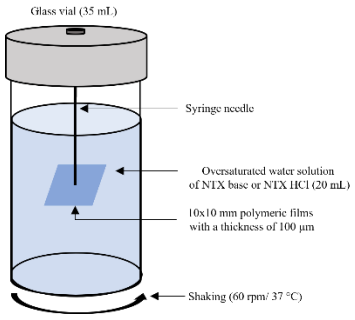


Figure 67 Depiction of the “immersion-method” to determine the equilibrium solubility of NTX base and NTX HCl in different types of EVA

For the determination of steady-state permeability of NTX forms through EVA films, vertical Franz-diffusion cell apparatus (Orchid Scientific, Maharashatra, India) was used. EVA films were clamped between the two halves of the apparatus with the effective diffusional area of 3.14 cm^2. The donor cells (5 mL) contained the oversaturated water-solution of NTX forms, while the acceptor cell (20 mL) contianed pure water. The cells were stirred at 20 rpm with a magnetic stirrer (20 rpm) and conditioned at 37 °C. Samples were taken (1 mL) at several time points (up to 30 hours) from the acceptor cells and replaced with a fresh media. The samples were then analysed for drug content according to the HPLC assay method described in *Section 2.2.4*.

The diffusion coefficients of NTX forms in different grades of EVA were calculated according to the following equation:

$$D_{NTX-EVA} = P/S$$

,where:

- D – diffusion coefficient (cm^2/h)
- P – permeability coefficient (mg/cm*h)
- S – solubility (mg/cm^3)

5.2.3 Hot-melt extrusion

The extrusion method is described in detail in the previous chapter, *Section 4.2.2*. The formulations prepared in the present study and the applied processing parameters are summarised in *Table 28*. The feeding rate remained constant (5 g/min) for each formulation.

Table 28 Compositions and processing parameters used for the formulations investigated in this study

Formulation	Component (%w/w)					Processing temp. (°C)	Screw speed (rpm)
	NTX HCl	NTX base	EVA18	EVA28	EVA39		
10NTX HCl_EVA18	10	-	90	-	-	140	30
10NTX HCl_EVA28	10	-	-	90	-	140	30
10NTX HCl_EVA39	10	-	-	-	90	140	30
10NTX base_EVA18	-	10	90	-	-	140	30
10NTX base_EVA28	-	10	-	90	-	140	30
10NTX base_EVA39	-	10	-	-	90	140	30

5.2.4 Purity profiling, drug content analysis and *in vitro* release testing of the implants

HPLC methods used in this study were the same as described in *Section 2.2.4*. Protocols for drug content analysis and *in vitro* testing was conducted as described in *Section 0*. Water-solubility of NTX base was determined as described in *Section 2.2.8* prior to the *in vitro* study to ensure perfect sink conditions. The measured 1.939±0.07 mg/mL value indicated that the applied *in vitro* testing protocol ensured perfect sink condition.

5.2.5 Morphological characterisation of the implants

DSC, SEM and Raman mapping was conducted as described in *Section 2.2.11-12* and *4.2.4*.

5.3 Results

5.3.1 Diffusion study

In order to investigate the influence of the differing lipophilicity of the NTX forms on the diffusion characteristic in different types of EVAs, two types of measurements were conducted. First, the equilibrium solubility of the NTX forms was determined by the "immersion method". The measured drug uptake in the thin polymer films after 6 weeks of conditioning in the oversaturated water solution of NTX base at 37 °C are shown in *Figure 68*. No detectable drug content could be measured in films immersed in NTX HCl solutions. The results clearly show that the diffused amount of NTX base in the polymeric films increased with increasing VA-content.

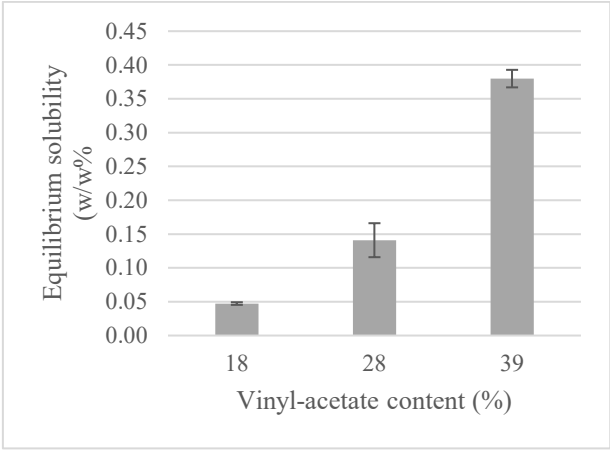


Figure 68 NTX base uptake in different types of EVAs at 37 °C.
Error bars represent ±1 standard deviation of n=3 replicates

As a second assessment, the steady-state permeability of NTX forms through different grades of EVA was measured by a Franz-diffusion cell apparatus. The diffused drug content measured in the acceptor cells as a function of time are plotted in *Figure 69*. No detectable drug content could be measured in the acceptor cells for NTX HCl. The permeability coefficients were calculated according to the following equation:

$$P = \frac{dM_t}{dt} * \frac{d}{A}$$

, where

- P – permeability (mg/cm*h)
- dM_t/dt – slope of the linear region on the time versus diffused drug content curve (mg/h)
- d – thickness of the membrane ($1*10^{-2}$ cm)
- A – effective diffusional area (3.14 cm^2)

The calculated values are summarised in *Table 29*. As can be seen, increasing VA-content resulted in higher permability coefficients as well as the calculated diffusion coefficients.

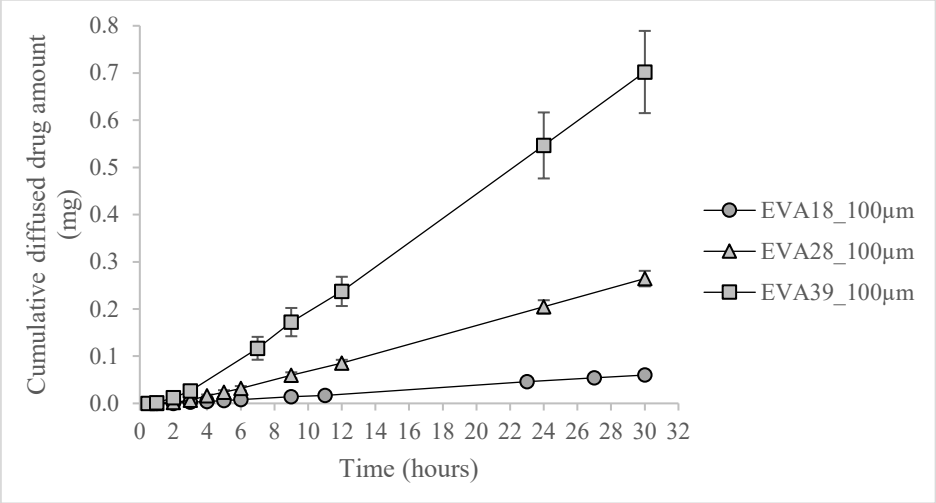


Figure 69 NTX base permeation through different grades of EVA.
Error bars represent ±1 standard deviation of n=3 replicates.

Table 29 Summary of the calculated parameters measured in the diffusion study

VA-content (%)	Solubility (%w/w)	Solubility (mg/cm^3)	Permeability (mg/cm*h)	Diffusion coefficient (cm^2/h)
			NTX HCl	
18	n.a	n.a	n.a	n.a
28	n.a	n.a	n.a	n.a
39	n.a	n.a	n.a	n.a
			NTX base	
18	0.0473	0.4469	$0.7*10^{-5}$	$1.57*10^{-5}$
28	0.1410	1.3321	$3.09*10^{-5}$	$2.32*10^{-5}$
39	0.3799	3.4759	$8.09*10^{-5}$	$2.33*10^{-5}$

5.3.2 Formulation study of NTX forms with different types of EVA

Each formulation could be manufactured efficiently with the selected processing parameters (140 °C/30 rpm). The NTX HCl-based implants had an off-white colour, while the NTX base-loaded implants were yellowish and more transparent than the NTX HCl based systems (*Figure 65*). Each implant had acceptable flexibility for clinical use as an IDDS.

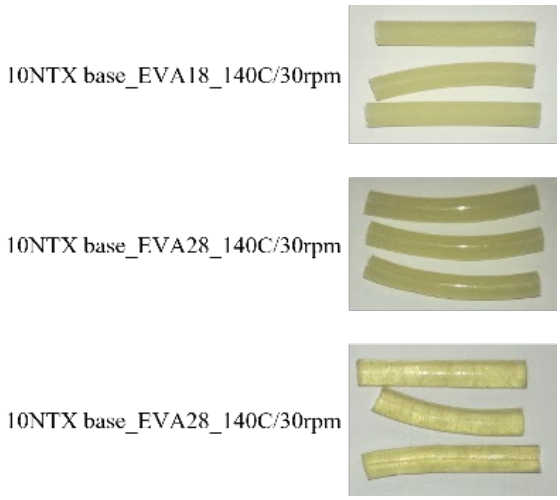


Figure 70 10w/w% NTX base-loaded implants produced using varying EVA grades

The average drug content of the implant batches was measured to determine the homogeneity and thus to compare the extrudability of each NTX form at a relatively low concentration level (10% w/w). The results indicate that each formulation contained close to the target concentration level. However, the variation of the measured values for NTX HCl-loaded systems was higher (%RSD>5) compared to the NTX base-loaded systems (%RSD<5), indicating a better homogeneity for the base form of NTX.

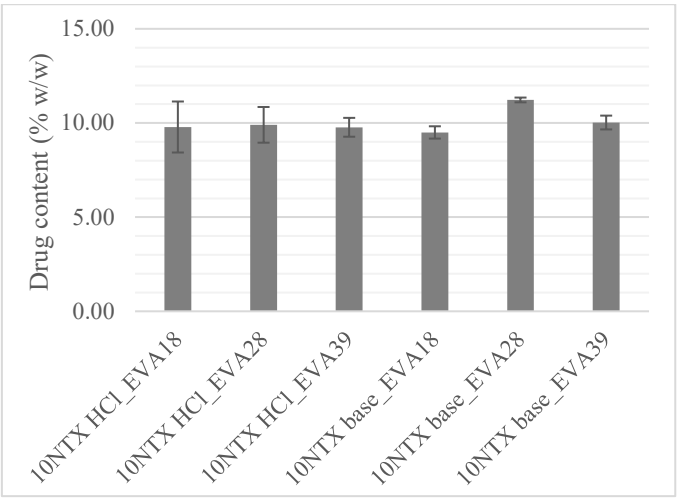


Figure 71 Measured drug concentration of implants produced using different NTX forms and varying EVAs. Error bars represent ±1 standard deviation of n=6 replicates.

Investigation of NTX degradation in the implants revealed that the NTX base tended to have significantly lower thermal stability in the formulations compared to NTX HCl (*Figure 72*). In NTX HCl-based systems the total impurity content was not higher than 0.05%, while the NTX base formulations showed more than a 0.40% of total impurity content. However, the raw NTX base had an acceptable degradation profile with only two detectable impurities (Impurity B and C) with very low concentrations. In NTX base-EVA formulations, new decomposition substances formed (Impurity D, Impurity G and one unknown impurity). Additionally, the results showed a more than 4-fold increase in the concentrations of the main oxidative by-product, Impurity B, significantly increasing the total impurity contents. Although the total impurity content did not exceed the 1.0% threshold limit, the measured concentrations of Impurity B in NTX base-loaded formulations were remarkably higher than its 0.1% limit, making the extrudates unsuitable for clinical applications. Moreover, a trend can also be seen on the purity profiles of NTX base-EVA systems, i.e., an increase in VA-content resulted in increased degradation.

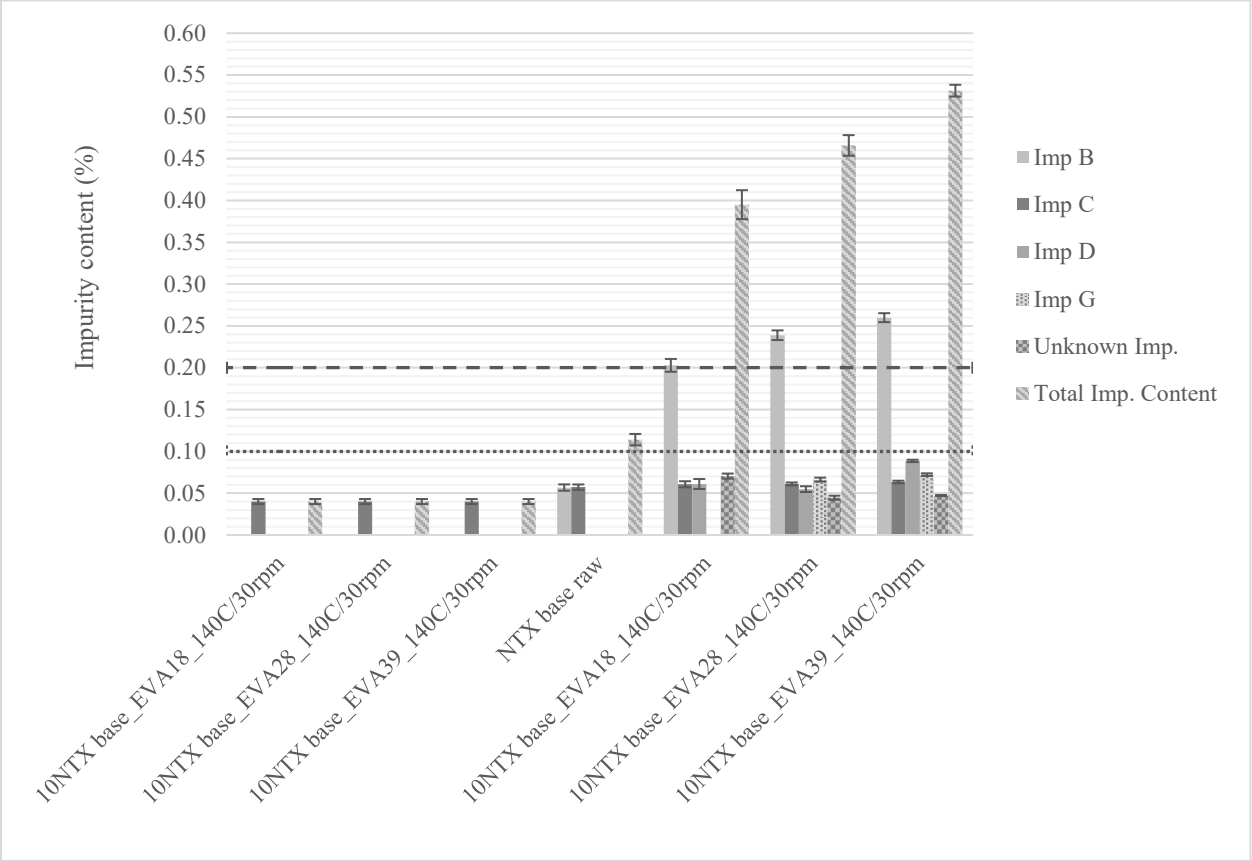
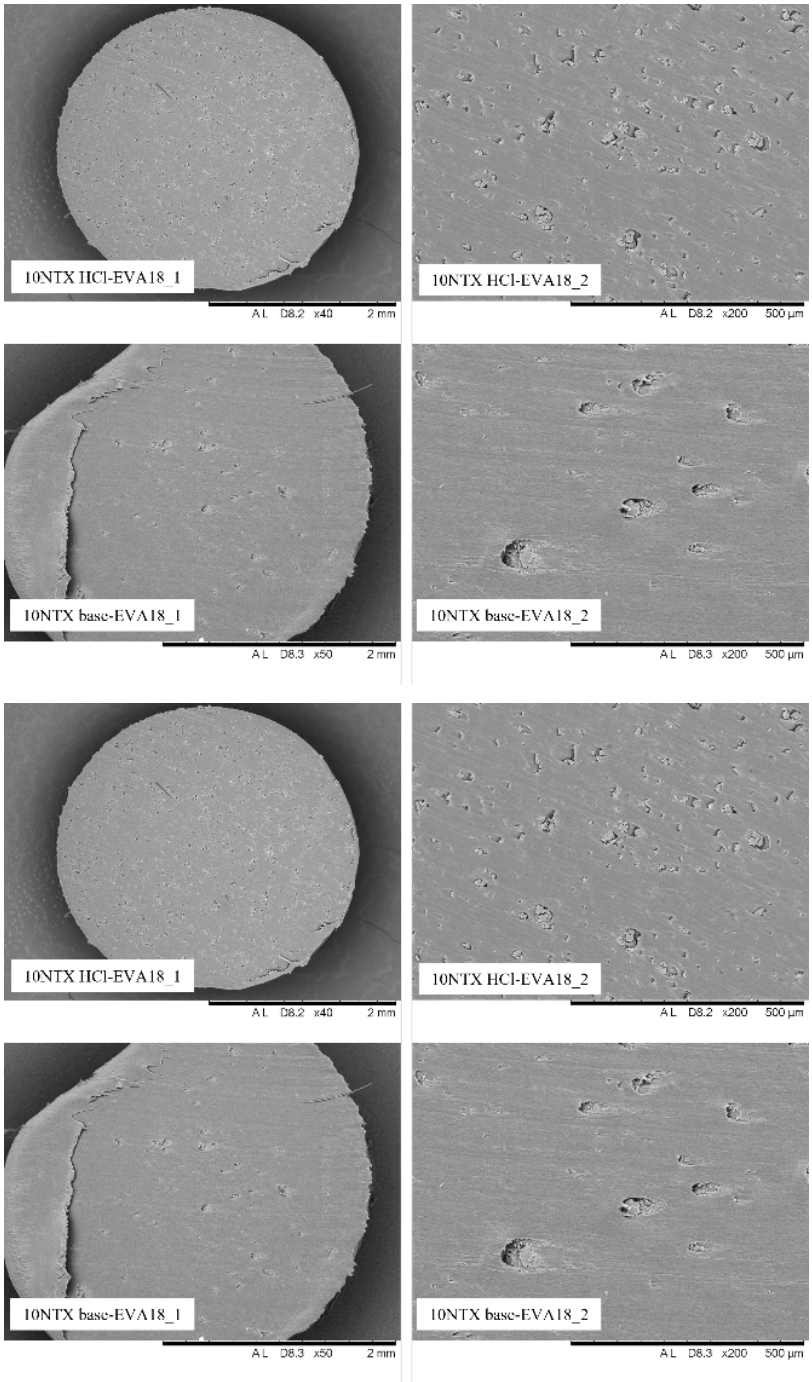


Figure 72 Detectable impurities of NTX in the implants prepared using different NTX forms and EVAs. The dotted line represents the 0.1% threshold limit for Impurity B and Unknown impurity, while the dashed line represents the 0.2% threshold limit for Impurity D and Impurity E according to Ph.Eur. monograph for NTX HCl. The 1.0% threshold limit for total impurity content is not indicated in this figure. Error bars represents the ±1 standard deviations of n=3 replicates.

The morphology of the implants was characterised by SEM. The cross-sectional images show the great difference between the systems containing the different forms of NTX (*Figure 73*). In the NTX HCl-loaded systems, homogeneously distributed particles are visible, while in the systems containing NTX base, no or only a small number of residual particles can be seen with less defined, flocculent structure. Significant differences can also be noticed between the NTX base formulations using different EVA grades. The images clearly show that as the VA-content of the EVA increases, the number of particle rich regions decrease, while in the case of EVA39, no particles are observed.



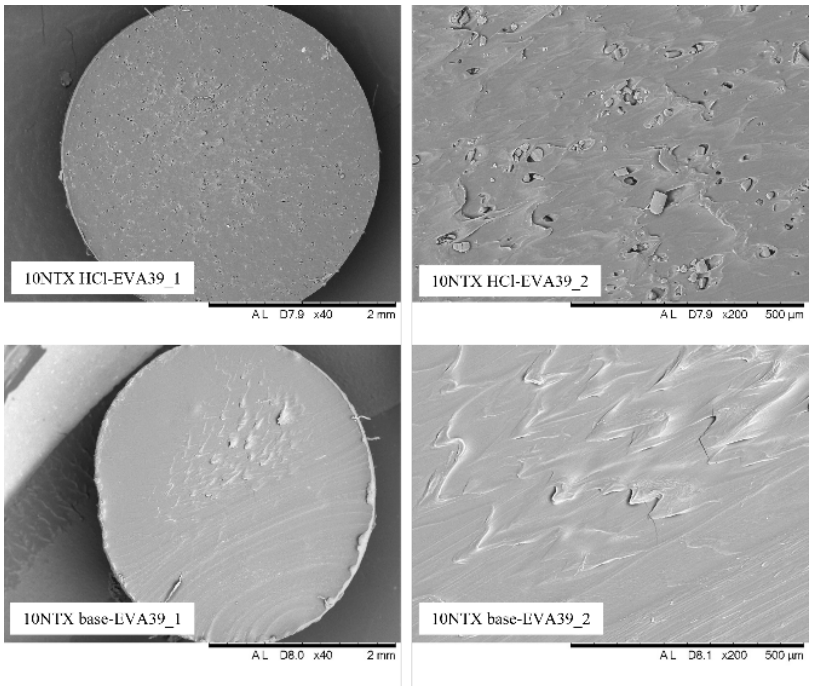


Figure 73 SEM images of the cross-sections of implants prepared using different NTX froms and EVA grades. The images coded with 1 were taken at 40x magnification, while the images coded with 2 represent 200 magnification from the centre (bulk) of the cross-sections.

The results described above suggest that the NTX base dissolved in the EVA during the HME process, and a significant proportion remained in a molecularly dispersed form within the EVA due to the rapid cooling after the process. In order to investigate the radial distribution of the solubilised and kinetically stabilised NTX base in the EVA matrices, Raman spectrometry was used, as the neutral form of NTX has no sufficient EDX activity to be investigated by the SEM equipment. The Raman spectra of NTX base has distinctive intensive characteristic peaks (609.9, 636.0, 1198.7 and 1643.3 cm^{-1}) that can be used to investigate its distribution in the presence of the EVA matrix polymers (*Figure 74*). The chemical maps were generated according to the correlation between the spectra of the pure NTX base and the measured points (*Figure 75*). The images demonstrate that the NTX base was well-distributed in the radial direction of the implants, with the highest homogeneity in the EVA39 system.

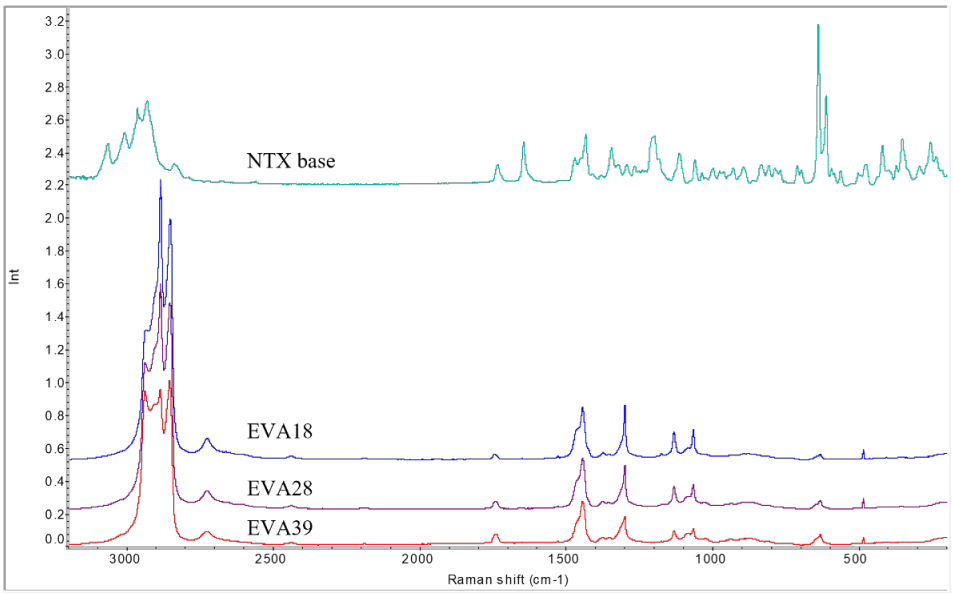


Figure 74 Representative average spectra of each material used for this study. 4 measurements were taken from each pure component. The spectra were then averaged, baseline-corrected and normalised.

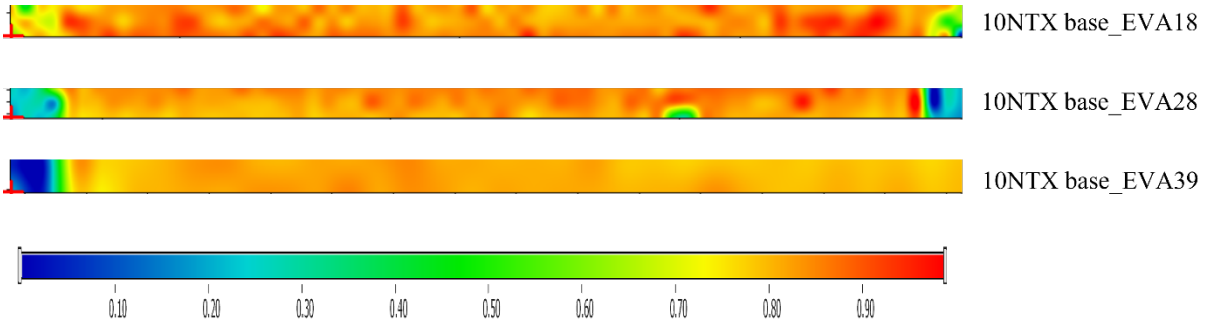


Figure 75 Chemical maps generated based on the correlation between the spectra of pure NTX base and the measure spectra on the analysed surface area with a spatial resolution of 30 µm. Low to high spectral concentrations (extent of correlation) in the images are described by colors blue to red.

Thermal investigations of the physical mixtures and the extrudates of NTX base-EVA systems were performed by DSC (*Figure 76*). In all cases, the DSC curves showed a broad glass transition of EVAs in the temperature range of approximately -48 to 0 °C. No significant shift of this thermal transition can be observed on the thermograms of the EVA extrudates compared to their physical mixtures. The curves also present the change in the crystalline structure of EVAs after HME, as their melting peaks in the range of 0 to 100 °C appeared at different temperatures compared to the related physical mixtures. However, the calculated overall crystallinities did not change significantly after the HME process (*Table 30*). Most importantly, the well-defined endothermic melting peak of NTX base at 176 °C can be seen with significantly lower intensities in the curves of the EVA18 and EVA28 extrudates, while on the curve of NTX base-EVA39 system, no peaks can be seen at 176 °C, suggesting that all of the NTX went through complete dissolution during HME, and remained stable upon cooling.

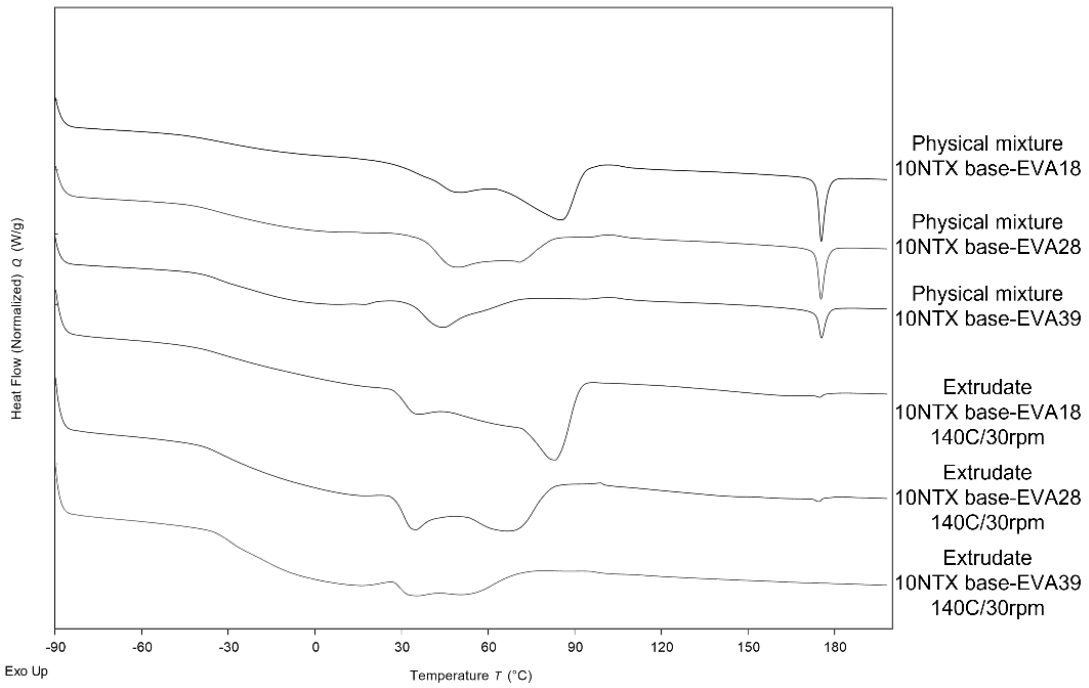


Figure 76 DSC scans of the physical mixtures of NTX base and different EVAs and the extruded implants

Table 30 Calculated crystallinites and glass transition of EVAs

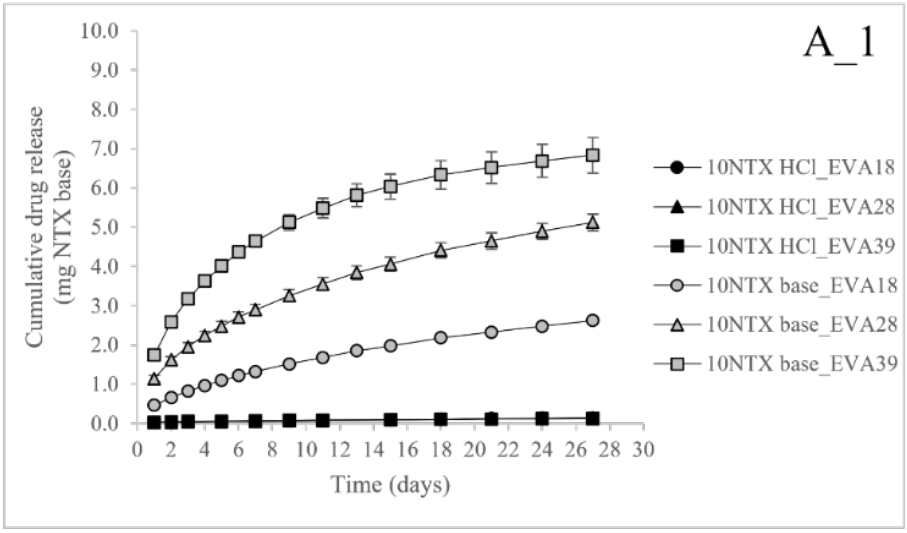
Sample	Crystallinity (%)		Glass transition (°C)
	NTX base		EVA
Physical mix_10NTX base_EVA18	100.00	22.35	-30.05
Physical mix_10NTX base_EVA28	100.00	11.66	-29.46
Physical mix_10NTX base_EVA39	100.00	5.41	-29.65
10NTX base_EVA18	0.21	19.74	-29.56
10NTX base_EVA28	0.26	11.03	-29.86
10NTX base_EVA39	0.00	4.03	-29.52

In vitro release study on the produced 10% w/w implants were conducted in purified water at 37°C. Each release data measured were calculated for the NTX base for better comparison. *Figure 77 A_1* and *A_2* show the NTX release from the implants produced using different types of NTX forms and EVAs. As can be seen, the NTX HCl-loaded implants have a significantly lower drug release rate compared to the NTX base-loaded implants ($p>0.05$). EVA18, EVA28 and EVA39 NTX base-loaded implants released 2.62±0.08 mg (29.78±2.02%), 5.12±0.21 mg (52.96±1.87%) and 6.83±0.45 mg (68.39±1.73%) NTX by day 27, respectively. On the other hand, NTX HCl-loaded implants released only approximately 0.13-0.15 mg NTX after the same period, equivalent to 2.51-2.81% of their total NTX base content (calculated from their NTX HCl loading). The daily release of NTX base appeared to be continuously decreasing over the

first 15 days, then stabilised, resulting in a 0.06, 0.07 and 0.09 mg/day daily release for EVA18, EVA28 and EVA29, respectively. Although the release rate of NTX-HCl-loaded systems stabilised after 8 days, their release rate was approximately more than 10-fold lower when compared to the NTX base-loaded implants, at approximately 0.004 mg/day.

In order to highlight the increased release performance of NTX base-loaded implants, data from the previous experimental chapter was used (*Section 4.3.3*) for comparison. The NTX HCl-loaded EVA28 systems were prepared using the same processing parameters, and their release performance was analysed under the same conditions. *Figure 77 B_1* and *B_2* demonstrate that the NTX base-loaded system with only a 10% w/w drug content has a drug release profile between the that of the 20 and 30% w/w NTX HCl-loaded implants. However, its release rate by day 27 becomes equal to the 20% w/w NTX HCl system at approximately 0.01 mg/day.

The release kinetics of the NTX base-loaded implants were further investigated by fitting the release data to several mathematical models (*Table 31*). The Higuchi model showed a good fit (r^2>0.95), indicating that the release occurred through diffusion. The applied Baker-Lonsdale model is based on solving Fick's basic differential equation for cylindrical geometry to a given set of appropriate initial and boundary conditions. This model also showed a good fit to the release data. Furthermore, the calculated diffusion coefficient of the model appeared to be in reasonable correlation with the coefficient experimentally determined in the previous study.



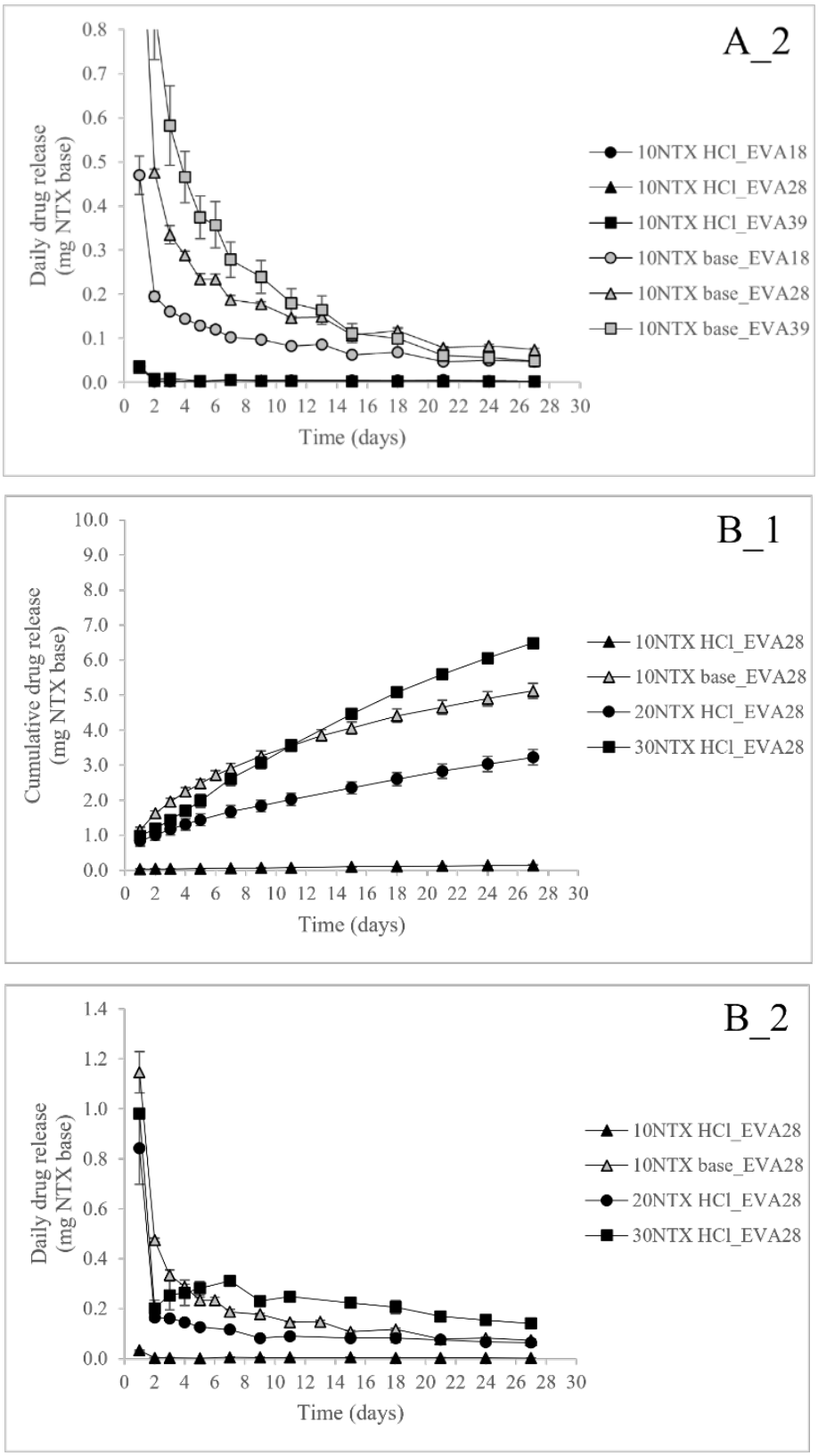


Figure 77 In vitro release of the produced implants. (A_1, B_1) Total NTX base released over time (mg total ±1 SD; n=3/group). (A_2, B_2) Daily NTX base release over tine (mg released/day; ±1 SD; n=3/group).

Table 31 Drug release kinetics of the NTX base-loaded implants

Formulation	Higuchi model	Baker-Lonsdale model[174] (Short time approximations)		Experimentally determined diffusion coefficient in EVAs
	$M_t/A=k_Ht^{1/2}$	$M_t/M_\infty=4*(D_{apparent}t/\pi R^2)^{1/2}-D_{apparent}t/R^2$ R=radius of the implant (0.15 cm)		
	r^2	$D_{apparent}$ (cm^2/h)	r^2	$D_{experimental}$ (cm^2/h)
10NTX base_EVA18	0.9993	$1.04*10^{-5}$	0.9995	$1.57*10^{-5}$
10NTX base_EVA28	0.9962	$2.35*10^{-5}$	0.9998	$2.32*10^{-5}$
10NTX base_EVA39	0.9751	$2.42*10^{-5}$	0.9871	$2.33*10^{-5}$

5.4 Discussion

As a preliminary investigation, the diffusion behaviour of the two forms of NTX in EVA was studied. The ”immersion method” results showed that only the base form diffused into the polymeric films (*Table 29*). This was not surprising as the experiments were conducted in water with a pH≈7. The NTX HCl salt form is an ionic compound that dissociates in water into $NTXH^+$ and Cl^- ions, and the diffusion of a highly polarised compound into a highly hydrophobic polymer is thermodynamically not preferable. However, as NTX has a pKa value of 8.13 at 37 °C, the water solution of NTX base contained approximately 7% of its non-ionised form, which remained constant as an excess amount of NTX base crystals was used in the solutions. The difference in NTX uptake by the different grades of EVA can be explained by their microstructures. EVA is a semi-crystalline polymer. The increasing number of VA-groups inhibit the crystallisation of polyethylene chain segments via a steric hindrance, decreasing the overall crystallinity and increasing the volume of amorphous regions in the polymer. This was confirmed by the DSC investigations of the physical mixtures, where the crystallinity of EVA18, EVA28 and EVA39 was measured 22.35, 11.66 and 5.41%, respectively (*Table 30*). As the molecular distances within the EVA crystals are smaller than the molecular size of NTX, the diffusion can only take place in the amorphous regions. As a consequence, the NTX uptake was higher in EVAs with higher VA-content.

The same explanation can be applied to the results of the Franz-diffusion cell experiments, where the calculated permeability appeared to be $0.7*10^{-5}$, $3.09*10^{-5}$ and $8.09*10^{-5}$ mg/cm*h for EVA18, EVA28 and EVA39 membranes, respectively (*Table 29*).

The processability of NTX base and NTX HCl at 10% w/w concentration level in different EVA grades was investigated. The results from the drug content assay measurements showed that the base form could be formulated with higher homogeneity compared to the HCl-salt form (*Figure 71*). Likely, the majority of the NTX base is dissolved in the molten polymers during the HME process resulting in a better mixing efficiency. The molecularly dispersed forms then remained stable in the extrudates due to the rapid cooling of the fibers upon exiting the extruder die. This was confirmed by SEM measurements, which demonstrated that in the NTX HCl-loaded implants, several NTX HCl particles could be visualised, while in the images of NTX base-loaded implants, only a few residual particles were observed in EVA18 and EVA28, and no particles were obsereved in EVA39 (*Figure 73*). The homogeneous distribution of the partly or completely dissolved NTX base in the radial direction of the implants was also verified by Raman mapping (*Figure 75*). In each measured point on the mapped areas, signals of NTX base could be detected, confirming the hypothesis that in each formulation, the NTX base was distributed at a molecular level, which was the most significantly expressed in the EVA39 system. DSC measurements also confirmed the base form's molecularly dispersed or amorphous morphology in the extrudates, as no melting peaks were detected or only with very low intensities related to the NTX base at 176 °C (*Figure 76*). According to the results mentioned above, it can be assumed with high certainty, that the NTX base-loaded implants were highly oversaturated with NTX.

In vitro release experiments revealed signifcant difference between the pure Fickian- and tortuosity-controlled mass transport. The amount of NTX released over 27 days from the 10% w/w NTX base implants were 20 to 45 fold greater compared to implants containing 10% w/w NTX HCl (*Figure 77*). This was not surprising, as in NTX-HCl implants, the drug is not permeable through the EVAs, due to its higher hydrophilicity and the drug loading was not high enough to form an interconnected network of pores. Therefore only drug crystals situated on or near the implant surface contributed to the release. On the other hand, the more lipophilic NTX base was able to diffuse across the amorphous region of the matrix polymers (previously confirmed in the diffusion study), resulting in a significantly higher release rate. The significant differences in drug release for the 10% w/w NTX base-loaded EVA polymers can also be explained by the different crystallinity and thus amorphicity of the EVA grades. EVAs with higher VA-content contain more amorphous regions, providing a larger area for molecular diffusion.

The fitted mathematical models verified that the mass transport from NTX base-EVA implants was based on diffusion (*Table 31*). Surprisingly, the diffusion coefficients of NTX in EVAs calculated by the Baker-Lonsdale model, which describes drug release considering pure Fickian-diffusion, showed a reasonable correlation with diffusion coefficient values determined in the diffusion study by solubility and permeability measurements.

Although the aforementioned results clearly show the advantages of the use of NTX base form, significant chemical degradation could be detected in these systems, whose extent was directly proportional to the VA-content and inversely proportional to the MFI of the EVA polymers used (*Figure 72*). The main degradation product appeared to be Impurity B (4,5α-epoxy-3,14-dihydroxymorphinan-6-one; noroxymorphone) which is an oxidative degradation product of NTX forming through an electron loss of the main compound[296,297]. Unfortunately, in each NTX base-EVA system, the concentration of this specific impurity was more than 2-fold higher than its threshold limit (0.1%) stated in the related Ph.Eur. monograph. The correlation between the VA-content and MFI of the EVAs used and the total impurity content of NTX can be explained by the different solubilisation efficiency and melt-flow properties of EVAs during HME, which was conducted at approximately 30 °C lower temperature (T_{proc}=140 °C) than the melting of NTX base (T_m=176 °C). First, it can be assumed that the dissolution of NTX base occurs via the interaction between the oxo-group of the VA side chains of EVAs and the hydroxyl-groups of NTX. Thus, increasing VA-content results in higher possibilities for interactions, increasing the efficiency of EVA for better solubilisation. When the drug loses its crystalline structure and becomes amorphous or molecularly dispersed, it tends to have lower thermal stability, as previously described in several studies[251,334] . Furthermore, since EVA39 has lower MFI (60.04) the other EVAs (EVA18-MFI159.73 and EVA28-MFI150.00), it is very likely that the dissolved drug went through degradation not only because of the heat stress, but also due to the increased shear stresses during the HME.

5.5 Conclusion

In this study novel, NTX base-loaded EVA implants were manufactured, their several CQAs were assessed and compared to NTX HCl-loaded EVA systems.

In the preliminary investigation, the diffusion behaviour of NTX forms in different types of EVAs was determined. The results indicated that the ionic HCl salt form of NTX had no diffusivity in EVAs, while the base form had. The formulation study showed that the NTX base could be solubilised in EVAs via a one-step HME with a T_{proc} 30 °C below its melting temperature, resulting in an oversaturated and kinetically stabilised system. Additionally, our results demonstrated that better homogeneity could also be achieved with the NTX base form due to its dissolution during the HME. However, significant thermal degradation was observed in the NTX base-loaded formulations, which was proportional to the VA-content and the MFI value of the EVAs applied. The *in vitro* release study of the produced implants showed that if the drug release mechanism was based on pure Fickian-diffusion through the polymeric matrices, a significantly higher drug release rate could be achieved with the same drug level. For example, 10% w/w NTX base-loaded EVA28 implants performed almost the same drug release that could be achieved with 20 or 30 %w/w NTX HCl-loaded EVA28 systems (*Figure 77 B_1*).

This study highlights the importance of the physicochemical characteristic of the applied API to be formulated with EVA and defines a promising step forward for further development.

6 General discussion and future works

6.1 General discussion

Drug addiction is one of the most pressing issues in today's society. Unfortunately, most pharmacological treatment options available are hard to access for certain groups, and their effectiveness is limited due to poor patient compliance. Therefore, there is an urgent need for advanced drug delivery strategies to address the challenges associated with the manufacturing costs and adherence to the conventional dosing regimens.

In this study, novel subcutaneously implantable long-acting EVA-based formulations of NTX were prepared using a cost-eefective one-step HME process, which is a solvent-free, continuous technology that can be easily scaled for mass production. The Implantable Drug Delivery Systems (IDDS) demonstrated sustained release for over 90 days, which can provide long-term delivery of NTX into the bloodstream from the subcutaneous tissue, eliminating mild or severe side effects due to the repetitive fluctuation in the API plasma concentration, which can otherwise be caused by conventional daily oral administration.

Firstly, appropriate analytical protocols were developed and validated. The influence of EVA grade and drug loading on the processability, homogeneity, stability and *in vitro* drug release was evaluated. The results demonstrated that a higher VA-content EVA resulted in slower drug release, whereas a lower MFI EVA influenced the processability and, consequently, the drug stability. Drug loading also had a great influence on the processability, homogeneity and *in vitro* release. Implants with higher drug loadings had a lower homogeneity with a higher drug release rate. An NTX HCl loading above 40% w/w resulted in an increased release rate that was insufficient to achieve long-term release. At the same time, implants with lower (below 35% w/w) NTX HCl loadings, showed significantly slower release than was expected. The data also revealed that the mechanism of drug release from the implants was mainly controlled by the diffusion of NTX HCl through a porous network filled with the release media. It was also demonstrated that the amorphisation of NTX HCl during the extrusion process had no significant impact on the production of degradation by-products. *In vivo* investigations showed that the 35 and 40% w/w implants provided long-term blood concentrations in male beagle dogs. Although the exhibited plasma levels were lower than was expected, our extraction studies proved that acceptable levels of NTX HCl was released from the implants, however, it accumulated in the surrounding capsule formed by inflammatory tissue response and did not diffuse into the bloodstream. This problem can be presumably solved by the administration of

anti-inflammatory drugs simultaneously or by positioning several implants close together to increase the diffusion of NTX HCl through the tissue and into the bloodstream. However, further animal studies would have been required to prove these assumptions.

To help with technology transfer and scale-up, a process window was determined for the final formulation of 35% w/w NTX HCl-EVA28 (MFI:25) with a diameter of 3 mm and a length of 40 mm. 6 different process settings were investigated to determine the impact of manufacturing process parameters (process temperature and screw speed) on the Critical Quality Attributes (CQAs) and, where appropriate, identify any relationships supported by statistical analyses. The study demonstrated the complex influence of processing temperature and screw speed on the drug content of the products, which was due to the morphological change of NTX HCl during the HME process. However, other performance characteristics were not influenced by these two process parameters or could be traced back to the complex evolution of the drug content. After selecting the most appropriate HME process settings, a larger batch size (approximately 100 implants) was manufactured, and their stability was assessed over 6 months under accelerated conditions (40 °C/ 75% RH). The implants stored in heat-sealed Alu/PE/PP sachet pouches showed adequate long-term stability under the accelerated conditions. Although a significant level of recrystallisation of the amorphous NTX HCl in the implants was observed after 6 months of storage, this phase transition did not affect the most critical attribute of the implants, namely their release rate of NTX HCl.

In summary, the primary objective of this dissertation, namely to develop a subcutaneous removable rod-shaped NTX HCl-loaded IDDS with acceptable CQAs and stability, was achieved. The therapeutically sufficient daily drug level in the bloodstream can be achieved and tailored to the patients' needs by using several implants.

In *Chapter 4*, for the first-time the release of a highly hydrophilic drug (NTX HCl) from EVA matrix, containing different cellulose-ether (CE) additives (HPC and HPMC) was studied. The main aim of this research was to investigate the influence of the competitive phenomena of dissolution, swelling and gelling of the CEs on the release performance of the IDDSs produced using a cost-effective, single-step HME process. We demonstrated that homogeneous ternary systems, confirmed by several analytical techniques (i.e., HPLC assay, SEM and Raman spectrometry), could be produced by the applied processing parameters on a laboratory-scale Kapex 7.5mm extruder. Approximately a 2 and a 4 fold increase in NTX HCl release could be obtained by incorporating only 5 and 10% w/w swelling- or pore-forming CE-additives into the 20% w/w NTX HCl-loaded implants, and the release mainly followed the highly preferable

zero-order kinetics. Moreover, our results also showed that the release rate from 50% w/w drug-loaded implants could be decreased advantageously by embedding only 5% w/w HPMC into the systems, providing a constant release of NTX HCl for approximately 40 days. In these systems, the release mainly occured via the diffusion of the dissolved NTX HCl through continuously forming pores and also through the hydrogel-network of the HPMC polymer.

These findings could be exploited to tailor drug release from the implants while signifcantly reducing the manufacturing costs. The lower NTX HCl-loaded ternary systems (with CE-additives) could provide approximately the same drug release as the higher drug-loaded binary systems, which would result in significant costs savings as the NTX HCl is more expensive than CE-additives.

Finally, in *Chapter 5*, it was shown for the first time that an oversaturated and kinetically stabilised monolithic solution of NTX and EVA could be produced via a one-step HME process using the more lipophilic neutral base form of the API. The different physicochemical characteristics of the NTX base resulted in a dissolution of NTX in the molten EVA matrices during the HME proces with a T_{proc} of 140 °C, approximately 40 °C below the T_m (176 °C) of NTX base. The majority of the NTX base remained in a molecularly dispersed form within the EVAs due to the rapid cooling of the extrduate after the processing, which was proven by several analytical techniques (e.g., SEM, DSC and Raman spectrometry). One of the main advantages of the solid solution systems was that they could be produced with better homogeneity compared to the NTX HCl-loaded two-phases solid dispersion systems owing to the better mixing efficacy of the base form during HME. However, significant oxidative degradation (above the acceptable limit) could be observed in the NTX base-loaded systems, with the extent of degradation directly proportional to the VA-content of theEVAs. These findings suggested that a higher ratio of VA-groups on the polyvinyl backbone resulted in a better solubilisation effect because of higher possibilities for interaction with the NTX base.The decomposition of NTX can presumably be reduced by using optimised process parameters and/or antioxidant additives (e.g., Vitamin-E-succinate, Vitamin-C), which is one of the subjects of our further work.

Another advantage of the solid solution formulations over the dispersion systems could be observed in their different release performances. Our results demonstrated that a significantly higher drug release rate could be achieved when the mass transport was based on pure Fickian-diffusion of the NTX molecules through EVA matrices, compared to the tortuosity-controlled release from the two-phase dispersion systems. For example, 10% w/w NTX base-loaded

EVA28 implants had almost the same drug release rate achieved with 20 or 30 % w/w NTX HCl-loaded EVA28 systems. The rate of Fickian diffusion was dependent on the VA-content and thus the crystallinity and hydrophobicity of the matrix polymer. EVAs with higher VA-content showed higher drug release because of the increased ratio of amorphous domains of EVAs, through which the diffusion of NTX could occur.

6.2 Future works

NTX HCl-loaded EVA28 implants

In order to advance the commercialisation of the NTX HCl-loaded EVA28 implants, further *in vivo* studies should be conducted. In the next studies, several implants would be placed close together in the subcutaneous tissue area, and both the plasma levels of NTX HCl and the level of inflammatory tissue response determined. Depending on the outcome of this study, further development focusing on incorporating a sufficient amount of anti-inflammatory agents (e.g., corticosteroids or triamcinolone) into the NTX HCl-EVA28 implants or administering them simultaneously *per os* should be considered.

NTX HCl-loaded EVA28 implants with CE additives

Further investigations (e.g., processability, homogeneity, purity, *in vitro* performance) on the composite systems with dimensions of 40 mm in length and 2 to 4 mm in diameter should be performed. This geometry is similar in dimensions to other subcutaneous implants currently available on the market and previously investigated in this thesis. After a proper process development step, a comparative *in vivo* study should be carried out, focusing on the difference between the pharmacokinetic profiles of the binary and ternary systems.

NTX base-loaded implants (co-extrusion and 3D-printing)

Our measurements showed that the base form of NTX has significant diffusivity through the EVA polymers. This finding can be exploited in the use of other product designs that can provide a preferable zero-order release rate of NTX. The following studies would aim to develop reservoir products prepared using different melt-based technologies, such as co-extrusion and 3D-printing. In these systems, the inner EVA core would contain the oversaturated form of NTX, while the outer layer would control the drug release. The composition of the core and the rate-controlling layer, and also their geometries (thickness) could be designed (using the experimentally determined diffusion coefficients) and manufactured based on the required pharmacokinetic profile.

Obviously, prior to any further development, the issue of the heat degradation of NTX base has to be addressed. As mentioned earlier, our further plans focusing on this topic include the optimisation of the HME processing parameters (T_{proc} and screw speed). After the appropriate HME process window is assessed, in which NTX base-EVA systems with acceptable purity profile, morphology and release performance can be produced, experiments utilising co-extrusion with other EVAs or 3D-printing (direct powder extrusion technology) can be started. Another interesting approach to decrease heat degradation of NTX would be the use of specific anti-oxidant additives, such as Vitamin-E-succinate (T_m=76 °C), a fine solid powder that can be easily fed, with the other two components, into the extruder. Our preliminary experiments showed that this specific additive is extrudable and miscible with EVAs. Furthermore, because of its low T_m, it can plasticise the system, providing the possibility to decrease the T_{proc}, therefore, decrease the heat stress that the molecularly dispersed NTX must endure.

References

[1] Blanco C, Volkow ND. Management of opioid use disorder in the USA: present status and future directions. Lancet 2019; 393 (10182): 1760-1772. doi:10.1016/S0140-6736(18)33078-2

[2] Skolnick P. The opioid epidemic: Crisis and solutions. Annu Rev Pharmacol Toxicol 2018; 58: 143-159. doi:10.1146/annurev-pharmtox-010617-052534

[3] United Nations Office on Drugs and Crime. World drug report 2020. [internet]. Vienna, Austria: United Nations; 2020 [cited 2021 May 17]. Available from: https://wdr.unodc.org/wdr2020/field/WDR20_BOOKLET_4.pdf

[4] Substance Abuse and Mental Health Services Administration. Key substance use and mental health indicators in the United States: Results from the 2019 national survey on drug use and helath. [internet]. Rockville, MD, USA: U.S Department of Health and Human Services; 2020 [cited 2021 May 18]. Available from: https://www.samhsa.gov/data/sites/default/files/reports/rpt29393/2019NSDUHFFRPDFWHTML/2019NSDUHFFR1PDFW090120.pdf

[5] World Health Organization. Opioid overdose. [internet]. 2021 [cited 2021 May 18] Available from: https://www.who.int/news-room/fact-sheets/detail/opioid-overdose#:~:text=Worldwide%2C%20about%20269%20million%20people,drug%20use%20disorders%20in%202018.

[6] Tsui JI, Evans JL, Lum PJ, Hahn JA, Page K. Association of opioid agonist therapy with lower incidence of hepatitis C virus infection in young adult injection drug users. JAMA Intern Med. 2014; 174 (12): 1974-1981. doi:10.1001/jamainternmed.2014.5416

[7] Tolia VN, Patrick SW, Bennett MM, et al. Increasing incidence of the neonatal abstinence syndrome in U.S. neonatal ICUs. N Engl J Med 2015; 372 (22): 2118-2126. doi:10.1056/NEJMsa1500439

[8] Compton WM, Volkow ND. Major increases in opioid analgesic abuse in the United States: concerns and strategies. Drug Alcohol Depend 2006; 81 (2): 103-107. doi:10.1016/j.drugalcdep.2005.05.009

[9] Srivastava AB, Gold MS. Beyond Supply: How We Must Tackle the Opioid Epidemic. Mayo Clin Proc 2018; 93 (3): 269-272. doi:10.1016/j.mayocp.2018.01.018

[10] Bodnar RJ. Endogenous opiates and behavior: 2014. Peptides 2016; 75: 18-70. doi:10.1016/j.peptides.2015.10.009

[11] Fields H. State-dependent opioid control of pain. Nat Rev Neurosci 2004; 5 (7): 565-575. doi:10.1038/nrn1431

[12] Listos J, Łupina M, Talarek S, Mazur A, Orzelska-Górka J, Kotlińska J. The Mechanisms Involved in Morphine Addiction: An Overview. Int J Mol Sci [internet]. 2019 [cited: 2022 April 14]; 20 (17): 4302. doi:10.3390/ijms20174302

[13] White JM, Irvine RJ. Mechanisms of fatal opioid overdose. Addiction 1999; 94 (7): 961-972. PMID:10707430

[14] Koob GF, Ahmed SH, Boutrel B, et al. Neurobiological mechanisms in the transition from drug use to drug dependence. Neurosci Biobehav Rev 2004; 27 (8): 739-749. doi:10.1016/j.neubiorev.2003.11.007

[15] Raehal KM, Bohn LM. β-arrestins: regulatory role and therapeutic potential in opioid and cannabinoid receptor-mediated analgesia. Handb Exp Pharmacol 2014; 219: 427-443. doi:10.1007/978-3-642-41199-1_22

[16] Nakamoto K, Kawasaki S, Kobori T, et al. Involvement of matrix metalloproteinase-9 in the development of morphine tolerance. Eur J Pharmacol 2012; 683 (1-3): 86-92. doi:10.1016/j.ejphar.2012.03.006

[17] Taylor AM, Castonguay A, Ghogha A, et al. Neuroimmune Regulation of GABAergic Neurons Within the Ventral Tegmental Area During Withdrawal from Chronic Morphine. Neuropsychopharmacology 2016; 41 (4): 949-959. doi:10.1038/npp.2015.221

[18] Koob GF, Stinus L, Le Moal M, Bloom FE. Opponent process theory of motivation: neurobiological evidence from studies of opiate dependence. Neurosci Biobehav Rev 1989; 13 (2-3): 135-140. doi:10.1016/s0149-7634(89)80022-3

[19] Gravitz L. Unravelling the mystery of opioid addiction. Nature 2019; 573(7773): S20-S21. doi:10.1038/d41586-019-02690-6

[20] Cicero TJ, Ellis MS. Understanding the demand side of the prescription opioid epidemic: Does the initial source of opioids matter? Drug Alcohol Depend 2017; 173 Suppl 1: S4-S10. doi:10.1016/j.drugalcdep.2016.03.014

[21] Compton WM, Jones CM, Baldwin GT, Harding FM, Blanco C, Wargo EM. Targeting Youth to Prevent Later Substance Use Disorder: An Underutilized Response to the US Opioid Crisis. Am J Public Health 2019; 109(S3): S185-S189. doi:10.2105/AJPH.2019.305020

[22] Behar E, Santos GM, Wheeler E, Rowe C, Coffin PO. Brief overdose education is sufficient for naloxone distribution to opioid users. Drug Alcohol Depend 2015; 148: 209-212. doi:10.1016/j.drugalcdep.2014.12.009

[23] Krieter P, Chiang N, Gyaw S, et al. Pharmacokinetic Properties and Human Use Characteristics of an FDA-Approved Intranasal Naloxone Product for the Treatment of Opioid Overdose. J Clin Pharmacol 2016; 56(10): 1243-1253. doi:10.1002/jcph.759

[24] U.S. Food and Drug Adminisration. Abuse-Deterrent Opioids – Evaluation and Labeling: Guidance for Industry [internet]. 2015 [cited: 2022 April 14] Available from: http://www.fda.gov/downloads/drugs/guidancecomplianceregulatoryinformation/guidances/ucm334743.pdf

[25] Morgan JR, Schackman BR, Leff JA, Linas BP, Walley AY. Injectable naltrexone, oral naltrexone, and buprenorphine utilization and discontinuation among individuals treated for opioid use disorder in a United States commercially insured population. J Subst Abuse Treat 2018; 85: 90-96. doi:10.1016/j.jsat.2017.07.001

[26] Mattick RP, Breen C, Kimber J, Davoli M. Methadone maintenance therapy versus no opioid replacement therapy for opioid dependence. Cochrane Database Syst Rev [internet]. 2009 [cited 2021 May18]; 2009(3): CD002209. doi:10.1002/14651858.CD002209.pub2

[27] Dasgupta N, Freifeld C, Brownstein JS, et al. Crowdsourcing black market prices for prescription opioids. J Med Internet Res [internet]. 2013 [cited 2021 May 18]; 15 (8): e178. doi:10.2196/jmir.2810

[28] Lev R, Petro S, Lee A, et al. Methadone related deaths compared to all prescription related deaths. Forensic Sci Int 2015; 257: 347-352. doi:10.1016/j.forsciint.2015.09.021

[29] Amato L, Davoli M, Minozzi S, Ali R, Ferri M. Methadone at tapered doses for the management of opioid withdrawal. Cochrane Database Syst Rev [internet]. 2005 [cited 2021 May 18]; 2005; (3): CD003409. doi:10.1002/14651858.CD003409.pub3

[30] Stotts AL, Dodrill CL, Kosten TR. Opioid dependence treatment: options in pharmacotherapy. Expert Opin Pharmacother 2009; 10 (11): 1727-1740. doi:10.1517/14656560903037168

[31] Fairley M, Humphreys K, Joyce VR, et al. Cost-effectiveness of treatments for opioid use disorder. JAMA Psychiatry [internet]. 2021 [cited 2021 May 18]; e210247. doi:10.1001/jamapsychiatry.2021.0247

[32] Gong C, Zou X, Chen W, Liu Y, Lu Q, Ling L. Factors associated with compliance among methadone maintenance treatment transfers: Evidence from audit records at clinics in

Guangdong, China. Int J Environ Res Public Health [internet] 2019 [cited 2021 May 18]; 16 (11): 2023. doi:10.3390/ijerph16112023

[33] Volkow ND, Jones EB, Einstein EB, Wargo EM. Prevention and treatment of opioid misuse and addiction: A review. JAMA Psychiatry 2019; 76 (2): 208-216. doi:10.1001/jamapsychiatry.2018.3126

[34] Falcon E, Browne CA, Leon RM, et al. Antidepressant-like effects of buprenorphine are mediated by kappa opioid receptors. Neuropsychopharmacology 2016; 41 (9): 2344-2351. doi:10.1038/npp.2016.38

[35] Fareed A, Vayalapalli S, Casarella J, Drexler K. Effect of buprenorphine dose on treatment outcome. J Addict Dis 2012; 31 (1): 8-18. doi:10.1080/10550887.2011.642758

[36] Nielsen S, Larance B, Degenhardt L, Gowing L, Kehler C, Lintzeris N. Opioid agonist treatment for pharmaceutical opioid dependent people. Cochrane Database Syst Rev [internet]. 2016 [cited 2021 May 18]; (5): CD011117. doi:10.1002/14651858.CD011117.pub2

[37] Blum K, Han D, Modestino EJ, et al. A systematic, intensive statistical investigation of data from the comprehensive analysis of reported drugs (CARD) for compliance and illicit opioid abstinence in substance addiction treatment with buprenorphine/naloxone. Subst Use Misuse 2018; 53 (2): 220-229. doi:10.1080/10826084.2017.1400064

[38] Mattick RP, Kimber J, Breen C, Davoli M. Buprenorphine maintenance versus placebo or methadone maintenance for opioid dependence. Cochrane Database Syst Rev [internet]. 2008 [cited 2021 May 18]; (2): CD002207. doi:10.1002/14651858.CD002207.pub3

[39] Lofwall MR, Walsh SL. A review of buprenorphine diversion and misuse: the current evidence base and experiences from around the world. J Addict Med 2014; 8 (5): 315-326. doi:10.1097/ADM.0000000000000045

[40] Tetrault JM, Fiellin DA. Current and potential pharmacological treatment options for maintenance therapy in opioid-dependent individuals. Drugs 2012; 72 (2): 217-228. doi:10.2165/11597520-000000000-00000

[41] Ford C, Halliday K, Lawson E, Browne E. Guidence for the use of substitute prescribing in the treatment of opioid dependence in primary care. Royal Collage of General Practioners [internet]. 2011 [cited 2021 May 18] Available from: https://www.rcgp.org.uk/revalidation-and-cpd/~/media/Files/SMAH/RCGP-Guidance-for-the-use-of-substitute-prescribing-in-the-treatment-of-opioid-dependence-in-primary-care-2011.ashx

[42] Substance Abuse and Mental Health Services Administration. Become a buprenorphine waivered practioner. [internet] [cited 2021 May 18] Available from: https://www.samhsa.gov/medication-assisted-treatment/become-buprenorphine-waivered-practitioner

[43] Rosenthal RN, Lofwall MR, Kim S, et al. Effect of Buprenorphine Implants on Illicit Opioid Use Among Abstinent Adults With Opioid Dependence Treated With Sublingual Buprenorphine: A Randomized Clinical Trial. JAMA 2016; 316 (3): 282-290. doi:10.1001/jama.2016.9382

[44] Rosenthal RN, Goradia VV. Advances in the delivery of buprenorphine for opioid dependence. Drug Des Devel Ther 2017; 11: 2493-2505. doi:10.2147/DDDT.S72543

[45] Blumberg H, Dayton HB. Naloxone, naltrexone, and related noroxymorphones. Adv Biochem Psychopharmacol 1973; 8 (0): 33-43. PMID: 4794989

[46] Martin WR, Jasinski DR, Mansky PA. Naltrexone, an antagonist for the treatment of heroin dependence. Effects in man. Arch Gen Psychiatry 1973; 28 (6): 784-791. doi:10.1001/archpsyc.1973.01750360022003

[47] O'Brien CP, Greenstein R, Ternes J, Woody GE. Clinical pharmacology of narcotic antagonists. Ann N Y Acad Sci 1978; 311: 232-240. doi:10.1111/j.1749-6632.1978.tb16779.x

[48] Verebey K. The clinical pharmacology of naltrexone: pharmacology and pharmacodynamics. NIDA Res Monogr 1981; 28: 147-158. PMID: 6791001

[49] Koehl JL, Zimmerman DE, Bridgeman PJ. Medications for management of opioid use disorder. Am J Health Syst Pharm 2019; 76 (15): 1097-1103. doi:10.1093/ajhp/zxz105

[50] Weerts EM, Kim YK, Wand GS, et al. Differences in delta- and mu-opioid receptor blockade measured by positron emission tomography in naltrexone-treated recently abstinent alcohol-dependent subjects. Neuropsychopharmacology 2008; 33 (3): 653-665. doi:10.1038/sj.npp.1301440

[51] Shulman M, Choo TH, Scodes J, et al. Association between methadone or buprenorphine use during medically supervised opioid withdrawal and extended-release injectable naltrexone induction failure. J Subst Abuse Treat [internet] 2021 [cited 2021 May 18]; 124: 108292. doi:10.1016/j.jsat.2021.108292

[52] Unterwald EM. Naltrexone in the treatment of alcohol dependence. J Addict Med 2008; 2 (3): 121-127. doi:10.1097/ADM.0b013e318182b20f

[53] Valbrun LP, Zvonarev V. The opioid system and food intake: Use of opiate antagonists in treatment of binge eating disorder and abnormal eating behavior. J Clin Med Res 2020; 12 (2): 41-63. doi:10.14740/jocmr4066

[54] Patten DK, Schultz BG, Berlau DJ. The safety and efficacy of low-dose naltrexone in the management of chronic pain and inflammation in multiple sclerosis, fibromyalgia, Crohn's disease, and other chronic pain disorders. Pharmacotherapy 2018; 38 (3): 382-389. doi:10.1002/phar.2086

[55] Kim PS, Fishman MA. Low-dose naltrexone for chronic pain: Update and systemic review. Curr Pain Headache Rep [internet]. 2020 [cited 2021 May 18]; 24 (10): 64. doi:10.1007/s11916-020-00898-0

[56] Lie MRKL, van der Giessen J, Fuhler GM, et al. Low dose Naltrexone for induction of remission in inflammatory bowel disease patients. J Transl Med [internet]. 2018 [cited 2021 May 18]; 16 (1): 55. doi:10.1186/s12967-018-1427-5

[57] Bolton MJ, Chapman BP, Van Marwijk H. Low-dose naltrexone as a treatment for chronic fatigue syndrome. BMJ Case Rep [internet]. 2020 [cited 2021 May 18]; 13 (1): e232502. doi:10.1136/bcr-2019-232502

[58] Liu WM, Scott KA, Dennis JL, Kaminska E, Levett AJ, Dalgleish AG. Naltrexone at low doses upregulates a unique gene expression not seen with normal doses: Implications for its use in cancer therapy. Int J Oncol 2016; 49 (2): 793-802. doi:10.3892/ijo.2016.3567

[59] Porter SJ, Somogyi AA, White JM. In vivo and in vitro potency studies of 6beta-naltrexol, the major human metabolite of naltrexone. Addict Biol 2002; 7 (2): 219-225. doi:10.1080/135562102200120442

[60] Yancey-Wrona JE, Raymond TJ, Mercer HK, Sadée W, Bilsky EJ. 6beta-naltrexol preferentially antagonizes opioid effects on gastrointestinal transit compared to antinociception in mice. Life Sci 2009; 85 (11-12): 413-420. doi:10.1016/j.lfs.2009.06.016

[61] U.S Food and Drug Administration. Revia® (naltrexone hydrochloride tablets USP). [internet] Silver Spring, MD, USA [cited 2021 May 4] Available from: https://www.accessdata.fda.gov/drugsatfda_docs/label/2013/018932s017lbl.pdf

[62] Meyer MC, Straughn AB, Lo MW, Schary WL, Whitney CC. Bioequivalence, dose-proportionality, and pharmacokinetics of naltrexone after oral administration. J Clin Psychiatry 1984; 45 (9): 15-19. PMID:6469932

[63] Dean RL. The preclinical development of Medisorb Naltrexone, a once a month long acting injection, for the treatment of alcohol dependence. Front Biosci 2005; 10: 643-655. doi:10.2741/1559

[64] Oncken C, Van Kirk J, Kranzler HR. Adverse effects of oral naltrexone: analysis of data from two clinical trials. Psychopharmacology (Berl). 2001; 154 (4): 397-402. doi:10.1007/s002130000666

[65] O'Malley SS, Krishnan-Sarin S, Farren C, O'Connor PG. Naltrexone-induced nausea in patients treated for alcohol dependence: clinical predictors and evidence for opioid-mediated effects. J Clin Psychopharmacol 2000; 20 (1): 69-76. doi:10.1097/00004714-200002000-00012

[66] Rohsenow DJ, Colby SM, Monti PM, et al. Predictors of compliance with naltrexone among alcoholics. Alcohol Clin Exp Res 2000; 24 (10): 1542-1549. PMID:11045863

[67] Volpicelli JR, Watson NT, King AC, Sherman CE, O'Brien CP. Effect of naltrexone on alcohol "high" in alcoholics. Am J Psychiatry 1995; 152 (4): 613-615. doi:10.1176/ajp.152.4.613

[68] Sullivan MA, Garawi F, Bisaga A, et al. Management of relapse in naltrexone maintenance for heroin dependence. Drug Alcohol Depend 2007; 91 (2-3): 289-292. doi:10.1016/j.drugalcdep.2007.06.013

[69] Wang R, Conner DP, Li BV. Bioavailability and bioequivalence aspects of oral modified-release drug products. AAPS J 2017; 19 (2): 360-366. doi:10.1208/s12248-016-0025-9

[70] Amidon GL, Lennernäs H, Shah VP, Crison JR. A theoretical basis for a biopharmaceutic drug classification: the correlation of in vitro drug product dissolution and in vivo bioavailability. Pharm Res 1995; 12 (3): 413-420. doi:10.1023/a:1016212804288

[71] van den Heuvel MW, van Bragt AJ, Alnabawy AK, Kaptein MC. Comparison of ethinylestradiol pharmacokinetics in three hormonal contraceptive formulations: the vaginal ring, the transdermal patch and an oral contraceptive. Contraception 2005; 72 (3): 168-174. doi:10.1016/j.contraception.2005.03.005

[72] Rogers E, Mehta S, Shengelia R, Reid MC. Four strategies for managing opioid-induced side effects in older adults. Clin Geriatr 2013; 21 (4)

[73] Tibbitt MW, Dahlman JE, Langer R. Emerging frontiers in drug delivery. J Am Chem Soc 2016; 138 (3): 704-717. doi:10.1021/jacs.5b09974

[74] Jin J, Sklar GE, Min Sen Oh V, Chuen Li S. Factors affecting therapeutic compliance: A review from the patient's perspective. Ther Clin Risk Manag 2008; 4 (1): 269-286. doi:10.2147/tcrm.s1458

[75] Fenton OS, Olafson KN, Pillai PS, Mitchell MJ, Langer R. Advances in biomaterials for drug delivery. Adv Mater 2018; e1705328. doi:10.1002/adma.201705328

[76] Hillery AM, Park K. editors. Drug delivery: Fundamentals & applications. 2nd ed. Boca Raton, Florida: CRC Press; 2017.

[77] Mikulic M. Pharmaceutical market: worldwide revenue 2001-2020. [internet] 2021 [cited: 2021 May 4] Available from: https://www.statista.com/statistics/263102/pharmaceutical-market-worldwide-revenue-since-2001/

[78] Grand View Research. Controlled release drug delivery market size, share & trends, analysis report by technology, by release mechanism, by application, by region, and segment forecast, 2020-2027. [internet] 2020 [cited: 2021 May 4] Available from: https://www.grandviewresearch.com/industry-analysis/controlled-release-drug-delivery-market

[79] Langer R. Drug delivery. Drugs on target. Science 2001; 293 (5527): 58-59. doi:10.1126/science.1063273

[80] Santos A, Sinn AM, Bariana M, Kumeria T, Wang Y, Losic D. Drug-releasing implants: current progress, challenges and perspectives. J Mater Chem B 2014; 2 (37): 6157-6182. doi:10.1039/c4tb00548a

[81] Stevenson CL, Santini JT Jr, Langer R. Reservoir-based drug delivery systems utilizing microtechnology. Adv Drug Deliv Rev 2012; 64 (14): 1590-1602. doi:10.1016/j.addr.2012.02.005

[82] Pan H, Shen P, Shu Q, et al. Efficacy and safety of sustained-release oxycodone compared with immediate-release morphine for pain titration in cancer patients: A multicenter, open-label, randomized controlled trial (SOCIAL). Medicine 2019 ;98 (24): e15505. doi:10.1097/MD.0000000000015505

[83] Nel A, Bekker LG, Bukusi E, et al. Safety, acceptability and adherence of dapivirine vaginal ring in a microbicide clinical trial conducted in multiple countries in sub-saharan Africa. PLoS One 2016; 11 (3): e0147743. doi:10.1371/journal.pone.0147743

[84] Borrego Y, Gómez-Fernández E, Jiménez R, Cantudo R, Almeida-González CV, Morillo R. Predictors of primary non-adherence to concomitant chronic treatment in HIV-infected

patients with antiretroviral therapy. Eur J Hosp Pharm 2018; 25 (3): 127-131. doi:10.1136/ejhpharm-2016-001000

[85] Kirkman MS, Rowan-Martin MT, Levin R, et al. Determinants of adherence to diabetes medications: findings from a large pharmacy claims database. Diabetes Care 2015; 38 (4): 604-609. doi:10.2337/dc14-2098

[86] Vernon A, Fielding K, Savic R, Dodd L, Nahid P. The importance of adherence in tuberculosis treatment clinical trials and its relevance in explanatory and pragmatic trials. PLoS Med 2019; 16 (12): e1002884. doi:10.1371/journal.pmed.1002884

[87] Ferdinand KC, Senatore FF, Clayton-Jeter H, et al. Improving medication adherence in cardiometabolic disease: Practical and regulatory implications. J Am Coll Cardiol 2017; 69 (4): 437-451. doi:10.1016/j.jacc.2016.11.034

[88] Choi HY, Oh IJ, Lee JA, et al. Factors affecting adherence to antihypertensive medication. Korean J Fam Med 2018; 39 (6): 325-332. doi:10.4082/kjfm.17.0041

[89] Bidwal M, Lor K, Yu J, Ip E. Evaluation of asthma medication adherence rates and strategies to improve adherence in the underserved population at a Federally Qualified Health Center. Res Social Adm Pharm 2017; 13 (4): 759-766. doi:10.1016/j.sapharm.2016.07.007

[90] Rolnick SJ, Pawloski PA, Hedblom BD, Asche SE, Bruzek RJ. Patient characteristics associated with medication adherence. Clin Med Res 2013; 11 (2): 54-65. doi:10.3121/cmr.2013.1113

[91] Offord S, Lin J, Mirski D, Wong B. Impact of early nonadherence to oral antipsychotics on clinical and economic outcomes among patients with schizophrenia. Adv Ther 2013; 30 (3): 286-297. doi:10.1007/s12325-013-0016-5

[92] Holt SR, Tobin DG. Pharmacotherapy for alcohol use disorder. Med Clin North Am 2018; 102 (4): 653-666. doi:10.1016/j.mcna.2018.02.008

[93] Sullivan MA, Bisaga A, Pavlicova M, et al. A randomized trial comparing extended-release injectable suspension and oral naltrexone, both combined with behavioral therapy, for the treatment of opioid use disorder. Am J Psychiatry. 2019; 176 (2): 129-137. doi:10.1176/appi.ajp.2018.17070732

[94] De Geest S, Sabaté E. Adherence to long-term therapies: evidence for action. [internet] Geneva, Switzerland: World Health Organization. 2003 [cited: 2021 May 4]. Available from: https://www.who.int/chp/knowledge/publications/adherence_full_report.pdf

[95] Osterberg L, Blaschke T. Adherence to medication. N Engl J Med 2005; 353 (5): 487-497. doi:10.1056/NEJMra050100

[96] McHugh KJ, Guarecuco R, Langer R, Jaklenec A. Single-injection vaccines: Progress, challenges, and opportunities. J Control Release 2015; 219: 596-609. doi:10.1016/j.jconrel.2015.07.029

[97] Lau CML, Yu Y, Jahanmir G, Chau Y. Controlled release technology for anti-angiogenesis treatment of posterior eye diseases: Current status and challenges. Adv Drug Deliv Rev 2018; 126: 145-161. doi:10.1016/j.addr.2018.03.013

[98] United States Pharmacopeia. Nomenclature guidelines [internet] Rockville, Maryland, USA. 2020 [cited 2021 May 4]. Available from: https://www.usp.org/sites/default/files/usp/document/usp-nomenclature-guidelines.pdf

[99] Martini LG, Coles M, Gravell K, Stephenson S, Thomson CM. The use of a hydrophobic matrix for the sustained release of a highly water soluble drug. Drug Dev Ind Pharm 2000; 26 (1): 79-83. doi:10.1081/ddc-100100330

[100] Malaterre V, Ogorka J, Loggia N, Gurny R. Oral osmotically driven systems: 30 years of development and clinical use. Eur J Pharm Biopharm 2009; 73 (3): 311-323. doi:10.1016/j.ejpb.2009.07.002

[101] Lipinski CA, Lombardo F, Dominy BW, Feeney PJ. Experimental and computational approaches to estimate solubility and permeability in drug discovery and development settings. Adv Drug Deliv Rev 2001; 46 (1-3): 3-26. doi:10.1016/s0169-409x(00)00129-0

[102] Keserü GM, Makara GM. The influence of lead discovery strategies on the properties of drug candidates. Nat Rev Drug Discov 2009; 8 (3): 203-212. doi:10.1038/nrd2796

[103] Waring MJ, Arrowsmith J, Leach AR, et al. An analysis of the attrition of drug candidates from four major pharmaceutical companies. Nat Rev Drug Discov 2015;14(7):475-486. doi:10.1038/nrd4609

[104] Aungst BJ. Optimizing oral bioavailability in drug discovery: An overview of design and testing strategies and formulation options. J Pharm Sci 2017; 106 (4): 921-929. doi:10.1016/j.xphs.2016.12.002

[105] Anselmo AC, Gokarn Y, Mitragotri S. Non-invasive delivery strategies for biologics. Nat Rev Drug Discov 2019; 18 (1): 19-40. doi:10.1038/nrd.2018.183

[106] Mitragotri S, Burke PA, Langer R. Overcoming the challenges in administering biopharmaceuticals: formulation and delivery strategies. Nat Rev Drug Discov 2014; 13 (9): 655-672. doi:10.1038/nrd4363

[107] McDowell A, Medlicott NJ. Chapter 4: Anatomy and physiology of the injection site: Implication for extended release parenteral systems. In: Wright JC, Burgess DJ, editors. Long Acting Injections and Implants. 1st ed. New York, NY, USA: Springer; 2012. p. 57-68.

[108] Jucker BM, Alsaid H, Rambo M, Lenhard SC, Hoang B, Xie F, Groseclose MR, Castellino S, Damian V, Bowers G, Gupta M. Multimodal imaging approach to examine biodistribution kinetics of Cabotegravir (GSK1265744) long acting parenteral formulation in rat. J Control Release 2017; 268: 102-112. doi: 10.1016/j.jconrel.2017.10.017

[109] Abraham G, Demiraj F, Ungemach FR. Comparison of the hypothalamic-pituitary-adrenal axis susceptibility upon single-dose i.m. depot versus long-acting i.v. triamcinolone acetonide therapy: a direct pharmacokinetic correlation. J Endocrinol 2006;191 (2): 491-6. doi: 10.1677/joe.1.06991

[110] Singh K, Sarafianos SG, Sönnerborg A. Long-acting anti-HIV drugs targeting HIV-1 reverse transcriptase and integrase. Pharmaceuticals 2019; 12 (2): 62. doi: 10.3390/ph12020062

[111] Hoffman AS. The origins and evolution of "controlled" drug delivery systems. J Control Release. 2008; 132 (3): 153-163. doi: 10.1016/j.jconrel.2008.08.012

[112] Macoul KL, Pavan-Langston D. Pilocarpine ocusert system for sustained control of ocular hypertension. Arch Ophthalmol 1975; 93 (8): 587-590. doi:10.1001/archopht.1975.01010020571003

[113] Quarterman JC, Geary SM, Salem AK. Evolution of drug-eluting biomedical implants for sustained drug delivery. Eur J Pharm Biopharm 2021; 159: 21-35. doi:10.1016/j.ejpb.2020.12.005

[114] Berger J, Dunn JD, Johnson MM, Karst KR, Shear WC. How drug life-cycle management patent strategies may impact formulary management. Am J Manag Care 2016; 22 (16 Suppl): S487-S495

[115] Rosen H, Abribat T. The rise and rise of drug delivery. Nat Rev Drug Discov 2005; 4 (5): 381-385. doi:10.1038/nrd1721

[116] International Federation of Pharmaceutical Manufacturers Associations. Pharmaceutical innovation platform [internet]. Geneva, Switzerland: Impremiere Genevoise; 2004 [cited:

2021 May 15]. Available from: https://www.who.int/intellectualproperty/Pharmaceutical_innovation.pdf

[117] Kumar A, Pillai J. Chapter 13: Implantable drug delivery systems. In: Grumezescu A, editor. Nanostructures for the engineering of cells, tissues and organs. 1st ed. Norwich, NY, USA: Elsevier; 2018: p. 473-511.

[118] Bally L, Thabit H, Hovorka R. Finding the right route for insulin delivery - an overview of implantable pump therapy. Expert Opin Drug Deliv 2017; 14 (9): 1103-1111. doi:10.1080/17425247.2017.1267138

[119] Maher S, Mazinani A, Barati MR, Losic D. Engineered titanium implants for localized drug delivery: recent advances and perspectives of Titania nanotubes arrays. Expert Opin Drug Deliv 2018; 15 (10): 1021-1037. doi:10.1080/17425247.2018.1517743

[120] Wong BS, Yoong SL, Jagusiak A, et al. Carbon nanotubes for delivery of small molecule drugs. Adv Drug Deliv Rev 2013; 65 (15): 1964-2015. doi:10.1016/j.addr.2013.08.005

[121] Anglin EJ, Cheng L, Freeman WR, Sailor MJ. Porous silicon in drug delivery devices and materials. Adv Drug Deliv Rev 2008; 60 (11): 1266-1277. doi:10.1016/j.addr.2008.03.017

[122] Lee SH, Park M, Park CG, Lee JE, Prausnitz MR, Choy YB. Microchip for sustained drug delivery by diffusion through microchannels. AAPS PharmSciTech 2012; 13 (1): 211-217. doi:10.1208/s12249-011-9743-6

[123] Sutradhar KB, Sumi CD. Implantable microchip: the futuristic controlled drug delivery system. Drug Deliv 2016; 23 (1): 1-11. doi:10.3109/10717544.2014.903579

[124] DiChristina M, Meyerson BS. Top 10 Emerging Technologies of 2017. Sci Am 2017; 317 (6): 28-39. doi:10.1038/scientificamerican1217-28

[125] Rodgers AM, Courtenay AJ, Donnelly RF. Dissolving microneedles for intradermal vaccination: manufacture, formulation, and stakeholder considerations. Expert Opin Drug Deliv 2018; 15 (11): 1039-1043. doi:10.1080/17425247.2018.1522301

[126] Gill HS, Prausnitz MR. Coated microneedles for transdermal delivery. J Control Release 2007; 117 (2): 227-237. doi:10.1016/j.jconrel.2006.10.017

[127] McGrath MG, Vrdoljak A, O'Mahony C, Oliveira JC, Moore AC, Crean AM. Determination of parameters for successful spray coating of silicon microneedle arrays. Int J Pharm 2011; 415 (1-2): 140-149. doi:10.1016/j.ijpharm.2011.05.064

[128] Vora LK, Moffatt K, Tekko IA, et al. Microneedle array systems for long-acting drug delivery. Eur J Pharm Biopharm 2021; 159: 44-76. doi:10.1016/j.ejpb.2020.12.006

[129] Economidou SN, Uddin J, Marques MJ, et al. A novel 3D printed hollow microneedle microelectromechanical system for controlled, personalizes transdermal drug delivery. Addit Manuf [internet]. 2021 [cited: 2021 May 16]; 38: 101815. doi:10.1016/j.addma.2020.101815

[130] Croxatto HB. NORPLANT: levonorgestrel-releasing contraceptive implant. Ann Med 1993; 25 (2): 155-160. doi:10.3109/07853899309164160

[131] Baum MM, Butkyavichene I, Gilman J, et al. An intravaginal ring for the simultaneous delivery of multiple drugs. J Pharm Sci 2012; 101 (8): 2833-2843. doi:10.1002/jps.23208

[132] Simpson SM, Widanapathirana L, Su JT, et al. Design of a drug-eluting subcutaneous implant of the antiretroviral tenofovir alafenamide fumarate. Pharm Res [internet]. 2020 [cited: 2021 May 16]; 37 (4): 83. doi:10.1007/s11095-020-2777-2

[133] Tiboni M, Campana R, Frangipani E, Casettari L. 3D printed clotrimazole intravaginal ring for the treatment of recurrent vaginal candidiasis. Int J Pharm [internet]. 2021 [cited: 2021 May 16]; 596: 120290. doi:10.1016/j.ijpharm.2021.120290

[134] van Laarhoven JA, Kruft MA, Vromans H. Effect of supersaturation and crystallization phenomena on the release properties of a controlled release device based on EVA copolymer. J Control Release 2002; 82 (2-3): 309-317. doi:10.1016/s0168-3659(02)00139-6

[135] Macoul KL, Pavan-Langston D. Pilocarpine ocusert system for sustained control of ocular hypertension. Arch Ophthalmol 1975; 93 (8): 587-590. doi:10.1001/archopht.1975.01010020571003

[136] Kukreja N, Onuma Y, Serruys PW. Xience V everolimus-eluting coronary stent. Expert Rev Med Devices 2009; 6 (3): 219-229. doi:10.1586/erd.09.1

[137] Fu Y, Kao WJ. Drug release kinetics and transport mechanisms of non-degradable and degradable polymeric delivery systems. Expert Opin Drug Deliv 2010; 7 (4): 429-444. doi:10.1517/17425241003602259

[138] Joseph J, Patel RM, Wenham A, Smith JR. Biomedical applications of polyurethane materials and coatings. Trans. IMF 2018; 96 (3): 121-129. doi:10.1080/00202967.2018.1450209

[139] Koutsamanis I, Paudel A, Nickisch K, Eggenreich K, Roblegg E, Eder S. Controlled-Release from High-Loaded Reservoir-Type Systems-A Case Study of Ethylene-Vinyl Acetate and Progesterone. Pharmaceutics [internet]. 2020 [cited: 2021 June 5]; 12 (2): 103. doi:10.3390/pharmaceutics12020103

[140] Darney PD. Hormonal implants: contraception for a new century. Am J Obstet Gynecol 1994;170(5):1536-1543. doi:10.1016/s0002-9378(94)05016-7

[141] Macoul KL, Pavan-Langston D. Pilocarpine ocusert system for sustained control of ocular hypertension. Arch Ophthalmol 1975; 93 (8): 587-590. doi:10.1001/archopht.1975.01010020571003

[142] Joseph J, Patel RM, Wenham A, Smith JR. Biomedical applications of polyurethane materials and coatings. Trans IMF 2018; 96 (3): 121-129. doi:10.1080/00202967.2018.1450209

[143] Liu X, Lei L, Hou JW, et al. Evaluation of two polymeric blends (EVA/PLA and EVA/PEG) as coating film materials for paclitaxel-eluting stent application. J Mater Sci Mater Med 2011; 22 (2): 327-337. doi:10.1007/s10856-010-4213-3

[144] Barnwal P, Das S, Mondal S, Ramasamy A, Maiti T, Saha A. Probuphine® (buprenorphine implant): a promising candidate in opioid dependence. Ther Adv Psychopharmacol 2017; 7 (3): 119-134. doi:10.1177/2045125316681984

[145] Kim J, Kim WJ, Kim SJ, Cho CW, Shin SC. Release characteristics of quinupramine from the ethylene-vinyl acetate matrix. Int J Pharm 2006; 315 (1-2): 134-139. doi:10.1016/j.ijpharm.2006.03.019

[146] Koutsamanis I, Spoerk M, Arbeiter F, Eder S, Roblegg E. Development of Porous Polyurethane Implants Manufactured via Hot-Melt Extrusion. Polymers [internet]. 2020 [cited: 2021 June 4]; 12 (12): 2950. doi:10.3390/polym12122950

[147] Lee SS, Hughes P, Ross AD, Robinson MR. Biodegradable implants for sustained drug release in the eye. Pharm Res 2010; 27 (10): 2043-2053. doi:10.1007/s11095-010-0159-x

[148] von Burkersroda F, Schedl L, Göpferich A. Why degradable polymers undergo surface erosion or bulk erosion. Biomaterials 2002; 23 (21): 4221-4231. doi:10.1016/s0142-9612(02)00170-9

[149] Xu Y, Kim CS, Saylor DM, Koo D. Polymer degradation and drug delivery in PLGA-based drug-polymer applications: A review of experiments and theories. J Biomed Mater Res B Appl Biomater 2017; 105 (6): 1692-1716. doi:10.1002/jbm.b.33648

[150] Pişkin E. Biodegradable polymers as biomaterials. J Biomater Sci Polym Ed 1995; 6 (9):775-795. doi:10.1163/156856295x00175

[151] Singh MP, Stefko J, Lumpkin JA, Rosenblatt J. The effect of electrostatic charge interactions on release rates of gentamicin from collagen matrices. Pharm Res 1995; 12 (8): 1205-1210. doi:10.1023/a:1016272212833

[152] Hu L, Sun Y, Wu Y. Advances in chitosan-based drug delivery vehicles. Nanoscale 2013; 5 (8): 3103-3111. doi:10.1039/c3nr00338h

[153] Dumanli AG. Nanocellulose and its Composites for Biomedical Applications. Curr Med Chem 2017; 24 (5): 512-528. doi:10.2174/0929867323666161014124008

[154] Nair LS, Laurencin CT. Biodegradable polymers as biomaterials. Prog. Polym. Sci 2007; 32 (8), 762–798. doi:10.1016/j.progpolymsci.2007.05.017

[155] Luckachan GE, Pillai CKS. Biodegradable polymers-A review on recent trends and emerging perspectives. J Polym Environ 2011; 19: 637–676. doi:10.1007/s10924-011-0317-1

[156] Shapira-Furman T, Serra R, Gorelick N, et al. Biodegradable wafers releasing Temozolomide and Carmustine for the treatment of brain cancer. J Control Release 2019; 295: 93-101. doi:10.1016/j.jconrel.2018.12.048

[157] Wang L, Chaw CS, Yang YY, et al. Preparation, characterization, and in vitro evaluation of physostigmine-loaded poly(ortho ester) and poly(ortho ester)/poly(D,L-lactide-co-glycolide) blend microspheres fabricated by spray drying. Biomaterials 2004; 25 (16): 3275-3282. doi:10.1016/j.biomaterials.2003.09.099

[158] Reed S, Smoot C, Shull D, Crumbling T, D'Ottavio J, Gabriele PD, Harris JJ, Nicholson CB, Ely J, inventors; Secant Group, assignee. Tunable, controlled-release, urethane-containing elastomers and processes of forming the same. Patent No.: US 10,918,764 B2. February 16, 2021. [internet] [cited: 2021 June 2] Available from: https://patentimages.storage.googleapis.com/eb/4c/b7/a1c08b0a56618a/US10918764.pdf

[159] U.S Food and Drug Administration. Use of international standard ISO 10993-1, "Biological evaluation of medical devices – Part 1: Evaluation and testing witihin a risk management process" [internet]. 2020 [cited: 2021 June 2] Available from: https://www.fda.gov/media/85865/download

[160] United States Pharmacopeia. Biological reactivity tests, in vivo [internet] Rockville, Maryland, USA. [cited 2021 June 2]. Available from: http://www.pharmacopeia.cn/v29240/usp29nf24s0_c88.html

[161] Shapira-Furman T, Serra R, Gorelick N, et al. Biodegradable wafers releasing Temozolomide and Carmustine for the treatment of brain cancer. J Control Release 2019; 295: 93-101. doi:10.1016/j.jconrel.2018.12.048

[162] Furra BJA, Hutchinsonb FG. A biodegradable delivery system for peptides: preclinical experience with the gonadotrophin-releasing hormone agonist Zoladex. J Control Release 1992; 21 (1): 117-127. doi:10.1016/0168-3659(92)90013-H

[163] Kimura H, Ogura Y. Biodegradable polymers for ocular drug delivery. Ophthalmologica 2001; 215 (3): 143-155. doi:10.1159/000050849

[164] Kent JS, Lewis DH, Sanders LM, Tice TR, inventors; Syntex USA LLC, assignee. Microencapsulation of water soluble active polypeptides. Patent No.: US 4,675189, June 23, 1987. [internet] [cited: 2021 June 2] Available from: https://patentimages.storage.googleapis.com/82/99/90/1311eef39bf1e5/US4675189.pdf

[165] Kim B, Lee SH, Choi TK, et al. Effectiveness of risperidone long-acting injection in first-episode schizophrenia: in naturalistic setting. Prog Neuropsychopharmacol Biol Psychiatry 2008; 32 (5): 1231-1235. doi:10.1016/j.pnpbp.2008.03.012

[166] Srivastava AB, Mariani JJ, Levin FR. New directions in the treatment of opioid withdrawal. Lancet 2020; 395 (10241): 1938-1948. doi:10.1016/S0140-6736(20)30852-7

[167] Dunn RL, English JP, Cowsar DR, Vanderbilt DP, inventors; Tolmar Therapeutics Inc., assignee. Biodegradable in situ forming implants and methods of producing the same. Patent No.: US 5,990,194, November 23, 1999. [internet] [cited: 2021 June 2] Available from: https://patentimages.storage.googleapis.com/57/70/43/e572db26b3c770/US5990194.pdf

[168] de Freitas CSM, Soares AN. Efficacy of Leuprorelide acetate (Eligard®) in daily practice in Brazil: a retrospective study with depot formulations in patients with prostate cancer. Int Braz J Urol 2020; 46 (3): 383-389. doi:10.1590/S1677-5538.IBJU.2019.0212

[169] Patra CN, Swain S, Sruti J, et al. Osmotic drug delivery systems: basics and design approaches. Recent Pat Drug Deliv Formul 2013; 7 (2): 150-161. doi:10.2174/1872211311307020007

[170] Liu S, Miyoshi M. Long-Term Constant Subcutaneous Drug Administration. Methods Mol Biol 2018; 1868: 17-22. doi:10.1007/978-1-4939-8802-0_3

[171] Leuprorelin implant (ALZA). DUROS, leuprolide acetate implant, leuprolide implant, Viadur. Drugs R D 1999; 2 (6): 425-426. doi:10.2165/00126839-199902060-00016

[172] Dash AK, Cudworth GC 2nd. Therapeutic applications of implantable drug delivery systems. J Pharmacol Toxicol Methods 1998; 40 (1): 1-12. doi:10.1016/s1056-8719(98)00027-6

[173] Kleiner LW, Wright JC, Wang Y. Evolution of implantable and insertable drug delivery systems. J Control Release 2014; 181: 1-10. doi:10.1016/j.jconrel.2014.02.006

[174] Siepmann J, Siepmann F. Modeling of diffusion controlled drug delivery. J Control Release 2012; 161 (2): 351-362. doi:10.1016/j.jconrel.2011.10.006

[175] Baker RW, Lonsdale HK. Controlled release: Mechanism and rate. In Tanquary AC, Lacey RE, editors. Controlled Release of Biologically Active Agents. 1st ed. New York, NY, USA: Plenum Press, 1973. p. 15-72.

[176] Almeida A, Brabant L, Siepmann F, et al. Sustained release from hot-melt extruded matrices based on ethylene vinyl acetate and polyethylene oxide. Eur J Pharm Biopharm 2012; 82 (3): 526-533. doi:10.1016/j.ejpb.2012.08.008

[177] Claeys B, Vervaeck A, Hillewaere XK, et al. Thermoplastic polyurethanes for the manufacturing of highly dosed oral sustained release matrices via hot melt extrusion and injection molding. Eur J Pharm Biopharm 2015; 90: 44-52. doi:10.1016/j.ejpb.2014.11.003

[178] Claeys B, De Bruyn S, Hansen L, De Beer T, Remon JP, Vervaet C. Release characteristics of polyurethane tablets containing dicarboxylic acids as release modifiers - a case study with diprophylline. Int J Pharm 2014; 477 (1-2): 244-250. doi:10.1016/j.ijpharm.2014.10.046

[179] Donelli G, Francolini I, Ruggeri V, Guaglianone E, D'Ilario L, Piozzi A. Pore formers promoted release of an antifungal drug from functionalized polyurethanes to inhibit Candida colonization. J Appl Microbiol 2006; 100 (3): 615-622. doi:10.1111/j.1365-2672.2005.02801.x

[180] Kim JE, Kim SR, Lee SH, Lee CH, Kim DD. The effect of pore formers on the controlled release of cefadroxil from a polyurethane matrix. Int J Pharm 2000; 201 (1): 29-36. doi:10.1016/s0378-5173(00)00388-4

[181] Kimball AB, Javorsky E, Ron ES, Crowley W Jr, Langer R. A novel approach to administration of peptides in women: Systemic absorption of a GnRH agonist via transvaginal ring delivery system. J Control Release 2016; 233: 19-28. doi:10.1016/j.jconrel.2016.04.035

[182] Verreck G, Decorte A, Heymans K, et al. The effect of pressurized carbon dioxide as a temporary plasticizer and foaming agent on the hot stage extrusion process and extrudate

properties of solid dispersions of itraconazole with PVP-VA 64. Eur J Pharm Sci 2005; 26 (3-4): 349-358. doi:10.1016/j.ejps.2005.07.006

[183] Costantini LC, Kleppner SR, McDonough J, Azar MR, Patel R. Implantable technology for long-term delivery of nalmefene for treatment of alcoholism. Int J Pharm 2004; 283 (1-2): 35-44. doi:10.1016/j.ijpharm.2004.05.034

[184] Higuchi T. Rate of release of medicaments from ointment bases containing drugs in suspension. J Pharm Sci 1961; 50: 874-875. doi:10.1002/jps.2600501018

[185] Higuchi T. Mechanism of sustained-action mediaction. Theoretical Analysis of rate of release of solid drugs dispersed in solid matrices. J Pharm Sci 1963; 52: 1145-1149. doi:10.1002/jps.2600521210

[186] Korsmeyer RW, Gurny R, Doelker E, Buri P, Peppas NA. Mechanism of solute release from porous hydrophilic polymers. Int J Pharm 1983; 15 (1): 25-35. doi: 10.1016/0378-5173(83)90064-9

[187] Peppas NA. Analysis of Fickian and non-Fickian drug release from polymers. Pharm Acta Helv 1985; 60 (4): 110-111.

[188] Tamani F, Bassand C, Hamoudi MC, Siepmann F, Siepmann J. Mechanistic explanation of the (up to) 3 release phases of PLGA microparticles: Monolithic dispersions studied at lower temperatures. Int J Pharm [internet]. 2021 [cited: 2021 May 4]; 596: 120220. doi:10.1016/j.ijpharm.2021.120220

[189] Nair LS, Laurencin CT. Biodegradable polymers as biomaterials. Prog Polym Sci 2007; 32 (8): 762-798. doi:10.1016/j.progpolymsci.2007.05.017

[190] Cai Q, Shi G, Bei J, Wang S. Enzymatic degradation behavior and mechanism of poly(lactide-co-glycolide) foams by trypsin. Biomaterials 2003; 24 (4): 629-638. doi:10.1016/s0142-9612(02)00377-0

[191] Cai Q, Shi G, Bei J, Wang S. Enzymatic degradation behavior and mechanism of poly(lactide-co-glycolide) foams by trypsin. Biomaterials 2003; 24 (4): 629-638. doi:10.1016/s0142-9612(02)00377-0

[192] Solorio L, Olear AM, Hamilton JI, et al. Noninvasive characterization of the effect of varying PLGA molecular weight blends on in situ forming implant behavior using ultrasound imaging. Theranostics 2012; 2 (11): 1064-1077. doi:10.7150/thno.4181

[193] Ji Y, Lesniak AK, Prudic A, et al. Drug release kinetics and mechanism from PLGA formulations. AIChE J 2016; 62 (11): 4055-4065. doi:10.1002/aic.15282

[194] Silva ATCR, Cardoso BCO, e Silva MESR, et al. Synthesis, characterization, and study of PLGA copolymer in vitro degradation. J Biomater Nanobiotechnol 2015; 6: 8-19. doi:10.4236/jbnb.2015.61002

[195] Desai KG, Mallery SR, Schwendeman SP. Formulation and characterization of injectable poly(DL-lactide-co-glycolide) implants loaded with N-acetylcysteine, a MMP inhibitor. Pharm Res 2008; 25 (3): 586-597. doi:10.1007/s11095-007-9430-1

[196] Siegel SJ, Kahn JB, Metzger K, Winey KI, Werner K, Dan N. Effect of drug type on the degradation rate of PLGA matrices. Eur J Pharm Biopharm 2006; 64 (3): 287-293. doi:10.1016/j.ejpb.2006.06.009

[197] D'Souza S, Faraj JA, Dorati R, DeLuca PP. Enhanced degradation of lactide-co-glycolide polymer with basic nucleophilic drugs. Advances in Pharmaceutics [internet]. 2015 [cited: 2021 April 14]. doi:10.1155/2015/154239

[198] Ding AG, Schwendeman SP. Determination of water-soluble acid distribution in poly(lactide-co-glycolide). J Pharm Sci 2004; 93 (2): 322-331. doi:10.1002/jps.10524

[199] Shifrovitch Y, Binderman I, Bahar H, Berdicevsky I, Zilberman M. Metronidazole-loaded bioabsorbable films as local antibacterial treatment of infected periodontal pockets. J Periodontol 2009; 80 (2): 330-337. doi:10.1902/jop.2009.080216

[200] Dorta MJ, Santoveña A, Llabrés M, Fariña JB. Potential applications of PLGA film-implants in modulating in vitro drugs release. Int J Pharm 2002; 248 (1-2): 149-156. doi:10.1016/s0378-5173(02)00431-3

[201] Langer R, Folkman J. Polymers for the sustained release of proteins and other macromolecules. Nature 1976; 263 (5580): 797-800. doi:10.1038/263797a0

[202] Siegel RA, Kost J, Langer R. Mechanistic studies of macromolecular drug release from macroporous polymers. I. Experiments and preliminary theory concerning completeness of drug release. J Control Release 1989; 8 (3): 223-236. doi: 10.1016/0168-3659(89)90044-8

[203] Zhang X, Mcauley KB, Goosen MFA. Towards prediction of release profiles of antibiotics from coated poly(DL-lactide) cylinder. J Control Release. 1995; 34: 175-179. doi: 10.1016/0168-3659(94)00124-D

[204] Zhou T, Lewis H, Foster RE, Schwendeman SP. Development of a multiple-drug delivery implant for intraocular management of proliferative vitreoretinopathy. J Control Release 1998; 55 (2-3): 281-295. doi:10.1016/s0168-3659(98)00061-3

[205] Jivraj I I, Martini LG, Thomson CM. An overview of the different excipients useful for the direct compression of tablets. Pharm Sci Technol Today 2000; 3 (2): 58-63. doi:10.1016/s1461-5347(99)00237-0

[206] Fialho SL, da Silva Cunha A. Manufacturing techniques of biodegradable implants intended for intraocular application. Drug Deliv 2005; 12 (2): 109-116. doi:10.1080/10717540590921432

[207] Kau YC, Chen DWC, Hsieh YT, et al. Compression molding of biodegradable drug-eluting implants for sustained release of metronidazole and doxycycline. J Appl Polym Sci 2013; 127: 554-560. doi: 10.1002/APP.37819

[208] Chasin B, Hollenbeck B, Brem H, et al. Interstitial drug therapy for brain tumors: a case study. Drug Dev Ind Pharm 1990; 16: 2579-2594. doi: 10.3109/03639049009058548

[209] Maturavongsadit P, Paravyan G, Kovarova M, Garcia JV, Benhabbour SR. A new engineering process of biodegradable polymeric solid implants for ultra-long-acting drug delivery. Int J Pharm X [internet]. 2020 [cited: 2021 April 16]; 3: 100068. doi:10.1016/j.ijpx.2020.100068

[210] Zema L, Loreti G, Melocchi A, Maroni A, Gazzaniga A. Injection Molding and its application to drug delivery. J Control Release. 2012; 159 (3): 324-331. doi:10.1016/j.jconrel.2012.01.001

[211] Welsh NR, Malcolm RK, Devlin B, Boyd P. Dapivirine-releasing vaginal rings produced by plastic freeforming additive manufacturing. Int J Pharm [internet]. 2019 [cited:2021 April 15]; 572: 118725. doi:10.1016/j.ijpharm.2019.118725

[212] Rathbone MJ, Bunt CR, Ogle CR, et al. Development of an injection molded poly(ε-caprolactone) intravaginal insert for the delivery of progesterone to cattle. J Control Release 2002; 85: 61-71. doi:10.1016/s0168-3659(02)00272-9

[213] Rothen-Weinhold A, Besseghir K, Vuaridel E, et al. Injection-molding versus extrusion as manufacturing technique for the preparation of biodegradable implants. Eur J Pharm Biopharm 1999; 48 (2): 113-121. doi:10.1016/s0939-6411(99)00034-x

[214] Zembko I, Ahmed I, Farooq A, et al. Development of disulfiram-loaded poly(lactic-co-glycolic acid) wafers for the localised treatment of glioblastoma multiforme: a comparison of manufacturing techniques. J Pharm Sci 2015; 104 (3): 1076-1086. doi:10.1002/jps.24304

[215] Malcolm RK, Woolfson AD, Toner CF, Morrow RJ, McCullagh SD. Long-term, controlled release of the HIV microbicide TMC120 from silicone elastomer vaginal rings. J Antimicrob Chemother 2005; 56 (5): 954-956. doi:10.1093/jac/dki326

[216] Malcolm RK, Boyd PJ, McCoy CF, Murphy DJ. Microbicide vaginal rings: Technological challenges and clinical development. Adv Drug Deliv Rev 2016; 103: 33-56. doi:10.1016/j.addr.2016.01.015

[217] Kotta S, Nair A, Alsabeelah N. 3D Printing Technology in Drug Delivery: Recent Progress and Application. Curr Pharm Des 2018; 24 (42): 5039-5048. doi:10.2174/1381612825666181206123828

[218] Norman J, Madurawe RD, Moore CM, Khan MA, Khairuzzaman A. A new chapter in pharmaceutical manufacturing: 3D-printed drug products. Adv Drug Deliv Rev 2017; 108: 39-50. doi:10.1016/j.addr.2016.03.001

[219] Breitenbach J. Melt extrusion: from process to drug delivery technology. Eur J Pharm Biopharm 2002; 54 (2): 107-117. doi:10.1016/s0939-6411(02)00061-9

[220] Crowley MM, Zhang F, Repka MA, et al. Pharmaceutical applications of hot-melt extrusion: part I. Drug Dev Ind Pharm 2007; 33 (9): 909-926. doi:10.1080/03639040701498759

[221] Repka MA, Battu SK, Upadhye SB, et al. Pharmaceutical applications of hot-melt extrusion: Part II. Drug Dev Ind Pharm 2007; 33 (10): 1043-1057. doi:10.1080/03639040701525627

[222] Repka MA, Shah S, Lu J, et al. Melt extrusion: process to product. Expert Opin Drug Deliv 2012; 9 (1): 105-125. doi:10.1517/17425247.2012.642365

[223] Maniruzzaman M, Boateng JS, Snowden MJ, Douroumis D. A review of hot-melt extrusion: process technology to pharmaceutical products. ISRN Pharm [internet]. 2012 [cited: 2021. May 1]; 436763. doi:10.5402/2012/436763

[224] Keen JM, Martin C, Machado A, Sandhu H, McGinity JW, DiNunzio JC. Investigation of process temperature and screw speed on properties of a pharmaceutical solid dispersion using corotating and counter-rotating twin-screw extruders. J Pharm Pharmacol 2014; 66 (2): 204-217. doi:10.1111/jphp.12106

[225] Follonier N, Doelker E, Cole ET. Evaluation of hot-melt extrusion as a new technique for the production of polymer-based pellets for sustained release capsules containing high loadings of freely soluble drugs. Drug Dev Ind Pharm 1994; 20 (8): 1323-1339. doi: 10.3109/03639049409038373

[226] Aitken-Nichol C, Zhang F, McGinity JW. Hot melt extrusion of acrylic films. Pharm Res 1996; 13 (5): 804-808. doi:10.1023/a:1016076306279

[227] Sato H, Miyagawa Y, Okabe T, Miyajima M, Sunada H. Dissolution mechanism of diclofenac sodium from wax matrix granules. J Pharm Sci 1997; 86 (8): 929-934. doi:10.1021/js960221w

[228] Zhang F, McGinity JW. Properties of sustained-release tablets prepared by hot-melt extrusion. Pharm Dev Technol 1999; 4 (2): 241-250. doi:10.1081/pdt-100101358

[229] Repka MA, Bandari S, Kallakunta VR, et al. Melt extrusion with poorly soluble drugs - An integrated review. Int J Pharm 2018; 535 (1-2): 68-85. doi:10.1016/j.ijpharm.2017.10.056

[230] Breitenbach J. Melt extrusion can bring new benefits to HIV therapy. Am J Drug Deliv 2006; 4: 61–64. doi:10.2165/00137696-200604020-00001

[231] Repka MA, Langley N, DiNunzio J, editors. Melt Extrusion: Materials, Technology and Drug Product Design. Berlin, Germany: Springer; 2013.

[232] Katz JI, Kaufman HE, Breslin C, Katz IM. Slow-release artificial tears and the treatment of keratitis sicca. Ophthalmology 1978; 85 (8): 787-793. doi:10.1016/s0161-6420(78)35611-6

[233] Schneider C, Langer R, Loveday D, Hair D. Applications of ethylene vinyl acetate copolymers (EVA) in drug delivery systems. J Control Release 2017 ; 262 :284-295. doi:10.1016/j.jconrel.2017.08.004

[234] van Laarhoven JA, Kruft MA, Vromans H. In vitro release properties of etonogestrel and ethinyl estradiol from a contraceptive vaginal ring. Int J Pharm 2002; 232 (1-2): 163-173. doi:10.1016/s0378-5173(01)00900-0

[235] Constantini LC. The development of ProNeura technology for the treatment of addiction. In Dean RG III, Bilsky E, Negus SS, editors. Opiate receptors and antagonists: From bench to clinic. 1st ed. Totowa, NJ, USA: Humana Press; 2009. p. 689-708.

[236] Patel RA, Bucalo LR, inventors; Titan Pharmaceuticals Inc., assignee. Implantable polymeric device for sustained release of buprenorphine. Patent No.: US 2021/0046000 A1. February 18, 2021. [internet] [cited: 2021 May 4] Available from: https://patentimages.storage.googleapis.com/de/c3/fc/0d10a2b7af9b3d/US20210046000A1.pdf

[237] Patel RA, Bucalo LR, Constantini LC, Kleppner S, inventors; Titan Pharmaceuticals Inc., assignee. Implantable polymeric device for sustained release of dopamine agonist. Patent No.:

US 9,278,163 B2 March 8, 2016. [internet] [cited: 2021 May 4] Available from: https://patentimages.storage.googleapis.com/8d/d7/81/6d3ec8f5549675/US9278163.pdf

[238] Patel RA, Sreedharan S, Bhonsle SR, inventors; Titan Pharmaceuticals Inc., assignee. Patent No.: US 2021/0007973 A1 January 14, 2021. [internet] [cited: 2021 May 4] Available from: https://www.patentguru.com/US2021007973A1

[239] Patel RA, Bucalo LR, inventors; Titan Pharmaceuticals Inc., assignee. Implantable polymeric device for sustained release of buprenorphine with minimal initial burst. Patent No.: WO 2007/139744 A2 December 6, 2007. [internet] [cited 2021 May 4] Available from: https://patentimages.storage.googleapis.com/07/c3/44/9b9fed8f9bdbd6/WO2007139744A3.pdf

[240] Chen W, Wu Z, Yang H, Guo S, Li D, Cheng L. In vitro and in vivo evaluation of injectable implants for intratumoral delivery of 5-fluorouracil. Pharm Dev Technol 2014; 19 (2): 223-231. doi:10.3109/10837450.2013.769568

[241] Clark MR, Johnson TJ, McCabe RT, et al. A hot-melt extruded intravaginal ring for the sustained delivery of the antiretroviral microbicide UC781. J Pharm Sci 2012; 101 (2): 576-587. doi:10.1002/jps.22781

[242] Islam MT, Scoutaris N, Maniruzzaman M, et al. Implementation of transmission NIR as a PAT tool for monitoring drug transformation during HME processing. Eur J Pharm Biopharm 2015; 96: 106-116. doi:10.1016/j.ejpb.2015.06.021

[243] Dadou SM, Tian Y, Li S, Jones DS, Andrews GP. The optimization of process analytical technology for the inline quantification of multiple drugs in fixed dose combinations during continuous processing. Int J Pharm [internet] 2021 [cited 2021 April 16]; 592: 120024. doi:10.1016/j.ijpharm.2020.120024

[244] Plumb K. Continuous processing in the pharmaceutical industry: Changing the mind set. Chem Eng Res Des 2005; 83 (A6): 730-738. doi: 10.1205/cherd.04359

[245] International Conference on Harmonisation of Technical Requirements for Registration of Pharmaceuticals for Human Use. ICH Harmonised Tripartite Guideline: Impurities in new drug products, Q3B (R2). [internet] [cited: 2021 May 6] Available from: https://www.ema.europa.eu/en/documents/scientific-guideline/ich-q-3-b-r2-impurities-new-drug-products-step-5_en.pdf

[246] Repka MA, Prodduturi S, Stodghill SP. Production and characterization of hot-melt extruded films containing clotrimazole. Drug Dev Ind Pharm 2003; 29 (7): 757-765. doi:10.1081/ddc-120021775

[247] Repka MA, Gerding TG, Repka SL, McGinity JW. Influence of plasticizers and drugs on the physical-mechanical properties of hydroxypropylcellulose films prepared by hot melt extrusion. Drug Dev Ind Pharm. 1999; 25 (5): 625-633. doi:10.1081/ddc-100102218

[248] Hughey JR, Keen JM, Brough C, Saeger S, McGinity JW. Thermal processing of a poorly water-soluble drug substance exhibiting a high melting point: the utility of KinetiSol® Dispersing. Int J Pharm 2011; 419 (1-2): 222-230. doi:10.1016/j.ijpharm.2011.08.007

[249] Dinunzio JC, Brough C, Hughey JR, Miller DA, Williams RO 3rd, McGinity JW. Fusion production of solid dispersions containing a heat-sensitive active ingredient by hot melt extrusion and Kinetisol dispersing. Eur J Pharm Biopharm 2010; 74 (2): 340-351. doi:10.1016/j.ejpb.2009.09.007

[250] Weatherley S, Mu B, Thompson MR, Sheskey PJ, O'Donnell KP. Hot-melt granulation in a twin screw extruder: effects of processing on formulations with caffeine and Ibuprofen. J Pharm Sci 2013; 102 (12): 4330-4336. doi:10.1002/jps.23739

[251] Petritz E, Tritthart T, Wintersteiger R. Determination of phylloquinone and cholecalciferol encapsulated in granulates formed by melt extrusion. J Biochem Biophys Methods 2006; 69 (1-2): 101-112. doi:10.1016/j.jbbm.2006.03.007

[252] Patterson JE, James MB, Forster AH, Lancaster RW, Butler JM, Rades T. Preparation of glass solutions of three poorly water soluble drugs by spray drying, melt extrusion and ball milling. Int J Pharm 2007; 336 (1): 22-34. doi:10.1016/j.ijpharm.2006.11.030

[253] Trey SM, Wicks DA, Mididoddi PK, Repka MA. Delivery of itraconazole from extruded HPC films. Drug Dev Ind Pharm 2007; 33 (7): 727-735. doi:10.1080/03639040701199225

[254] Hughey JR, DiNunzio JC, Bennett RC, et al. Dissolution enhancement of a drug exhibiting thermal and acidic decomposition characteristics by fusion processing: a comparative study of hot melt extrusion and KinetiSol dispersing. AAPS PharmSciTech. 2010;11(2):760-774. doi:10.1208/s12249-010-9431-y

[255] Huang S, O'Donnell KP, Delpon de Vaux SM, O'Brien J, Stutzman J, Williams RO 3rd. Processing thermally labile drugs by hot-melt extrusion: The lesson with gliclazide. Eur J Pharm Biopharm 2017; 119: 56-67. doi:10.1016/j.ejpb.2017.05.014

[256] Ma X, Huang S, Lowinger MB, et al. Influence of mechanical and thermal energy on nifedipine amorphous solid dispersions prepared by hot melt extrusion: Preparation and physical stability. Int J Pharm 2019; 561: 324-334. doi:10.1016/j.ijpharm.2019.03.014

[257] Zhu Y, Mehta KA, McGinity JW. Influence of plasticizer level on the drug release from sustained release film coated and hot-melt extruded dosage forms. Pharm Dev Technol 2006; 11 (3): 285-294. doi:10.1080/10409230600767551

[258] Verhoeven E, Vervaet C, Remon JP. Xanthan gum to tailor drug release of sustained-release ethylcellulose mini-matrices prepared via hot-melt extrusion: in vitro and in vivo evaluation. Eur J Pharm Biopharm 2006; 63 (3): 320-330. doi:10.1016/j.ejpb.2005.12.004

[259] Del Valle EMM. Cyclodextrins and their uses: a review. Process Biochem. 2004; 39: 1033–1046. doi: 10.1016/S0032-9592(03)00258-9

[260] Maniruzzaman M, Morgan DJ, Mendham AP, Pang J, Snowden MJ, Douroumis D. Drug-polymer intermolecular interactions in hot-melt extruded solid dispersions. Int J Pharm. 2013; 443 (1-2): 199-208. doi:10.1016/j.ijpharm.2012.11.048

[261] Loxley A. Devices and implant systems by hot-melt-extrusion. In Douroumis D, editor. Hot-melt extrusion: Pharmaceutical aplications. 1st ed. Hoboken, NJ, USA: John Wiley & Sons, Ltd.; 2012. P. 301-321.

[262] Munjal M, ElSohly MA, Repka MA. Chemical stabilization of a Delta9-tetrahydrocannabinol prodrug in polymeric matrix systems produced by a hot-melt method: role of microenvironment pH. AAPS PharmSciTech [internet] 2006 [cited 2021 April 13]; 7 (3): 71. doi:10.1208/pt070371

[263] Crowley MM, Zhang F, Koleng JJ, McGinity JW. Stability of polyethylene oxide in matrix tablets prepared by hot-melt extrusion. Biomaterials 2002; 23 (21): 4241-4248. doi:10.1016/s0142-9612(02)00187-4

[264] Haser A, Cao T, Lubach JW, Zhang F. In Situ Salt Formation during Melt Extrusion for Improved Chemical Stability and Dissolution Performance of a Meloxicam-Copovidone Amorphous Solid Dispersion. Mol Pharm 2018; 15 (3): 1226-1237. doi:10.1021/acs.molpharmaceut.7b01057

[265] Hussain MA, Shefter E. Naltrexone-3-salicylate (a prodrug of naltrexone): synthesis and pharmacokinetics in dogs. Pharm Res 1988; 5 (2): 113-115. doi:10.1023/a:1015944302567

[266] Stinchcomb AL, Swaan PW, Ekabo O, et al. Straight-chain naltrexone ester prodrugs: diffusion and concurrent esterase biotransformation in human skin. J Pharm Sci 2002; 91 (12): 2571-2578. doi:10.1002/jps.10239

[267] Sullivan MF, Kalkwarf DR. Sustained release of naltrexone from glyceride implants. Natl Inst Drug Abuse Res Monogr Ser 1976; (4): 27-32. PMID:967232

[268] Misra AL, Pontani RB. An improved long-acting delivery system for narcotic antagonists. NIDA Res Monogr 1981; 28: 254-264. PMID:6791009

[269] Gray AP, Robinson DS. Naltrexone zinc tannate: a prolonged-action narcotic antagonist complex. J Pharm Sci 1974; 63 (1): 159-161. doi:10.1002/jps.2600630147

[270] Sidman KR, Arnold DL, Steber WD, et al. Use of synthetic polypeptides in the preparation of biodegradable delivery vehicles for narcotic antagonists. Natl Inst Drug Abuse Res Monogr Ser 1976; (4): 33-38. PMID:967233

[271] Lehman TM, Pyati P, Peterson GR. Inhibition of drug metabolism by chronically administered naltrexone. Life Sci 1979; 25 (18): 1591-1600. doi:10.1016/0024-3205(79)90442-9

[272] Chiang CN, Hollister LE, Kishimoto A, Barnett G. Kinetics of a naltrexone sustained-release preparation. Clin Pharmacol Ther 1984; 36 (5): 704-708. doi:10.1038/clpt.1984.243

[273] Comer SD, Collins ED, Kleber HD, Nuwayser ES, Kerrigan JH, Fischman MW. Depot naltrexone: long-lasting antagonism of the effects of heroin in humans. Psychopharmacology (Berl) 2002; 159 (4): 351-360. doi:10.1007/s002130100909

[274] U.S Food and Drug Administration. Vivitrol® (naltrexone for extended-release injectable suspension USP). [internet] Silver Spring, MD, USA [cited 2021 May 4] Available from: https://www.accessdata.fda.gov/drugsatfda_docs/label/2010/021897s015lbl.pdf

[275] Dunbar JL, Turncliff RZ, Dong Q, Silverman BL, Ehrich EW, Lasseter KC. Single- and multiple-dose pharmacokinetics of long-acting injectable naltrexone. Alcohol Clin Exp Res 2006; 30 (3): 480-490. doi:10.1111/j.1530-0277.2006.00052.x

[276] Kamali H, Khodaverdi E, Hadizadeh F, Yazdian-Robati R, Haghbin A, Zohuri G. An in-situ forming implant formulation of naltrexone with minimum initial burst release using mixture of PLGA copolymers and ethyl heptanoate as an additive: In-vitro, ex-vivo, and in-vivo release evaluation. J Drug Deliv Sci Technol 2018; 47: 95-105. doi:10.1016/j.jddst.2018.06.027

[277] Gooberman LL, Malmberg GJ, Tripp AR, inventors; TRIPP, assignee. Opiate antagonist implant and process of preparation therefor. Patent No.: WO 98/30171. 16 July, 1998. [internet] [cited 2021 May 14] Available from: https://patentimages.storage.googleapis.com/fe/13/23/60e4e8b1f65aa5/WO1998030171A1.pdf

[278] Olsen L, Christophersen AS, Frogopsahl G, Waal H, Mørland J. Plasma concentrations during naltrexone implant treatment of opiate-dependent patients. Br J Clin Pharmacol 2004; 58 (2): 219-222. doi:10.1111/j.1365-2125.2004.02122.x

[279] Ramenskaya GV, Shikh EV, Arzamastsev AP, Kukes VG. Pharmacokinetic study of the new domestic hypodermic form of nlatrexone: prodetoxon depot tablets. Pharm Chem J 2005; 39: 1-3. doi: 10.1007/s11094-005-0066-3

[280] Navin S, Kunal S, inventors; Rusan Pharma Ltd., assignee. Implantable naltrexone tablets. Patent No.: WO 2017/033208 A2. 2 March, 2017. [internet] [cited 2021 May 14] Available from: https://patentimages.storage.googleapis.com/2b/6f/fa/2a85de6b9e96c3/WO2017033208A2.pdf

[281] Hulse GK, Arnold-Reed DE, O'Neil G, Chan CT, Hansson R, O'Neil P. Blood naltrexone and 6-beta-naltrexol levels following naltrexone implant: comparing two naltrexone implants. Addict Biol 2004; 9(1): 59-65. doi:10.1080/13556210410001674103

[282] Hulse GK, Low VH, Stalenberg V, et al. Biodegradability of naltrexone-poly(DL) lactide implants in vivo assessed under ultrasound in humans. Addict Biol 2008; 13 (3-4): 364-372. doi:10.1111/j.1369-1600.2007.00081.x

[283] Lobmaier PP, Kunøe N, Gossop M, Katevoll T, Waal H. Naltrexone implants compared to methadone: outcomes six months after prison release. Eur Addict Res 2010; 16 (3): 139-145. doi:10.1159/000313336

[284] Wermeling DP, Banks SL, Hudson DA, et al. Microneedles permit transdermal delivery of a skin-impermeant medication to humans. Proc Natl Acad Sci USA 2008; 105 (6): 2058-2063. doi:10.1073/pnas.0710355105

[285] Brogden NK, Banks SL, Crofford LJ, Stinchcomb AL. Diclofenac enables unprecedented week-long microneedle-enhanced delivery of a skin impermeable medication in humans. Pharm Res 2013; 30 (8): 1947-1955. doi:10.1007/s11095-013-1036-1

[286] Ehrich E, inventor; Alkermes Inc., assignee. Naltrexone long acting formulations and methods of use. Patent No.: US 7,919,499 B2. 5 April, 2011. [internet] [cited 2021 May 14] Available from: https://patentimages.storage.googleapis.com/76/11/01/48ba9849b5c1fd/US7919499.pdf

[287] International Conference on Harmonisation of Technical Requirements for Registration of Pharmaceuticals for Human Use. ICH Harmonised Tripartite Guideline: Validation of analytial procedures, Q2 (R1). [internet] [cited: 2021 May 6] Available from: https://www.ema.europa.eu/en/documents/scientific-guideline/ich-q-2-r1-validation-analytical-procedures-text-methodology-step-5_en.pdf)

[288] Kolter K, Karl M, Gryczke A. Hot-Melt Extrusion with BASF Pharma Polymers: Extrusion Compendium. 2nd ed. [internet]. Ludwigshafen, Germany: BASF SE Pharma Ingredients & Services; 2012 [cited 2021 June 3]. Available from: https://pharma.basf.com/files/ebooks/Hot-Melt-Extrusion-Book.pdf

[289] Henderson AM. Ethylene-vinyl acetate (EVA) copolymers: A general review. IEEE Electra Insulk Mag [internet]. 1993 [cited 2021 June 4]; 9 (1): 30-38. Available from: https://ieeexplore.ieee.org/stamp/stamp.jsp?tp=&arnumber=249923

[290] Bremner T, Rudin A, Cook DG. Melt flow index values and molecular weight distributions of commercial thermoplastics. J Appl Polym Sci 1990; 41 (7-8): 1617-1627. doi: 10.1002/app.1990.070410721

[291] DuPont de Nemours Inc..DuPont™ Elvax® EVA resins for adhesives, sealants and wax blends [internet]. 2012 [cited 2021 June 4] Available from: https://www.nevicolor.it/produkte/polymer-suchen/dupont/elvax/documenti/elvax-adhesives-wax-blends.pdf

[292] International Conference on Harmonisation of Technical Requirements for Registration of Pharmaceuticals for Human Use. ICH Harmonised Tripartite Guideline: Good Manufacturing Practice Guide for Active Pharmaceutical Ingredients, Q7 (R1). [internet] [cited: 2021 May 6] Available from: https://database.ich.org/sites/default/files/Q7%20Guideline.pdf

[293] Kim H, Burgess DJ. Effect of drug stability on the analysis of release data from controlled release microspheres. J Microencapsul 2002; 19 (5): 631-640. doi:10.1080/02652040210140698

[294] Abdelkader H, Wu Z, Al-Kassas R, Brown JE, R.G. Alany RG. Preformulation characteristics of the opioid growth factor antagonist-naltrexone hydrochloride: stability and

lipophilicity studies. J Drug Del Sci Tech 2011; 21 (2): 157–163. doi: 10.1016/S1773-2247(11)50017-6

[295] Kaufman JJ, Semo NM, Koski WS. Microelectrometric titration measurement of the pKa's and partition and drug distribution coefficients of narcotics and narcotic antagonists and their pH and temperature dependence. J Med Chem 1975; 18 (7): 647-655. doi:10.1021/jm00241a001

[296] Garrido JMPJ, Delerue-Matos C, Borges F, Macedo TRA, Oliveira AM. Voltametric oxidation of drugs of abuse I. Morphine and metabolites. Electroanalysis 2004; 16 (17): 1419-1426. doi:10.1002/elan.200302966

[297] Garrido JMPJ, Delerue-Matos C, Borges F, Macedo TRA, Oliveira AM. Voltametric oxidation of drugs of abuse III. Heroin and metabolites. Electroanalysis 2004; 16 (18): 1497-1502. doi:10.1002/elan.200302975

[298] Andhariya JV, Choi S, Wang Y, Zou Y, Burgess DJ, Shen J. Accelerated in vitro release testing method for naltrexone loaded PLGA microspheres. Int J Pharm 2017; 520 (1-2): 79-85. doi:10.1016/j.ijpharm.2017.01.050

[299] Brown CK, Friedel HD, Barker AR, et al. FIP/AAPS joint workshop report: dissolution/in vitro release testing of novel/special dosage forms. AAPS PharmSciTech 2011; 12 (2): 782-794. doi:10.1208/s12249-011-9634-x

[300] Shin SC, Lee HJ. Controlled release of triprolidine using ethylene-vinyl acetate membrane and matrix systems. Eur J Pharm Biopharm. 2002; 54 (2): 201-206. doi:10.1016/s0939-6411(02)00051-6

[301] Koutsamanis I, Eder S, Beretta M, et al. Formulation and processability screening for the rational design of ethylene-vinyl acetate based intra-vaginal rings. Int J Pharm 2019; 564: 90-97. doi:10.1016/j.ijpharm.2019.04.041

[302] Almeida A, Possemiers S, Boone MN, et al. Ethylene vinyl acetate as matrix for oral sustained release dosage forms produced via hot-melt extrusion. Eur J Pharm Biopharm 2011; 77 (2): 297-305. doi:10.1016/j.ejpb.2010.12.004

[303] Camacho J, Díez E, Ovejero G, Díaz I. Thermodynamic interactions of EVA copolymer-solvent systems by inverse gas chromatography measurements. J Appl Polym Sci 2013; 128 (1): 481-486. doi: 10.1002/app.38193

[304] Ritger PH, Peppas NA. A simple equation for description of solute release I. Fickian and non-fickian release from non-swellable devices in the form of slabs, spheres, cylinders or discs. J Control Release 1987; 5 (1): 23-36. doi: 10.1016/0168-3659(87)90034-4

[305] Siegel RA. Porous systems. In Siepmann J, Siegel RA, Rathbone MJ, editors. Fundamentals and applications of controlled release drug delivery. 1st ed. New York, NY, USA: Springer; 2012. p. 229-251.

[306] Pace NL, Parrish RG, Lieberman MM, Wong KC, Blatnick RA. Pharmacokinetics of naloxone and naltrexone in the dog. J Pharmacol Exp Ther 1979; 208 (2): 254-256. PMID:762657

[307] Darville N, van Heerden M, Erkens T, et al. Modeling the time course of the tissue responses to intramuscular long-acting paliperidone palmitate nano-/microcrystals and polystyrene microspheres in the rat. Toxicol Pathol 2016; 44 (2): 189-210. doi:10.1177/0192623315618291

[308] Matić J, Alva C, Witschnigg A, et al. Towards predicting the product quality in hot-melt extrusion: Small scale extrusion. Int J Pharm X [internet]. 2020 [cited 2021 August 12]; 2: 100062. doi:10.1016/j.ijpx.2020.100062

[309] Thiele W. Twin-screw extrusion and screw design. In Ghebre-Sellassie I, Martin CE, Zhang F, DiNunzio J, editors. Pharmaceutical Extrusion Technology. 2nd ed. Boca Raton, FL, USA: CRC Press; 2020. p. 71-93.

[310] Rathore AS, Winkle H. Quality by design for biopharmaceuticals. Nat Biotechnol 2009; 27 (1): 26-34. doi:10.1038/nbt0109-26

[311] Simões MF, Pinto RMA, Simões S. Hot-melt extrusion in the pharmaceutical industry: toward filing a new drug application. Drug Discov Today 2019; 24 (9): 1749-1768. doi:10.1016/j.drudis.2019.05.013

[312] Alshetaili A, Alshahrani SM, Almutairy BK, Repka MA. Hot Melt Extrusion Processing Parameters Optimization. Processes [internet]. 2020 [cited 2021 August 12]; 8(11):1516. https://doi.org/10.3390/pr8111516

[313] Sarraf AG, Cherkaoui S, Jordan O, Gurny R, Doelker E. Controlled drug release from melt-extrudates through processing parameters: a chemometric approach. Int J Pharm 2015; 481 (1-2): 9-17. doi:10.1016/j.ijpharm.2014.12.046

[314] Maddineni S, Battu SK, Morott J, Soumyajit M, Repka MA. Formulation optimization of hot-melt extruded abuse deterrent pellet dosage form utilizing design of experiments. J Pharm Pharmacol 2014; 66 (2): 309-322. doi:10.1111/jphp.12129

[315] N Politis S, Colombo P, Colombo G, M Rekkas D. Design of experiments (DoE) in pharmaceutical development. Drug Dev Ind Pharm 2017; 43 (6): 889-901. doi:10.1080/03639045.2017.1291672

[316] Butreddy A, Bandari S, Repka MA. Quality-by-design in hot melt extrusion based amorphous solid dispersions: An industrial perspective on product development. Eur J Pharm Sci [internet]. 2021 [cited 2021 August 12]; 158: 105655. doi:10.1016/j.ejps.2020.105655

[317] Eitzlmayr A, Matic J, Khinast J. Analysis of flow and mixing in screw elements of corotating twin-screw extruders via SPH. AIChE J 2017; 63: 2451-2463. doi:10.1002/aic.15607

[318] International Conference on Harmonisation of Technical Requirements for Registration of Pharmaceuticals for Human Use. ICH Harmonised Tripartite Guideline: Stability testing of new drug substances and and products, Q1A (R2). [internet] [cited: 2022 April 14] Available from: https://database.ich.org/sites/default/files/Q1A%28R2%29%20Guideline.pdf

[319] Brandrup J, Immergut EH, Grulke EA, editors Polymer handbook. 4th ed. Hoboken, NJ, USA: Wiley ;1999

[320] Shah VP, Tsong Y, Sathe P, Liu JP. In vitro dissolution profile comparison--statistics and analysis of the similarity factor, f2. Pharm Res 1998; 15 (6): 889-896. doi:10.1023/a:1011976615750

[321] Brum J, Burnett D. Quantification of surface amorphous content using dispersive surface energy: the concept of effective amorphous surface area. AAPS PharmSciTech 2011; 12 (3): 887-892. doi:10.1208/s12249-011-9655-5

[322] Wang Y, Snee RD, Keyvan G, Muzzio FJ. Statistical comparison of dissolution profiles. Drug Dev Ind Pharm 2016; 42 (5): 796-807. doi:10.3109/03639045.2015.1078349

[323] Yuksel N, Kanik AE, Baykara T. Comparison of in vitro dissolution profiles by ANOVA-based, model-dependent and -independent methods. Int J Pharm 2000; 209 (1-2): 57-67. doi:10.1016/s0378-5173(00)00554-8

[324] Omidian H, Park K. Swelling agents and devices in oral drug delivery. J Drug Del Sci Tech 2008; 18 (2): 83-93. doi: 10.1016/S1773-2247(08)50016-5

[325] Mandal A, Clegg JR, Anselmo AC, Mitragotri S. Hydrogels in the clinic. Bioeng Transl Med 2020; 5 (2): 1-12. doi: 10.1002/btm2.10158

[326] McBride JW, Boyd P, Dias N, et al. Vaginal rings with exposed cores for sustained delivery of the HIV CCR5 inhibitor 5P12-RANTES. J Control Release 2019; 298: 1-11. doi:10.1016/j.jconrel.2019.02.003

[327] Teller RS, Rastogi R, Johnson TJ, Blair MJ, Hitchcock RW, Kiser PF. Intravaginal flux controlled pump for sustained release of macromolecules. Pharm Res 2014; 31 (9): 2344-2353. doi:10.1007/s11095-014-1331-5

[328] Ma D, Djemai A, Gendron CM, et al. Development of a HPMC-based controlled release formulation with hot melt extrusion (HME). Drug Dev Ind Pharm 2013; 39 (7): 1070-1083. doi:10.3109/03639045.2012.702350

[329] Luebbert C, Stoyanov E, Sadowski G. Phase behavior of ASDs based on hydroxypropyl cellulose. Int J Pharm X [internet]. 2020 [cited 2021 October 8]; 3: 100070. doi:10.1016/j.ijpx.2020.100070

[330] Hsu TT, Langer R. Polymers for the controlled release of macromolecules: effect of molecular weight of ethylene-vinyl acetate copolymer. J Biomed Mater Res 1985; 19 (4): 445-460. doi:10.1002/jbm.820190409

[331] Gao P, Skoug JW, Nixon PR, Ju TR, Stemm NL, Sung KC. Swelling of hydroxypropyl methylcellulose matrix tablets. 2. Mechanistic study of the influence of formulation variables on matrix performance and drug release. J Pharm Sci 1996; 85 (7): 732-740. doi:10.1021/js9504595

[332] Baumgartner S, Kristl J, Peppas NA. Network structure of cellulose ethers used in pharmaceutical applications during swelling and at equilibrium. Pharm Res 2002; 19 (8): 1084-1090. doi:10.1023/a:1019891105250

[333] Brittain HG, Dickanson DA, Hotz J, Lyons SL, Ramstack M, Wright SG, inventors; Alkermes Inc., assignee. Polymorphic forms of naltrexone. Patent No.: US 7,279,579 B2. October 9, 2007. [internet]. [cited 2021 October 23] Available from: https://patentimages.storage.googleapis.com/ff/ee/04/7786be9ac36c8d/US7279579.pdf

[334] Davis DA, Miller DA, Santitewagun S, Zeitler A, Su Y, Williams RO. Formulating a heat- and shear-labile drug in an amorphous solid dispersion: Balancing drug degradation and crystallinity. Int J Pharm [internet]. 2021 [cited 2021 October 14]; 3: 100092. doi: 10.1016/j.ijpx.2021.100092